Mechanism and function of Cdc123 mediated eIF2 assembly

DISSERTATION ZUR ERLANGUNG DES DOKTORGRADES

DER NATURWISSENSCHAFTEN (DR. RER. NAT.)

DER FAKULTÄT FÜR BIOLOGIE UND VORKLINISCHE MEDIZIN

DER UNIVERSITÄT REGENSBURG

vorgelegt von Sven Vanselow

aus

Esslingen a.N.

im Jahr 2020

Das Promotionsgesuch wurde eingereicht am

13.11.2020

Die Arbeit wurde angeleitet von

Prof. Dr. Wolfgang Seufert

Unterschrift:

Table of contents

Abstract

The eukaryotic initiation factor 2 (eIF2) is a protein complex which is conserved among all eukaryotes and has a homolog in archaea, called archaeal initiation factor 2 (aIF2). It fulfills essential functions in protein synthesis and is made up of three subunits (α, β and γ). Together with GTP and the initiator tRNA Met-$tRNA_i^{Met}$ ($tRNA_i$), eIF2 forms the ternary complex (TC). eIF2 leads $tRNA_i$ to the ribosomal 40S subunit and scans the mRNA in collaboration with other initiation factors. Upon binding of $tRNA_i$ to a start codon, γ-phosphate of the GTP and subsequently all initiation factors are released (Algire et al., 2005). The ribosomal subunits join to form an active 80S ribosome and elongation phase, in which the peptide chain is synthesized, commences. eIF2 is involved in selection of the right start codon and important for the accuracy of protein synthesis. It is a hub for central regulational mechanisms, which adjust cell metabolism under conditions of stress. Amino acid starvation, unfolded protein stress and other stress factors activate certain kinases, which phosphorylate eIF2α, reduce TC activity and thus protein synthesis rate (Pakos-Zebrucka et al., 2016). On a molecular level, defects in eIF2 lead to inefficient protein synthesis and inaccurate selection of start codons, hence affecting cell growth and increasing susceptibility to exogenous stressors. In humans, several rare mutations of eIF2γ are known which negatively affect the activity of eIF2 and lead to organ dysfunction and neuronal defects in particular. The molecular cause is lowered TC activity, since binding of $tRNA_i$ and assembly of trimeric eIF2 are affected (Borck et al., 2012; Young-Baird et al., 2019c).

This work pays particular attention to the assembly mechanism of eIF2. To date, no dedicated scaffold protein or chaperone that necessary for aIF2 assembly in archaea is known. In eukaryotes however, previous studies established that the protein Cdc123 is indispensable for assembly of the the α-, β- and γ-subunits to active trimeric eIF2 (Perzlmaier et al., 2013). Meanwhile, little is known about the order of assembly and the individual functions of each subunit as well as Cdc123. However, the mechanism of complex formation is of great interest to understand molecular causes of eIF2-related hereditary defects. Here, detailed studies of eIF2 subunit interactions and eIF2-Cdc123 interactions will be presented. The majority of experiments were performed in the budding yeast *S. cerevisiae*. Thanks to its ease of handling and fast replication, it is an ideal model organism for fundamental cellular processes. The high conservation of the translation process in general and eIF2 in particular allow for conclusions about the respective processes in human cells. In yeast, the endogenous proteins and, by heterologous expression, the human proteins were investigated. Some results were verified in human cell culture. At the end, a model for stepwise assembly of eIF2 will be presented and individual roles of each eIF2 subunit and Cdc123 will be discussed.

Zusammenfassung

Der eukaryotische Initiationsfaktor 2 (eIF2) ist ein Proteinkomplex, der in allen Eukaryonten essentielle Funktionen in der Proteinsynthese übernimmt und als archaeeller Initiationsfaktor 2 (aIF2) auch in Archaeen konserviert ist. Er besteht aus drei Untereinheiten (α, β und γ) und bindet in seiner aktiven Form GTP und die Initiator-tRNA Met-$tRNA_i^{Met}$ ($tRNA_i$), wodurch ein ternärer Komplex (TC) gebildet wird. eIF2 führt die $tRNA_i$ zur ribosomalen 40S-Untereinheit, wo in Zusammenarbeit mit anderen Initiationsfaktoren die mRNA gescannt wird. Bei korrekter Basenpaarung der tRNA mit dem Startcodon werden zunächst das γ-Phosphat des GTPs aus eIF2 und dann die Initiationsfaktoren freigesetzt (Algire et al., 2005). In der Folge bilden die ribosomalen Untereinheiten ein aktives 80S-Ribosom und die Elongationsphase, bei der die Peptidkette synthetisiert wird, beginnt. eIF2 ist also an der Auswahl des Startcodons beteiligt und somit für die Genauigkeit der Translationsinitiation mitverantwortlich. eIF2 ist Ansatzpunkt für zentrale Regulationsmechanismen, die in Stresssituationen zu einer Anpassung des Zellmetabolismus führen. So können Aminosäuremangel oder Stress durch ungefaltete Proteine Kinasen aktivieren, die eIF2α phosphorylieren, die Menge an aktivem eIF2 dadurch reduzieren und die Proteinsyntheserate senken (Pakos-Zebrucka et al., 2016). Defekte in eIF2 können auf molekularer Ebene eine ineffizientere Proteinsynthese und ungenauere Auswahl von Startcodons zur Folge haben. Folglich führen sie zu langsamerem Zellwachstum und einer erhöhten Anfälligkeit für exogene Stressfaktoren. Beim Menschen sind mehrere seltene Mutationen von eIF2γ bekannt, die die Aktivität des Komplexes negativ beeinflussen und zu schweren körperlichen Missbildungen der Organe, insbesondere aber des zentralen Nervensystems führen. Die molekularen Ursachen liegen dabei in der verringerten Bildung von aktiven TCs, da die Bindung der $tRNA_i$ oder die Assemblierung des trimeren eIF2-Komplexes beeinträchtigt sind (Borck et al., 2012; Young-Baird et al., 2019c).

In dieser Arbeit soll der Assemblierung von eIF2 besondere Aufmerksamkeit gewidmet werden. Für den archaellen Faktor aIF2 ist nicht bekannt, dass ein Gerüstprotein oder Chaperon für seine Assemblierung benötigt wird. In Eukaryonten hingegen ist, wie vorherige Studien zeigen konnten, das Protein Cdc123 für die Assemblierung der α-, β- und γ-Untereinheiten zum trimeren Komplex unabdingbar (Perzlmaier et al., 2013). Über die Reihenfolge, sowie die individuellen Funktionen jeder Untereinheit und Cdc123 während der Assemblierung ist indes wenig bekannt. Der Mechanismus der Komplexbildung ist jedoch von großem Interesse, um die molekularen Ursachen von eIF2-Mutationserkrankungen zu verstehen. In dieser Arbeit sollen detaillierte Untersuchungen zu Interaktionen der eIF2-Untereinheiten miteinander und mit dem Assemblierungsfaktor Cdc123 vorgestellt werden. Die Mehrzahl der Experimente wurde in der Hefe *S. cerevisiae* durchgeführt. Durch ihre einfache Handhabung und hohe Zellteilungsrate ist sie ein idealer Modellorganismus für grundlegende zelluläre Prozesse. Dank der hohen Konservierung des Translationsprozesses im Allgemeinen und eIF2 im Besonderen können auch Rückschlüsse auf die entsprechenden Vorgänge im Menschen gezogen werden. Es wurden dabei die Proteine der Hefe untersucht, durch heterologe Expression im Hefeorganismus jedoch auch die entsprechenden Proteine des Menschen. Einige Ergebnisse wurden durch Untersuchungen in menschlicher Zellkultur verifiziert. Am Ende soll ein neues Modell zur schrittweisen Assemblierung des eIF2 vorgestellt und auf die Funktionen der einzelnen Untereinheiten und Cdc123 eingegangen werden.

1 Introduction

1.1 Translation initiation

Gene expression in all living cells roughly happens in three major steps: First, transcription of sequence information from DNA to pre-messenger RNA (pre-mRNA) by the cell's transcription machinery, which is made up of RNA polymerase II, transcription factors and additional regulating factors. Secondly, pre-mRNA must be processed. Freshly synthesized pre-mRNAs contain non-coding sequences and must be cut and spliced by the spliceosome. The mRNA is then capped at the 5' end with an m^7G-guanosine cap and the 3'-end is extended with a poly-adenine tail. These modifications ensure stability and proper recognition of the mRNA by the ribosome and serve as a way for the cell to discriminate between cellular RNA and potentially dangerous foreign RNA. The last step in gene expression is translation. In translation initiation, the 40S ribosomal subunit binds mRNA and an initiator tRNA (Met-$tRNA_i^{Met}$, in the following text referred to as $tRNA_i$). Together with a set of initiation factors, the mRNA is scanned and a start codon is selected. After joining of 40S with the 60S ribosomal subunit, elongation phase begins, in which the polypeptide chain is synthesized by the 60S subunit. Elongation of the chain continues until the stop codon of the open reading frame enters the ribosome and is recognized by the eukaryotic release factor (eRF). The polypeptide chain is released, the ribosomal subunits and all translation factors dissociate from the mRNA and the ribosomal subunits are recycled. All steps of translation are catalyzed or facilitated by protein factors, which are named after the respective step of translation in which they are active: initiation factors, elongation factors and termination factors (information taken from Alberts, 2004).

Translation initiation is a central process in cellular biochemistry and the most complex step in translation. It is the main target for translational regulation. While regulation of gene expression happens mostly on a transcriptional level, researchers have long realized the importance of translational regulation, especially when a rapid and global response is needed (Reynolds, 2002). Translation initiation is the process in which mRNAs are recognized and prepared for translation of their open reading frame (ORF). These steps include guiding the mRNA and the methionylated initiator tRNA to the ribosome, cyclizing and scanning the mRNA and selecting the right start codon (Jackson et al., 2010). There are different ways in which mRNAs can be selected. The majority of cellular mRNAs are translated canonically, i.e. through recognition of their 5'-cap and in interaction with all main translation initiation factors. Some mRNAs with unusual properties can enter the ribosome in non-canonical ways (Kwan and Thompson, 2019). Viral RNAs either hijack their host cell's translation initiation machinery or find alternative ways to bypass control mechanisms (Jan et al., 2016).

1.1.1 Cap-dependent translation initiation

Translation initiation in eukaryotes is vastly more complex than in prokaryotes and necessitates a high number of protein factors that regulate and direct the process. Whereas bacteria directly bind the start site of an open reading frame via base pairing of ribosomal RNA with nucleotides close to the start codon, eukaryotic ribosomes bind the mRNA at its 5'-cap (which does not exist in prokaryotes) and scan the mRNA until a start codon is recognized. This complicated process requires 11 initiation factors consisting of 24 gene products in yeast. In mammals, some initiation factors have become more complex, such as eIF3, which consists of only 6 subunits in

yeast, but 13 subunits in humans. Some other initiation factors or domains are not structurally, but functionally conserved or fulfill their function in different ways (Dever et al., 2016). Generally, translation initiation is similar in mammals and yeasts.

1.1.1.1 mRNA properties

Eukaryotic mRNAs, unlike their counterparts in prokaryotes, are monocistronic, which means they contain only one major ORF. The ORF in the vast majority of cases starts with an AUG start codon and ends with one of three stop codons: UAG, UAA or UGA. The coding sequence is flanked by 5'- and 3'-untranslated regions (UTRs), which in interaction with other factors regulate localization, stability and the rate at which an mRNA is translated (Mayr, 2019). Today, the 5'-UTR is often referred to as 'leader sequence', as what was thought to not contain any coding sequences often contains upstream ORFs (uORFs) and can give rise to a plethora of small peptides (Starck et al., 2016). uORFs often inhibit translation of the main ORF of the mRNA but lose their inhibiting properties under certain conditions (see sections 1.1.2.1, 1.1.4). The structure of the 5'-leader also influences translation of an mRNA. Highly structured mRNAs, in which the 5'-leader forms folds and hairpins, rely on RNA helicases for efficient translation initiation. In yeasts, 5'-leaders are typically shorter and less structured than in higher eukaryotes (Kertesz et al., 2010). As mentioned, translation usually starts at an AUG start codon. However, not only the sequence of the codon, but also its sequence context influences the efficiency of translation initiation. Optimal context in *S. cerevisiae* are adenine-rich sequences upstream of AUG, position -3 being the most critical (Hinnebusch, 2011). This start codon context bias, while being significant, is less pronounced in yeast compared to higher eukaryotes. The optimal sequence for start-codon context differs between eukaryotic species, though a consensus sequence, named Kozak sequence, has been established (Kozak, 1987).

1.1.1.2 Initiator tRNA (Met-tRNA$_i^{MET}$)

Each codon of an mRNA is bound by a unique tRNA carrying the encoded amino acid. Interestingly, AUG encodes methionine both at the start of and within the coding region, yet two different tRNAs are used for the start codon and internal AUG codons. Differing sequences and post-transcriptional modifications in the tRNAs set the two methionylated tRNAs apart and prevent elongator tRNA (tRNA$_e$) Met-tRNA$_e^{Met}$ from functioning in translation initiation vise versa. tRNA$_i$ seems to be particularly sensitive when it comes to modifications, as lack of modifications strongly impairs translation initiation (Anderson et al., 1998) .

1.1.1.3 43S Preinitiation complex (PIC) formation

Initiator tRNA must be guided to the 40S subunit by eIF2. This trimeric protein complex consists of three subunits, eIF2α, β and γ. Domain 1 of the γ-subunit is related to the family of small G-proteins and hydrolyzes GTP during translation initiation (see section 1.1.3.1). After each round of translation initiation, GDP must be released by the guanosine exchange factor (GEF) eIF2B to allow GTP to bind. Active eIF2 then binds tRNA$_i$ to form TC. All eIF2 subunits contribute to binding tRNA$_i$ so that the dissociation constant (K_D) is in the nanomolar range (Naveau et al., 2013). TC is a hub for translational regulation. Stress, e.g. from amino acid depletion or unusual amounts of unfolded protein, activates kinases like Gcn2 or PERK that phosphorylate eIF2α. eIF2-P acts as an inhibitor of eIF2B and lowers the amount of TC available in the cell. This, in turn, lowers global translation activity but selectively increases translation of a set of mRNAs

that contain uORFs and code for proteins that mediate the cell's response to the aforementioned stress conditions (section 1.1.4). Details of eIF2 assembly and regulation can be found in section 1.1.3. TC forms a multifactor complex (MFC) together with eIF1, eIF3 and eIF5, which is stabilized by multiple interactions of the proteins with each other. eIF1 in particular can bind all initiation factors at the same time: eIF2β, the C-terminal domain of eIF5 and eIF3c. In addition, eIF2β and eIF5 bind directly to each other (Dever et al., 2016). Together with the ribosomal 40S subunit and eIF1A, which sits at the A site of the 40S subunit, MFC forms the 43S PIC. This opens up the mRNA entry channel on the 40S subunit, which is critical for mRNA binding and scanning in subsequent steps (Hinnebusch, 2014). Whether the MFC is a distinct complex that always binds to 40S as a whole or whether it serves as a reservoir for translation initiation factors (TIFs), is not clear (Aitken and Lorsch, 2012). In the 43S PIC, eIF1 is positioned at the P site and, together with eIF1A, prevents robust interaction of $tRNA_i$ with the P site. eIF3 is the largest factor among those present in 43S PIC and interacts with the solvent exposed side of the ribosome through various contacts (Valásek et al., 2003). eIF5 is a guanosine dissociation inhibitor (GDI) and a GTPase activating protein (GAP) for eIF2. It prevents dissociation of GTP/ GDP from eIF2γ and also stimulates hydrolysis of GTP (Jennings and Pavitt, 2010).

1.1.1.4 mRNA activation

Eukaryotic mRNA is not directly recognized by the ribosome. First, it must be activated by a group of TIFs that bind its 5'-cap and poly-A-tail and circularize the mRNA. eIF4E and the Poly-A binding protein (PABP) Pab1 bind the 5'-cap and the poly-A-tail, respectively, and recruit the scaffolding protein eIF4G, which bridges eIF4E and Pab1, forming a circle. Secondary structures in the 5'-mRNA leader interfere with the progression of translation initiation by hindering 43S recruitment and mRNA scanning. The scaffold protein eIF4G also binds Ded1 and eIF4A. These DEAD-box RNA helicases are thought to unwind secondary structures in RNA. Consistent with this assumption, translation of mRNAs with long and highly structured 5'-leaders is particularly sensitive to lack of Ded1 (Gupta et al., 2018). eIF4A's RNA helicase activity, on the other hand, seems to mainly promote 43S recruitment to RNA by creating a stretch of single-stranded RNA for the complex to bind to (Sen et al., 2015). eIF4B, together with eIF4G, enhances the ATPase and RNA helicase activities of eIF4A (Andreou and Klostermeier, 2014). The proteins eIF4A, -B and –G together are also referred to as eIF4F. Finally, the mRNA complex, held together by eIF4G, unites with the 43S PIC to form the scanning competent 48S PIC.

1.1.1.5 48S PIC formation, mRNA scanning and start codon recognition

In mammals, eIF4G contacts eIF3c, d and e to bring the MFC and mRNA together. These eIF3 subunits are not conserved in yeast, where joining of the mRNA activation complex with 43S PIC is mediated by binding of the eIF5 C-terminal domain (CTD) to eIF4G. In 43S PIC, eIF5-CTD is bound to eIF2β and eIF3c (Asano et al., 2001; Yamamoto et al., 2005). Since the eIF4F complex binds mRNA at its 5' end, 43S is also recruited to that part of the transcript. This ensures start of translation at the first AUG codon. Complex joining is further enhanced by interactions of eIF4B with eIF3 and Rps20, a small subunit (SSU) associated ribosomal protein; this may implicate a role for eIF4B in recruiting mRNA to the entry channel of the 40S subunit (Zhou et al., 2014). The factors eIF1 and eIF1A prevent $tRNA_i$ from binding to the P site, and A site, respectively, so the ternary complex cannot fully engage with the P site (P_{OUT} state). P_{OUT} is further promoted by interaction of the scanning inhibitor elements in the eIF1A-NTT with eIF5-CTD and eIF1

(Hinnebusch, 2017). eIF1 and eIF1A also open up the mRNA entry channel of the 40S subunit and allow the 43S PIC to slide along the mRNA in 3' direction (Passmore et al., 2007). GTP hydrolysis by eIF2γ is stimulated by eIF5 and can take place before start codon recognition (Algire et al., 2005). Selection of the start codon is mainly directed by base pairing between the $tRNA_i$'s CAU-anticodon with the AUG codon. Mutational studies revealed that mutation of the anticodon to CCU and the start codon to a matching AGG allowed translation of a *HIS4* mRNA (Cigan et al., 1988a). Once the anticodon of $tRNA_i$ recognizes an AUG start codon in good context, engagement of TC with the P site induces a conformational change in the preinitiation complex that weakens its interaction with eIF1 (Maag et al., 2005). The factor's dissociation triggers release of the free phosphate (P_i) still associated with TC. The release is enhanced by movement of the eIF1A C-terminal tail (CTT) away from the P site and towards eIF5. It is assumed that eIF5, whose N-terminal domain resembles eIF1, moves into the gap left by eIF1 and also stimulates P_i release (Nanda et al., 2009). The unstructured NTT of eIF2β, which was previously bound to eIF1 now interacts with the eIF5-CTD, which allows the scanning inhibitor elements of eIF1A, also bound to eIF5-CTD, to move to and stabilize the codon-anticodon helix. The head of the 40S subunit moves downwards to the body and the mRNA channel tightens. In this closed conformation of the 48S PIC, further movement of the mRNA is prevented (Llácer et al., 2015). In many of the translation initiation factors, including eIF1, eIF1A, eIF2α, β and γ, eIF3 subunits and in 18S rRNA, mutations have been identified that increase translation initiation from near-cognate start codons, e.g. UUG, and AUG codons in suboptimal context. Termed "suppressor of initiation codon" (Sui^-), these mutations seem to favor transition to a closed conformation of the ribosome and full engagement of TC with the P site (P_{IN} state). This makes selection of the start codon less stringent. eIF1 in particular seems to have a critical role as "gate keeper" of start codon selection, as reduced levels of eIF1 protein confer a Sui^- phenotype, whereas overexpression of the factor increases stringency of start codon selection and even suppresses other Sui^- mutations. The gene encoding eIF1 was named *SUI1* in yeast, owing to its gatekeeping function. Interestingly, the *SUI1* mRNA contains an AUG start codon in poor context. Relaxed start codon selection thus increases expression of eIF1, which partially restores the accuracy of translation initiation (Martin-Marcos et al., 2011). Study of the structural properties of 48S PIC revealed the importance of adenine-rich sequences for the recognition of start codons. Arginine residues in domain 1 of eIF2α are in contact with nucleotides upstream of the AUG start codon and specifically recognize adenine residues at position -3. The interaction seems to slow down mRNA scanning to facilitate start codon recognition (Hinnebusch, 2017). Movement of the initiation factors upon AUG recognition closes the mRNA entry channel and tightens the P site. This likely prevents the PIC from moving away from the start codon.

1.1.1.6 Subunit joining

Since eIF2 is positioned at the intersubunit face, its release is necessary before joining of 40S with 60S to form an active 80S ribosome can take place. The association of eIF2 with $tRNA_i$ is dependent on its GTP-bound state. Release of P_i weakens its affinity for $tRNA_i$ and facilitates eIF2 release from the PIC. Evidence suggests that eIF2 remains in complex with eIF5 as it leaves the PIC and that the eIF2 • eIF5 complex is the main cytoplasmic reservoir of eIF2 (Singh et al., 2006). Subunit joining is mediated by an interaction between C-terminal amino acids of eIF1A with domain 4 of eIF5B (Acker et al., 2006). eIF5B also contacts $tRNA_i$ and stabilizes it on the PIC

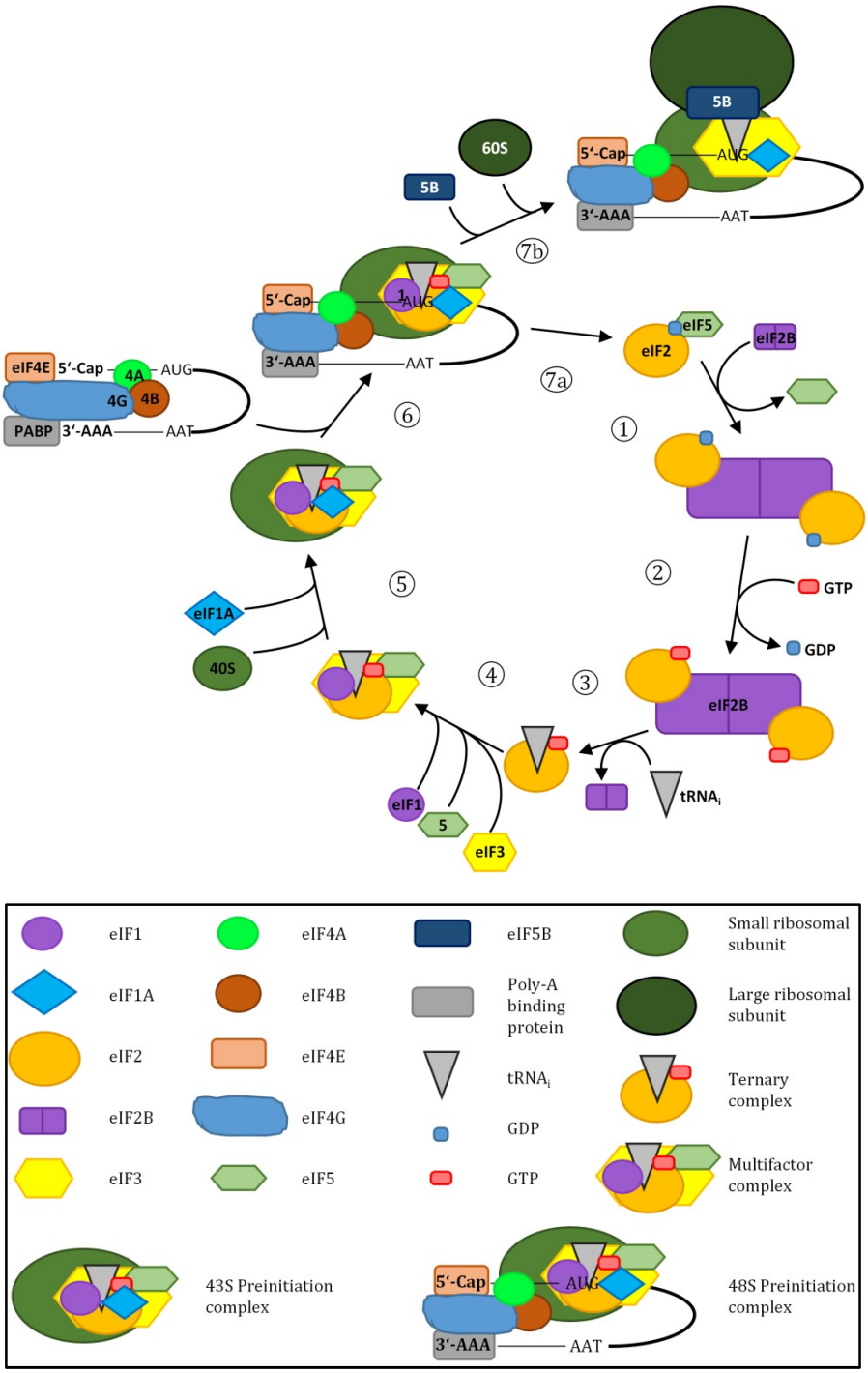

Figure 1: Schematic overview of translation initiation. (1) eIF2 • GDP is in complex with its GAP/ GDI eIF5. eIF2B replaces eIF5, exerting its GDI displacement activity via its γ- and ε-subunits. (2) eIF2B catalyzes release of GDP, allowing GTP to bind. (3) Ternary complex formation is completed by displacement of eIF2B by $tRNA_i$. (4) Ternary complex forms an MFC together with eIF5, eIF1 and eIF3. (5) The MFC and eIF1A bind the 40S ribosome. 43S PIC is formed. (6) eIF2E and PABP, held together by the scaffold protein eIF4G, bind to the 5'-cap and the Poly-A tail of an mRNA. eIF4G also binds eIF4A and, together with eIF5B, stimulates its helicase activity to resolve secondary mRNA structures for easier attachment of the 43S PIC. The activated mRNA complex and 43S PIC join to form a scanning competent 48S PIC. eIF2, stimulated by eIF5, hydrolyzes GTP during scanning but does not release P_i yet. (7A) Upon start codon recognition, P_i and eIF1 are released and eIF2 • GDP, in complex with eIF5, dissociates from the ribosome. (7b) Subunit joining is catalyzed by interaction of eIF5B with eIF1A. Elongation commences and the remaining eIFs quickly dissociate. Figure inspired by drawings by Hinnebusch et al. (Hinnebusch, 2014), Dever et al. (Dever et al., 2016), Jackson et al. (Jackson et al., 2010) and Perzlmaier (Perzlmaier, 2012).

to prevent its dissociation, preventing the PIC from returning to the open, scanning competent state (Lee et al., 2002). The release of eIF5B and eIF1A from 80S ribosomes marks the second step in translation initiation that depends on GTP hydrolysis. It is catalyzed by the central G domain of eIF4B. Without GTP hydrolysis, release of eIF5B and eIF1A is impaired, resulting in slow cell growth. Mutations that suppress the slow growth phenotype often weaken eIF5B association with the ribosome and result in leaky scanning, which suggests that GTP hydrolysis represents another quality control step and checkpoint (Shin et al., 2002). With $tRNA_i$ engaged with the P site and an empty A site, the fully assembled ribosome is ready to bind the first elongator tRNA and start protein synthesis. Not all initiation factors instantly dissociate from the ribosome during translation; some can remain attached for a while but fall off during elongation.

1.1.2 Alternative translation initiation pathways

Besides canonical, 5'-cap dependent translation initiation, alternative pathways for mRNAs to enter the ribosome exist that are mostly used by mRNAs with unusual structures, some mRNAs coding for regulatory proteins or viral RNAs (Kwan and Thompson, 2019).

1.1.2.1 Reinitiation

As mentioned above, a part of the translation initiation machinery remains attached to the ribosome for a short time during elongation. Translation of very short ORFs, e.g. uORFs, can be terminated with the SSU and some of the initiation factors, e.g. eIF3 still attached (Szamecz et al., 2008). In this case, the 40S subunit resumes scanning after reaching the stop codon. Dissociation of eIF2 is a mandatory step in translation initiation, so reinitiation on the same mRNA can only take place if the scanning SSU can catch a new TC before reaching the next start codon. This mechanism of reinitiation is used to quickly increase the translation of certain transcripts in reaction to changing conditions, e.g. the *GCN4*/ *ATF4* mRNAs (for details, see section 1.1.4).

1.1.2.2 IRES

Internal Ribosome Entry Structures (IRES) are secondary structures in the 5'-leader of mRNAs that can recruit ribosomes independently of a 5'-cap. They were first discovered in picornaviridae. Since viral RNAs often do not have access to cellular mRNA processing factors, IRES offers a way to circumvent that step in mRNA quality control. There are four types of IRES, none of which require the cap-binding eIF4E. However, they differ in their need for other initiation factors (Jackson et al., 2010). Some cellular mRNAs use IRES to recruit ribosomes under stress conditions. In fungi, such mRNAs often encode heat shock proteins, proteins involved in cell wall synthesis or metabolism. Under conditions where cap-dependent translation initiation is suppressed, translation of those mRNAs can be rapidly upregulated for a quick response to changing conditions (Peguero-Sanchez et al., 2015). In mammals, an example for IRES-dependent mRNAs are pro-apoptotic proteins, as caspases cleave several factors required for cap-dependent initiation (Spriggs et al., 2005).

1.1.2.3 Leaky scanning

Ribosomes rarely scan past AUG start codons in optimal context. If, however, the context is poor, e.g. due to non-adenine nucleotides at positions -3 or -4, or the start codon is UUG, leaky scanning frequently occurs (Cigan et al., 1988b). Likewise, a lower abundance of or defects in

some translation initiation factors can increase the frequency of skipping AUG codons in suboptimal context (Fekete et al., 2007). If a start codon is skipped, scanning continues and initiation usually occurs at the next strong start codon. Thus, leaky scanning can result in proteins with longer or shorter N-termini, if the second start codon is in frame with the skipped one, or in a different protein, if it is out of frame (Kochetov, 2008). Two prominent examples for leaky scanning in yeast are the genes *GRS1* and *ALA1*, which encode acyl-tRNA synthases. Initiation at their upstream non-AUG start codons produces an N-terminal tail that mediates import to mitochondria. Initiation at the downstream, in-frame AUG start codon results in the cytoplasmic protein (Chang and Wang, 2004).

1.1.3 Function, interactions and regulation of eIF2

Being the carrier of $tRNA_i$, a key factor in start codon selection and the main target for translational regulation, eIF2 is a central actor in protein synthesis. The three subunits of eIF2, eIF2α, β and γ, are highly conserved among all eukaryotes and archaea. The central subunit of the complex, eIF2γ, is related to the $tRNA_e$ binding elongation factors eEF1A and bacterial EF-Tu. It contains a G-domain which binds and hydrolyzes GTP and thus belongs to the family of small GTPases. Assembly of trimeric eIF2 is mediated by the ATP grasp protein Cdc123. Since GTP is hydrolyzed to GDP in each round of translation initiation, GDP must first be released by the decameric eIF2B complex to allow GTP to bind. eIF2-GTP then forms a ternary complex with $tRNA_i$. During stress conditions, eIF2α is phosphorylated, which turns eIF2 into an inhibitor of its GEF, lowers TC levels and activates *GCN4*/ *ATF4* expression. In yeast, the three subunits α, β and γ were named Sui2, Sui3 and Gcd11/Sui4, as they were identified in mutational analyses where yeast strains with relaxed start codon selection (Sui^- phenotype) were studied (Cigan et al., 1988b; Huang et al., 1997). The name Gcd11 stems from the "general control derepressed" phenotype, in which *GCN4* expression is permanently active. Some mutations in Gcd11 and other *GCD* genes affect TC formation, which activates ISR independently of eIF2α phosphorylation (Harashima and Hinnebusch, 1986).

The human eIF2 components are referred to as eIF2α, -β and –γ, while the gene names are EIF2S1, 2 and 3. Sometimes, the gene nomenclature is used for the gene products as well.

1.1.3.1 eIF2 composition

The γ-subunit is the central protein of the eIF2 complex. It binds the α- and β-subunit and GTP. The protein consists of three domains that are conserved among eukaryotes (see figure 2, 3) and archaea and the homologous elongation factors eEF1A (eukaryotes), EF-1A (archaea) and EF-Tu (bacteria) (Schmitt et al., 2010). Domain 1, also called G-domain because it binds and hydrolyzes GTP, is the largest of the three domains and can vary in length between species. While archaea have the N-terminally shortest G-domain, budding yeasts' eIF2γ possesses a long N-terminal extension of 90 AA, most of which is not essential for growth. The domain contains conserved G-motifs that bind the G-nucleotide (see figure 2): The NKxD (G4), SAQL (G5) and GKS/T (G1) motifs and the mobile switch 1 (G2) and switch 2 (G3) regions (Roll-Mecak et al., 2004). The switch motifs change their conformation depending on whether GDP or GTP is bound (Yatime et al., 2006). Based on structural data from archaeal IF2, domain 1 is also responsible for binding the β-subunit via multiple amino acid contacts (Sokabe et al., 2006). Domain 1 possesses a

characteristic ribbon that protrudes out of the domain core towards domain 2. In yeast, the ribbon is stabilized by four cysteines, coordinating a zinc ion. In mammals, three of four cysteines are not conserved and the ribbon is instead held together by hydrophobic interactions. Mutation of the cysteines severely affects growth in yeast (Roll-Mecak et al., 2004). Domain 2 contacts the α-subunit, mostly with a loop structure and two conserved amino acids at the end of the domain (Yatime et al., 2006). According to those data, the α- and β-subunits do not directly contact each other. Domain 3 is responsible for binding the assembly factor Cdc123 (Panvert et al., 2015).

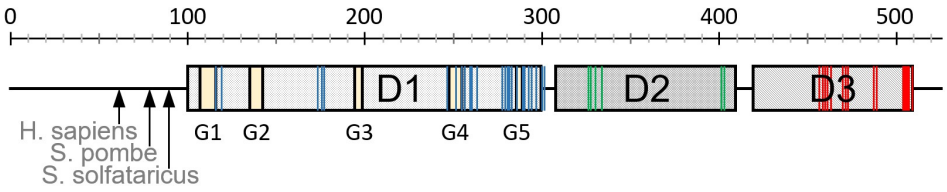

Figure 2: Schematic view of eIF2γ. Domains 1-3 are labeled as D1-3. The start of N-termini in different species is annotated at the N-terminal tail. G-Motifs are indicated as yellow boxes and labeled as G1-5. Contacts to eIF2β are indicated as blue lines, contacts to eIF2α in green, residues involved in Cdc123 interaction in red. The scale on top shows amino acid positions.

```
yeast       MSDLQDQEPSIIINGNLEPVGEPDIVEETEVVAQETQETQDADKPKKKVAFTGLEEDGET   60
human       ----------------------------------------------------MA----GGEA   6
archaea     ------------------------------------------------------------   0

yeast       EEEKRKREFEEGGGLPEQPLNPDFSKLNPLSAEIINRQATINIGTIGHVAHGKSTVVRAI   120
human       GVT-----LGQPHLSRQDLTTLDVTKLTPLSHEVISRQATINIGTIGHVAHGKSTVVKAI   61
archaea     ------------------------------MAWPKVQPEVNIGVVGHVDHGKTTLVQAI   29
                                          . *  :***.:*** ***:*:*:**

yeast       SGVQTVRFKDELERNITIKLGYANAKIYKCQEPTCPEPDCYRSFKSDKEISPKCQRPGCP   180
human       SGVHTVRFKNELERNITIKLGYANAKIYKLDDPSCPRPECYRSCGSSTPDEFPTDIPGTK   121
archaea     TGIWTSKHSEELKRGMTIKLGYAETNIGVCE--SCKKPEAYVT-------EPSCKSCGSD   80
            :*: * :..:**:*.:********:::*   :  :* .*:.* :       .   .  *

yeast       GRYKLVRHVSFVDCPGHDILMSTMLSGAAVMDAALLLIAGNESCPQPQTSEHLAAIEIMK   240
human       GNFKLVRHVSFVDCPGHDILMATMLNGAAVMDAALLLIAGNESCPQPQTSEHLAAIEIMK   181
archaea     DEPKFLRRISFIDAPGHEVLMATMLSGAALMDGAILVVAANEPFPQPQTREHFVALGIIG   140
            .. *::*::**:*.***::**:***.***:**.*:*::*.**  ***** **:.*: *:

yeast       LKHVIILQNKVDLMREESALEHQKSILKFIRGTIADGAPIVPISAQLKYNIDAVNEFIVK   300
human       LKHILILQNKIDLVKESQAKEQYEQILAFVQGTVAEGAPIIPISAQLKYNIEVVCEYIVK   241
archaea     VKNLIIVQNKVDVVSKEEALSQYRQIKQFTKGTWAENVPIIPVSALHKINIDSLIEGIEE   200
            :*:::*:***:*:: :..* .: ..*  * :** *:..**:*:**  * **: : * * :

yeast       TIPVPPRDFMISPRLIVIRSFDVNKPGAEIEDLKGGVAGGSILNGVFKLGDEIEIRPGIV   360
human       KIPVPPRDFTSEPRLIVIRSFDVNKPGCEVDDLKGGVAGGSILKGVLKVGQEIEVRPGIV   301
archaea     YIKTPYRDLSQKPVMLVIRSFDVNKPGTQFNELKGGVIGGSIIQGLFKVDQEIKVLPGLR   260
             * .* **:  .* ::*********** :.::***** ****::*::*:.:**:: **:

yeast       TKDDKGKIQCKPIFSNIVSLFAEQNDLKFAVPGGLIGVGTKVDPTLCRADRLVGQVVGAK   420
human       SKDSEGKLMCKPIFSKIVSLFAEHNDLQYAAPGGLIGVGTKIDPTLCRADRMVGQVLGAV   361
archaea     V-EKQGKVSYEPIFTKISSIRFGDEEFKEAKPGGLVAIGTYLDPSLTKADNLLGSIITLA   319
              :.:**:  :***::* *:   .:::: * ****:.:** :**:* :**.::*.::
```

```
yeast        GHLPNIYTDIEINYFLLRRLLGVKTDGQKQ-AKVRKLEPNEVLMVNIGSTATGARVVAVK   479
human        GALPEIFTELEISYFLLRRLLGVRTEGDKKAAKVQKLSKNEVLMVNIGSLSTGGRVSAVK   421
archaea      DAEVPVLWNIRIKYNLLERVVGAK-----EMLKVDPIRAKETLMLSVGSSTTLGIVTSVK   374
             .    :  ::.*.* **.*::*.:     :  **  :  :*.**:.:** :* . * :**

yeast        ADMARLQLTSPACTEI-NEKIALSRRIEKHWRLIGWATIKKGTTLEPIA---   527
human        ADLGKIVLTNPVCTEV-GEKIALSRRVEKHWRLIGWGQIRRGVTIKPTVDDD   472
archaea      KDEIEVELRRPVAVWSNNIRTVISRQIAGRWRMIGWGLVEI-----------   415
              *  .: *  *...   . : .:**::  :**:***. :.
```

Figure 3: Alignment of yeast eIF2γ (Gcd11) against human eIF2γ and aIF2γ from *Sulfolobus solfataricus* by clustal ω. Gaps are indicated as hyphens (-), AAs conserved among all three species as asterisks (*), moderately conserved AAs as colons (:) or dots (.).

The α-subunit is structurally conserved in eukaryotes and archaea. In eukaryotes, it contains an acidic C-terminal extension. Like eIF2γ, eIF2α has three domains: Domain 1 is a β-barrel, domain 2 is made of an α-helical structure and domain 3, which establishes contact to eIF2γ, is a mixed β-barrel/ α-helix. Whereas domain 1 and 2 form one rigid structure, domain 3 is flexible relative to the other two domains (Naveau, et al., 2010). In eukaryotes, the phosphorylation of Serine 51 in response to stress conditions activates *GCN4*/ *ATF4* expression (see section 1.1.4).

The β-subunit is composed of three conserved central domains and eukaryote specific extensions at the N- and C-terminus. The conserved part consists of a short α-helix, roughly 20 AA in length, a mixed α-β-domain, which mediates the interaction with the γ-subunit and a zinc binding domain. The N-terminal, eukaryote-specific domain contains basic lysine patches and is important for binding to eIF5 and eIF2B. Its absence in archaea can be explained with their lack of IF5 and IF2B (Naveau et al., 2010).

All subunits contribute to binding $tRNA_i$ and lack of either subunit significantly reduces affinity for the amino acid carrier. While the γ-subunit on its own can bind $tRNA_i$, affinity is increased by one order of magnitude by addition of eIF2α, and three orders of magnitude with eIF2β. (Naveau et al., 2013). This is in contrast to the situation in archaea, where the γ- and α-subunit bind $tRNA_i$ together and the β-subunit plays only a minor role. The eukaryote-specific, N- and C-terminal extensions contribute significantly to eIF2β's binding properties (Schmitt et al., 2012).

1.1.3.2 Cdc123

Large protein complexes and RNA-protein complexes often require assembly factors or scaffold proteins to make assembly kinetically possible. Small protein complexes like eIF2, which consists of only three subunits, usually assemble without help from external factors. Surprisingly, the protein Cdc123 was found to be the dedicated assembly factor for eIF2 some years ago (Perzlmaier et al., 2013; Richter, 2006).

Genetic analysis of temperature-sensitive (ts) 3Y1 rat fibroblasts strains revealed mutants that were unable to enter cell cycle from quiescence (Ohno & Kimura, 1984; Ohno et al., 1984). In one of the mutants, systematically named 3Y1tsD123, the effect was attributed to a gene unknown at the time. Termed *D123* after the number of the ts mutant, the gene was necessary for G1-S transition in the rat fibroblasts. Using a human cDNA library, Okuda et al. succeeded in 1996 to identify a gene that complemented the ts-allele under restrictive temperature (Okuda

and Kimura, 1996). A single nucleotide exchange, leading to mutation of alanine 109 to valine, caused rapid degradation of *D123* by the proteasome (Okuda et al., 1999; Okuda & Kimura, 1996). At the permissive temperature of 34 °C, cellular levels were already lowered to 1/8th of that in the reference 3Y1 cell line, and again lowered by 75% at 40 °C. Thus, while *D123* is an essential gene, its cellular concentration is not a limiting factor for cell cycle entry. Treatment with proteasome inhibitors resored the stability of the mutated *D123* in 3Y1tsD123 cells (Okuda et al., 2001). Human *D123* is ubiquitously expressed, as indicated by the presence of mRNA and protein in most tissues. Highest expression levels were found in testes (Onisto et al., 1998).

Homologs of the gene were later discovered in many eukaryotic species (for an alignment of the proteins in yeast and human, see figure 4) and due to its importance in cell cycle entry, the gene became generally known as Cell division cycle 123 (*CDC123*). The *CDC123* gene is essential in all species in which it exists. However, a direct function in cell cycle was already doubted by Ohno et al. in 1984, because transformation with Simian Virus 40 (SV40) of the 3Y1tsD123 cell line overrode G1 arrest but lead to cell death quickly thereafter. *D123*'s involvement in cell cycle entry was therefore assumed to be of secondary nature (Ohno and Kimura, 1984). Studies in yeast revealed positive regulation of Cdc123 expression levels by nutrient availability and a link between Cdc123, E3 ubiquitin ligases Chf1/2 and Gcd11 levels. Bieganowski et al. discovered that Chf1 and -2 ubiquitinate Gcd11 for proteasomal degradation, but Cdc123 stabilizes Gcd11 by destabilizing the E3 ligases themselves (Bieganowski et al, 2004). High availability of nutrients thus increases the abundance of eIF2, which seems plausible, since protein synthesis is one of the most energy-consuming processes in rapidly dividing yeast cells. Deletion of Chf1 and 2, however, did not suppress the essentiality of Cdc123. Consequentially, protection of Gcd11 from Chf1/2 mediated degradation is not the most important function of Cdc123. Later, the essential function of Cdc123 was shown to be in translation initiation (Richter, 2006). Without Cdc123, integrity of the eIF2 complex was compromised, as shown by decreased binding of Gcd11 to Sui2 in co-immunoprecipitation. Work by Perzlmaier et al. (Perzlmaier, 2012) expanded on the importance of Cdc123 in eIF2 assembly. From co-immunoprecipitation, complementation and shutdown assays, Cdc123 emerged as the dedicated assembly factor of eIF2 (see section 1.1.3.3).

Structural analysis and PSI-BLAST of Cdc123 revealed its membership in the superfamily of ATP-grasp enzymes (Burroughs et al., 2015; Panvert et al., 2015). These enzymes use ATP to transfer functional groups to other molecules; examples include biotin carboxylases, various dipeptide synthetases and tubulin tyrosin ligase (Fawaz et al., 2011). Whether Cdc123 catalyzes a post-translational modification of eIF2 proteins and whether this could be a step in eIF2 assembly is unclear. Homologs of Cdc123 have been identified in most eukaryotes and often their assigned function is in G1-S transition. A search for homologous proteins (https://www.ebi.ac.uk/interpro/entry/InterPro) reveals gene products with significant sequence homology even in some archaea, bacteria and viruses, although no function has been attributed to these proteins.

Cdc123 consists of two domains that are rigid enough to be crystallized (Panvert et al., 2015) and a C-terminal part that seems to be relatively flexible (unpublished data). The protein binds

ATP between its two domains in a similar way other ATP grasp proteins do. The nucleotide is bound with a K_D of ~ 70 µM and the association stabilizes the structure of Cdc123.

```
yeast      MSSQEYTTFIDIPVTRAQVEHCSYSFWSSLYPKYVPKSIVLKSLPKKFIQYLEQDGIKLP 60
human      -------------MKKEHVLHCQFSAWYPFFRGVTIKSVI-LPLPQNVKDYLLDDGTLVV 46
                      :.: :* **.:* *  ::   . **::   **::. :** :**  :

yeast      QEENSRSVYTEEIIRNEDNDYSDWEDDEDTATEFVQEVEPLIDFPELHQKLKDALNELG- 119
human      SGRDDPPTHS-QPDSDDEAEEIQWSDDENTATLT------APEFPEFATKVQEAINSLGG 99
           . .:.  .:: :   ::: :  :*.***:***          :***:  *:::*:*.**

yeast      AVAPKLNWSAPRDATWILPNNTMKCNEVNELYLLLNASNYIMHDLQRAFKGCVDGDDIKG 179
human      SVFPKLNWSAPRDAYWIAMNSSLKCKTLSDIFLLFKSSDFITRDFTQPFIHCTDDSPDPC 159
           :* *********** **  *.::**: :.:::**:::*::* :*: : *  *.*..

yeast      LKFDLVLRQWCDMNPALEFRVFVKNAHIVGATQRDLN-YYDYLDELSDTFKDLIDEIVHD 238
human      IEYELVLRKWCELIPGAEFRCFVKENKLIGISQRDYTQYYDHISKQKEEIRRCIQDFFKK 219
           ::::****:**:: *. *** ***: :::* :*** . ***::.: .: ::  *:::.:.

yeast      VVLPKFPDKSFVLDVYIPRPFNKIFIVDINPFARKTDSLLFSWNEIAAIAPPKNDVEDYE 298
human      HIQYKFLDEDFVFDIYRD-SRGKVWLIDFNPFGEVTDSLLFTWEELISENNLNGDFSEVD 278
            :  ** *:.**:*:*     .*::::*:***.. ******:*:*: :    :.*..: :

yeast      LRLVTRHNTGRFASKE---------HSENHVPQDLVEASLNPEAIRELTQKWKELLSQQA 349
human      AQE---QDSPAFRCTNSEVTVQPSPYLSYRLPKDFVDLSTGEDAHK-----LIDFLKLKR 330
            :    :::  * ..:         : . ::*:*:*: * . :* :       ::*. :

yeast      KEESSDSENET    360
human      NQQEDD-----    336
           :::..*
```

Figure 4: Alignment of yeast Cdc123 against human Cdc123 by clustal ω. Gaps are indicated as hyphens (-), identical AAs as asterisks (*), moderately conserved AAs as colons (:) or dots (.).

1.1.3.3 eIF2 assembly

Under normal conditions, the assembly of eIF2 subunits into a trimeric complex requires Cdc123 binding to the C-terminus of eIF2γ. Truncation by just a few amino acids impairs binding of the assembly factor and, consequently, of eIF2α and –β. Cells without Cdc123 are not viable and shutdown of Cdc123 synthesis quickly results in G1 arrest. However, simultaneous overexpression of eIF2α and –γ restores eIF2 assembly by mass action and partially rescues cell growth in *S. cerevisiae* (Perzlmaier et al., 2013). Overexpression of eIF2γ alone or in combination with eIF2β is not sufficient. The model proposed by Perzlmaier et al. describes Cdc123 binding to eIF2γ as a requisite step in translation initiation that possibly induces an allosteric change in the γ-subunit, allowing α and β to bind (figure 5). Since overexpression of γ and α rescues assembly, binding of α was discussed as the second step in assembly, followed by binding of the β-subunit.

Recently, different mutations have been described in the human eIF2γ encoding gene EIF2S3, which cause a form of X-linked intellectual deficiency, called MEHMO syndrome (Borck et al., 2012; Gregory et al., 2019; Stanik et al., 2018; Young-Baird et al., 2019c), and related illnesses. MEHMO syndrome is characterized by and named after the symptoms microcephaly, epilepsy, hypogonadism, mental deficiency and obesity. Some of these genetic variants seem to affect eIF2 assembly, including one where the *EIF2S3* gene contains a nonsense mutation at the 3'-end,

resulting in a truncated protein. The binding of $tRNA_i$ is particularly impaired, leading to low TC levels. Importantly, eIF2α coprecipitated increased amounts of Cdc123, but lower amounts of eIF2γ and eIF2β in mutant cells compared to wild type cells (Young-Baird et al., 2019). Possibly, the C-terminal truncation of γ, while not affecting Cdc123 binding itself, makes the interaction unproductive. Based on those observations, Young-Baird et al. proposed a different eIF2 assembly model in which Cdc123 binds both the α-subunit and a putative γβ-dimer, transiently self-dimerizes and thereby facilitates eIF2 assembly (see figure 5 below). Consistent with this, it is thought that eIF2γ binds the β-subunit cotranslationally (Shiber et al., 2018).

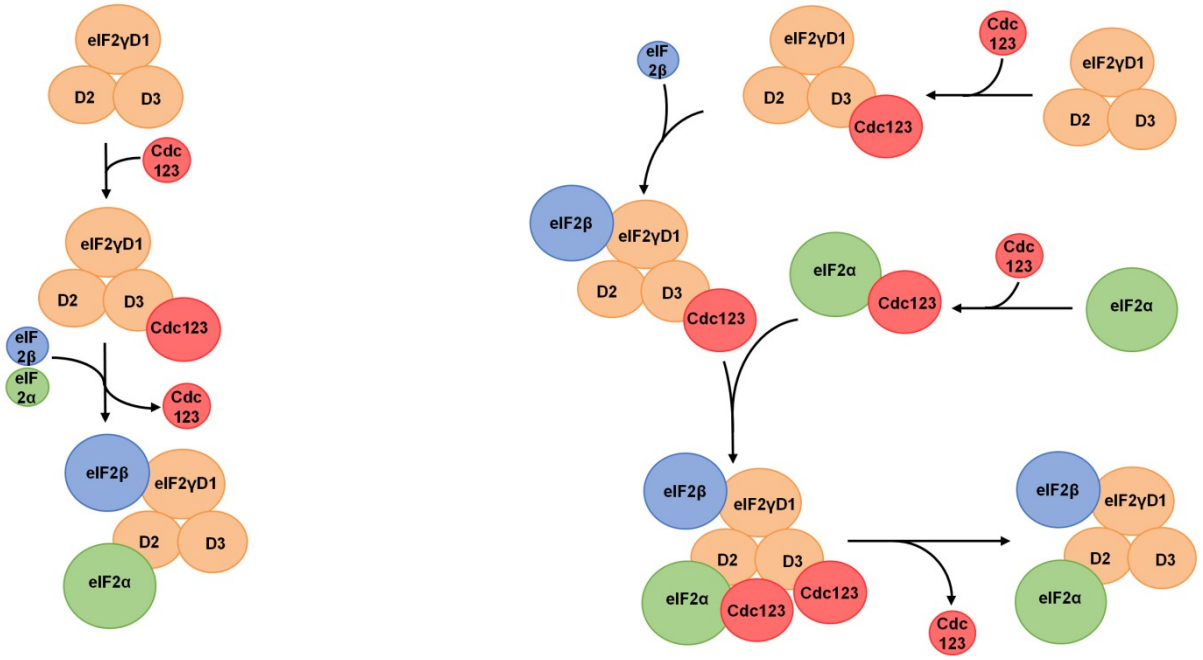

Figure 5: Alternative models for eIF2 assembly. On the left side, a model by Perzlmaier et al. is shown, in which Cdc123 binds to domain 3 of eIF2γ, induces an allosteric change in the protein to enable binding of eIF2α and –β. The model on the right by Young-Baird et al. (Young-Baird et al., 2019a) proposes an alternative mechanism, where Cdc123 binds to both eIF2γβ and eIF2α. Dimerization of Cdc123 facilitates joining of eIF2γβ dimer with eIF2α. In both models, Cdc123 dissociates after completion of the assembly.

1.1.3.4 eIF2 recycling by eIF2B

During translation initiation, eIF2γ hydrolyzes GTP to GDP and releases P_i upon start codon recognition. Studies indicate that the GAP eIF5 remains attached to eIF2 after translation initiation (Jennings et al., 2013). Both eIF2 and eIF5 are abundant proteins, whereas the cellular concentration of eIF2B is up to one order of magnitude lower (Wang et al., 2012). Thus, the eIF5-eIF2 complex contains the largest part of cytoplasmic eIF2. Before the eIF2 complex can be reused for another round of translation initiation, eIF2γ must be recharged with GTP. The dissociation rate of GDP from eIF2 is fairly slow in yeast, at 0.1 x min^{-1}, and even slower in mammals, at 0.005 x min^{-1} (Jennings and Pavitt, 2010). For this reason, eIF2, like many other GTPases, requires a GEF for efficient GDP release. In yeast, eIF5 stabilizes eIF2-GDP even more, making it a guanosine dissociation inhibitor (GDI). In mammals, no such effect could be found (Sokabe et al., 2012). eIF2B, the GEF of eIF2, must displace eIF5 to catalyze release of GDP.

eIF2B is a decameric complex, consisting of the five different subunits α-ε that assemble into a di-pentamer which contains two molecules of each subunit. Each pentamer can be further divided into the catalytic eIF2Bγε and the regulatory eIF2Bαβδ subcomplexes. The CTDs of both eIF5 and eIF2Bε interact with eIF2β (see section 1.1.3.1 for eIF2 structure). For eIF2B's GDI displacement factor (GDF) activity, its γ-subunit, encoded by the *GCD1* gene in *S. cerevisiae*, must act together with the ε-subunit (Jennings and Pavitt, 2014). The ε-subunit contains the GEF domain at its C-terminus and possesses weak GEF activity on its own. The eIF2Bγε subcomplex can exert full GDF and GEF activity in vitro. eIF2 has an affinity for GDP that is 100 times higher than that for GTP. As the ratio of GDP to GTP concentration in the cytoplasm is roughly 1:10, the ratio between eIF2 • GDP to eIF2 • GTP would be 10:1. eIF2B lowers the affinity of eIF2 to the G-nucleotide by a factor of 100 to help reaching the equilibrium quickly. Release of eIF2B from eIF2 is coupled with binding of $tRNA_i$ to eIF2, which can only take place when GTP, not GDP, is bound to eIF2γ. The coupling of GDP release with TC formation dramatically shifts the equilibrium towards GTP binding and the final eIF2 • GDP to TC ratio is at around 1:1 (Bogorad et al., 2018). As of today, it is thought that eIF2B exerts an allosteric effect on eIF2 to destabilize GDP binding.

1.1.4 eIF2B regulation and integrated stress response

The integrated stress response is one of the best studied mechanisms of translational control. The α-subunit of eIF2 is phosphorylated at serine 51 and turned into an inhibitor of eIF2B. In *S. cerevisiae*, Gcn2 is the only such kinase and is activated in response to amino acid starvation. Mammals possess three additional kinases that respond to different stressors but all phosphorylate eIF2α serine 51, too. Specifically, ER stress, caused by misfolded proteins, activates PERK, dsRNA, which is a sign of viral infection, activates PKR and lack of heme, high concentrations of heavy metals or heat shock activate HRI (Holcik and Sonenberg, 2005). The response to eIF2α phosphorylation is dependent on the regulatory eIF2B subunits α, β and δ. In the current model of eIF2B inhibition, eIF2α-P, in complex with eIF2γβ, binds eIF2Bα, β and δ tightly and prevents interaction of eIF2Bε with eIF2γ. This also prevents interaction of non-phosphorylated eIF2 • GDP complexes with the same eIF2B and limits the pool of active eIF2B in the cytoplasm (Dever et al., 2016). Additionally, some evidence indicates that $tRNA_i$ competes with eIF2B for the same binding site on eIF2α and the altered structure of eIF2α-P inhibits the binding of $tRNA_i$ and thus the dissociation of eIF2B (Gordiyenko et al., 2019). As more and more TC is used in translation initiation but eIF2 • GDP complexes are not sufficiently recycled, the cellular TC concentration decreases. This causes the global rate of translation initiation and protein synthesis to drop significantly. Lower protein synthesis saves energy and amino acids, which is important when the cell lacks nutrients, and slows down the replication rate of viruses during a viral infection. In the case of heat shock or an excess of misfolded proteins, the cell is given time and resources to resolve the issue. Paradoxically, some mRNAs are translated at much higher rates under these conditions. One of the most prominent examples is *GCN4* in yeast, or its homolog *ATF4* in mammals. The *GCN4* mRNA possesses four uORFs in front of the *GCN4* coding ORF. Translation is mostly initiated at the start codon of uORF1, as it is the ORF closest to the 5' end. It encodes a peptide of only 3 amino acids. Shortly after initiation, translation is

terminated and in ~50% of cases, eIFs needed for scanning are still attached, allowing the ribosome to resume scanning.

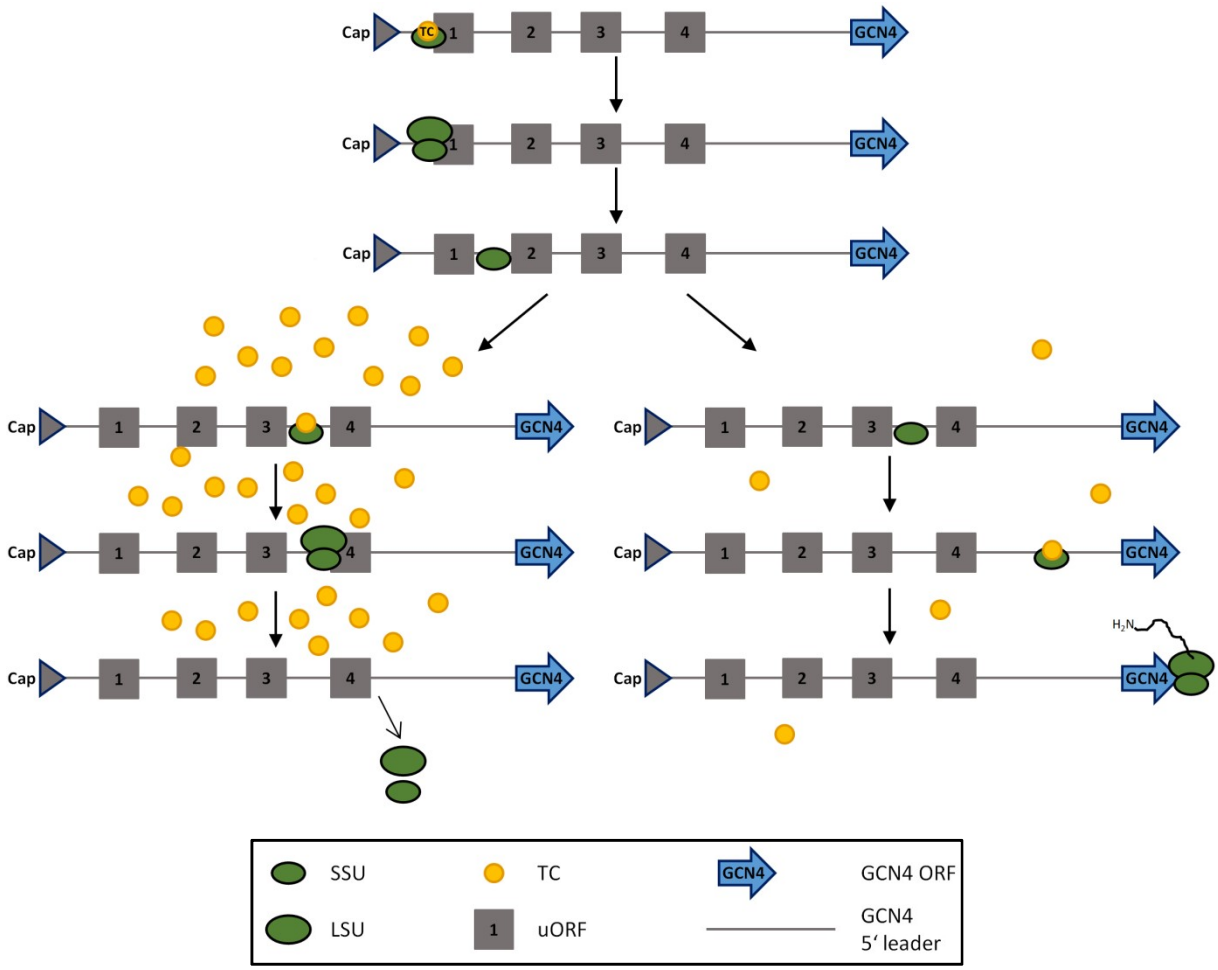

Figure 6: Translational regulation of GCN4 expression. Translation of the GCN4 mRNA initially starts at the AUG start codon of uORF1. After termination, a proportion of 40S ribosomes retain initiation factors eIF3 and eIF4 and resume to mRNA scanning. Abundant TC (left side) leads to reinitiation at one of the downstream uORFs (2-4) and dissociation of the ribosome from the transcript. If TC concentration is low (right side), the scanning 40S subunit often does not acquire a new TC before scanning past the last uORF and reinitiates at the GCN4 ORF more frequently.

For reinitiation, a new TC must be acquired by the scanning ribosome. Under optimal growth conditions, TCs are abundant and reinitiation takes place at one of the downstream uORFs 2-4. Termination at these uORFs leads to dissociation of the ribosome from the mRNA, likely due to interaction of the GC-rich environment of their stop codons with ribosomal RNA (Hinnebusch, 2005). When TC levels are decreased due to eIF2α phosphorylation, about half of the scanning ribosomes acquire a new TC only after passing uORF4 (see figure 6). Translation is then initiated at the start codon of the *GCN4* ORF. The *GCN4* gene product is a transcription factor that regulates the expression of a variety of genes, most of which are involved in amino acid synthesis.

In rapidly dividing yeast cells, a large proportion of eIF2B is not diffusely localized in the cytoplasm like other translation initiation factors, but forms higher order structures. These so called eIF2B bodies seem to be the most active pool of eIF2B. Photobleaching assays showed

that its substrate eIF2 can move into and out of those bodies, but events that reduce translation activity also reduce the movement of eIF2 into the eIF2B bodies (Campbell et al., 2005).

1.2 Cell cycle in *S. cerevisiae*

The cell cycle has been extensively studied in budding yeast and the fission yeast *Schizosaccharomyces pombe* (*S. pombe*). While its regulation is simpler in yeasts than in mammals, many mechanisms and individual proteins are conserved (Alberts, 2004). Studying the cell cycle in yeast has greatly helped understanding the fundamentals of the eukaryotic cell cycle in general (Lee and Nurse, 1988).

1.2.1 Cell cycle progression

Cell cycle in *S. cerevisiae*, as in other eukaryotic species, can be subdivided into four phases (figure 7): G1, S, G2 and M phase. In early G1 (gap phase 1), cells mostly grow in size to prepare the ground for cell cycle entry. In late G1, final preparations take place: The budding site is defined by an increase of cytoskeletal regulators at the site (Howell and Lew, 2012) and the chromosomal origins of replication are licensed by assembly of pre-replication complexes on the DNA (Diffley, 2004). If pro-mitotic signals outweigh anti-mitotic signals, the cells enter S-Phase (synthesis phase). The cells start forming a bud that will later become the daughter cell. They replicate their genome and the spindle pole body. These structures are the seeds of microtubule assembly, similar to centrosomes in higher eukaryotes. During G2 phase (gap phase 2), success and fidelity of DNA replication as well as other prerequisites for cell division are checked. G2 phase is relatively short in yeasts but longer in higher eukaryotes, likely due to the higher complexity of those organisms and larger genome size. In higher eukaryotes and some fungi, the transition from G2 phase to M phase is clearly defined by the breakdown of the nuclear envelope and condensation of the chromatin. Microtubuli attach to the centromers of the chromosomes and align them in the equatorial plane. The budding yeast *S. cerevisiae*, as many other simple eukaryotes, undergoes a closed mitosis, where the nuclear membrane remains intact. M-phase (mitosis) marks the separation of mother cell and daughter cell nuclei. This process is again subdivided into four mitotic phases and ends with cytokinesis. In Prophase, the chromosomes condensate and the spindle poles attach to opposite sides of the replicated chromosomes. In metaphase, motor proteins, attached to the spindle apparatus, pull the chromosomes towards opposing poles of the daughter and mother cell. At the transition of metaphase to anaphase, controlled by the mitotic spindle checkpoint, the tension increases and as soon as the cell passes the checkpoint, the sister chromatids are segregated 1:1 between mother and daughter cells (Marston, 2014). The daughter cell also receives proteins, mitochondria, ribosomes and one spindle pole from the mother cell. Finally, the daughter cell is separated by contraction of the bud neck and remodeling of the cell wall during cytokinesis (Howell and Lew, 2012). Both cells then undergo G1 phase again to grow in size and prepare for another cell division.

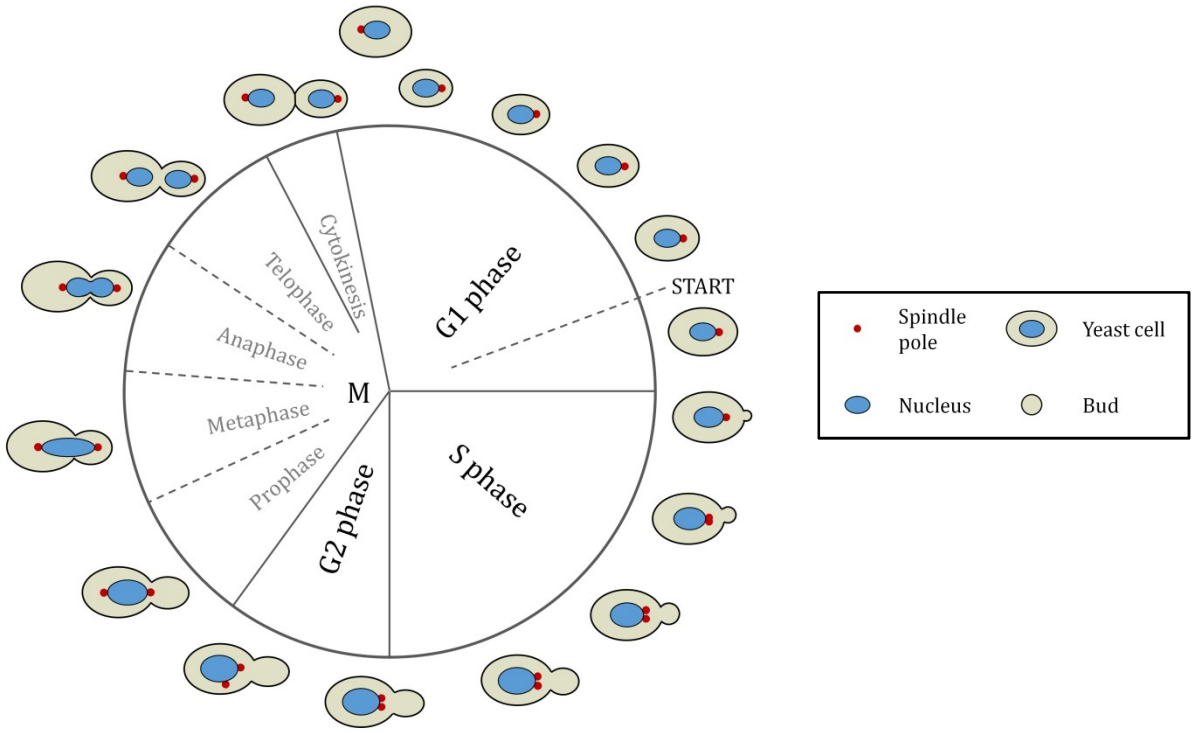

Figure 7: Schematic overview of cell cycle in *S. cerevisiae*. During G1 phase, the cell grows and increases its biosynthetic capacity in preparation for cell division. In late G1, the cell passes the START point and is determined to go through mitosis. After some last preparations, e.g. bud site selection and licensing of origins of replication, the cell enters S phase. During this phase, genomic DNA and spindle poles are replicated. Fidelity of DNA replication and general preparedness for mitosis are checked in G2 phase. In M phase, the genetic material and spindle poles are distributed equally between mother and daughter cell. Proteins, ribosomes and organelles are distributed asymmetrically. At the end of mitosis, the bud neck contracts and the daughter cell is separated completely in cytokinesis. Figure inspired by figures from Humphrey et al., Perzlmaier (Humphrey and Pearce, 2005; Perzlmaier, 2012).

1.2.2 Regulatory mechanisms in cell cycle

Cell division is highly regulated, as cells are particularly vulnerable to environmental conditions and unresolved problems in their cellular biochemistry during that phase. In G1, multiple signaling pathways engage in a tug-of-war to decide whether to enter S-phase or not. The step at which cells decide to divide is usually called “START” in yeast cells and “restriction point” in higher eukaryotes. Entry into S phase is the most tightly controlled step in cell cycle, as it is irreversible and cells are determined to go through mitosis regardless of changes in conditions, once they have passed START. In yeast, pro-mitotic signals are high availability of nutrients and large cell size. Negative signaling is triggered by nutrient deprivation, pheromone sensing, small cell size, DNA damage and other stress signals (Longhese et al., 1998; Newcomb et al., 2003).

In the 1970s, many cell cycle genes were identified by Hartwell et al. They randomly mutagenized yeasts to create temperature sensitive strains that arrested in different stages of the cell cycle at a restrictive temperature (Hartwell et al., 1974). Subsequent identification of the affected genes led to the discovery of genes that were important at certain stages of the cell cycle. Some of the discovered key regulators are a group of proteins known as cyclin dependent kinases (CDKs). CDKs drive cell cycle by phosphorylation of many proteins that have a function

in cell cycle. Depending on the substrate, those phosphorylations can have an activating or inhibiting effect, dissolve protein complexes or target proteins for proteasomal degradation. Following phosphorylation, some targets are recognized by large SCF and APC/C complexes (Cardozo and Pagano, 2004; Yamano, 2019). SCF is named after Skp1, Cullin and F-box proteins, which are part of the complex. It contains ubiquitin ligases, which attach ubiquitin chains to targets, various other proteins and a substrate-defining F-box protein. Polyubiquitinated proteins are recognized by proteasomes and quickly degraded. The anaphase promoting complex, or cyclosome (APC/C), works in a similar fashion, but its main function is control of the mitotic spindle checkpoint.

While the expression of CDKs is relatively stable throughout the cell cycle, their activity is dependent on complex formation with Cyclins. Cyclins are named after the periodic increase and decrease of their cellular concentrations during cell cycle and each cell cycle phase has a characteristic profile of cyclin expression (Evans et al., 1983). They regulate the activity and expression of various proteins to drive cell cycle in the intended direction. Cdk1, also known as Cdc28, is a key regulator of cell cycle in yeast. It associates with G1, S, and G2/M cyclins that define its substrate specificity and activity. In total, six CDKs exist in *S. cerevisiae*, but Cdk1 is the only essential one and sufficient to promote cell cycle progression. Owing to the higher complexity of their cell cycle regulation, many more CDKs exist in mammals, including three homologs of yeast Cdk1, which can all complement temperature-sensitive mutants in yeast. Cdk1 is a serine/threonine kinase that recognizes over 70 substrates with the consensus sequence S/T-P-X-K/R. In many of those substrates, multiple phosphorylation sites are located in unstructured, non-conserved regions (Enserink and Kolodner, 2010).

Besides cyclins, CDK activating kinases (CAKs) and CDK inhibitors (CKI) regulate the activity of CDKs. CDKs are completely inactive without cyclins, because a flexible, so-called T-loop blocks their active center and many amino acid side chains in the active center are poorly positioned. CDK activating kinase 1 phosphorylates a threonine inside Cdk1's T-loop to facilitate cyclin binding. Only after cyclin binding, Cdk1 is phosphorylated multiple times for full activity (Enserink and Kolodner, 2010). Cdk1 activity is low in early G1 due to low cyclin concentrations, and increases in late G1, as cyclin 3 expression increases. Cyclin 3 is highly unstable and its cellular concentration is almost proportional to its synthesis rate (Tyers et al., 1992). In S, G2 and M-phase, different cyclins are expressed and degraded to adjust Cdk1 activity. Cyclin degradation and CKI reexpression in anaphase once again decrease its activity as the cell exits mitosis.

1.2.3 Cell cycle entry

Cln-Cdk1 complexes target various proteins and protein complexes during cell cycle to overcome inhibitory checkpoints and to activate the expression of genes needed for cell cycle progression. The CKIs Sic1 and Far1 are expressed between M/G1 and G1/S phases and inhibit Cln-Cdk1 complexes. Conversely, active Cln-Cdk1 complexes can phosphorylate Sic1 and Far1 to target them for degradation by SCF^{Cdc4} (Haase and Wittenberg, 2014). Thus, a steady increase of active Cln-Cdk complexes does not lead to slow progression through the cell cycle, but to rapid, switch-like transitions. Far1 inhibits Cln3-Cdk1 complexes throughout G1. As the amount of

Cln3-Cdk1 complexes surpasses the inhibitory capacity of Far1, pro-mitotic Cln3-Cdk1 wins the upper hand, resulting in sudden degradation of Far1 and rapid derepression of remaining inactive Cln3-Cdk1 complexes.

Expression of S-phase specific genes depends on the two transcription factors MBF and SBF. They are bound to the promoters of genes involved in DNA replication and cell cycle progression. SBF is a heterodimer of Swi4 and Swi6 whereas MBF contains Mbp1 and Swi6. Whi5, the functional homolog of retinoblastoma protein (Rb), a suppressor of cell cycle entry and tumor suppressor in higher eukaryotes, forms a complex with SBF to repress its pro-transcriptional activity.

An interesting finding has been that cellular concentration of Cln3 is stable throughout G1 and its activity relative to cell size remains at the same level before START. Whi5, however, is synthesized during G2-, S- and M-phase in a size-independent manner and thus reaches its highest concentration in small, newborn cells in early G1. Its dilution during cell growth in G1 gradually shifts the balance towards relatively higher Cln3 activity. Phosphorylation of Whi5 by Cln3-Cdk1 leads to its dissociation from SBF and expression of SBF target genes. This form of size-dependent cell cycle entry ensures that cells possess a sufficient protein synthesis capacity and organelle activity to go through mitosis successfully (Schmoller et al., 2015). Others have proposed constant Whi5 concentrations, but rapidly increasing Cln3 concentrations shortly before START due to increased glycolytic flux and protein synthesis as the primary mechanism for passing START (Dorsey et al., 2018; Litsios et al., 2019). The general requirement of a high enough biosynthetic capacity for cell cycle entry is uncontroversial. Cells that are subjected to increasing doses of cycloheximide, which blocks the translocation step in 80S ribosomes, demonstrated increasingly prolonged G1-phase and larger sizes (reviewed in Polymenis and Aramayo, 2015).

SBF target genes include Cln1 and Cln2, which form complexes with Cdk1. These complexes, like Cln3-Cdk1, phosphorylate Whi5, which further decreases nuclear Whi5 concentration. The positive feedback loop activates SBF/MBF even more and the cells irreversibly pass START. The mechanism of Cln3-Cdk1-mediated MBF activation is not exactly known but could be similar to that observed in SBF regulation. MBF activates the expression of S-phase cyclins Clb5/6. Their complexes with Cdk1 are inhibited by Sic1 at first, but overcome inhibition by the same mechanism as Cln3-Cdk1 complexes. Clb5/6-Cdk1 complexes then promote DNA replication and finalize entry into S phase. Their activity is also needed for assembly of the mitotic spindle (Schwob and Nasmyth, 1993).

1.3 Aim of this work

Translation initiation is a field in cellular biology that has been studied in great detail by numerous scientists. Over the last four decades, more and more detailed knowledge on how mRNAs are recognized, scanned and translated into proteins has been accumulated. Advances in structural biology have paved the way for a mechanistic understanding of translation. Some of the greatest successes include crystalization of entire ribosomes (Ben-Shem et al., 2010) or the deciphering of the mRNA scanning mechanism (Hinnebusch, 2017). Recently, the structure of

eIF2-eIF2B complexes has been published in several papers and revealed interesting details about the mechanism of GDP exchange and its inhibition by eIF2α phosphorylation (Anand et al., 2018; Gordiyenko et al., 2019; Kashiwagi et al., 2019). Yet, a relatively low number of publications focus on eIF2 and its interesting assembly mechanism: Unlike most protein complexes of its size, the trimeric eIF2 complex requires a dedicated assembly factor or chaperone, called Cdc123, for assembly.

This thesis is intended to increase the understanding of eIF2 assembly, with a focus on the individual roles of each subunit and Cdc123. In biochemical assays, a variety of mutated eIF2 subunits were used to define assembly intermediates and get a better understanding of the subunit interactions that take place during assembly. Based on the obtained data, a refined model for stepwise assembly of eIF2 by Cdc123 will be presented. Some experimental results indicated a possible intramolecular self-interaction of the γ-subunit that is influenced by Cdc123; thus, the special role of the eIF2γ-Cdc123 interaction was another focus of this work. Finally, defective eIF2 assembly and its consequences for cellular development were investigated.

Since the central protein of eIF2, the γ-subunit, is notoriously hard to express in *E. coli*, the proteins were studied in their natural hosts, i.e. *S. cerevisiae* and the human HEK cell line. In addition, the human proteins were expressed and studied in yeast cells. The majority of results were obtained by protein biochemistry methods, complemented with genetic assays, flow cytometric cell cycle profiling and live-cell microscopy. In order to create a starting point for future studies, new potential interaction partners of Cdc123 in human cells and yeast were identified using mass spectrometry.

2 Results

2.1 Stepwise assembly of eIF2 by Cdc123

This part of the thesis focuses on developing a new, more detailed model for stepwise eIF2 assembly by the eIF2 chaperone Cdc123. Most experiments were conducted in *S. cerevisiae*, but some of the most important findings were replicated and verified in human cell culture, using a modified cell line based on HEK-293T.

2.1.1 Integrity of the eIF2γ N-terminus is necessary for eIF2 assembly

Due to its poor expression in *E. coli*, full length Gcd11 is inaccessible to in-vitro analysis; structural information on the trimeric eIF2 complex and subunit interaction platforms are therefore derived from studies on the homologous archaeal IF2 complex (see section 1.1.3.1). In yeast, eIF2γ (Gcd11) has a non-conserved N-terminal tail (NTT). Domain 1, also known as G-domain, binds GTP and contains the active center for GTP hydrolysis. The contact to eIF2β is mostly made via the C-terminal part of domain 1; eIF2α is contacted via domain 2 and Cdc123 by domain 3. Successive N-terminal truncation of Gcd11 was used to find the essential core of eIF2 that is needed for assembly. Gcd11 has a total length of 527 amino acids. Different truncated variants of Gcd11 were conditionally expressed in yeast cells under control of the galactose-inducible *GAL1* promoter (p*GAL1*, see table 26) in addition to the yeasts' endogenous Gcd11. The longest truncated protein, starting at AA 61, had only its yeast-specific NTT removed, whereas the shortest variant, Gcd11(410-527) contained only domain 3. Controls with full-length Gcd11 and a strain with no additional Gcd11 were included. Each protein was tagged with N-terminal 3xFLAG peptide (->^{FLAG}Gcd11) for FLAG-immunoprecipitation (detailed description of cell lysis, protein sample preparation and IP in section 5.5). Yeast cells were grown overnight in XY medium with raffinose as a carbon and energy source (XY-R), and induced for two hours with 2% galactose (XY-RG) to express their respective variant of Gcd11. Yeasts were lyzed mechanically and lysates were incubated with αFLAG agarose beads to pull down ^{FLAG}Gcd11. After elution with hot Laemmli sample buffer (LSB), samples were analyzed via Western Blot to detect Sui2, Sui3 and Cdc123; by visual quantification of the co-precipitated binding partners, the capacity of each Gcd11 variant to assemble into eIF2 could was analyzed. All antibodies that were used for this experiment and all following experiments are listed in table 4.3.1. The results are shown in figure 8. Removal of the non-conserved NTT did not have any significant effect on co-precipitation of Sui2, Sui3 and Cdc123. A very mild effect on binding of Sui2 was detected when up to 81 AAs were removed, which indicates that this part of Gcd11 is dispensable for eIF2 assembly. A drastic reduction of eIF2γ-α and γ-β complexes was observed when at least 91 AAs were missing. There is no evidence for a direct involvement of these amino acids in eIF2α and –β binding, so the likely reason for loss of binding is a structural defect of domain 1. The drastic effect not only on binding of eIF2β, but also eIF2α, is not entirely clear, but could point towards dependency of eIF2α binding on eIF2β (which is unlikely, as will be shown in part 2.1.2) or interdomain communication in eIF2γ. Some residual Sui2 binding was maintained in the versions up to 310-527, whereas for Sui3 binding the entire G-domain was required. These observations conform to the subunit binding platforms found in archaea (Sokabe et al., 2006; Yatime et al., 2005). For Cdc123 binding, domain 3 alone was sufficient. Strikingly, the two shortest Gcd11 variants coprecipitated higher amounts of Cdc123. It seems that these variants

are less capable of releasing Cdc123, despite interactions with Sui2 and Sui3 not being fundamentally different in variant 310-527 compared to 201-527. Interdomain communication as a requirement for Cdc123 release and lack thereof in variant 310-527, must be considered as as a possible explanation.

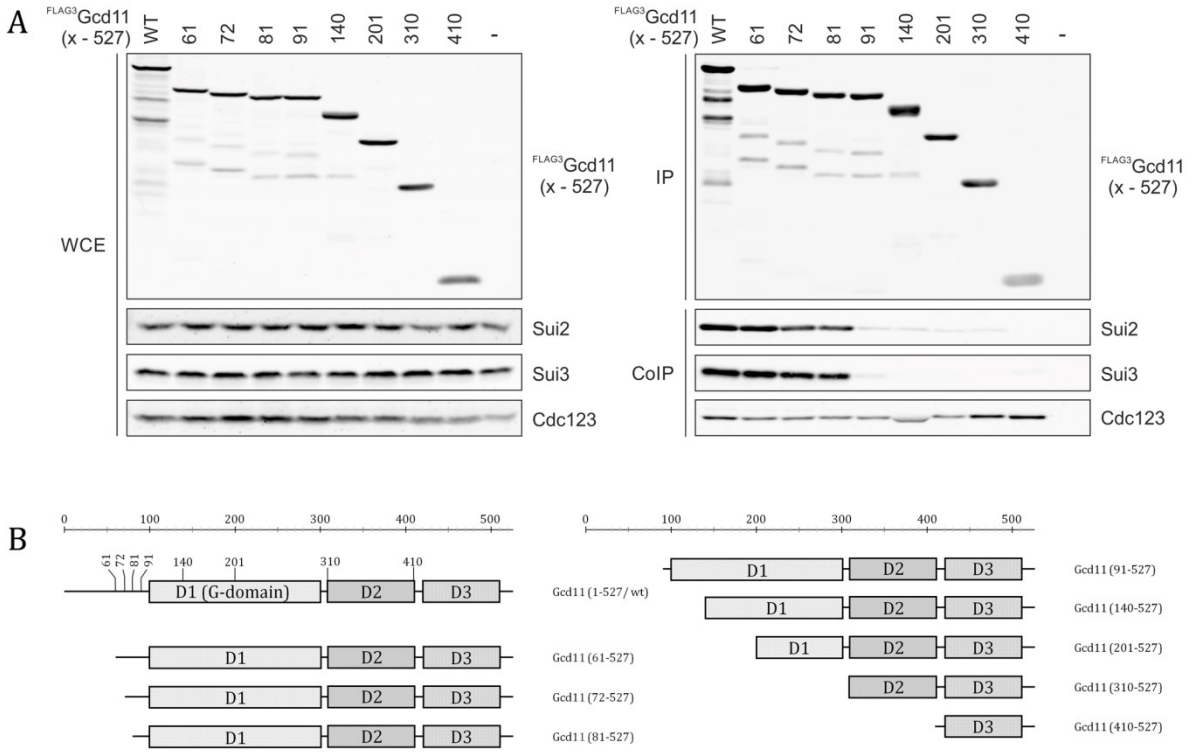

Figure 8: N-terminal truncation of Gcd11 and its effect on eIF2 assembly. A: FLAG-tagged, successively truncated variants of Gcd11 were analyzed for their capability to form eIF2 complex via Co-IP and Western Blot. On the left side, whole cell extracts (WCE) are depicted; the right side shows precipitated FLAGGcd11 and coprecipitated Sui2, Sui3 and Cdc123. The respective variants of FLAGGcd11 in each sample are indicated on top of the figure (x-527), x being the starting amino acid, shown on top of each lane. Each box is annotated with the protein that was detected. Strains: K700, W15011, W14924, W15009, W15010, W14925, W14926, W14927, W14928, W14929. **B:** Schematic representation of each Gcd11 variant. Structured domains are shown as boxes, non-conserved tails and spacers are shown as lines. The scale on top shows amino acid positions.

2.1.2 Binding of eIF2α and –β to eIF2γ require Cdc123, but are independent of each other

Defects in eIF2 are lethal in yeast, as demonstrated by the inviability of eIF2 subunit and Cdc123 null mutants. Deletion of *CDC123*, however, can be rescued by combined overexpression of eIF2γ and eIF2α. Together with the previous finding from this work, that binding of eIF2α and –β, upon N-terminal truncation, were lost in concert, this seems to indicate an interdependency of the two subunits in binding to eIF2γ. In order to unravel such potential dependencies, point mutations were introduced into Gcd11 by site-directed mutagenesis (QuikChange protocol, section 5.1.1.2). According to structural data from archaea, these point mutations should disturb interaction with Sui2 or Sui3, respectively. To create a Sui2 binding mutant, the AA exchange

D403R was introduced, which reverses polarity of the affected AA side chain and should strongly repulse Sui2. The homologous AA in *S. solfataricus* aIF2γ, D301, interacts with aIF2α (Yatime et al., 2006). A conserved valine residue at pos. 281 was mutated to disturb interaction with Sui3. The homologous amino acid in humans, I222, was implicated in a form of X-linked intellectual deficiency (XLID) and its mutation to threonine impairs eIF2β binding; the respective AA in *P. furiosus* aIF2γ, I178, was identified as an AA involved in aIF2β binding (Borck et al., 2012; Sokabe et al., 2006). Again, the amino acid was mutated to arginine (V281R) to maximize the effect. The proteins, together with known Cdc123 binding mutant Gcd11(1-514) were expressed with N-terminal 3xFLAG tags from exogenous constructs, but under control of p*GCD11* (for details on promoters, see table 26) to achieve expression levels similar to endogenous Gcd11. As before, Co-IPs were performed and Sui2, Sui3 and Cdc123 were detected in Western Blots.

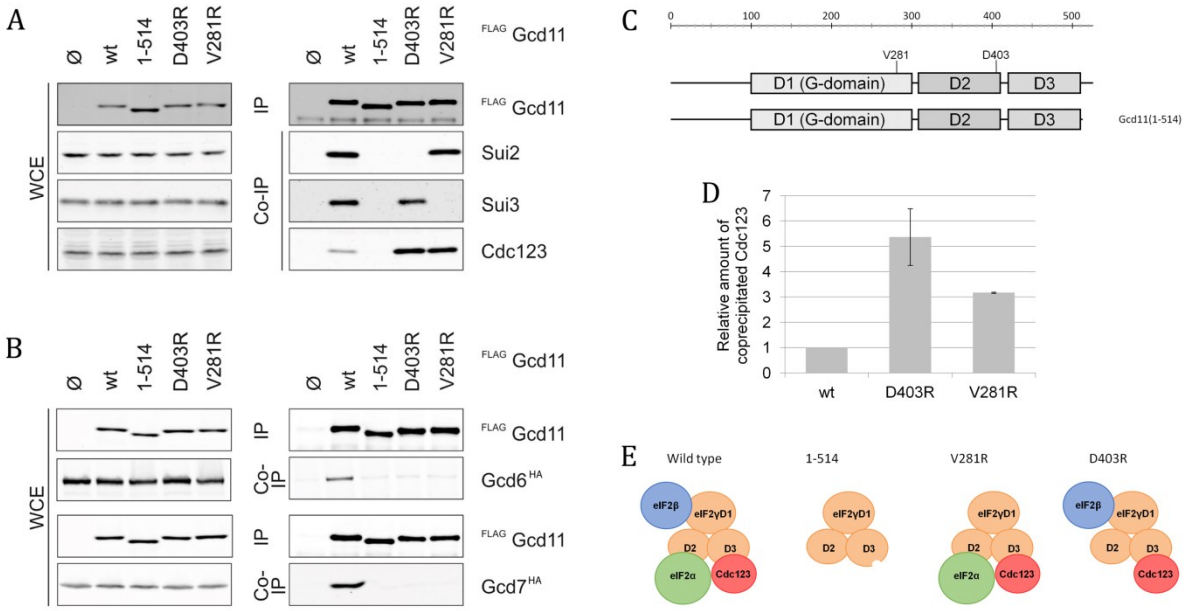

Figure 9: Effects of selective eIF2α/ eIF2β binding mutants on eIF2 assembly. A: Immunoprecipitation of mutated ^{FLAG}Gcd11 and detection of coprecipitated Sui2, Sui3, Cdc123. The respective Gcd11 variant in each sample is indicated on top of the figure. Strains: W12626, W12783, W15419, W15558, W15416. **B:** Yeast strains used in figure A were cross bread against strains with endogenously tagged Gcd6/7. Coprecipitation was analyzed by Western Blotting. Strains in top two panels: W15500, W15512, W15506, W15771, W15503. Starins in bottom two panels: W15501, W15513, W15507, W15772, W15504. **C:** Schematic representation of the Gcd11 variants. The scale on top indicates amino acid positions. **D:** Quantification of coprecipitated Cdc123 for wild type Gcd11 and mutants D403R, V281R. **E:** Schematic model of eIF2 assembly intermediates found in each sample.

The Cdc123 binding mutant Gcd11(1-514), unsurprisingly, was unable to bind either Sui2 or Sui3. However, the Gcd11 variants D403R and V281R, while being completely unable to bind Sui2 and Sui3, respectively, retained their ability to bind the respective other subunit (figure 9A, B). A reproducible, slight decrease of Sui3 binding was found for Gcd11(D403R), but overall, evidence clearly shows relative independence of eIF2α and eIF2β binding. Similar to the N-terminally truncated Gcd11 variants 310-527 and 410-527, the Sui2 and Sui3 binding mutants were able to coprecipitate more Cdc123 than the wild type protein. The extent of the effect was

quantified in triplicates. The signal from coprecipitated Cdc123 was normalized on precipitated ^{FLAG}Gcd11 and compared to the wild type protein (figure 9D; for raw data, see table S1). A five-fold increase for D403R, and a three-fold increase for V281R in terms of complex formation with Cdc123 was found. Since the same effect was observed in different Gcd11 assembly mutants, a common cause, namely accumulation of Cdc123-containing assembly intermediates, seems likely.

From our current understanding of eIF2-eIF2B interaction, one can infer that partially assembled eIF2 is unlikely to have a robust interaction with eIF2B, since all eIF2 subunits form contacts with eIF2B subunits in vivo (Gordiyenko et al., 2019). To confirm this, the yeast strains were cross-bred with other strains in which the endogenous copies of Gcd6 or Gcd7 (ε- and β-subunits of eIF2B in *S. cerevisiae*) were C-terminally tagged with 3xHA peptide. Co-IPs were performed for these new strains and Gcd6/7 were detected in IP eluates. As expected, only wild type Gcd11 precipitated Gcd6 and Gcd7 (figure 9B).

2.1.3 Quantification of Cdc123-eIF2 subunit interaction

A necessary step in elucidating the order of eIF2 assembly is the quantification of naturally occurring eIF2 assembly intermediates. This excludes the use of overexpression constructs and tags that alter protein function. Thus, yeast strains with endogenously N-terminally 3xFLAG-tagged eIF2 subunits were used. Use of the same epitope for each protein allows detection with the same antibody, enabling comparative protein quantification via Western Blot. Previously, polyclonal sera against each protein had been used to verify natural expression levels and incorporation into eIF2 complexes (data by Lea Neumann-Arnold). Then, a monoclonal αFLAG antibody (M2 by Sigma) was used to quantify eIF2 subunits in a Co-IP experiment. Coprecipitation of Cdc123 was quantified with an αCdc123 serum. For each sample, the amount of Cdc123 was measured in relation to precipitated eIF2 subunits. The quantification was performed in triplicates. One of the Western Blots (WBs) is shown in figure 10A. As expected, Gcd11 precipitated the highest amount of Cdc123, as it is the primary interaction partner of Cdc123. A lower amount of complexes containing eIF2β was detected (~20% relative to eIF2γ-Cdc123 complexes), and significantly fewer complexes containing Sui2 (<5%, see figure 10B; for raw data, see table S2).

Next, the experimental setup was reversed and a strain with endogenously tagged Cdc123, with a 3xFLAG tag at its C-terminus, was used to quantify the amounts of coprecipitated Sui2, Sui3 and Gcd11 relative to precipitated Cdc123^{FLAG}. Sui2 was 13xMYC-tagged in anticipation of the weak expected signal. Again, the experiment was replicated three times. This time, the enrichment of each coprecipitated protein in the IP eluates in comparison to whole cell extracts (WCEs) was compared between samples and Gcd11 was set to 100%. As previously, the strongest interaction could be detected for the pair Cdc123-Gcd11 (100%). A weaker interaction was found for Cdc123-eIF2β (40%) and less yet for Cdc123-eIF2α (<5%), confirming the findings from the first experiment (figures 10C, D; for raw data, see table S3).

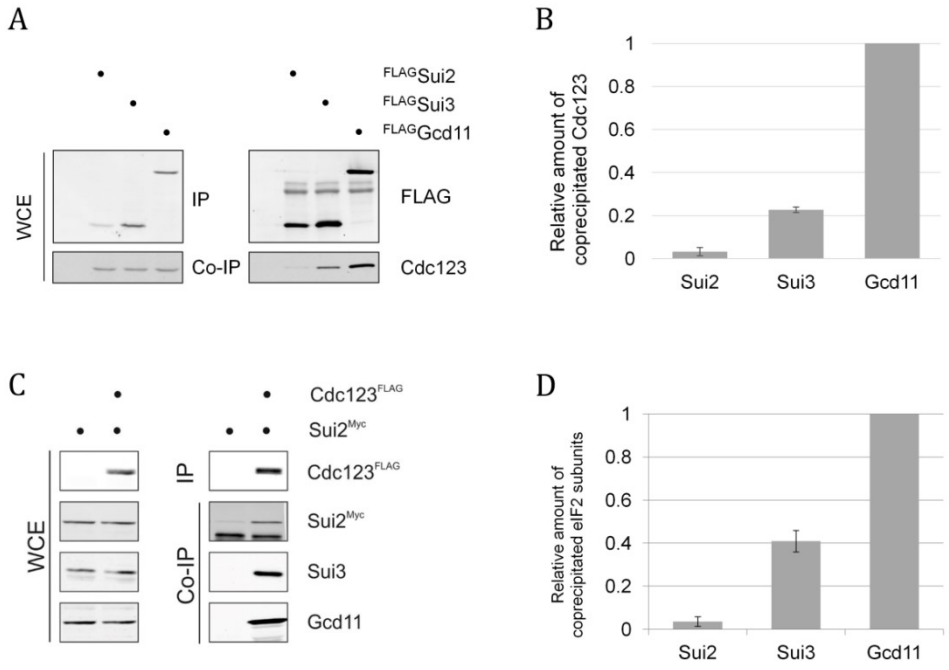

Figure 10: Quantification of Cdc123-eIF2 subunit interactions. A: Co-Immunoprecipitation of Cdc123 with FLAG-tagged eIF2 subunits. Indicated on top is the FLAG-tagged eIF2 subunit in each sample. Strains: W10953, W15228, W15230, W15232. **B:** Quantitative analysis of Cdc123 binding to eIF2 subunits. **C:** Co-Immunoprecipitation of eIF2 subunits with Cdc123^{FLAG}. The presence of Cdc123^{FLAG} and Sui2^{MYC} is indicated for each sample. Strains: W9878, W14424 **D:** Quantitative analysis of eIF2 subunit binding to Cdc123. Enrichment of each prey protein in IP samples over WCEs was used as a proxy for complex abundance.

2.1.4 eIF2α binds Cdc123 directly, but eIF2β does not

The quantification of eIF2 assembly intermediates had revealed that a high amount of eIF2γ-Cdc123, a moderate amount of complexes with eIF2β and Cdc123 and a very small amount of complexes with eIF2α and Cdc123 could be purified from growing yeast cells. Gcd11 is the primary interaction partner for Cdc123 and binds all three interaction partners directly during assembly. Direct interactions between eIF2α or –β with Cdc123 have not been established yet but could explain the differing amounts of assembly intermediates. To test whether eIF2α and -β establish direct contacts to Cdc123 during eIF2 assembly, mutants were created that cannot bind Gcd11. If no direct contact occurs in the cell and eIF2α/β are connected to Cdc123 only through Gcd11, loss of interaction with Gcd11 would also abolish binding of Cdc123. If, however, Cdc123 binding could be detected despite lack of Gcd11 interaction, the binding of Cdc123 would have to be direct.

First, two mutants of Sui3 were created where conserved amino acids, whose archaeal homologs were known to interact with aIF2γ, were exchanged (Sokabe et al., 2006). This resulted in the two double mutants Sui3(Y131A, S132A) and Sui3(L134R, L135R), in the following text referred to as YS/AA and LL/RR. The Sui3 variants were expressed with N-Terminal 3xFLAG tags and dependent on the repressible p*GAL1*, because overexpression of Sui3, and Sui3 mutants in particular, had been demonstrated to be toxic for yeast cells before. Co-IPs were performed to investigate binding of Gcd11, Sui2 and Cdc123. Both Sui3 variants were unable to bind Gcd11,

which confirms the high conservation of IF2 structure throughout living organisms. In addition, no measurable amounts of Cdc123 and Sui2 could be detected in IP eluates (figure 11A). Thus, no Sui3-Sui2 and Sui3-Cdc123 complexes were pulled down from yeast cell lysates which points to the indirect nature of those interactions. To rule out the possibility of a severe structural defect in the mutants that makes them completely nonfunctional, the yeast strains were cross-bred against a strain with endogenously, C-terminally 13xMYC tagged Tif5. In yeast, Tif5 is synonymous with eIF5. Being a known interaction partner for eIF2β, Tif5 should interact with Sui3 independently of Gcd11 and confirm the selectiveness of the Sui3 point mutations, if found in the IP eluates. Indeed, Tif5 interaction was not affected in the mutants Sui3(YS/AA) and Sui3(LL/RR), confirming their usefulness for the eIF2 assembly assay (figure 11A).

Next, Sui2 mutants were created accordingly (Yatime et al., 2006). The two mutants Sui2(L205E) and Sui2(V220E) were expressed from the strong, constitutive *TEF2* promoter (p*TEF2*, see table 26), with a 3xFLAG tag at their N-terminus. The constructs and a wild type Sui2 control were introduced into a yeast strain with C-terminally 3xMYC tagged endogenous Cdc123. The tag served to enhance signal strength. Co-IPs were performed and according to expectations, wild type Sui2, but none of the mutants were able to yield Gcd11 or Sui3 signals in the IP samples. This, again, confirms that no direct interaction between the α- and β-subunit takes place. For Cdc123, however, no decrease in signal strength could be observed, compared to wild type Sui2 (figure 11B); Sui2-Cdc123 binding thus must be independent of Gcd11. This is interesting for two reasons: First, complexes containing Sui2 and Cdc123 are significantly less abundant than complexes containing eIF2β and Cdc123. A possible explanation is that the interaction, while direct, is very short-lived. Maybe, eIF2 assembly is quickly completed and Cdc123 dissociates, once eIF2α joins the complex. Secondly, eIF2γ-α-Cdc123 does not seem to contribute significantly to the total amount of complexes containing eIF2α and Cdc123, which opens up the possibility for a function of binary eIF2α-Cdc123 complexes, as proposed in the assembly model by Young-Baird et al. (see section 1.1.3.3). The very low abundance of such complexes, however, is not consistent with that model.

Protein Sui2(L205E) migrated significantly slower than the other variants, which cannot be explained by the altered charge alone. An insertion, introduced during mutagenesis, can be ruled out because the gene was sequenced. One possible explanation could be a drastic change in 3D-structure that is not resolved by denaturation in hot LSB.

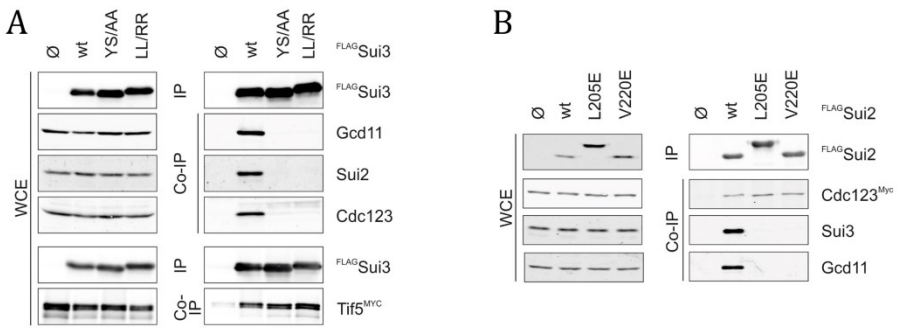

Figure 11: Characterization of Sui2-Cdc123 and Sui3-Cdc123 interactions. A: Immunoprecipitation of ^{FLAG}Sui3. The Sui3 variant in each probe is specified on top. Strains in top four panels: K700, W15193, W15428, W15429. Strains in bottom two panels: W15773, W15441, W15444, W15447. **B:** Immunoprecipitation of ^{FLAG}Sui2. The Sui2 variant in each sample is specified on top. Strains: W5077, W15714, W15720, W15723.

2.1.5 eIF2α binding is the rate-limiting step in eIF2 assembly

In the previous experiment, an interesting relationship between eIF2α and Cdc123 had been revealed. The direct, but seemingly short-lived interaction raises questions about the exact role of eIF2α in eIF2 assembly; possibly, it could compete with Cdc123 for eIF2γ and release the assembly factor once eIF2 assembly is completed. To test this hypothesis, a strain with endogenous Cdc123^{FLAG} was transformed with overexpression constructs of Sui2 and Sui3. Cdc123^{FLAG} was pulled down and the amount of coprecipitated Gcd11 was analyzed. With Sui2, but not Sui3 overexpression, the amount of Gcd11 was reduced, indicating a decrease in Cdc123-Gcd11 complexes (data by Franziska Wojciech). This experiment was taken further but using overexpressed wild type Sui2 and the mutated Sui2 variants L205E and V220E. Again, overexpression of wild type Sui2 caused a decrease of Cdc123-Gcd11 complexes, whereas the effect was absent in the mutants. Thus, a high abundance of Sui2 can speed up eIF2 assembly, as shown by the decrease in Cdc123 containing assembly intermediates (figure 12A). Sui2 can only exert this effect together with Gcd11; a mere sequestration of Cdc123, leading to a decrease of its binding to Gcd11, can be ruled out.

If an increase in Sui2 abundance increases the rate of eIF2 assembly, its decrease should slow the assembly down and lead to an increase of assembly intermediates. Cdc123^{FLAG} constructs were introduced into two diploid yeast strains, one of which possessed only one *SUI2* gene copy. The heterozygous deletion was expected to reduce Sui2 protein levels to about 50%. An IP of Cdc123^{FLAG} was carried out and Sui2, Sui3 and Gcd11 were detected using antisera. Indeed, the level of Sui2 in the heterozygous strain was markedly lower, at about 50% of the homozygous strain. Coprecipitation of Sui3 was significantly increased and a moderate increase was seen for Gcd11 (figure 12C), indicating an increase of eIF2γ-Cdc123 and eIF2γβ-Cdc123 complexes in the heterozygous strain. This, in turn, implies that eIF2 assembly occurs at a lower rate.

In conclusion, the data support a model in which the Cdc123-Gcd11 complex binds eIF2β first. Then, eIF2α binds, directly interacts with Cdc123 and quickly provokes its release from eIF2. In this model, the trimeric eIF2γβ-Cdc123 complex is relatively stable, until it encounters eIF2α. Upon its binding, eIF2 assembly is completed. Higher cellular concentrations of eIF2α speed up the assembly, because the average time until an eIF2α molecule contacts the eIF2γβ-Cdc123

complex is shorter. Accordingly, lower eIF2α concentrations have the opposite effect. However, it is entirely possible that the assembly does not always occur in this order. The collected data is compatible with a second pathway existing where eIF2γ-Cdc123 binds eIF2α first, Cdc123 is released and eIF2β completes the assembly.

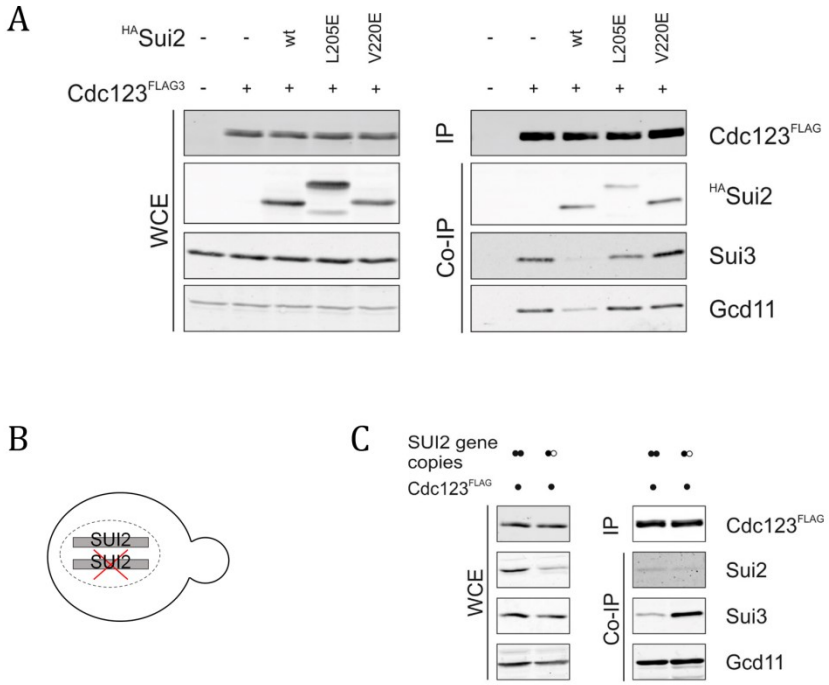

Figure 12: Role of eIF2α and new model for eIF2 assembly. A: p*GAL1* overexpression of different HA-tagged Sui2 variants in a strain with Cdc123^{FLAG}. Immunoprecipitation of Cdc123^{FLAG} and detection of ^{HA}Sui2, Sui3 and Gcd11. Presence of ^{HA}Sui2 variants and Cdc123^{FLAG} is indicated on top of the figure. Strains: K699, W14058, W15914, W15915, W15916. **B:** Schematic model of heterozygous Sui2 deletion in a diploid strain. **C:** IP of Cdc123^{FLAG} in a strain with heterozygous *SUI2* deletion and a homozygous strain with two copies as control. Presence of Cdc123^{FLAG} and the number of *SUI2* copies are indicated on top of the figure; black dots represent *SUI2* gene copies, empty dot represents gene deletion. Strains: W15910, W15911.

The investigation of aforementioned human eIF2γ variant 1-464SQQ* in human cells by Young-Baird et al. gave rise to an alternative model of eIF2 assembly. IP of eIF2α and eIF2β in normal cells and cells with the mutated EIF2S3 allele led to the observation, that a higher proportion of Cdc123-eIF2α and Cdc123-eIF2β complexes were present in the mutant cells. It was concluded that Cdc123 forms complexes with eIF2γβ and eIF2α. In the suggested model, the Cdc123 proteins would probably catalyze the formation of eIF2 by self-dimerization. The I->SQQ* mutation hinders the association of the two preassembly complexes, which leads to a higher proportion of assembly intermediates. Cdc123 dimers, however, have not been found so far, despite multiple attempts, including some from the Seufert lab. The existence of stable Cdc123-eIF2α dimers would also suggest that a significant amount of such complexes can be purified from living cells. However, experiments performed in this work found a vastly lower abundance of Cdc123-eIF2α complexes than Cdc123-eIF2γ complexes in both yeast and human cells (see sections 2.1.3, 2.1.7). It would be useful to determine the effect of eIF2γ overexpression on the abundance of Cdc123-eIF2α complexes. If Cdc123 occured in complex

with both proteins prior to completion of eIF2 assembly, one would expect a competition between the two eIF2 subunits for the assembly factor and thus a decrease in Cdc123-eIF2α complexes upon eIF2γ overexpression. To this end, yeast strains with endogenously FLAG-tagged Cdc123, MYC-tagged Sui2, and optionally, a Gcd11 overexpression construct were used in a Co-IP, with yeast strains lacking the FLAG-tagged Cdc123 as negative control. Unfortunatelly, visible bands for Sui2^{MYC} were visible in the negative control and the positive samples did not show significantly stronger signals that would justify a definitive answer (figure 13). An interesting piece of information that the experiment revealed was the fact that Gcd11 coprecipitation was not any higher in the Gcd11 overexpression strain, compared with the control, suggesting that most Cdc123 molecules are bound to Gcd11 at any given time.

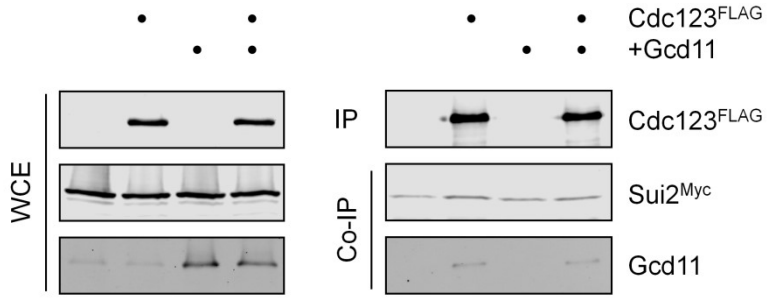

Figure 13: IP of Cdc123^{FLAG} and detection of Sui2^{MYC} and Gcd11 coprecipitation. Indicated next to the panels are the detected proteins. On top of the figure, the expression of Cdc123^{FLAG} and overexpression of Gcd11 are indicated; Sui2^{MYC} was present in every strain used in this experiment. Strains: W17923, W17924, W17925, W17926.

2.1.6 Human eIF2γ binds heIF2α, -β and hCdc123 in vivo

Due to the high versatility and ease of cultivation, yeast is regularly used as a model organism to understand fundamental cellular processes in all eukaryotes. However, a necessary prerequisite for drawing any general conclusions from experiments in yeast is a sufficient level of conservation of the process in question. For eIF2 assembly, this means that interactions that take place in yeast must be verified in human cells and mutations of homologous amino acids or domains should have similar consequences for eIF2 assembly in both species.

In order to verify that the observed interactions of heIF2γ with its partners can be reproduced in a human cell culture model, the cell line Flp-In™ T-REx™-293 was stably transfected with a 3xFLAG-heIF2γ construct for overexpression of human eIF2γ (heIF2γ, see section 5.4 for cell culture methods). A few of the obtained clonal transfected cell lines were tested for protein expression. For the selected strain, which was clone number 3, expression conditions, i.e. the duration of induction and the concentration of tetracycline for induction were optimized (figure 14A-C). The highest expression level of heIF2γ was achieved with induction for two days and a tetracycline concentration of 2 µg/ml at a cell confluency of 80-100% at the time of induction. Accumulation of human eIF2γ over the course of two days indicates that the protein is very stable with a half-life of more than one day.

Transfected cells were grown in five 75 cm^2 flasks to a confluency of 100% and induced by addition of 20 ml Dulbecco's modified eagle medium (DMEM) + 10% fetal bovine serum (FBS) (DMEM + 10 % FBS will be referred to as DMEM in the following text) with 2 µg/ml tetracyclin

for two days. Untransfected cells were used as the negative control and subjected to the same treatment. The total cell count was around 150 million. Cells were lyzed and subjected to IP as described in section 5.5, using 25 µl αFLAG M2 affinity matrix and lysate with an estimated total protein content of ~30 mg. After incubation at 4 °C for 2 hours, elution was performed three times with 25 µl 3xFLAG elution buffer (3xFLAG peptide stock diluted 1:20 in cell lysis buffer) for 30 minutes each. Roughly 60 µl of the eluate were retrieved and boiled with 20 µl 4x LSB. The samples were run on four SDS-gels to detect ^{FLAG}heIF2γ itself and its three putative interaction partners, the endogenous proteins heIF2α, -β and hCdc123. For each gel, 2 OD_{595} of WCE samples (corresponding to 1/700 of total sample) and 10 µl of IP eluates (~1/10 of total sample) were used. For the detection of heIF2α and –β, commercially available, polyclonal antibodies were used. ^{FLAG}heIF2γ was detected with M2 α-FLAG antibody. For hCdc123, affinity purified polyclonal antibody (for the method, see section 5.5.9) from rabbit serum was used. As shown in figure 14D, interactions of eIF2γ with all putative interaction partners could clearly be reproduced in human cells.

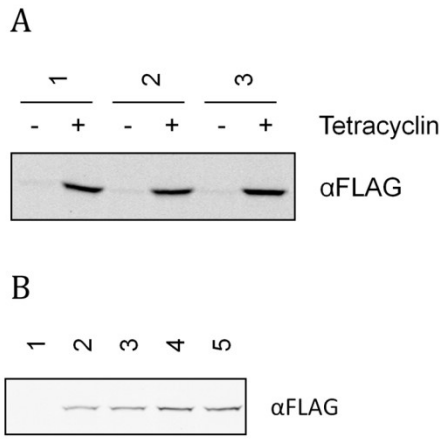

C

Sample number	Induction time	Tet conc. (µg/ µl)	FLAG signal
1	0 d	0	0
2	1 d	1	1.60
3	1 d	2	2.10
4	2 d	1	3.33
5	2 d	2	3.35

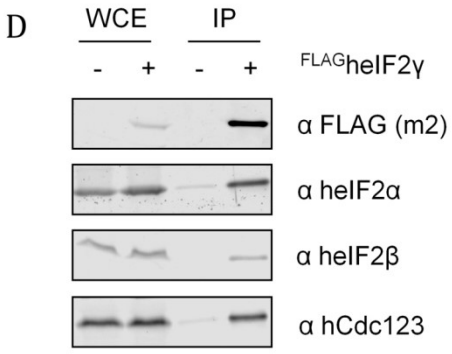

Figure 14. Overexpression and IP of ^{FLAG}heIF2γ in HEK-293T cells A: Test expression of three clonal, ^{FLAG}heIF2γ-transfected strains of Flp-In™ T-REx™-293. For each sample, strain number (1-3) and use of 2 µg/ ml tetracyclin (+/-) is indicated above the figure. **B:** Optimization of expression conditions for ^{FLAG}heIF2γ. 1-5 are five different conditions, listed in the table in (C). **C:** Assessment of expression conditions, tabular display. For conditions 1-5, induction time, tetracyclin concentration and resulting protein levels (dimensionless number) are listed. **D:** Immunoprecipitation of ^{FLAG}heIF2γ and analysis of coprecipitated interaction partners. The two lanes on the left show the input, the two lanes on the right the IP samples. For each box, the used antibody is indicated.

Unlike in yeast, where ^{FLAG}eIF2γ immunoprecipitation pulls down high amounts of eIF2α and –β, no enrichment of these proteins was observed. The low level of eIF2 complexes with the overexpressed ^{FLAG}eIF2γ protein could stem from a negative effect of the tag on eIF2 assembly, which seems unlikely, as no such effect was observed in yeast and the N-terminus seems to be dispensable for assembly. It could also hint towards naturally high numbers of free eIF2 subunit proteins in humans, whch raises the question what function free eIF2 subunits might serve. A third option could be low eIF2 complex formation due to the high cell density in the cultures that were used for the IP. While the supply of fresh nutrients was ensured by frequent medium exchanges, it cannot be ruled out that the high cell density lead to a reduction in eIF2 levels as a means of lowering protein synthesis. Nevertheless, the verification of eIF2 complex formation and binding of hCdc123 to heIF2γ in live human cells helped confirming the significance of all findings in yeast for the understanding of translation initiation in humans. Furthermore, the functionality of all antibodies for the detection of endogenous eIF2 subunits and Cdc123 in human cells was verified.

2.1.7 eIF2 assembly intermediates occur in similar relative amounts in yeast and humans

Next, the relative amounts of assembly intermediates in human cells were analyzed. A new cell line, based on Flp-In™ T-REx™-293, was created that expressed human ^{FLAG}Cdc123. Immunoprecipitation of the protein and detection of heIF2α, -β and –γ in the IP eluate can reveal the degree of enrichment of each binding partner in the IP eluate compared to WCE signals. From previous results in yeast, the greatest enrichment would be expected for heIF2γ, the lowest for heIF2α. Again, successfully transfected strains were identified by test expression and expression conditions were optimized (figure 15A-C).

The IP was performed in a similar fashion as for ^{FLAG}eIF2γ, with cell lysate, prepared from roughly 150 million cells, containing a total of ~35 mg of protein. Four SDS gels were run, with 2 OD_{595} of WCE samples (corresponding to 1/800 of total sample) and 10 µl of IP eluates (~1/10 of total sample). ^{FLAG}hCdc123, heIF2α, -β and –γ were detected with polyclonal antibodies and the relative band intensities for WCE and IP samples were compared (figure 15D). According to expectations and compatible with the eIF2 assembly model established in *S. cerevisiae*, low amounts of heIF2α, a larger amount of heIF2β and a high amount of heIF2γ in complex with hCdc123 were coprecipitated. It is thus reasonable to conclude is that eIF2 assembly, and the role of Cdc123 in assembly, are fundamentally similar in yeast and human. In the Western Blot, a thin band appeared just below the strong band that represents ^{FLAG}hCdc123. Running at a similar height as would be expected for untagged, endogenous hCdc123, appearance of the band in the IP eluates could have been evidence for Cdc123 dimerization, which had been proposed by other researchers before (Young-Baird et al., 2019b). However, the band was detectable with αFLAG antibody F7425. It is thus a C-terminally truncated form of hCdc123, still containing the FLAG-tag and not the endogenous protein. Accordingly, no substantial evidence for Cdc123 dimerization exists to this date.

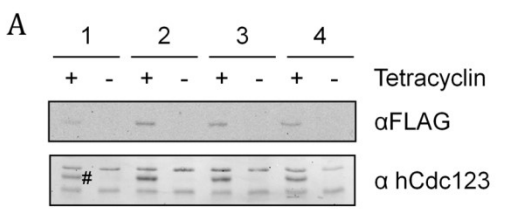

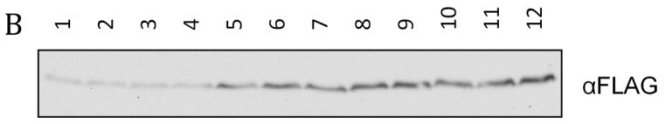

C

Sample number	Induction time	Tet conc. (µg/ µl)	FLAG signal
1	8	0.5	0.14
2	8	1.0	0.15
3	8	1.5	0.16
4	8	2.0	0.18
5	24	0.5	0.47
6	24	1.0	0.68
7	24	1.5	0.59
8	24	2.0	0.78
9	48	0.5	0.84
10	48	1.0	0.68
11	48	1.5	0.75
12	48	2.0	1.00

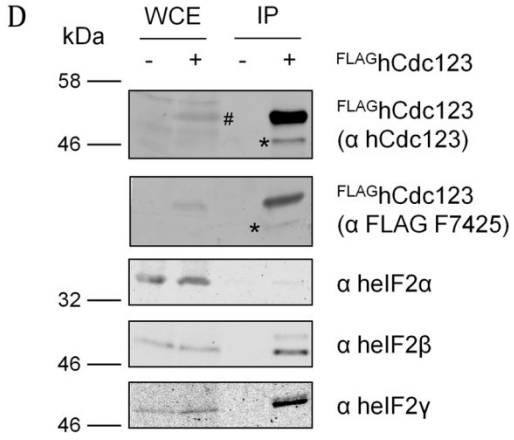

Figure 15. Overexpression and IP of ^{FLAG}hCdc123 in HEK-293T cells A: Test expression of three clonal, ^{FLAG}hCdc123-transfected strains of Flp-In™ T-REx™-293. For each sample, strain number (1-4) and use of 1 µg/ µl tetracyclin (+/-) is indicated above the figure. **B:** Optimization of expression conditions for ^{FLAG}hCdc123. 1-12 are twelve different conditions, listed in the table in (C). **C:** Assessment of expression conditions, tabular display. For conditions 1-12, induction time, tetracyclin concentration and resulting protein levels (dimensionless number) are listed. **D:** Immunoprecipitation of ^{FLAG}hCdc123 and analysis of coprecipitated interaction partners. The two lanes on the left show the input, the two lanes on the right the IP samples. All samples were run four times to detect ^{FLAG}hCdc123, eIF2α, -β and -γ. For each box, the used antibody is indicated. # = ^{FLAG}Cdc123 * = degraded ^{FLAG}Cdc123

2.1.8 Assembly of human eIF2 can be modeled in yeast and hCdc123 facilitates heIF2 assembly

Introduction of one exogenous gene into mammalian cells can be achieved relatively quickly with the Flp-In™ T-REx™-293 cell line, but testing different mutants of multiple proteins in the same cell line is extremely time consuming and resource intensive. Testing the interactions of human eIF2 proteins and human Cdc123 in yeast to assess the effect of mutations and the role of the proteins would be a great tool to study aspects of human eIF2 assembly.

To start off, interaction between heIF2γ and heIF2α was tested in Yeast-two-hybrid (Y2H) assays (for details of the method, see section 5.5.8). Plasmids, based on pJG4-5 and pEG202, containing heIF2γ and heIF2α, were cotransformed into reporter strain W276. As a negative control, the reporter strain was transformed with pEG202_heIF2α and empty pJG4-5, lacking an insert. Six colonies from each transformation plate were chosen, spotted on SRG-HT plates and grown for three days at 25 °C. Then, the Y2H reaction mix was prepared and poured onto the plate and they were incubated at 37 °C. Since no blue coloring of any of the spots was observed

after four hours, the plate was incubated for 24 hours. After the prolonged incubation time, a faint blue coloring was observed in the positive samples while the negative control remained uncolored. It was assumed, that the interaction between heIF2γ and –α was too weak to yield a strong reporter signal. Besides method specific effects that frequently occur in Y2H tests, the lack of human Cdc123 in the reporter strain was one possible explanation for the weak interaction. To test this hypothesis, the reporter strain was transformed with a construct for ^{FLAG}hCdc123 overexpression. A few transformants were tested for ^{FLAG}hCdc123 expression (figure 16A). Clones 1-4 were chosen for a repetition of the Y2H. A negative control and a regular reporter strain were included. After only a few hours of incubation, the modified reporter strain, but not the default one, showed an intense blue coloring (figure 16B). Presence of ^{FLAG}hCdc123 had indeed strengthened the interaction between heIF2γ and –α significantly, demonstrating that hCdc123 was needed for the interaction and that it could fulfill this function in the yeast system. Furthermore, the interaction was not dependent on heIF2β.

Next, several variants of heIF2γ were tested in the same assay (figure 17D). The first version was full-length heIF2γ (with AAs 1-472), followed by the variants 1-457, 1-464 and 1-464SQQ*. The latter was the variant found in some patients with MEHMO syndrome (Moortgat et al., 2016). The deletion of four nucleotides close to the 3' end of the gene causes a frameshift mutation that results in replacement of AAs 465-472 IKPTVDDD by SQQ, followed by a premature stop. The third variant 1-464 represented the truncated version of that protein without the three additional AAs. Variant 1-457 served as a model for total lack of hCdc123 binding capability. From previous studies on eIF2 assembly in yeast, it was suspected that the mutation of the C-terminus, found in heIF2γ(1-464SQQ*), could cause a defect in hCdc123 binding and thus affect eIF2 assembly. Again, a Y2H assay was performed. The experiment revealed a total lack of interaction between heIF2γ(1-457) and –α, and a very weak one for the mutants 1-464 and 1-464SQQ* that is hardly visible in the photograph (figure 16C). It was concluded, that the MEHMO variant of heIF2γ indeed had a defect in its binding of heIF2α, likely caused by defective interaction with hCdc123.

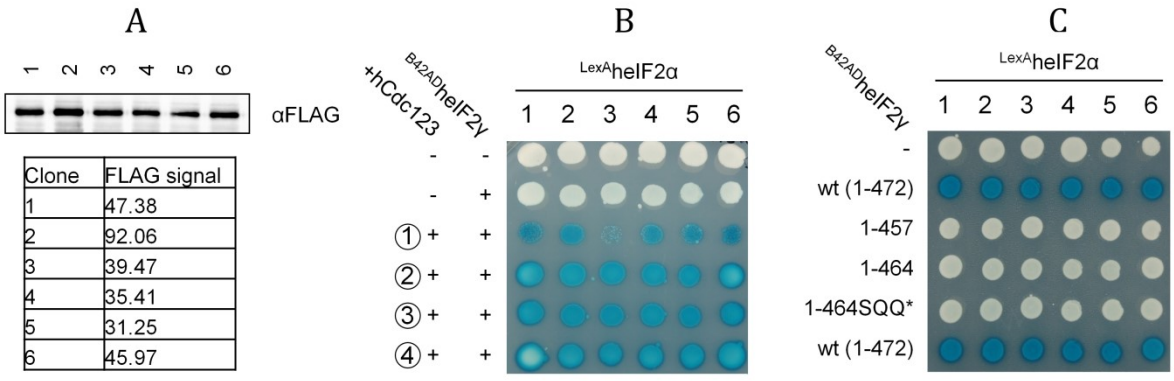

Figure 16: Analysis of heIF2γ-α interaction in Y2H assays. A: Test of a modified Y2H reporter strain, expressing ^{FLAG}hCdc123. 1-6 are six clones from the yeast transformation. **B:** Y2H assay using the original reporter W276 and 4 clones of the reporter strain + ^{FLAG}hCdc123 (1-4). A reporter with en empty pJG4-5 vector and pEG202-heIF2α was used as negative control. W276 served as reference. Four modified reporter strains were used for comparison. Of each transformed reporter strain, six colonies were chosen and spotted on SRG-HT (above the figure, 1-6). **C:** Y2H assay of interaction between different variants of heIF2γ and heIF2α, using modified reporter strain clone 3 (W15023).

To further investigate eIF2 assembly in the aforementioned variants of heIF2γ, all of them were ligated into expression vectors in which they would be expressed under control of the yeast *GCD11* promoter. The vector also added an N-terminal 3xFLAG-tag for easier detection and use of the proteins in Co-IPs. They were introduced into yeast strains that already expressed ^{MYC}heIF2α, ^{HA}heIF2β or ^{MYC}hCdc123. Expression levels were adjusted to similar cellular amounts by testing different transformants for their expression levels. The newly created strains were used to study interaction of heIF2γ with each of its interaction partners in Co-IPs. The capability of each variant to interact with heIF2α,-β and hCdc123 was compared to that of full length heIF2γ by analyzing the amounts of formed complexes. All proteins were detected and quantified with monoclonal antibodies against their tag. The experiment clearly revealed a lack of heIF2α and-β binding for all modified variants of heIF2γ (figure 17A). However, only variant 1-457 was unable to bind hCdc123. Since heIF2γ was coexpressed with only heIF2α, -β or hCdc123, one possible outcome of the IP could have been a lack of interaction with eIF2α and -β in all variants, as no hCdc123 was present in those cells. Full length heIF2γ nevertheless displayed a pronounced ability to form complexes with its eIF2 partners. This can be explained by yCdc123 complementing hCdc123 to some degree. Indeed, hCdc123 has been shown to rescue deletion of yCdc123 (Kachroo et al., 2015). In the Y2H assay, the dependence on hCdc123 seems to be a lot stronger. Yeast Cdc123 is naturally expressed at low levels, at a few thousand molecules per cell (Breker et al., 2013; Chong et al., 2015). This low number of proteins is unlikely to interact with a significant fraction of heIF2γ molecules, since heIF2γ was expressed from the high copy 2µ plasmid pJG4-5 under control of the strong *GAL1* promoter. With variants 1-464 and 1-464SQQ* on the other hand, the assembly defect was clearly seen in the IP. Since binding of hCdc123 was intact, the lack of eIF2α and -β binding cannot be explained by a lack of binding alone. It seems plausible that the interaction is unproductive and does not result in the modification of heIF2γ that is assumed to be necessary for eIF2 assembly.

To test interactions of the different heIF2γ variants with all of the three tested proteins at the same time and further define the role of hCdc123, a yeast strain had to be created that expresses all proteins at the same time. First, a parent strain, expressing ^{MYC}heIF2α, ^{HA}heIF2β and ^{MYC}hCdc123, was created to serve as a vessel for different heIF2γ mutants. The aforementioned ^{FLAG}heIF2γ variants were then introduced into the strain and expression levels were adjusted. IPs were performed analogously and heIF2 complexes were detected in WBs. This time, some interesting differences compared to the IP with only two proteins in the same strain were observed (figure 17B). The shortest heIF2γ variant 1-457 behaved similarly. Interaction with hCdc123 and eIF2β was absent, though a very small amount of eIF2α was detected in Co-IP. For heIF2γ variants 1-464 and 1-464SQQ*, however, the interaction with heIF2a and –β improved significantly. Compared to full-length heIF2γ, the reduction of complex formation with –α and –β was less severe. Possibly, the interaction of yCdc123 with heIF2γ is a lot more fragile than the respective intra-species protein interaction. Truncation or mutation of the C-terminus in heIF2γ might disproportionally affect those kinds of interactions, resulting in a synthetic interaction defect. Without additional hCdc123, heIF2γ is not modified and cannot bind heIF2α and –β. Co-expression of all human eIF2 subunits and hCdc123 together improved heIF2 assembly in the mutants, as the interaction between the human proteins seems to be more stable compared to the interspecies protein interaction. Interaction of heIF2γ with –α being most affected in the

MEHMO allele is consistent with the findings in Young-Baird et al.'s study of the disease (Young-Baird et al., 2019b).

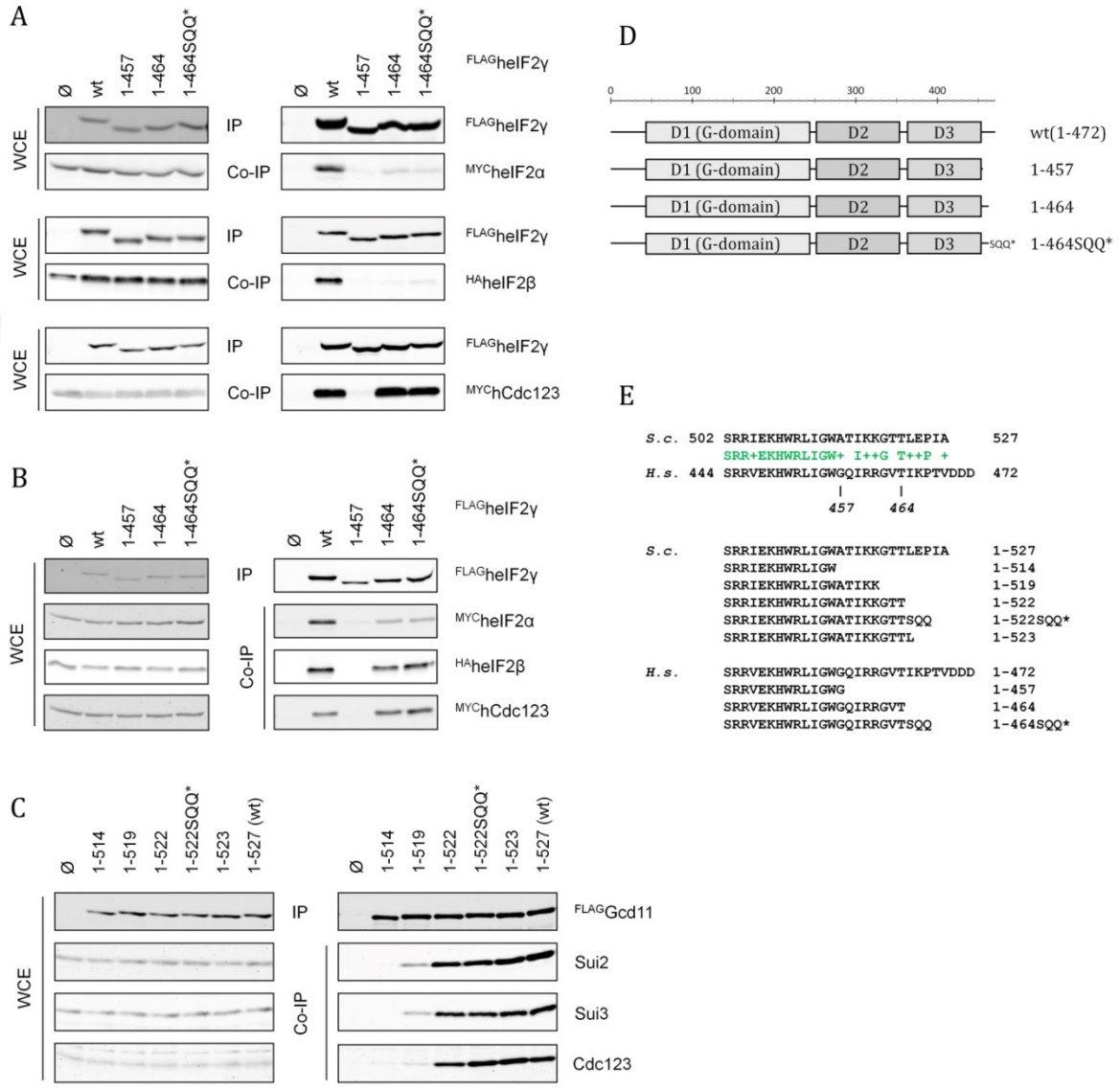

Figure 17: Study of human eIF2-Cdc123 interactions in yeast. A: Coexpression of different variants of ^{FLAG}heIF2γ and ^{MYC}eIF2α, ^{HA}heIF2β or ^{MYC}hCdc123 in separate yeast strains. IP of ^{FLAG}heIF2γ variants and detection of coprecipitated heIF2 subunits and hCdc123 via WB. The ^{FLAG}heIF2γ versions in each sample are indicated above the figure. Strains in top two panels: W14736, W15260, W15261, W15262, W15263. Strains in the middle two panels: W15026, W15125, W15126, W15127, W15128. Strains in bottom two panels: W15034, W15129, W15130, W15131, W15132. **B:** Coexpression of all four human proteins in yeast. IP of ^{FLAG}heIF2γ and detection of coprecipitated binding partners. Strains: W18017, W15350, W16360, W16361, W16362. **C:** IP of various Gcd11 variants including two homologs of the heIF2γ variants 1-464 and 1-464SQQ*. Detection of coprecipitated Sui2, Sui3 and Cdc123. Strains: W12626, W12790, W12788, W16160, W12786, W16199, W12784. **D:** Schematic representation of heIF2γ variants used in the Co-IPs and Y2Hs. **E:** Sequence alignment of the eIF2γ C-termini in yeast and human. Sequence alignment of C-termini of all heIF2γ and Gcd11 variants.

Meanwhile, one interesting finding, concerning species differences between humans and yeast stood out. In yeast, C-terminally truncated Gcd11 had shown severe defects in Cdc123 binding,

but less affected Sui2 and Sui3 binding. For the human proteins, the binding of hCdc123 was mostly intact in the heIF2γ mutants 1-464 and 1-464SQQ*, but interaction with heIF2α and –β was still affected. In order to define possible species differences, the heIF2γ variants were recreated in yeast (see figure 17E). Binding of Sui2, Sui3 and Cdc123 was compared between Gcd11 variants in Co-IPs (figure 17C).

Indeed, not only binding of Cdc123, but also of Sui2 and Sui3 was intact in the Gcd11 variants 1-522 and 1-52SQQ*, that are homologous to heIF2γ 1-464 and 1-464SQQ*. The extreme C-terminus is not as conserved as most other parts of eIF2γ, so the mode of Cdc123 binding might have diverged during evolution. This, however, does not mean that the molecular function of Cdc123 is different – instead, non-productive eIF2γ-Cdc123 complexes could simply be less stable in yeasts than in humans and not survive the protein preparation techniques used for IPs. Moreover, the C-terminus of human eIF2γ is a bit longer than that of yeast eIF2γ, which means that more amino acids were missing from heIF2γ(1-464SQQ*) compared to the yeast homolog. This, and the fact that the frameshift mutant's ability to form assembly intermediates seemed to profit slightly from the three aberrant amino acids SQQ, indicates that the mere number of AAs missing from the C-terminus is a relevant factor.

2.1.9 Reduced TC formation could be the cause of all EIF2S3 related illnesses

The rare genetic condition MEHMO can be caused by a variety of mutations in the human EIF2S3 gene. Three of the identified mutations, namely I222T, I259M and 1-464SQQ*, are linked to reduced TC formation (Borck et al., 2012; Moortgat et al., 2016; Young-Baird et al., 2019c). A forth mutation, P432S, was recently identified in patients with X-linked hypopituitarism with glucose dysregulation and mild cognitive defects (Gregory et al., 2019). These patients don't display the typical severe signs associated with MEHMO syndrome. Study of the yeast homolog of heIF2γ(P432S), the Gcd11 variant P490S, revealed a mild increase in Gcn4 levels, which prompted the authors to infer reduced TC formation, in addition to relaxed start-codon selection to be the cause of the disease. However, eIF2 assembly was not studied directly in the publication. To identify the molecular defect at the root of the symptoms seen in patients, a construct for expression of heIF2γ(P432S) in yeast was created and introduced into the existing heIF2α, -β, hCdc123 expression strain. An IP was performed and P432S was compared to full length heIF2γ, as well as variants 1-457 and 1-464SQQ* in terms of eIF2 assembly (figure 18). The eIF2 assembly defect in the P432S mutant was, surprisingly, even worse than in the 1-464SQQ* variant, which causes a much more severe complex of symptoms in patients. As with 1-464SQQ*, binding of

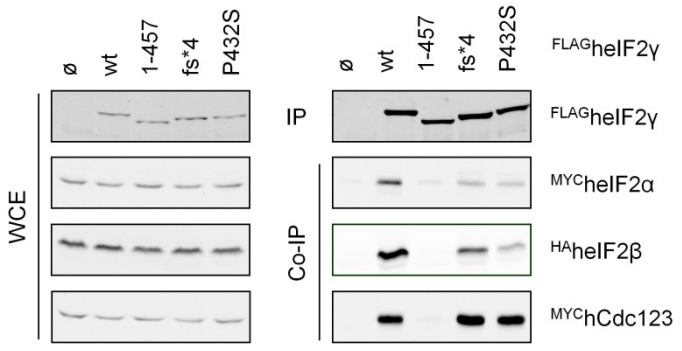

Figure 18: IP of ^{FLAG}heIF2γ variants, including P432S. Coprecipitated ^{MYC}eIF2α, ^{HA}heIF2β and ^{MYC}hCdc123 were detected with antibodies against the tags. The ^{FLAG}heIF2γ versions in each sample are indicated above the figure. Strains: W18017, W15350, W16360, W16362, W18018

hCdc123 was intact, but binding of heIF2α, and heIF2β in particular, was reduced. Binding of human $tRNA_i$ would be difficult to test in yeast, as this depends on eIF2B, too, so this aspect was not investigated. It is nevertheless likely that the differences between the MEHMO allele 1-464SQQ* and the milder P432S mutant can be traced back to differences in TC formation that are in part caused by slow eIF2 assembly. Not all subtleties of human eIF2 and Cdc123 interactions can be investigated in yeast; however, the data indicate that the eIF2 assembly defect plays a major role in the etiology of the newly found syndrome. P432 is located in domain 3 of heIF2γ and conserved among all eIF2γ orthologs. Located in domain 3's β-barrel structure and close to known Cdc123-interacting residues, its mutation could impact the productiveness of the heIF2γ-Cdc123 interaction, similar to the 1-464SQQ* mutation.

2.1.10 Mass spectrometry confirms interaction partners of Cdc123 and hints at function in the nucleus

The essential function of Cdc123 as an eIF2 assembly factor is well established, but some studies have implicated the protein in other functions related to eIF2 regulation, e.g. destabilization of the E3 ubiquitin ligases Chf1/2 (see section 1.1.3.2). Here, possible functions in which Cdc123 might be involved in yeast and human were studied by indentifying in-vivo binding partners. This was achieved by pulling down FLAG-tagged Cdc123 from yeast and human cells and identifying all coprecipitated proteins by mass spectrometry. Yeast $Cdc123^{FLAG}$ was overexpressed in yeast cells and ^{FLAG}hCdc123 in Flp-In™ T-REx™-293. For the yeast protein, around 200 OD cells and for the human protein, ~150 million cells were lysed. The proteins were pulled down by α-FLAG IP. IPs were performed with M2 αFLAG beads and y/hCdc123 were eluted by incubation with 3xFLAG peptide solution. For both proteins, negative controls, i.e. cells without the y/hCdc123 expression constructs, were included in the procedure. Of each IP eluate, 4 µl, corresponding to 5% of the total volume were loaded onto SDS gels to verify precipitation of Cdc123 and estimate the amount of purified protein contained in the samples (figure 19A/B). For each IP, bands running at the expected heights for FLAG-tagged y/hCdc123 and y/heIF2γ were found. For yeast, the band at around 50 kDa is likely $yCdc123^{FLAG}$, whereas the band at 55 kDa could be coprecipitated Gcd11 (figure 19A). For the human proteins, band 1 likely represents ^{FLAG}hCdc123 and heIF2γ is contained in band 2. For the quantification of protein bands, a dilution series with bovine serum albumin (BSA) was used to correlate the signal strengths of the bands of interest to the amount of protein contained in the BSA bands. To demonstrate the procedure, the standard curve and quantification for the ^{FLAG}hCdc123-IP is shown in figures 19C and D. According to the quantification, the band representing $yCdc123^{FLAG}$ contained around 500 ng of protein whereas roughly 300 ng of protein were contained in band 1 of figure 19B.

For the following mass spectrometry, 35 µl of each IP eluate were run on 4-12% gradient polyacrylamide gels (figure 20). From the gels, samples were prepared for mass spectrometry analysis as described in section 5.5.10. The trypsin fragments of every protein in the IP eluates were identified in the mass spectrometry based on their molecular weight. The software which was used to process the date assigned a score to every identified protein, based on the number of unique peptides found. Some proteins were only found in the positive samples (A) and can be

considered bona fide interaction partners of y/hCdc123. Other proteins were found in the control samples (B), too. Since the score of a protein loosely correlates with the amount of protein in the sample, proteins with a score at least 3 times higher in the positive sample compared to the respective control were regarded as direct or indirect binding partners of Cdc123. A selection of the proteins that were identified as interaction partners of Cdc123 in yeast and humans are listed in tables 1-5 (for the complete list of, see table S4, 5). For both yeast and human Cdc123, eIF2γ and –β were among the highest scoring proteins (score > 1000). In human cells, eIF2α was also found, albeit with a relatively low score (260). Besides heIF2γ itself, one of the highest scoring proteins was the heIF2γ-like (heIF2γL) protein, which is encoded by the EIF2S3B gene on chromosome 12. The high interaction score indicates both high abundance and strong interaction with hCdc123. As of 2020, no distinct function has been assigned to heIF2γL. The severity of MEHMO syndrome indicates that eIF2γL cannot functionally replace eIF2γ, despite only seven amino acid exchanges. A variety of translation initiation factors with reasonably high scores were found for both Cdc123 orthologs. For yCdc123, the two E3 ubiquitin ligases Dma1/2, also known as Chf1/2 were identified with high scores, corroborating their association with Cdc123, that was reported before (Bieganowski et al., 2004). In the human sample, the homologous proteins RNF8 and Chfr were not found. Strikingly, nuclear proteins, including nuclear pore and nucleolar proteins were found for both Cdc123 orthologs, indicating that Cdc123 might fulfill a function in the nucleus. Rrp12, Nop7 (PESC) and Mak5 in yeast, and Treacle protein (TCOF1), Nopp140 (NOLC1) and Nop58 in HEK are examples of proteins that are involved in the processing of preribosomal RNA and according to the MS data, interact with Cdc123. Proteins with a dual function in translation and pre-ribosome processing are not unheard of; human eIF6 is both involved in subunit joining during translation initiation and participates in the assembly of pre-60S particles (Sanvito et al., 1999). Interestingly, heIF6 was identified in this study as a binding partner of Cdc123 (see table 2), which could indicate the participation of both proteins in the same complex, e.g. the pre-60S processing machinery.

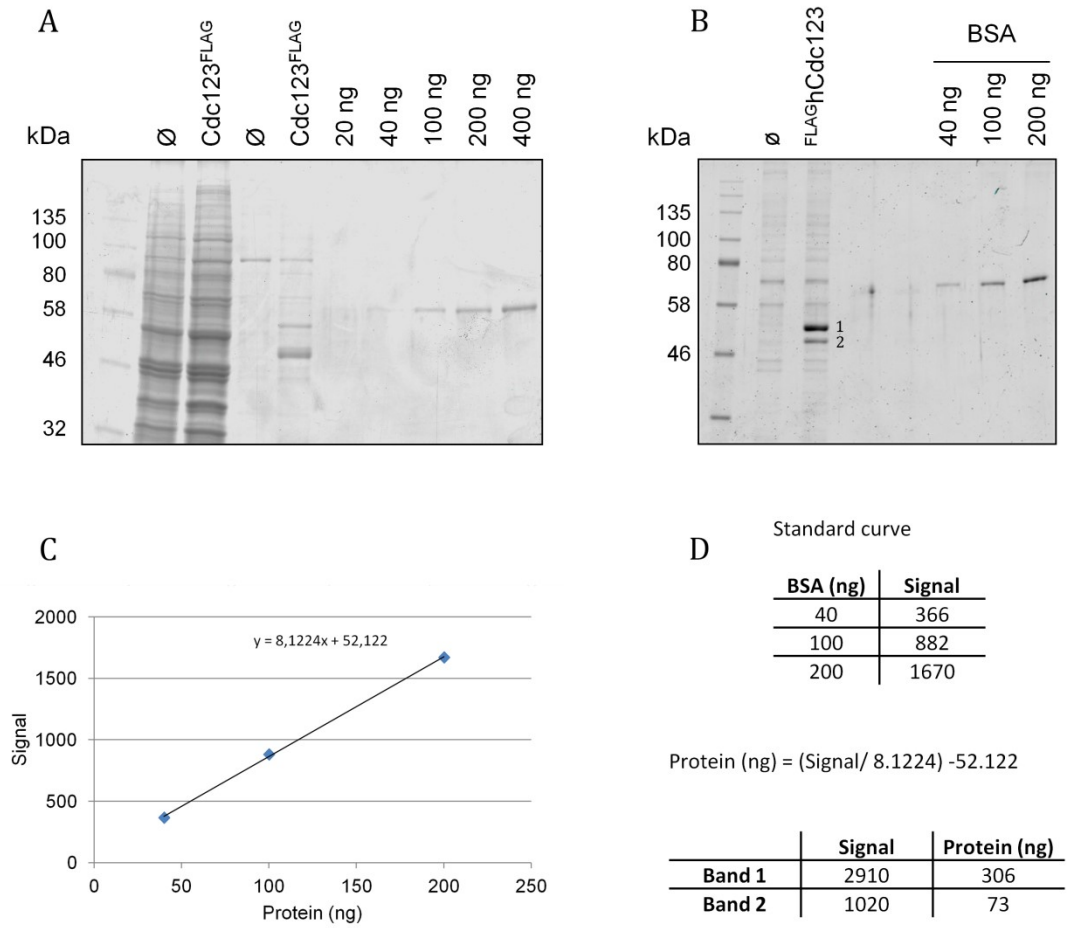

Figure 19: Coomassie analysis of purified Cdc123 from *S. cerevisiae* and *H. sapiens*. Defined amounts of pure BSA were included to draw a standard curve. **A**: Coomassie staining of WCEs and IP eluates of Cdc123^{FLAG} expressing yeast strain (W14058) and negative control (K699). **B**: IP eluates of ^{FLAG}hCdc123 expressing Flp-In™ T-REx™-293 cells and negative control. **C**: Standard curve derived from BSA bands in figure B. **D**: Standard curve in tabellary form, formula to quantify protein yield in IP eluates and quantification of two protein bands in the IP eluate.

To categorize the totality of interaction partners systematically and in an unbiased manner, the gene ontology database was used as a reference. In this database, every protein is categorized by the biological process it is involved in, its cellular localization and its molecular function. The webtool WebGestalt was used to analyze biological processes that were overrepresented in the lists of interaction partners for Cdc123 in yeast and human. The previous presumption, that many of Cdc123's interaction partners, in both yeast and human cells, are involved in processes in the nucleus, was thereby confirmed (figure 21). For yeast, nuclear transport was most enriched, whereas for human Cdc123, processes related to ribosome biogenesis were highlighted in particular. Note that only for the human protein, translation initiation was included in the list of enriched processes. Both this and the different nucleus-related processes that were enriched for yeast and human Cdc123 could be due to the number of proteins included in the reference database. If a biological process includes a very large amount of proteins, identification of a few from the list might not lead to the inclusion of said process in the report.

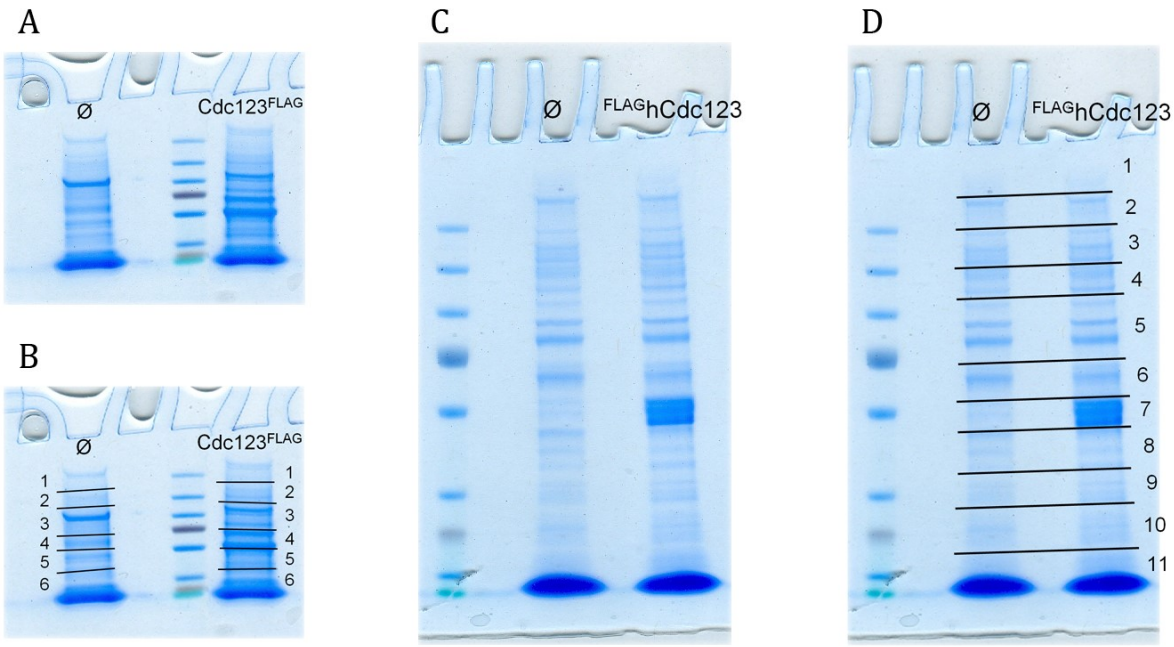

Figure 20: Gradient gels with immunoprecipitated yCdc123^{FLAG} and ^{FLAG}hCdc123. A, C: αFLAG IP eluates of cells expressing FLAG-tagged Cdc123 and a negative control without the protein. **B, D**: Lanes were cut into pieces in the process of sample preparation.

Table 1: Translation initiation factors associated with yeast Cdc123^{FLAG} in vivo. *A = Cdc123 sample, B = control sample*

		Scores			Peptides	
Accession	**Name**	**A**	**B**	**A/B**	**A**	**B**
sp|P32481|IF2G_S. c.	Eukaryotic translation initiation factor 2 subunit gamma	3344	832	4.02	43	16
sp|P09064|IF2B_S. c.	Eukaryotic translation initiation factor 2 subunit beta	1159	205	5.64	15	4
sp|P32501|EI2BE_S. c.	Translation initiation factor eIF-2B subunit epsilon	410	117	3.50	9	3
sp|P09032|EI2BG_S. c.	Translation initiation factor eIF-2B subunit gamma	228	32	7.25	5	1
sp|P12754|EI2BD_S. c.	Translation initiation factor eIF-2B subunit delta	227	56	4.08	5	1
sp|Q03195|RLI1_S. c.	Translation initiation factor RLI1	134			2	

Table 2: Translation initiation factors associated with human ^{FLAG}hCdc123 in vivo. *A = Cdc123 sample, B = control sample*

		Scores			Peptides	
Accession	**Name**	**A**	**B**	**A/B**	**A**	**B**
sp|P20042|IF2B_H. s.	Eukaryotic translation initiation factor 2 subunit 2	4655	202	23.0	55	4
sp|P41091|IF2G_H. s.	Eukaryotic translation initiation factor 2 subunit 3	4067	184	22.1	52	5
sp|Q2VIR3|IF2GL_H. s.	Eukaryotic translation	3124			41	

	initiation factor 2 subunit 3B					
sp|P55010|IF5_H. s.	Eukaryotic translation initiation factor 5	1384	64	21.8	23	2
sp|O75821|EIF3G_H. s.	Eukaryotic translation initiation factor 3 subunit G	553	168	3.3	11	4
sp|P05198|IF2A_H. s.	Eukaryotic translation initiation factor 2 subunit 1	260	75	3.4	5	2
sp|P56537|IF6_H. s.	Eukaryotic translation initiation factor 6	256			6	
sp|P78344|IF4G2_H. s.	Eukaryotic translation initiation factor 4 gamma 2	212			5	
sp|Q9UI10|EI2BD_H. s.	Translation initiation factor eIF-2B subunit delta	207	51	4.0	5	1
sp|O60841|IF2P_H. s.	Eukaryotic translation initiation factor 5B	188	56	3.4	4	2
sp|O75822|EIF3J_H. s.	Eukaryotic translation initiation factor 3 subunit J	119			3	

Table 3: Proteins of the nucleus associated with yeast Cdc123^{FLAG} in vivo*. A = Cdc123 sample, B = control sample*

		Score			**Peptides**	
Accession	**Name**	**A**	**B**	**A/B**	**A**	**B**
sp|P30822|XPO1_S. c.	Exportin-1	1013	169	6.00	23	4
sp|Q12754|RRP12_S. c.	Ribosomal RNA-processing protein 12	700	160	4.38	15	5
sp|P47054|NU192_S. c.	Nucleoporin NUP192	622	33	18.63	15	1
sp|Q04175|SXM1_S. c.	Importin beta SMX1	525	129	4.07	11	3
sp|P53261|PESC_S. c.	Pescadillo homolog	507	80	6.34	9	3
sp|P29469|MCM2_S. c.	DNA replication licensing factor MCM2	475			10	
sp|P32337|IMB3_S. c.	Importin subunit beta-3	432	69	6.30	10	2
sp|P38112|MAK5_S. c.	ATP-dependent RNA helicase MAK5	365	57	6.40	8	1
sp|P38811|TRA1_S. c.	Transcription-associated protein 1	310			6	
sp|P33418|XPOT_S. c.	Exportin-T	276			7	
sp|P35729|NU120_S. c.	Nucleoporin NUP120	237	31	7.65	6	1
sp|P32767|KA122_S. c.	Importin beta-like protein KAP122	211			4	
sp|P38712|RRP3_S. c.	ATP-dependent rRNA helicase RRP3	192	33	5.82	5	1
sp|P49687|NU145_S. c.	Nucleoporin NUP145	191	32	6.01	4	1
sp|P47108|URB2_S. c.	Nucleolar pre-ribosomal-associated protein 2	186			5	
sp|P25293|NAP1_S. c.	Nucleosome assembly protein	710	211	3.36	13	4

Table 4: Proteins of the nucleus associated with human ^{FLAG}hCdc123 in vivo. *A = Cdc123 sample, B = control sample*

		Scores			Peptides	
Accession	**Name**	**A**	**B**	**A/B**	**A**	**B**
sp|Q13428|TCOF1_H. s.	Treacle protein	717.2	71.3	10.0	16	2
sp|Q14978|NOLC1_H. s.	Nucleolar and coiled-body phosphoprotein 1	480			10	
sp|Q9Y2X3|NOP58_H. s.	Nucleolar protein 58	468	59	8.0	7	2
sp|Q13547|HDAC1_H. s.	Histone deacetylase 1	352			9	
sp|O60684|IMA7_H. s.	Importin subunit alpha-7	192			4	
sp|P62304|RUXE_H. s.	Small nuclear ribonucleoprotein E	171	44	3.9	3	1
sp|Q99733|NP1L4_H. s.	Nucleosome assembly protein 1-like 4	146			4	
sp|Q8WTT2|NOC3L_H. s.	Nucleolar complex protein 3 homolog	146			4	
sp|P62306|RUXF_H. s.	Small nuclear ribonucleoprotein F	140	40	3.5	2	1
sp|Q8NFH3|NUP43_H. s.	Nucleoporin Nup4	130			3	
sp|Q9Y3C1|NOP16_H. s.	Nucleolar protein 16	124			3	
sp|Q5C9Z4|NOM1_H. s.	Nucleolar MIF4G domain-containing protein 1	104			2	
sp|P52294|IMA5_H. s.	Importin subunit alpha-5	102			3	

Table 5: Ubiquitin ligases DMA1/2, also known as Chf1/2 found in association with yCdc123^{FLAG}. *A = Cdc123 sample, B = control sample*

		Scores			Peptides	
Accession	**Name**	**A**	**B**	**A/B**	**A**	**B**
sp|P53924|DMA2_S. c.	E3 ubiquitin-protein ligase DMA2	1445			21	
sp|P38823|DMA1_S. c.	E3 ubiquitin-protein ligase DMA1	788			10	

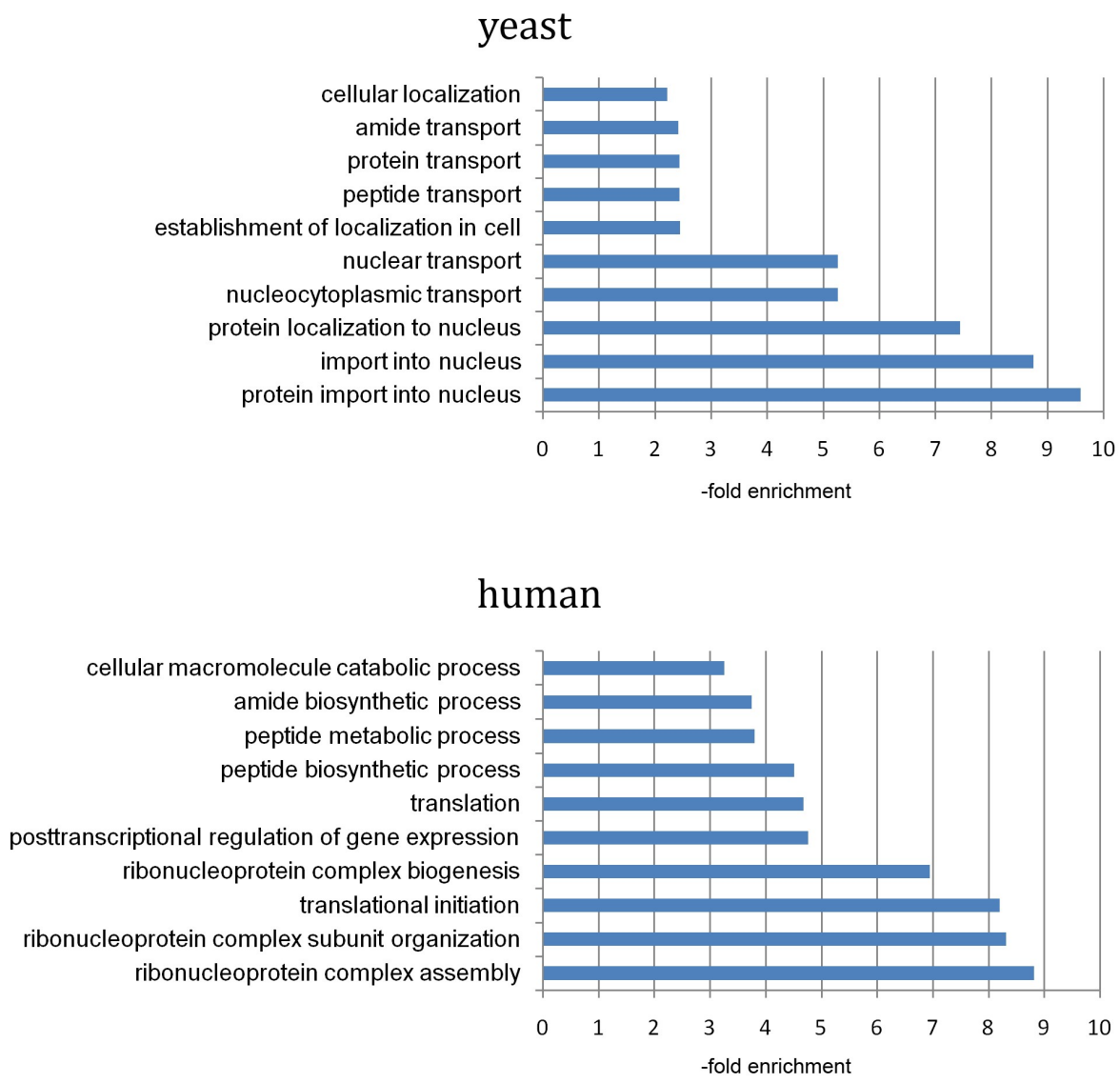

Figure 21: Enrichment of specific biological processes among Cdc123 binding partners, based on the gene ontology database. Upper diagram shows interaction partners of yeast Cdc123, lower diagram shows interaction partners of human Cdc123.

2.2 Cdc123-eIF2γ interaction and eIF2γ interdomain interaction

While there is little doubt that Cdc123 is required for eIF2 assembly, the mechanism of its action is unclear. Its membership in the ATP grasp protein family gave rise to speculations about a covalent modification of eIF2γ that facilitates eIF2α and –β binding. However, such a modification has yet to be identified. SILAC mass spectrometry had previously been used to identify post-translational modifications in Gcd11 that are introduced by Cdc123, but did not lead to positive results. The second possibility is that Cdc123 has an allosteric effect on eIF2γ. This effect could rely on binding of Cdc123 or a permanent reorganization of eIF2γ's 3D-structure. This part of the thesis attempts to uncover what kind of mechanism is likely to be behind Cdc123's function.

2.2.1 Gcd11 residue R510 is involved in interaction with Cdc123

The earliest mention of residue R510 is in a publication by Dorris et al. in 1995. Review of a set of Gcd11 mutants identified the mutation R510H in a yeast strain with relaxed start codon recognition and slow growth (Dorris et al., 1995). The residue is at the interface of eIF2γ-40S subunit interaction and its mutation to histidine activates *GCN4* expression (Shin et al., 2011). Recent, unpublished structural studies demonstrated that the C-terminal helix of Cdc123 establishes a direct contact to R510 via its AA D323. To test the importance of R510 for eIF2 assembly, the Gcd11 mutant R510D was created. Reversal of the AA's polarity weakens the contact to the positively charged AA D323 in Cdc123. To test the function of the mutated protein, a strain with heterozygous Gcd11 deletion was transformed with a construct for expression of ^{FLAG}Gcd11(R510D) under control of the *GCD11* promoter. The strain was sporulated and a tetrad dissection was performed. The mutation turned out to be deleterious for Gcd11 function, as no haploid spore with Gcd11(R510D), but without endogenous Gcd11, could form a colony (figure 22A). One of the haploid yeasts, positive for Gcd11(wt) and Gcd11(R510D), was chosen to test the mutant's ability to assemble into eIF2. Binding of Cdc123 and the other eIF2 subunit proteins was quantified by FLAG-IP of ^{FLAG}Gcd11 (figure 22B). The mutation seemed to cause a phenotype similar to the truncated Gcd11 variant 1-519, where a defect in Cdc123 binding resulted in reduced interaction with Sui2 and Sui3. The results were thus consistent with the earlier finding that AA R510 interacts with Cdc123.

After confirming the importance of R510 for Cdc123 binding, its interaction with Cdc123 residue D323 had to be further tested. If interaction between R510 of Gcd11 and D323 of Cdc123 was mediated by electrostatic attraction between the differently charged AA residues, mutual exchange of amino acids might rescue binding. To this end, the Cdc123(D323R) mutant was created. Originally, FLAG-tagged wt and mutated Gcd11, as well as MYC-tagged wt and mutated Cdc123 were going to be expressed constitutively from the strong *TEF2* promoter. It was planned to introduce the FLAG-*GCD11* constructs into MATα yeasts and the MYC-*CDC123* constructs into MATa strains. The strains would then be combined by cross breeding. However, the combination of Gcd11(R510D) and Cdc123(wt) or Cdc123(D323R) resulted in only a very low number of diploid yeast colonies after selection, none of which expressed the mutated *GCD11* allele. It was concluded, that Gcd11(R510D) protein was toxic when coexpressed with high quantities of Cdc123. Thus, Gcd11 was expressed conditionally under control of the repressible *GALL* promoter, a modified version of p*GAL1* with moderately lower strength (see

table 26). Cross-breeding with Cdc123-expressing strains was successful and an IP was performed. Interaction between Gcd11(R510D) and Cdc123(wt) was significantly reduced, compared to interaction between the wild type proteins. The mutation D323R of Cdc123 on the other hand did not cause a significant interaction defect. Interestingly, the interaction with Gcd11(R510D) was somewhat rescued when both proteins were mutated, again confirming the contact between the two amino acids (figure 22C).

Mutation of R510 might cause a structural change in addition to affecting interaction with AA D323 in hCdc123, as it affected interaction between the two proteins more severely than the D323R mutation and could not be fully rescued. This structural effect could also be responsible for its toxicity in combination with increased amounts of Cdc123. The effect was investigated in more detail in section 2.2.2.

In the Western Blot, Cdc123 appeared as a double band and it is likely that the differing mobility is caused by phosphorylation (see figure 22C). Gcd11(R510D) shifted the ratio between phosphorylated (upper) and unphosphorylated (lower) bands towards more phosphorylated Cdc123. It is possible that free Cdc123 is phosphorylated at a higher rate and its attachment to Gcd11 inhibits phosphorylation. Consistent with this assumption, the shift was more pronounced for Cdc123(wt) than Cdc123(D323R). The mutated variant of Cdc123 was mostly unphosphorylated. To explain this phenomenon, further testing would be required.

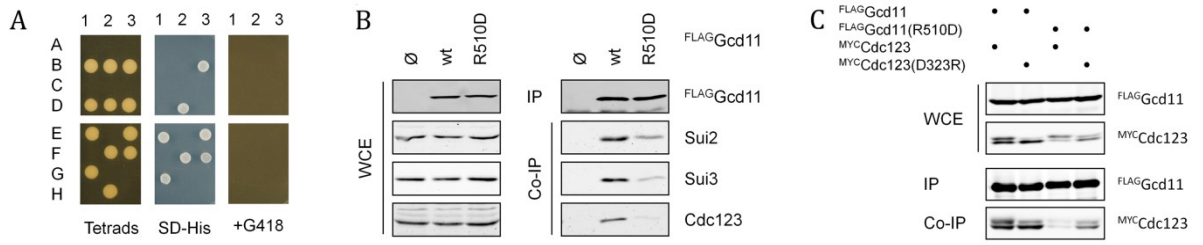

Figure 22: Test of Gcd11(R510D) function. A: Tetrad dissection of a diploid strain with heterozygous *GCD11* deletion, expressing Gcd11(R510D) at endogenous levels (W15907). The two panels on the left, labeled with the caption "Tetrads", show haploid yeast colonies that germinated from tetrads of the diploid strain. The four panels, labeled with SD-His and +G418 show marker tests, where growth on SD-His represents the exogenous, HIS3-coupled *GCD11(R510D)* gene and deletion of endogenous *GCD11* is indicated by growth on medium XY-D+G418. **B:** IP of ^{FLAG}Gcd11 and analysis of coprecipitated binding partners. Strains: W12626, W12783, W15907. **C:** IP of ^{FLAG}Gcd11, detection of coprecipitated ^{MYC}Cdc123. Indicated on top are the respective variants of ^{FLAG}Gcd11 and ^{MYC}Cdc123 in each sample. Strains: W15678, W15679, W15680, W15681.

2.2.2 Gcd11(R510D) exerts a dominant negative effect if assembled into eIF2

To further analyze the growth defect caused by Gcd11(R510D), the yeast strains, expressing Gcd11 variants conditionally and overexpressing Cdc123, were spotted on XY-D (repressive) and XY-RG (inducing) plates. As expected, coexpression of Gcd11(R510D) with Cdc123, wild type or D323R mutant, negatively impacted cell growth (figure 23).

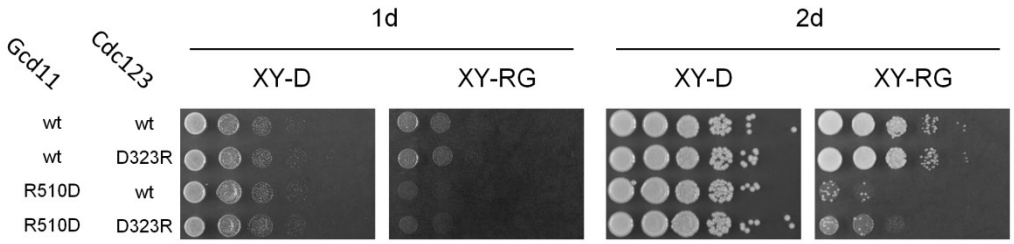

Figure 23: Spot growth test of yeasts expressing Gcd11(wt) or Gcd11(R510D) in combination with high levels of Cdc123(wt) and Cdc123(D323R). Yeasts were spotted on XY-D (repressive conditions) and XY-RG (inductive conditions). Growth was documented after one and two days. Strains: W15678, W15679, W15680, W15681.

To test how overexpression of Cdc123 affects the incorporation of Gcd11(R510D) into eIF2 complexes, IPs were performed with strains expressing ^{FLAG}Gcd11 under control of p*GALL* and Cdc123 under control of p*GAL1*. In this new configuration, the R510D mutation reduced binding of Cdc123 to some degree, but binding of Sui2 and Sui3 was unaffected (figure 24). Cdc123 overexpression thus seems to restore assembly of Gcd11(R510D) into trimeric eIF2. Since this configuration also disrupted cell growth, it was concluded, that Gcd11(R510D) could exert a dominant negative effect if incorporated into eIF2 complexes.

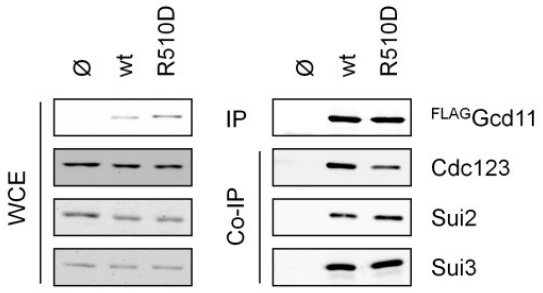

Figure 24: Overexpression of ^{FLAG}Gcd11 (wt/R510D) and Cdc123, immunoprecipitation of ^{FLAG}Gcd11 and detection of coprecipitated Cdc123, Sui2 and Sui3.

Finally, interaction with eIF2B, eIF5 and the 40S ribosomal subunit was tested. Since the difference between wild type and mutant Gcd11 was more pronounced at endogenous expression levels than with overexpression of both Gcd11 and Cdc123, both variants had to be tested. Strains with Gcd11 expression at endogenous levels and strains with p*GAL1* mediated Gcd11 + Cdc123 overexpression were cross-bred against strains with C-terminally 13xMYC-tagged Tif5, Gcd6, Gcd7 and Rps2 to test their coprecipitation. Rps2 is a protein of the small ribosomal subunit that is coprecipitated as a component of 40S, if Gcd11 indeed binds the ribosome. According to expectations, interaction with Gcd6 and Gcd7 was reduced in the mutant. Only fully assembled eIF2 can bind to its GEF eIF2B and the R510D mutant (see section 2.1.2). Since the R510D variant displayed a significant reduction in Sui2 and Sui3 binding, an impairment of eIF2B interaction was to be expected. The effect was quite significant at endogenous Gcd11 expression levels (figure 25A) but less so when Gcd11 and Cdc123 were overexpressed (figure 25B). Likewise, a slight reduction in Tif5 binding was observed in the low expression strain; the effect, however, was weaker than for Gcd6/7, as binding of Tif5 depends on eIF2β, but not –α. For Rps2, the opposite effect was observed. Gcd11(wt) did not coprecipitate Rps2 in an amount that was significantly above the signal in the negative control. Gcd11(R510D) on the other hand, despite yielding a slightly weaker FLAG signal in the IP compared to Gcd11(wt), coprecipitated more Rps2 (figure 25A). This could mean that monomeric Gcd11 can bind the 40S ribosome and that residue R510, despite being at the 40S-Gcd11 interface, is not important for the interaction.

Being mostly in a pool of free proteins due to its assembly defect, a larger fraction of R510D mutants could bind to 40S ribosomes. Alternatively, the aberrant eIF2 complex with Gcd11(R510D) might bind 40S for an extended period of time, possibly because it does not function properly in translation initiation.

To conclude, the toxicity of Gcd11(R510D) is likely exacerbated by high amounts of Cdc123 because this enables the mutated protein to be incorporated into more eIF2 complexes. These aberrant complexes then disturb processes downstream of eIF2 assembly. Since binding to eIF2B and 40S was altered, one can assume that TC formation, translation initiation or both processes are affected and the dominant negative effect of Gcd11(R510D) is exerted by sequestration of eIF2B or other components of the translation initiation machinery.

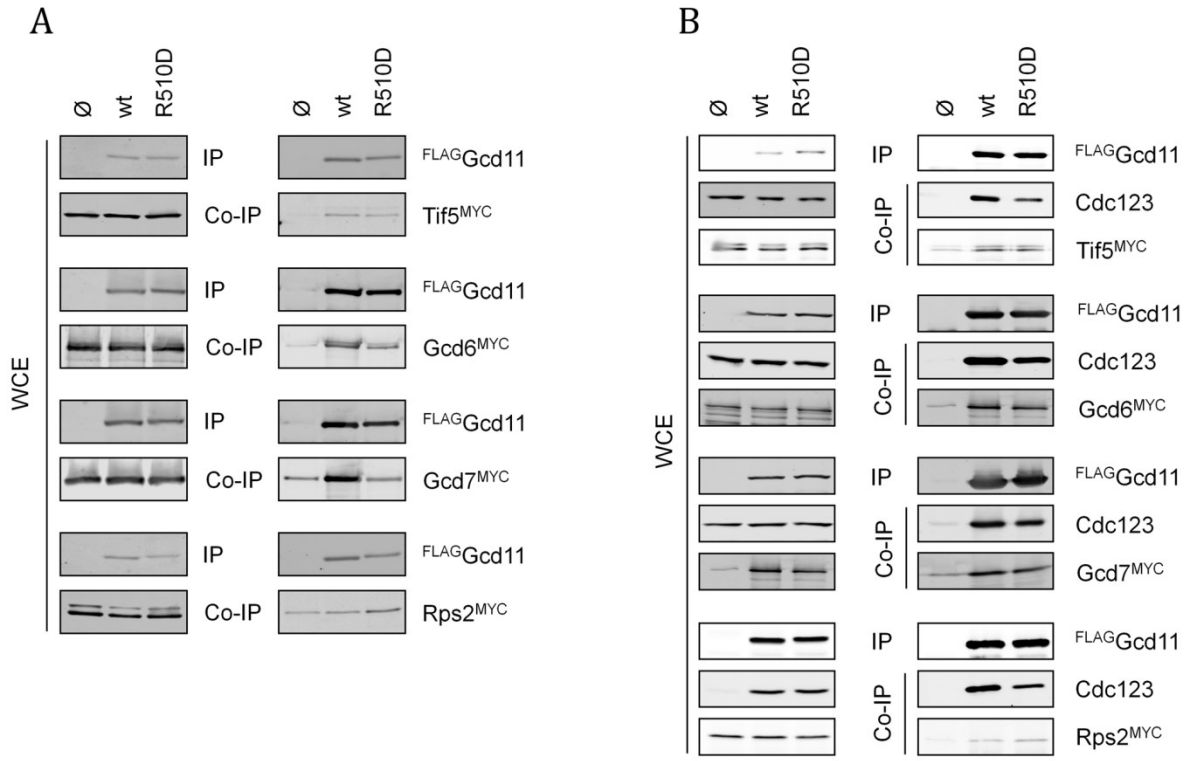

Figure 25: Immunoprecipitation of ^{FLAG}Gcd11 wt/R510D in strains with C-terminally 13xMYC-tagged Tif5, Gcd6, Gcd7 and Rps2. Detection of MYC-tagged proteins. **A**: IPs in strains with Gcd11 at endogenous levels. Strains in top two panels: W17931, W15469, W17934. Strains in two upper middle panels: W17932, W15470, W17935. Strains in two lower middle panels: W17933, W15471, W17936. Strains in bottom two panels: W16286, W16287, W17937. **B**: IPs in strains with overexpression of ^{FLAG}Gcd11 and Cdc123. Strains in top three panels: W16030, W16018, W16022. Strains in three upper middle panels: W16031, W16019, W16023. Strains in three lower middle panels: W16032, W16020, W16024. Strains in bottom three panels: W16033, W16021, W16025.

2.2.3 Interdomain interaction in eIF2γ

Cdc123 is sometimes described as an eIF2γ chaperone, hinting at its putative role in altering eIF2γ structure. A change in eIF2γ structure could be the main mechanism of activating eIF2 assembly – in other words, eIF2γ is initially synthesized and folded in an immature state that is incompatible with binding of eIF2α and -β. Several observations hint towards a communication between the C-terminus of eIF2γ with domain 1 that is indispensable for eIF2 assembly. For

example, structural impairments of domain 1, caused by modest N-terminal truncation (mutant 91-527) or mutation of the zinc ribbon (C150A, C174A) cause a loss of eIF2α binding, despite no known interactions of eIF2α with domain 1.

To test whether eIF2γ is capable of self-interaction, binding of Gcd11 fragments to each other was tested in Y2H. A domain 1+2 fragment (D1+2) was coexpressed with a domain 3 fragment (D3) and a domain 1 fragment (D1) was coexpressed with a domain 2+3 (D2+3) fragment in the reporter strain W276. In both cases, the N-terminal fragment was tagged with the activator domain, while the C-terminal fragment was tagged with LexA.

While no interaction was detected between D1+2 and D3, a visible activation of reporter gene lacZ was observed for D1 and D2+3. D3 on its own could be too small or lack certain structural properties to interact with D1. D1-D3 interaction had been observed previously in archaea via the Sw2 motif in domain 1 (Roll-Mecak et al., 2004) and could be key to understanding the mechanism of Cdc123-mediated modification of eIF2γ. If Cdc123 did indeed affect the positioning of eIF2γ domains to each other, its overexpression in the Y2H reporter strain would likely influence the self-interaction. A modified reporter strain, overexpressing Cdc123 with p*TEF2* was created and the Y2H experiment was repeated. This time, no interaction between D1 and D2+3 was detected. This could mean that domain 3 or domains 2 and 3 of Gcd11 are modified by Cdc123 in a way that prevents interaction. The ability to self-interact could be a feature of immature Gcd11, not yet able to form a trimeric eIF2 complex. Alternatively, Cdc123 might compete with D1 for interaction with D2+3, provided that its binding to D3 is incompatible with Gcd11 self-interaction. However, expression levels of genes inserted into pEG202 are extremely high due to the high plasmid copy number and the strong ADH1 promoter, which makes sequestration of all D2+3 peptides by Cdc123 unlikely.

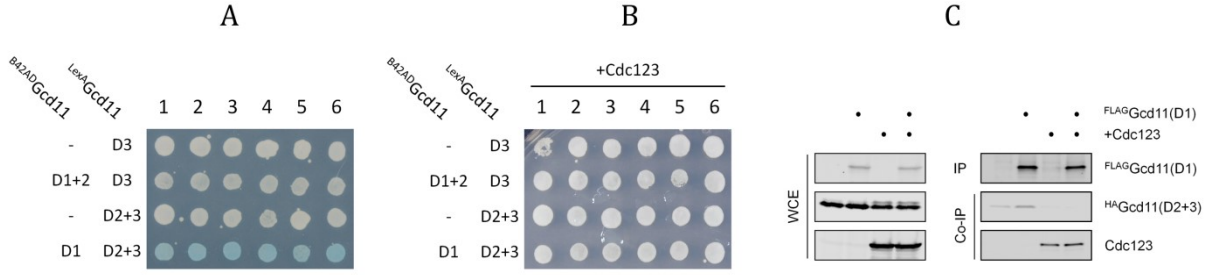

Figure 26: Self-interaction in Gcd11: D1 fragment binds D2+3 fragment. Cdc123 interrupts the interaction. **A**: Test of interaction between D1+2 and D3 as well as D1 with D2+3 in reporter strain W276. On the left, the B42-AD and LexA-tagged Gcd11 fragments are indicated. **B**: Test of the same interactions in reporter strain W16901 with additional overexpression of Cdc123. **C**: Immunoprecipitation of ^{FLAG}Gcd11(D1), detection of coprecipitated ^{HA}Gcd11(D2+3). Test was performed in strains with and without additional overexpression of Cdc123. Presence of ^{FLAG}Gcd11(D1) and Cdc123 in each sample is indicated on top of the figure. Strains: W17918, W17919, W17920, W17921.

The interaction was then investigated in Co-IP to strengthen the significance of the observations in Y2H. D1 was expressed with an N-terminal FLAG-tag at the expression level of endogenous Gcd11, ^{HA}Gcd11(D2+3) was expressed conditionally with p*MET3*. The IP was carried out in a strain with just the two proteins and in one which additionally overexpressed Cdc123. In both cases, a negative control without ^{FLAG}Gcd11(D1) was included. The experiment showed that D1 and D2+3 did indeed form complexes (figure 26C), albeit in low quantities. Overexpression of Cdc123 prevented the coprecipitation of ^{HA}Gcd11(D2+3). Together with the Y2H, this is a good indication that interaction of the C-terminal part of Gcd11 with domain 1 is a mechanism relevant for its function and regulation. Reorganization of interdomain orientation in eIF2γ or refolding of a loop or protrusion by Cdc123 could be the mechanism by which eIF2 assembly is catalyzed.

2.2.4 eIF2γ assembly mutants sequestrate Cdc123

Mutant proteins that lack certain amino acids or domains for binding their interaction partners are usually dead protein mass, whose synthesis takes up a small portion of the cell's resources but does not otherwise interfere with cellular biochemistry. In some cases however, dysfunctional proteins exert a dominant negative effect that is often dose-dependent, i.e. overexpression is more harmful than expression at endogenous levels (Veitia, 2007).

N-terminal truncation mutants (see section 2.1.1), expressed at high levels with p*GAL1*, were tested for their effect on cell growth via spot tests (for the method, see section 5.2.4) on agar plates that repressed Gcd11(mut) expression (XY-D) or induced it (XY-RG, XY-G). The spotted plates were incubated at 25 °C for two days and documented. Indeed, a dominant negative effect was observed in all variants where at least 90 AAs from their N-terminus had been removed (figure 27). The effect correlated perfectly with their unability to bind Sui2 and Sui3.

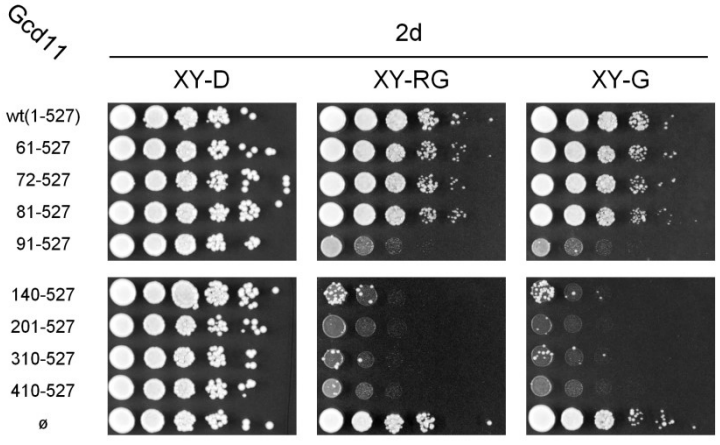

Figure 27: Effect of overexpressed, N-terminally truncated Gcd11 on cell growth. Cells were grown for two days at 25 °C. For each yeast strain, the respective overexpressed Gcd11-variant is indicated. Growth medium is denoted above the panels. Strains: W15011, W14924, W15009, W15010, W14925, W14926, W14927, W14928, W14929, K700.

For an in-depth analysis of the underlying cause, Gcd11(201-527) was chosen. A new variant, Gcd11(201-514), was created, to test if the protein's toxicity had to do with its ability to bind Cdc123, but not Sui2 and Sui3. By truncating the C-terminus, the protein's Cdc123-interaction platform was compromised (see section 1.1.3.1). The new variant was compared to Gcd11(wt) and the variants 201-527 and 1-514 it was based on. A new spot test was performed on XY-R (non inducing) and XY-RG (inducing). The plates were documented after one and two days. Again, Gcd11(201-527) inhibited cell growth significantly, whereas the wild type and 1-514 variant, as expected, did not have any effect. The dual-truncated protein Gcd11(201-514) lost its toxicity upon C-terminal truncation (figure 28), indicating that the ability of variant 201-527 to bind Cdc123, but not Sui2 and Sui3, was responsible for the negative effect on cell growth. It was hypothesized that the protein, due to its high abundance, bound most of the Cdc123 and prevented it from interacting with endogenous Gcd11. Unable to bind Sui2 and Sui3 and form TC, Gcd11(201-527) could not fulfill the function of endogenous Gcd11 and disrupted translation initiation. This hypothesis was tested by repetition of the growth test in strains that had been created by cross-breeding the haploid, Gcd11-overexpressing strains with a strain that also overexpressed Cdc123. If the hypothesis was right, overexpression of Cdc123 should leave sufficient assembly factor molecules to endogenous Gcd11 to assemble into trimeric eIF2 and TC, even when high amounts of Cdc123 are sequestrated by the Gcd11 mutant. According to expectations, growth of yeast cells expressing Gcd11(201-527) was rescued by overexpression of Cdc123, confirming the hypothesis (figure 28).

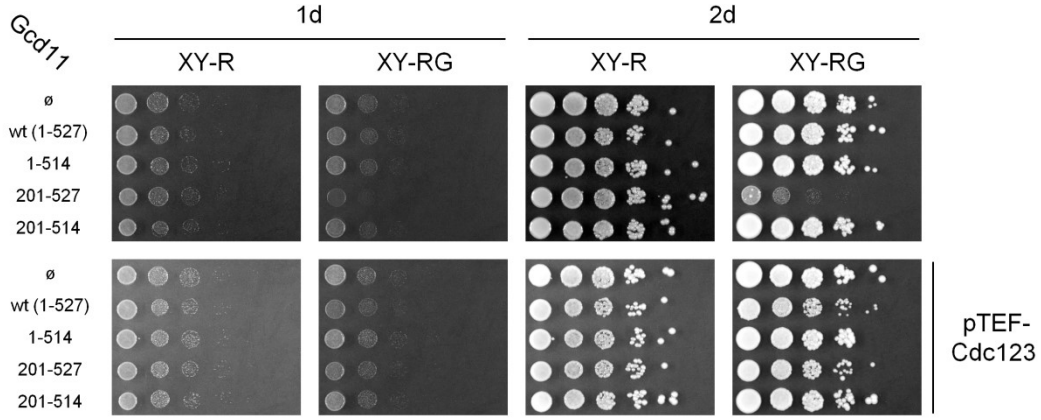

Figure 28: Dominant negative effect of Gcd11(201-527) is suppressed by Cdc123 overexpression. Cells were grown for one or two days at 25 °C. For each yeast strain, the respective overexpressed Gcd11-variant is indicated. Growth medium is denoted above the panels. The upper panels show a growth test in strains without additional Cdc123. Strains: W11164, W15011, W16200, W16201, W16202. The lower panels show growth of yeast strains in which Cdc123 was overexpressed alongside the Gcd11 mutants. Strains: W18061, W18062, W18063, W18064, W18065.

The Gcd11 point mutants V281R and D403R, which are characterized by their unability to bind Sui3 and Sui2, respectively, can be expressed at endogenous levels without significantly affecting the rate of cell division. The double mutant Gcd11(V281R, D403R), however, is too toxic for constitutive expression and must be expressed from a repressible promoter to prevent expression during growth phase of the yeast culture. Its unability to bind Sui2 and Sui3, as well as its ability to bind Cdc123 was confirmed in Co-IP (figure S1). The double mutant's and the

single mutants' potential toxicity as well as suppression of toxicity by overexpression of Cdc123 were tested via spot growth test on XY-R (non-inducing) and XY-RG (inducing). The strains expressed Gcd11 mutants under control of p*GALL*. By cross-breeding against the Cdc123 overexpression strain, strains for testing the effect of Cdc123 overexpression were created. Similar to Gcd11(201-527), the double mutant Gcd11(V281R, D403R) suppressed cell growth nearly completely. The single mutants, upon overexpression, showed a moderate toxicity (figure 29). A defect in binding just one of the eIF2 subunits thus leads to a less severe effect than inability to bind any of the two proteins, despite an equal inability to form functional TC. This suggests that Cdc123 is more stably attached to Gcd11 when none of the other subunits bind. Cdc123 may dissociate more frequently from Gcd11(mut)-Sui2/3 dimers, offering a chance for functional, endogenous Gcd11 to "catch" a Cdc123 molecule. Consistent with the assumed function of Sui2 as the primary Cdc123 release factor, Gcd11(D403R) had a stronger effect on growth than Gcd11(V281R). As before, overexpression of Cdc123 restored cell viability in each strain.

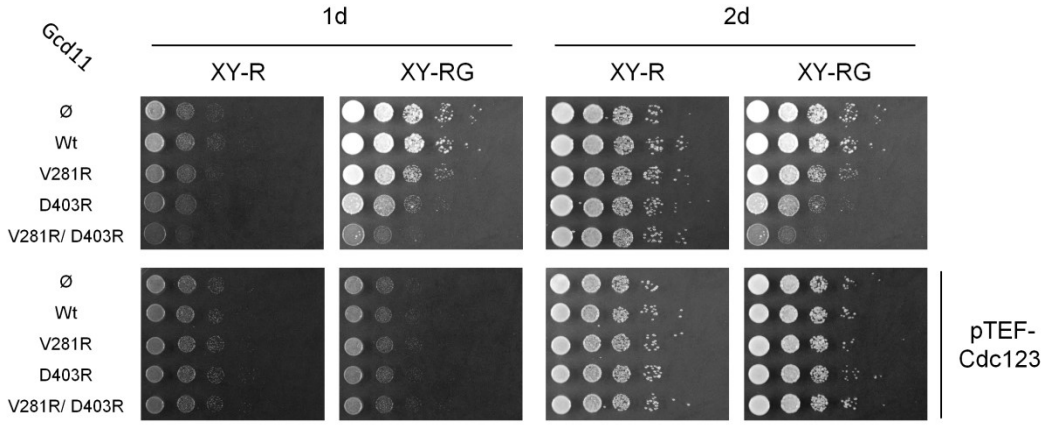

Figure 29: Dominant negative effect of Gcd11 assembly mutants is suppressed by Cdc123 overexpression. Cells were grown for one or two days at 25 °C. For each yeast strain, the respective overexpressed Gcd11-variant is indicated. Growth medium is denoted above the panels. The upper panels show a growth test in strains without additional Cdc123. Strains: K700, W15672, W16441, W16442, W16443. The lower panels show growth of yeast strains in which Cdc123 was overexpressed alongside the Gcd11 mutants. Strains: W17745, W17747, W17747, W17748, W17749.

2.2.5 Characterization of domain 1 mutants of Gcd11

Integrity of domain 1 of eIF2γ is essential for eIF2 assembly, as shown previously (section 2.1.1). It is homologous to G-domains of other members of the family of small GTPases. Besides binding eIF2β, it coordinates and hydrolyzes GTP in its active center. In this next part of this work, a set of D1 mutants, exerting dominant negative effects on cell growth, were investigated. The mutations affect GTP binding or D1 structure and, except for one mutant, cannot be expressed constitutively. The first mutant was N-terminally truncated protein Gcd11(91-527), that was earlier characterized in sections 2.1.1 and 2.2.4. Two further variants were the cysteine mutants C150A and C174A. The cysteines coordinate a zinc ion and support the structure of a protrusion in domain 1 (figure 30A). Next, two GTP binding mutants were created. Two amino acids in the G1 motif, S114 and T115 were mutated to alanine (mutant ST/AA) and K250 in G4 was mutated

to alanine as well (figure 30B). The last variant was ΔSw1, in which AAs 128-138, which make up the switch 1 motif, were deleted. Gcd11(ΔSw1), out of the six mutants, is the only one that can be expressed constitutively at the level of endogenous Gcd11, but causes a slow growth phenotype.

Since all proteins were toxic to yeast cells, expression constructs with the repressible *MET3* promoter (table 26) were created. The vector also contained a 3x FLAG tag upstream of the insert. Expression strains with similar protein levels were created.

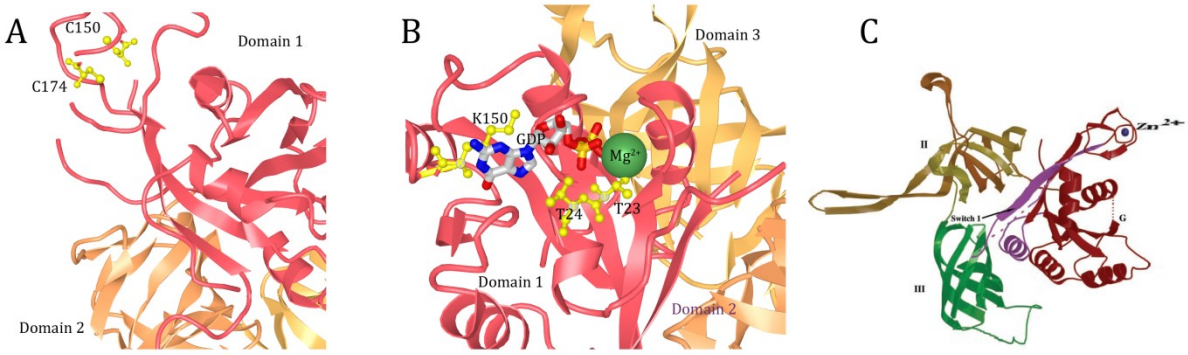

Figure 30: G-domain mutants used in this study. A: C150 and C174 in Gcd11 (PDB ID 6QG6, from Gordiyenko et al. 2019) **B:** GDP/GTP binding AAs T23, T24 and K150 in *S. solfataricus*, homologous to S114, T115 and K250 in *S. cerevisiae* (PDB ID 4RD6, from Panvert et al. 2015). **C:** Switch 1 region (purple) in M. jannaschii eIF2γ (from Roll-Mecak et al. 2004).

2.2.5.1 Integration of D1 mutants into eIF2 complexes

The ability to assemble into trimeric eIF2 was analyzed for each protein by αFLAG-IP. Yeasts were grown under repressive conditions during growth phase (XY-D + 0.33 mM Met). The medium was changed to SD-Met two hours prior to harvest to derepress the *MET3* promoter and activate expression of the exogenous Gcd11 construct. Each IP was performed twice and coprecipitated Sui2, Sui3 and Cdc123 were quantified. The signals were correlated with the FLAG signals in the IP and values from the IP of ^{FLAG}Gcd11(wt) served as reference (figure 31; raw data in tables S6, S7). Each mutant had a characteristic binding profile. Cdc123 binding was slightly reduced in most mutants, to around 60-80%. Exceptions were variant 91-527, where no difference was seen, and ΔSw1, where binding of Cdc123 was increased to ~200%. Mutant 91-527 had been characterized before and results were consistent with earlier observations, where Sui2 and Sui3 binding were reduced significantly. In the cysteine mutants, hardly any binding of Sui2 and Sui3 was observed, similar to the situation in N-terminal truncation mutants (section 2.1.1). It seems likely, that loss of the zinc ribbon structure, similar to the removal of too many AAs from the N-terminus, affects the overall structure of domain 1, which disrupts eIF2 assembly. G-motif mutants K250A and ST/AA displayed a moderate reduction in Sui2 binding, K250A additionally a severe defect in Sui3 binding, which could be a consequence of K250's close proximity to eIF2β binding amino acids (figure 2).

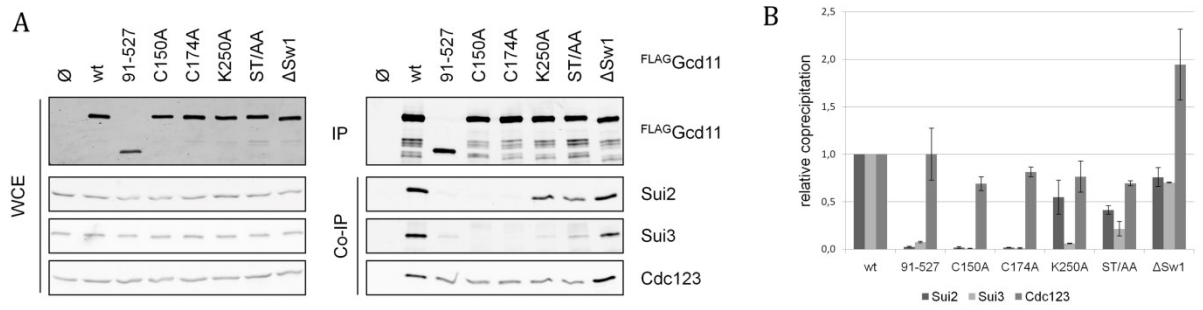

Figure 31: IP of ^{FLAG}Gcd11 G-domain mutants and quantification of coprecipitated binding partners. A: WB scan of one IP replicate. The respective variant of ^{FLAG}Gcd11 in each sample is indicated on top of the figure. Strains: K700, W12629, W17422, W17423, W17424, W17425, W17426, W17427. **B:** Quantification of coprecipitated binding partners relative to precipitated ^{FLAG}Gcd11 with ^{FLAG}Gcd11(wt) as reference. Experiment was performed in duplicates; the diagram shows averages.

2.2.5.2 Effect of D1 mutants on assembly of endogenous eIF2

Next, the effects of each mutant on the assembly of endogenous eIF2 were investigated. For this purpose, HA-tagged Gcd11-mutants were expressed conditionally with p*MET3* in a strain with endogenously FLAG-tagged Gcd11. Yeasts were grown under repressive conditions overnight, then expression of ^{HA}Gcd11 variants was induced by switch to SD-Met medium. Samples were taken at the time point of induction (t = 0h) and 0.25 h, 0.75 h, 2.5 h and 6 h after induction. With each sample, an αFLAG IP was performed. This way, the amounts of Sui2, Sui3 and Cdc123 that still participated in the assembly of endogenous eIF2 were monitored. For every yeast strain, except the one expressing ^{FLAG}Gcd11(wt), the Gcd11 mutants' toxicity was observed after one hour, with growth slowing down quickly. Interestingly, a lot less protein was retrieved from yeast samples from 2 h time points, and 6 h time points in particular. Possibly, this effect can be attributed to the depletion of TCs and thus the shutdown of protein synthesis. For Gcd11(wt), the curves show what would be expected for a simple competition for eIF2 subunits between endogenous and exogenous Gcd11 (figure 32, for Western Blot pictures, see figure S2). In the end, the amount of coprecipitated Sui2 and Sui3 was reduced to 30-40%, compatible with a 2.5x relative overexpression of the exogenous ^{HA}Gcd11. Cdc123 seemed to associate mostly with the endogenous protein; however, protein quantification by Western Blot is not strictly linear and varies between antibodies. Therefore, comparisons will be drawn mostly between the same proteins in different samples, not between different proteins, that are detected using different antisera. For variants C150A and C174A, the mechanism of affecting endogenous Gcd11 function looked similar (figure 32). First, Cdc123 was taken away from endogenous Gcd11, and then binding of Sui2 and Sui3 was affected more and more over time. Since C150 and C174 are unable to bind Sui2 and Sui3 themselves, coprecipitation levels did not drop initially, but were affected later on, indicating that the effect was indeed caused by Cdc123 sequestration. Due to their unability to assemble into eIF2, the mutant proteins remain attached to the assembly factor, depleting the pool of free Cdc123. With ΔSw1, this relatively simple explanation does not work, since the protein does bind Sui2 and Sui3. It could be the case that deletion of Sw1 indirectly affects the release of Cdc123. This would lead to the formation of a stable, tetrameric eIF2-Cdc123 complex, effectively sequestrating Cdc123 and Sui2/ Sui3. As we will see later, this

hypothetical tetrameric complex, if existent, is still able to bind eIF2B. Since ΔSw1 is unable to bind GTP, its binding to eIF2B could lead to the formation of unproductive complexes and inhibit eIF2 recycling. The mutants K250A and ST/AA, presumably unable to bind GTP, did not affect eIF2 assembly as dramatically as the three aforementioned variants (figure 32). Their toxicity could be caused by a combined effect on eIF2 assembly, similar to that of C150 and C174, and on eIF2B activity. While their ability to form eIF2 is reduced, the aberrant eIF2 complexes, once assembled, would bind eIF2B tightly; with no GDP or GTP bound to the γ-subunit, the guanosine exchange could not be catalyzed and eIF2B would be trapped. Since the cellular concentration of eIF2B is only 10-50% that of eIF2, according to PaxDb (Wang et al., 2012), even a small or moderate amount of aberrant eIF2 complexes would inhibit eIF2B activity.

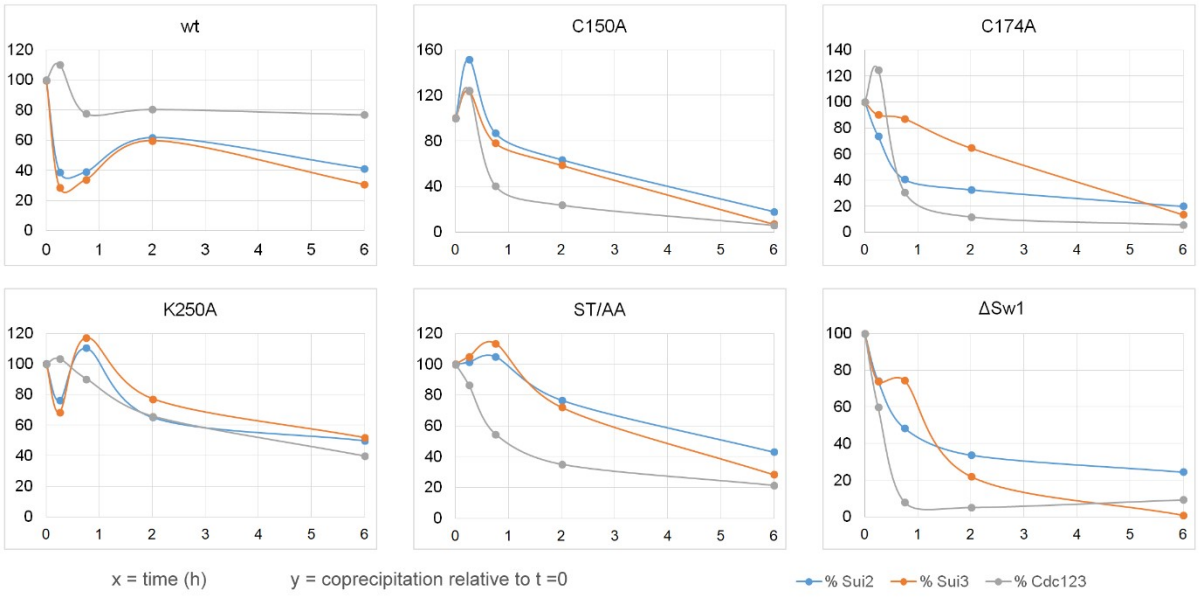

Figure 32: Effect of Gcd11 mutants on assembly of endogenous eIF2. For each diagram, the respective Gcd11 variant is denoted at the top. All values were calculated by dividing the signal from coprecipitated Sui2, Sui3 or Cdc123 by the FLAG signal; then, the start value at t = 0 was set to 100%. Strains: W16899, W16903, W16904, W16905, W16906, W16907.

2.2.5.3 Suppression of dominant negative effects by overexpression of eIF2 subunits and Cdc123

Overexpressing proteins that are involved in the affected pathway can suppress the dominant negative effect of some aberrant proteins, as seen for eIF2 assembly mutants in section 2.2.4. Identifying such proteins can also deliver additional information about the mechanism underlying the dominant negative effect. Yeast strains, conditionally (p*MET3*) expressing wild type Gcd11 or Gcd11 D1 mutants, were crossbred against strains overexpressing Sui2, Sui3, Cdc123 or combinations of the three proteins (see table 18). Growth of the resulting strains was tested under inductive and suppressive conditions in a dilution spot test. To this end, all diploid strains were grown overnight under suppressive conditions (XY-D + 0.33 mM Met), washed in water and spotted on SD++ and SD-Met. The results are summarized in table 6 (for spot test pictures, see figure S3). For mutants 91-527, C150A and C174A, the spot test confirmed the previous assumption that their toxicity is caused by sequestration of Cdc123. Indeed, the sole

overexpression of Cdc123, or its overexpression in combination with Sui2 and Sui3, restored growth back to normal. Overexpression of Sui2 seemed to help to some degree, too. Being a Cdc123 release factor, Sui2 might dissolve stable Gcd11(mut)-Cdc123 complexes occasionally and allow endogenous Gcd11 to bind the assembly factor. The toxic effect of mutant Gcd11(ΔSw1) could not be significantly suppressed by any of the combinations; only Sui2, Sui2/3 combination and Sui3/Cdc123 combination possibly helped alleviating the effect a bit. This is consistent with the earlier supposition that Gcd11(ΔSw1) affects eIF2B function, not only eIF2 assembly. Toxicity of Gcd11(ST/AA) and Gcd11(K250A) was suppressed by overexpressing Cdc123; for K250A, the positive effect was reversed when in addition, Sui3 was coexpressed, and the ST/AA strain did not tolerate additional Sui2 or Sui3. In the case of K250A, growth was restored again when Cdc123, Sui3 and Sui2 were coexpressed with the Gcd11 mutant. Possibly, overexpression of Cdc123 and Sui3 leads to the titration of Sui2 in the K250A mutant because of the formation of stable, non-functional eIF2 complexes. Adding a Sui2 overexpression construct then restores the level of available Sui2. This finding provides some interesting implications for the eIF2 assembly mechanism, too. Sui3 overexpression seems to rescue the integration of Gcd11(K250A) into trimeric eIF2 complexes by mass action. This would explain why Sui2 was not sequestrated without Sui3 overexpression and seems to indicate that dimeric eIF2γ-α complexes are less stable then trimeric eIF2. This is despite the fact that it was demonstrated earlier that binding of Sui2 and Sui3 to Gcd11 are not strictly interdependent (see section 2.1.2). To explain why overexpression of only Cdc123, but not combinations with Sui2 or Sui3 alleviated toxicity of the ST/AA variant, one can speculate that additional Sui2 and Sui3 further enhanced assembly of the mutated Gcd11 variant into eIF2 complexes, which then inhibited eIF2B function. Mutant K250A was earlier shown to bind Sui3 very poorly – Sui2 overexpression thus was not sufficient to drive eIF2 assembly, whereas for ST/AA, whose affinity for Sui2 and Sui3 was only slightly reduced, overexpression of either subunit was sufficient. This also explains why the toxicity of ST/AA could not be fully suppressed with additional Cdc123.

Table 6: Suppression of dominant negative effects of Gcd11 D1 mutants by overexpression of eIF2 subunits, Cdc123 and combinations thereof*. Indicated in the top row are the respective Gcd11 variants; overexpressed proteins are indicated in the column on the left. +++ = restoration of normal growth; ++ = significant improvement of growth; + = weak effect on growth; (+) = very weak or dubious effect on growth*

	91-527	C150A	C174A	K250A	ST/AA	ΔSw1
+Sui2	+	+	+	++		+
+Sui3						
+Cdc123	+++	+++	+++	+++	++	
+Sui2/3	+	(+)	(+)			+
+Sui2/Cdc123	++	++	++	+++		
+Sui3/Cdc123	++	++	+++			+
+Sui2/3/Cdc123	+++	+++	+++	+++		

2.2.6 Stabilization of eIF2γ by Cdc123

As described before, the earliest established link between Cdc123 and eIF2 function was the proposed inhibition of proteasomal degradation of Gcd11 (see section 1.1.3.2). Destabilization of Chf1 and 2, E3 ligases that mark Gcd11 for proteasomal degradation, was found to be a way in which Cdc123 increased eIF2 activity (Bieganowski et al., 2004). This mechanism, however, was found to be non-essential. Here, a second mechanism of Cdc123-mediated eIF2γ stabilization will be discussed.

2.2.6.1 hCdc123 increases the expression level of heIF2γ in the yeast system

The differences seen in heIF2γ IPs between strains expressing heIF2γ with only one interaction partner, and strains expressing eIF2γ together with -α, -β and hCdc123 necessitated a deeper look into the role of hCdc123. Using sporulation and tetrad dissection, strains with different combinations of heIF2α, -β, γ and hCdc123 were created. Western blot analysis of the strains showed that the expression levels of heIF2γ varied greatly between the resulting strains, despite originating from the same parent strain. A systematic analysis revealed that hCdc123 was the deciding factor that determined the level of heIF2γ protein. With hCdc123, the level of heIF2γ was roughly 10x higher than without it. Interestingly, the effect was only seen for the wild type protein and the variant 1-464SQQ*, but not variant 1-457 (figure 33). Somewhat paradoxically, the most truncated version seemed to be expressed at a high level in absence of hCdc123, but this can be attributed to the selection process. The selection of strains with similar expression levels of heIF2γ was performed in a background strain that already contained hCdc123. For heIF2γ(1-457), a transformant that compensated the naturally low level of heIF2γ(1-457) with a very high number of genomic plasmid integrations was chosen unintentionally. This was later confirmed by Anna Dlugosch via qPCR analysis, where the number of genomic integrations was determined (Dlugosch, 2019). Expression of heIF2α and -β had no significant impact on cellular levels of heIF2γ. Since only hCdc123 seemed to influence heIF2γ expression levels and the effect occurred only in those variants of heIF2γ that bind it, it was concluded that an interaction between the two proteins that is dependent on a physical interaction stabilizes heIF2γ.

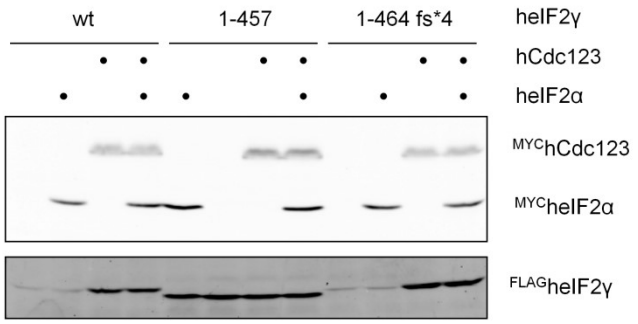

Figure 33: Characterization of haploid daughter strains, created by sporulation and tetrad dissection of strains expressing heIF2α, -β and hCdc123 together with a variant of heIF2γ (W15350, W16360, W16362). Indicated on top are presence of heIF2α, hCdc123 and the respective heIF2γ version of the parent strain. All strains express heIF2β.

2.2.6.2 Substoichiometric amounts of hCdc123 increase heIF2γ expression

How hCdc123 increases cellular levels of heIF2γ in yeast was unclear at this point. One possibility was protection of heIF2γ from degradation by direct binding of hCdc123. In this case,

hCdc123 would have to be expressed at least at similar or higher levels than heIF2γ for the effect to occur. If, however, hCdc123 introduced a modification into heIF2γ that made it more resistant to degradation, substoichiometric amounts would be sufficient. To test this hypothesis, expression levels of heIF2γ were tested in various strains with a defined gene dose of EIF2S3 (heIF2γ) and varying levels of human Cdc123. A yeast strain, expressing ^{FLAG}heIF2γ was transformed with three different constructs for expression of ^{FLAG}hCdc123. Three promoters, p*TEF2*, p*GCD11* and p*CDC123* (table 26) from yeast were used to achieve a wide span of expression levels. During transformation, plasmids can integrate between one and up to ten times, increasing the diversity of expression levels. Use of the same tag for both proteins allowed an accurate measurement of relative expression levels. Various transformants were analyzed and nine of them were selected for a direct comparison in Western Blot. Quantification of WB signals showed that the putative stabilization effect did not require equimolar amounts of the two proteins, as hCdc123 stabilized heIF2γ even at a tenth the amount of heIF2γ. It can thus be concluded that the stabilization does not rely on physical protection, but a transient interaction, during which heIF2γ is modified, is probably sufficient.

A

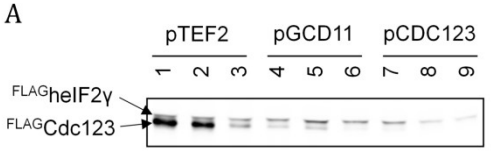

B

	1	2	3	4	5	6	7	8	9
hCdc123	129.9	101.9	21.4	7.7	10.7	2.3	2.3	0.4	0.2
heIF2γ	24.4	22.9	14.6	17.2	29.5	19.6	17.4	5.7	3.6

C

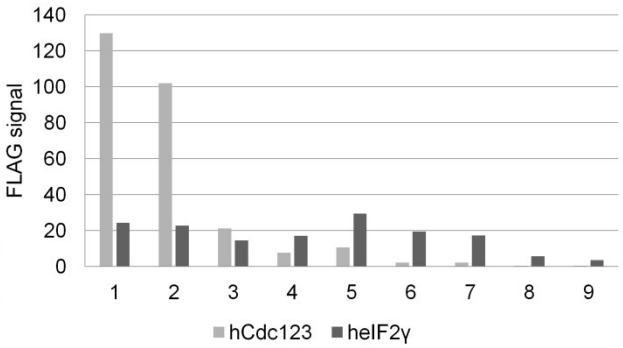

Figure 34: Influence of hCdc123 abundance on heIF2γ levels. A: Western Blot of nine strains, based on W16353 with a fixed EIF2S3 gene dose and different expression constructs for hCdc123. As ^{FLAG}heIF2γ and ^{FLAG}hCdc123 have similar running properties in SDS-PAGE, each protein is indicated on the left side of the panel. B: Quantification of FLAG signals for each strain. The numbers are dimensionless and proportional to signal strengths in the scan. C: Graphic depiction of the quantification.

2.2.6.3 hCdc123 stabilizes heIF2γ in a transient interaction

The stability of heIF2γ was further characterized in heIF2γ shutdown assays. Two strains, one of which expressed hCdc123 whereas the other one did not, were transformed with a construct for galactose-dependent expression of ^{FLAG}heIF2γ. Synthesis of heIF2γ was induced overnight by cultivation in XY-RG liquid medium and shut down in the morning by transferring the cells to XY-D. Samples were taken at different time points, starting at the time point of medium switch (t = 0) to monitor the decrease of heIF2γ over time. FLAG signals were quantified and compared to the signal at t = 0 for both strains. As expected, the signal intensity in the strains without hCdc123 decreased quickly, whereas the decrease of heIF2γ in presence of hCdc123 was slow and can be attributed mostly to the dilution effect during cell proliferation (figure 36A, B; for raw data, see table S8).

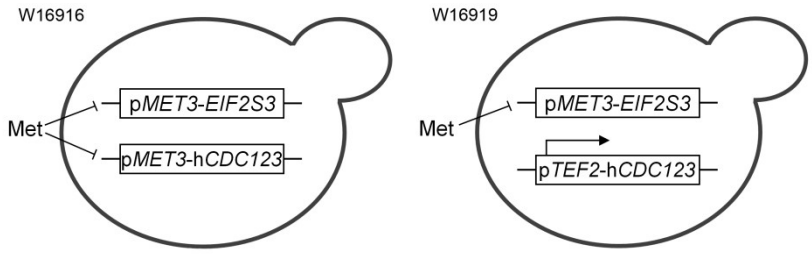

Figure 35: Schematic representation of yeast strains W16916, W16919 for heIF2γ shutdown assay. The boxes represent heIF2γ and hCdc123 alleles. Methionine represses transcription of all genes that are controlled by p*MET3*. The hCdc123 allele that is controlled by pTEF2 remains active.

In a second shutdown assay, it was asked, whether initial expression of hCdc123 would permanently stabilize heIF2γ. For this purpose, two strains were created. In both strains, heIF2γ was expressed conditionally under control of p*MET3*. However, strain 1 expressed hCdc123 under control of p*MET3* as well, whereas strain 2 expressed the protein constitutively (see figure 35). For the assay, both strains were cultivated in SD-Met overnight to allow synthesis of both proteins in both strains. *MET3* promoter was inactivated by transfer of the cultivated cells to XY-D + 33 µM methionine. Samples were taken at t = 0 and seven more time points and ^{FLAG}heIF2γ, as well as ^{MYC}hCdc123 signals were analyzed via WB. The decrease of heIF2γ concentration in both strains was slow and very similar to each other (figure 36 C, D; for raw data, see tables S9, S10). Human Cdc123 on the other hand was degraded quicker than heIF2γ and became virtually undetectable after six hours.

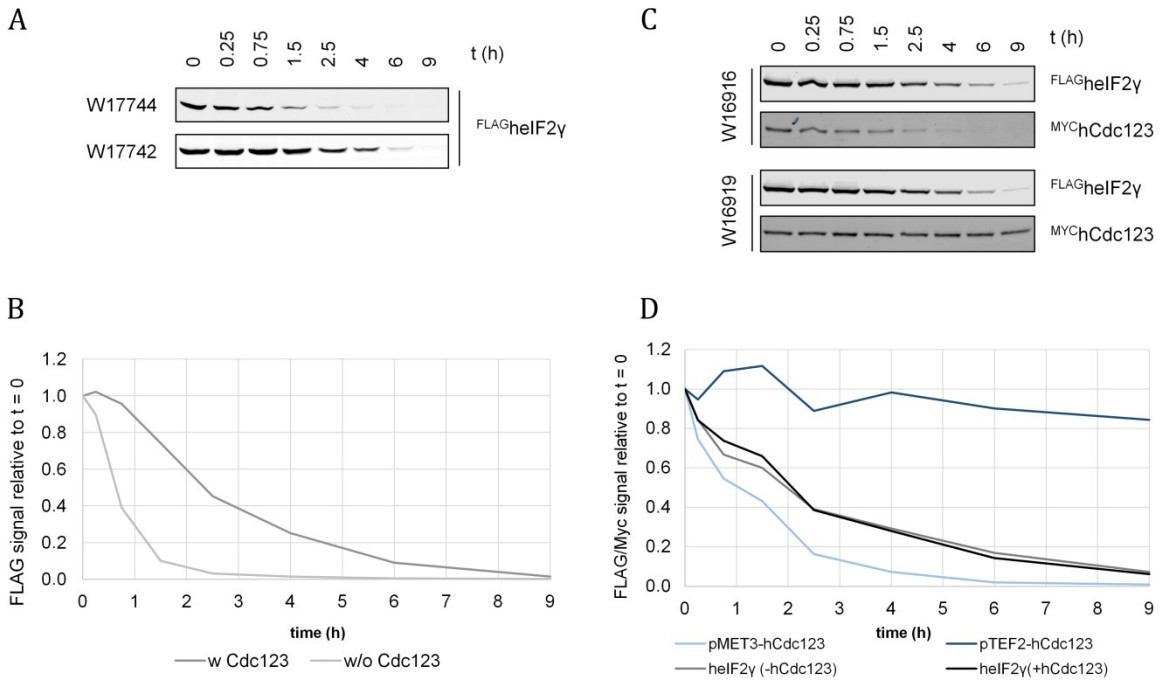

Figure 36: Effect of hCdc123 on stability of heIF2γ in yeast. **A, B:** Shutdown experiment with heIF2γ (p*GALL*) in strains with (W17742) and without (W17744) hCdc123. The values in the diagram were normalized to the value at t = 0. **C, D:** Shutdown experiment with heIF2γ (p*MET3*) in strains with constitutive (*pTEF2, W16919)* or conditional (p*MET3, W16916*) expression of hCdc123. The values in the diagram were normalized onto the value at t = 0.

It seems likely, that heIF2γ, once coming in contact with hCdc123, is modified in a way that stabilized the protein permanently, since even after the time point of six hours, no difference in heIF2γ levels between the two strains was observed. In conclusion, the two human proteins interact in yeast and hCdc123 introduces a stabilizing modification into heIF2γ. This modification, interestingly, seems to be distinct from the modification needed to prepare heIF2γ for heIF2 assembly, since the variant 1-464SQQ* was stabilized just as much as the wt protein.

2.2.7 The C-terminus of hCdc123 and interaction with heIF2γ

Unpublished data from crystallographic studies showed that the C-terminus of hCdc123 reaches over the ATP binding site in Cdc123 and contacts heIF2γ. Human Cdc123 has a total length of 336 AAs and consists of two domains (see section 1.1.3.2). C-terminal truncation of Cdc123 in yeast, which has a total length of 360 amino acids, increasingly leads to loss of function. Here, two variants of C-terminally truncated hCdc123, 1-292 and 1-314, and the mutant Y304G were studied in terms of complementation of yCdc123, binding of heIF2γ and support of heIF2 assembly. The truncated proteins lack AAs in the C-terminal part that contacts domain 3 of heIF2γ. They correspond to yeast Cdc123 with AAs 1-315 and 1-328 (figure 37). Residue Y304 interacts with the ATP binding site (unpublished data) and is not conserved in yeast, where tyrosine is replaced by asparagine. Its mutation likely interferes with ATP-related functions of hCdc123.

```
                      315/292     318/304   328/314
                         |           |         |
yeast   LRLVTRHNTGRFASKE---------HSENHVPQDLVEASLNPEAIRELTQKWKELLSQQA  349
human   AQE---QDSPAFRCTNSEVTVQPSPYLSYRLPKDFVDLSTGEDAHK-----LIDFLKLKR  330
         :    :::  * ..:         : . ::*:*:*: * . :* :       ::*. :
yeast   KEESSDSENET  360
human   NQQEDD-----  336
        :::::*
```

Figure 37: Alignment of the C-terminal parts of Cdc123 in yeast and human. The residues, relevant for this section, are highlighted. Gaps are indicated as hyphens (-), identical AAs as asterisks (*), moderately conserved AAs as colons (:) or dots (.).

2.2.7.1 Complementation of yCdc123

Cdc123 is conserved and functionally interchangeable between yeast and humans. Complementation tests in yeast can thereby indicate the functionality of a given hCdc123 variant. It is noteworthy that expression at endogenous levels, e.g. with pCdc123, is not sufficient. Complementation is not perfect and requires overexpression of the human protein.

To test complementation of yCdc123, a diploid yeast strain with heterozygous deletion of *CDC123* was transformed with expression constructs of hCdc123. The deletion had been achieved by replacement of the y*CDC123* gene with the KanMX6 cassette, which confers resistance to G418. The h*CDC123* construct was coupled with *LEU2*. *TEF2* promoter was chosen to achieve sufficient expression levels. For all three variants of hCdc123, strains which expressed hCdc123 at similar levels were selected. They were sporulated and tetrad dissections were performed. All colonies that formed from the haploid spores were subjected to a growth test on SD-Leu and XY-D+G418 to test for the h*CDC123* alleles and deletion of y*CDC123*, respectively.

The wild type control showed a growth pattern that indicated full complementation. Spores that had received at least one gene copy of human or endogenous *CDC123* had germinated and grew at normal rates. C-terminal truncation of hCdc123 reduced protein function considerably. In absence of endogenous Cdc123, version 1-314 allowed growth of yeast colonies at very low rates, whereas variant 1-292 did not complement at all. Mutant Y304G complemented yCdc123 comparably well, but not perfectly (figure 38). In essence, C-terminal truncation of hCdc123 leads to loss of function in a similar way as in yCdc123. Variant hCdc123(1-314) corresponds to yCdc123(1-328) and, depending on the strain background, yeast variants 1-325 or 1-326 are the shortest variants that can support cell growth. Amino acids upstream of AA328(y)/AA312(h) are moderately conserved (figure 37), which explains why removal of more amino acids shuts down Cdc123 function. AA Y304, despite its lack of conservation, seems to assume a conserved function in yeast, since its mutation to alanine interferes with complementation. However, it cannot be ruled out that the amino acid exchange alters the structure of the C-terminal part in a way that reduces its functionality in yeast.

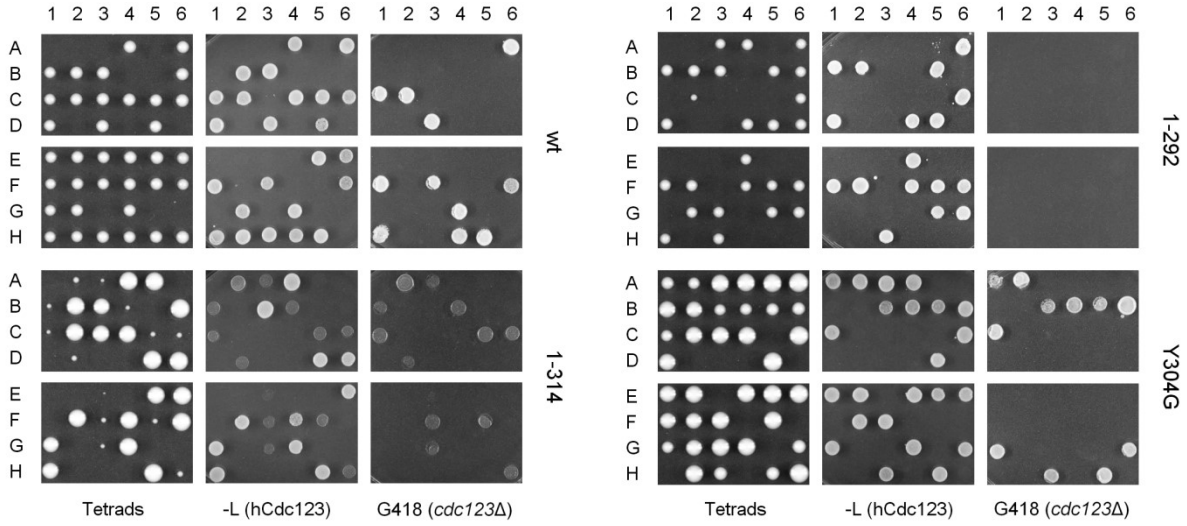

Figure 38: Complementation of yCdc123 by mutated hCdc123 variants was tested by tetrad dissection of strains, heterozygous for Cdc123 deletion and transformed with hCdc123 variants (W15568, W15573, W15578, W15581). The respective hCdc123 variant is indicated on the right of each batch of tetrads. From left to right, the panels show spore colonies on XYD (Tetrads), growth test on SD-Leu, representing expression of hCdc123 and growth on XYD+G418, indicating the deletion.

2.2.7.2 Binding of hCdc123 to heIF2γ is not sufficient to facilitate eIF2 assembly

As seen above, hCdc123 loses its ability to complement yCdc123 upon truncation of its C-terminal parts and mutation of Y304 results in a moderate reduction of functionality. Employing IP of ^{FLAG}hCdc123 variants, their ability to facilitate heIF2 assembly in yeast was tested. Yeast strains were created that expressed ^{HA}heIF2β and ^{MYC}heIF2γ together with ^{FLAG}hCdc123. Both truncated proteins showed a moderate decrease in heIF2γ binding, variant 1-314 an accordingly weaker interaction with heIF2β. For mutant 1-292, the defect in heIF2β binding was even more pronounced. Variant Y304G, which coprecipitated heIF2γ in similar quantities as the wild type protein, still had a visible defect in heIF2β binding (figure 39 A). These results confirm earlier

observations, that for full functionality, hCdc123 requires an intact ATP binding site in addition to binding heIF2, and link ATP binding to heIF2 assembly.

As shown earlier, hCdc123 supports the binding of heIF2γ to –α in Y2H. Reporter strains with similar expression levels of all hCdc123 variants were used to test how the mutations affected this function of hCdc123. The Y2H assay was performed as described before in section 2.1.8. The truncated proteins 1-314 and 1-292 performed very poorly, yielding hardly any or no blue coloring of the reporter strain. The Y304 mutant, which had failed to precipitate heIF2β at levels similar to the wild type in the IP, supported the γ-α interaction well. One might propose that the signal increase can be mostly attributed to stabilization of heIF2γ, which requires binding of the two proteins to each other. This would conform to the observation, that truncated hCdc123 has a lower affinity for heIF2γ. However, this explanation must be ruled out, as Anna Dlugosch demonstrated in her Bachelor thesis, that both proteins are indeed capable of stabilizing heIF2γ, albeit less effectively than hCdc123(wt) (Dlugosch, 2019). The differing capabilities of hCdc123 mutants to enhance eIF2α or –β binding to eIF2γ might be attributable to different binding requirements for the α- and β-subunits. It is also possible, that heIF2 can only be modulated reliably in yeast strains with all four proteins (heIF2α, -β, γ and hCdc123).

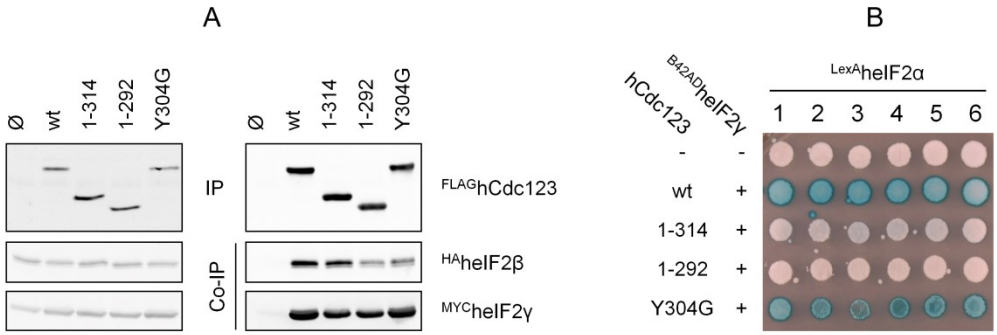

Figure 39: Investigation of different hCdc123 variants and their ability to facilitate heIF2 assembly. **A:** Immunoprecipitation of ^{FLAG}hCdc123 and detection of coprecipitated ^{HA}heIF2β and ^{MYC}heIF2γ. The respective variant of ^{FLAG}hCdc123 in each sample is indicated on top of the figure. Strains: W15164, W15165, W17059, W17060, W17061. **B:** Y2H assay in which the ability of hCdc123 variants to enhance heIF2γ-α interaction was analyzed. Strains: W276, W15023, W15592, W15593, W15594.

2.3 eIF2 dysfunction and cell cycle

The original identification and naming of Cdc123 as a cell cycle protein stems from the fact that G1 arrest is the most noticeable defect that occurs if Cdc123 is dysfunctional. Later, the underlying cause of G1 arrest was identified: Cdc123 is essential for eIF2 assembly, TC formation and thus protein synthesis in general. These processes come to a halt if Cdc123 is lacking or inactive. Cells that are overall unfit to enter cell cycle, e.g. because of a lack of nutrients, or in this case, lack of protein synthesis, often arrest at the most stringent check point of cell cycle, the START point. Defects of eIF2 subunits similarly lead to G1 arrest, or slow growth.

2.3.1 Haploinsufficiency in strains with heterozygous deletion of eIF2 subunits

Diploid cells lacking one copy of *SUI2*, *SUI3*, *GCD11* or *CDC123* are viable, but, depending on which genes are deleted, may display a mild slow growth phenotype. Average doubling time was tested in diploid yeast strains with heterozygous deletions of either of the genes. Four separate overnight cultures of each variant and the unaltered strain K842, on which all four strains were based, were inoculated with a defined amount of cells and grown at 25 °C. By comparing OD_{600} before and after the cultivation, doubling time was determined. Among the eIF2 subunit genes, *SUI2* was the most critical, while deletion of one copy of *GCD11* was most tolerated. Deletion of one *CDC123* allele did not cause a slow growth phenotype at all (figure 40; for raw data, see table S11). Expression of *CDC123* is roughly 5-10 times lower than that of the eIF2 subunits (Breker et al., 2013), as a transient interaction with eIF2γ is sufficient for eIF2 assembly and eIF2 most likely does not need Cdc123, once it is assembled. This, and the fact that Cdc123 is not directly involved in translation initiation, may explain why diploid yeast cells tolerate the loss of one allele. Sui2 is rate limiting in eIF2 assembly, as shown in section 2.1.5, so it is not surprising that yeasts with only one copy show significant haploinsufficiency. With respect to *SUI3* and *GCD11* deletions, the differing doubling times lack a clear explanation.

A

	doubling time (h)	**MSE (h)**
wt	1.73	0.021
- / *SUI2*	2.38	0.040
- / *SUI3*	2.17	0.043
- / *GCD11*	1.92	0.036
- / *CDC123*	1.74	0.005

B

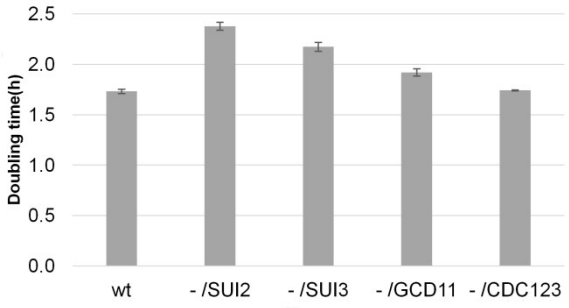

Figure 40: Doubling time of diploid yeast strains with heterozygous deletion of *SUI2*, *SUI3*, *GCD11* and *CDC123* in comparison to the unaltered strain K842 (wt). -/*SUI2*, etc. = heterozygous deletion of the respective gene. Strains: K842, W12626, W8907, W9883, W4443. **A:** Tabellary doubling times. MSE = Mean square error. **B:** Graphic depiction of doubling times with MSE.

2.3.2 Gcd11(1-521) is the minimal requirement for cell viability

As a model for eIF2 dysfunction, yeast with C-terminally truncated Gcd11 was used, as the modification affects all aspects of eIF2 assembly, including interaction of Cdc123. The model was used to investigate the connection between eIF2 function and cell cycle in terms of cell cycle progression and requirements for cell cycle entry. The pFA6a system (see section 5.2.3) was used to establish diploid, heterozygous yeast strains with truncated, endogenous *GCD11* alleles, coding for Gcd11 variants 1-519, 1-520, 1-521 and 1-522. For each strain, the intact 3'-end of one *GCD11* gene copy was replaced with an alternative, shorter 3'-end and a KanMX6 resistance cassette, which was used to select for transformed cells. The diploid yeast strains were sporulated and their tetrads dissected, to test the viability of their offspring with only the truncated *GCD11* allele and to obtain the haploid daughter strains. All viable colonies that had emerged from germinated spores were spotted on XY-D+G418 plates to test for the truncated

alleles. The analysis showed that *GCD11(1-521)* was the shortest allele to support cell growth. The haploid colonies were visibly smaller than the colonies with an intact *GCD11* allele. Variants 1-519 and 1-520 did not give rise to viable haploid yeasts and those with *GCD11(1-522)* grew at normal rates, indistinguishable from yeasts with wild type *GCD11* (figure 41). For all following experiments, *GCD11(1-521)* was chosen, as it showed visibly impaired eIF2 function, but was still viable. Two colonies, one MATa and one MATα, were selected and used in all following experiments. These strains and all strains derived from them are referred to as G521 in the following text.

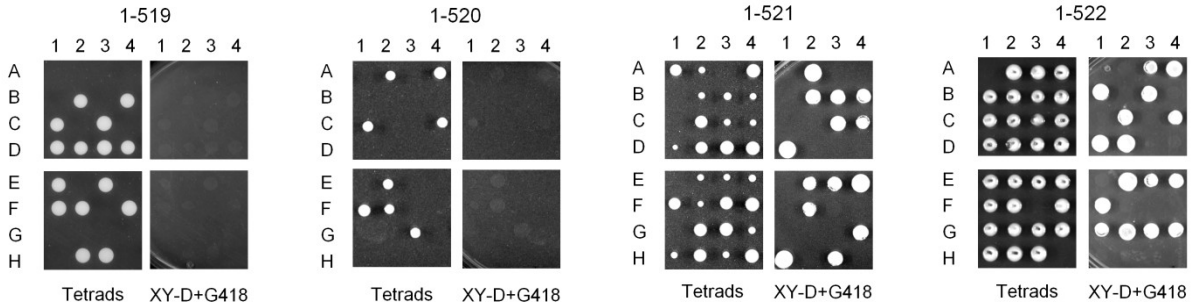

Figure 41: Tetrad dissection of four heterozygous yeast strains with one truncated *GCD11* allele. For each strain, the respective truncated Gcd11 variant is indicated on top. Colonies that had emerged from germinated spores were spotted on XYD+G418 to test for presence of the 3'-truncated allele. Diploid strains with Gcd11(1-521): W15565. Derived haploid strains: W15566, W15567.

2.3.3 Activation of ISR in G521

Reduced eIF2 function often goes along with activation of the ISR, which can be tested by measuring Gcn4 expression. Gcn4 expression was tested in G521 and K699 in a β-galactosidase reporter assay. The strains were transformed with a reporter plasmid in which the lacZ gene was fused to the 5'-leader of Gcn4 (described in Hinnebusch, 1985). As explained in section 1.1.4, low TC abundance favors the translation of mRNAs with such uORFs, hence increasing expression of the lacZ reporter gene. The assay was performed as explained in section 5.2.5. K699 had a β-galactosidase activity corresponding to 6.2±1.7 Miller units, whereas the expression was increased by a factor of 5 in G521, at 31.8±4.9 Miller units (for raw data, see table S12). These results meet the expectations for a strain with C-terminally truncated Gcd11, in which TC formation is likely reduced.

Next, Gcd11 expression in G521 was analyzed in comparison to that of K699. In a Western Blot quantification, Gcd11(1-521) expression was found to be only ~33% of Gcd11(wt). Since C-terminal truncation affects Cdc123 binding and this interaction was found to be important for eIF2γ stability in a different experiment (see 2.2.6), increased degradation could be the underlying cause for the low expression level. Alternatively, the C-terminus might contain an important epitope for antibodies in the αGcd11 serum. Whether this is the case could be verified with FLAG-tagged versions of both

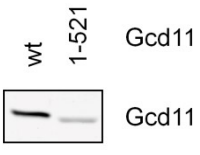

Figure 42: Gcd11 expression compared between K699 (wt) and W15566 (G521). Gcd11 was detected with a polyclonal αGcd11 serum.

proteins. The reduced amount of Gcd11 is unlikely to be the main cause of slow growth in G521, since the expected 50% reduction in the diploid strain, analyzed in section 2.3.1 had no major impact on doubling time.

2.3.4 Haploid yeasts with Gcd11(1-521) have a longer G1 phase

Growth- and cell division properties of G521 were characterized to specify the nature of its slow growth phenotype. Its generation time in XY-D at 25 °C, determined by overnight cultivation, was 2.8-3 hours, as opposed to 1.75 hours for the reference strain K699. To this end, the cell cycle profile was analyzed by flow cytometry (see section 5.2.2). The altered strain showed a significant shift to G1 phase and a smaller proportion of cells in G2/M, compared to K699. Then, cell cycle profiling was repeated in XY medium with glucose, glycerol and acetate to assess the impact of poor carbon sources that are not anaerobically fermentable on both strains. Interestingly, a significant G1 shift was observed for both K699 and G521 in poor carbon sources, but the impact of Gcd11 truncation was no longer visible in the cell cycle profile (figure 43A, B; for exact numbers, see table S13). Two models, explaining the effect, are conceivable. First, the bad carbon sources could create a new bottle neck for cell metabolism that makes the reduced eIF2 activity in G521 mostly irrelevant. Second, cross-talk between glucose signaling and eIF2 function, e.g. via the ISR, could make G521 less susceptible to a response that prolongs G1 phase in media with suboptimal carbon sources. Note that while cell cycle profiles of K699 and G521 were very similar in XY-Gly and XY-A, doubling time was still longer in G521, though the difference was smaller than in XY-D (3 h vs. 3.5 h in XY-Gly). *GCN4* expression itself had no negative effect on G521, as deletion of *GCN4* did not normalize doubling time or cell cycle profile (figure 43C). Forward scatter (FSC) data from K699 and G521 was used to estimate average cell size. The data suggested that G521 cells were slightly larger in size, which could be a mechanism of compensation for lower biosynthetic capacity (figure 43D).

Another marker for G1 phase is the expression level and the localization of Sic1. The inhibitor of G1/S transition is expressed in G1 phase and localized in the nucleus, where it inhibits Clb-Cdk1 complexes (see section 1.2.3). The degradation of Sic1 marks an important step for passing START. Overall Sic1 expression in a yeast culture thus depends on the proportion of cells in G1. Indeed, WB analysis of G521 in comparison to wild type cells showed increased Sic1 expression, consistent with cell cycle profiles (figure 44A). Sic1 localization and abundance was then investigated in confocal microscopy. Based on G521, a strain with $Sic1^{GFP}$ and 3xCherry-NLS was created by cross-breeding and tetrad dissection. The GFP tag allows visualization of Sic1, whereas the red fluorescent 3xCherry protein with the nuclear localization signal (NLS) from Swi5 marks the nucleus. Static images of the Gcd11(wt) strain and G521, grown in XY-D or XY-Gly were taken. Using the nucleus counter plugin from ImageJ, the total numbers of nuclei, indicated by the red mCherry-NLS signal, were compared to the numbers of nuclear $Sic1^{GFP}$ signals. For the wild type strain, grown in XY-D, 18±4.7% of cells had a nuclear $Sic1^{GFP}$ signal above the threshold, whereas for 37±5.5% of G521 cells in the same medium, this was the case. The difference disappeared in XY-Gly medium, where 43±6.6% of wt cells and 40±6.9% of G521 cells had a nuclear $Sic1^{GFP}$ signal (see figure 44B, C and table 7, for detailed data see table S14/S15).

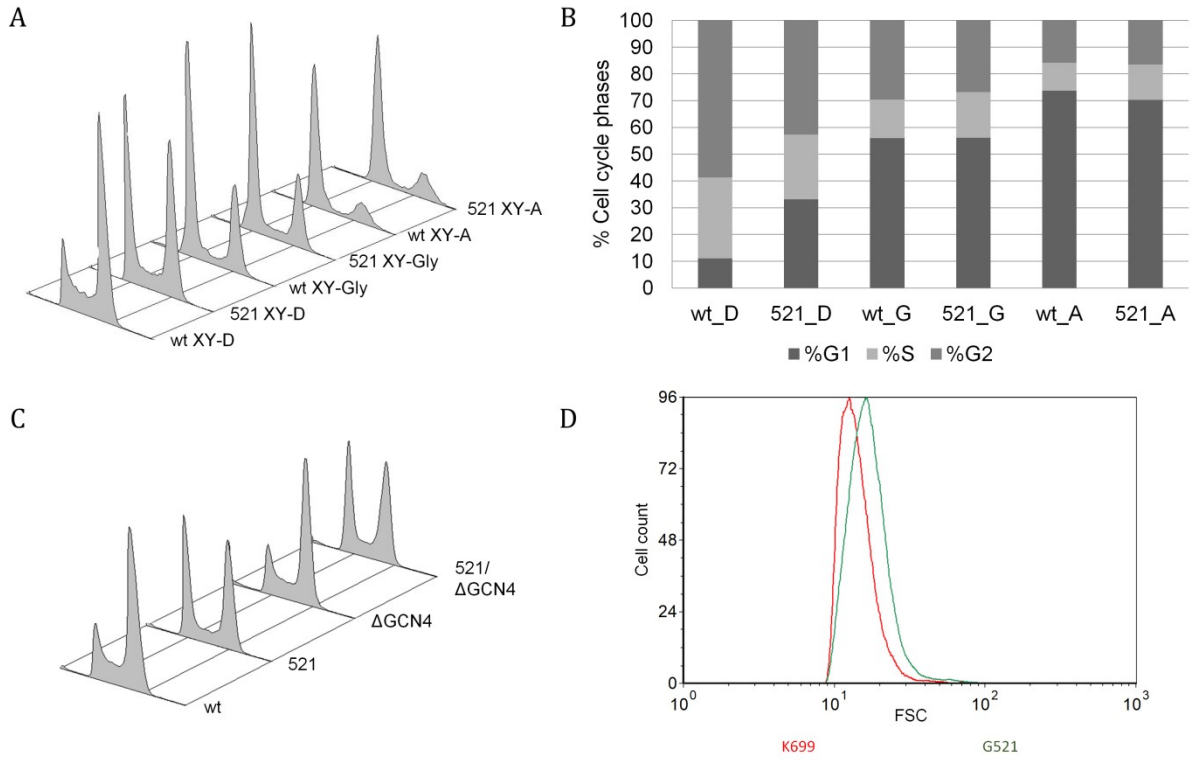

Figure 43: Flow cytometric analysis of strain G521 in comparison to K699. **A:** Cell cycle profiling of K699 (wt) and W15566 (G521) in XY medium with three different carbon sources: Glucose (D), glycerol (Gly/G) and acetate (A). **B:** Graphic display of cell cycle phase distribution in (A). wt_D = wild type strain, grown in XY-D medium, etc. **C:** Cell cycle profiling in K699 and G521 and derived strains with GCN4 deletion. Strains: K699, W15566, W14785, W15747. **D:** Forward scatter plotted against cell count as a surrogate for average cell size in K699 and G521.

Quantification of nuclear Sic1 can thus be used as an additional tool to assess the proportion of yeast cells in G1 phase. The data corroborated the flow cytometric- and Western Blot data. To summarize, slow growth of eIF2 deficit mutants is associated and primarily caused by an extended G1 phase.

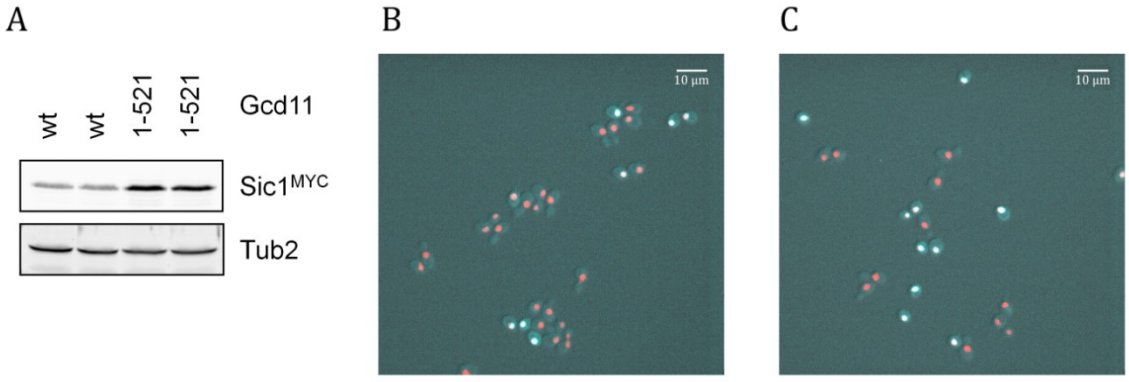

Figure 44: Quantification of Sic1 expression and localization. A: WB quantification of Sic1 levels in wild type yeast strains (MATa and MATα) and MATa and –α variants of G521 (from left to right), grown in XY-D. Sic1 was C-terminally MYC-tagged for antibody detection. Strains: W4331, W4332, W16293, W16294. **B, C:** Static images of yeast strains based on K699 (B, W13701) and G521 (C, W15753) with GFP-tagged Sic1 and 3xCherry-NLS.

Table 7: Summary of nuclear Sic1 quantification

Gcd11	Medium	% Sic1 in Nucleus	% no Sic1	MSE (%)
wt	XY-D	18.1	81.9	4.7
wt	XY-Gly	42.9	57.1	6.6
1-521	XY-D	36.6	63.4	5.5
1-521	XY-Gly	39.6	60.4	6.9

2.3.5 Smaller birth size in cells with impaired eIF2 function

For an in-depth analysis of cell cycle progression in G521, cell division of individual cells had to be observed over a longer period of time. Morphological changes, e.g. bud formation and cytokinesis can be studied best if the cell borders are visible at a high resolution (see section 5.2.6). For G521 and the wild type reference, strains with N-terminally GFP tagged Sso1 were created. Sso1 is a membrane-associated t-SNARE protein and its fusion with GFP creates a fusion protein that visibly highlights the cell borders. The strains were grown in XY-D and placed in an iBidi chamber, covered by a piece of SD++ agarose. During the recording, the cells were kept at 30 °C. Pictures were taken in 15 min intervals for the wt strain and 20 min intervals for G521 (see figure 45A, B). Thereby, phototoxic stress was kept at a minimum during the 6-8 h long recordings. The time lapses were taken to analyze bud formation, cytokinesis, time intervals between these events, cell size and the relationship between those parameters. An inverse relationship between cell size at the time point of cytokinesis and the time interval until formation of a bud was observed (figure 45C). This time interval roughly corresponds to the duration of G1 phase. Unsurprisingly, G1 phase takes longer in small cells, since they contain smaller amounts of mitochondria, ribosomes and proteins of the DNA replication machinery, whose biochemical activity is vital for the progression through cell cycle. They need to grow to a certain size first to be fit for mitosis. In G521 cells, G1 phase took longer for cells of all sizes, as their impaired ribosomal machinery takes longer for that growth to take place. Some of the smallest cells needed up to 2.5 h for their progression through G1 and generally, cells were more heterogeneous in G521 than the wild type strain. These results are also a reminder that the doubling time of a given strain, grown under defined conditions, is merely an average of millions of cells in the culture, while individual cells may take significantly shorter or longer to complete one cycle of cell division.

A very different observation was made for the time needed to complete the cell cycle. The time from the start of bud formation to cytokinesis can be used as a morphological proxy for progression through S-, G2- and M-phase. Here, no correlation was found between cell volume and time needed; in addition, no significant difference between wt and G521 was observed (figure 45D). These data fit to the idea that the requirements for cell cycle entry must be fulfilled before the START checkpoint can be passed, but cells fully commit to cell cycle once having passed the checkpoint. This also suggests that G521 can indeed compensate its metabolic insufficiencies to pass through mitosis, undisturbed by its decreased biosynthetic capacity.

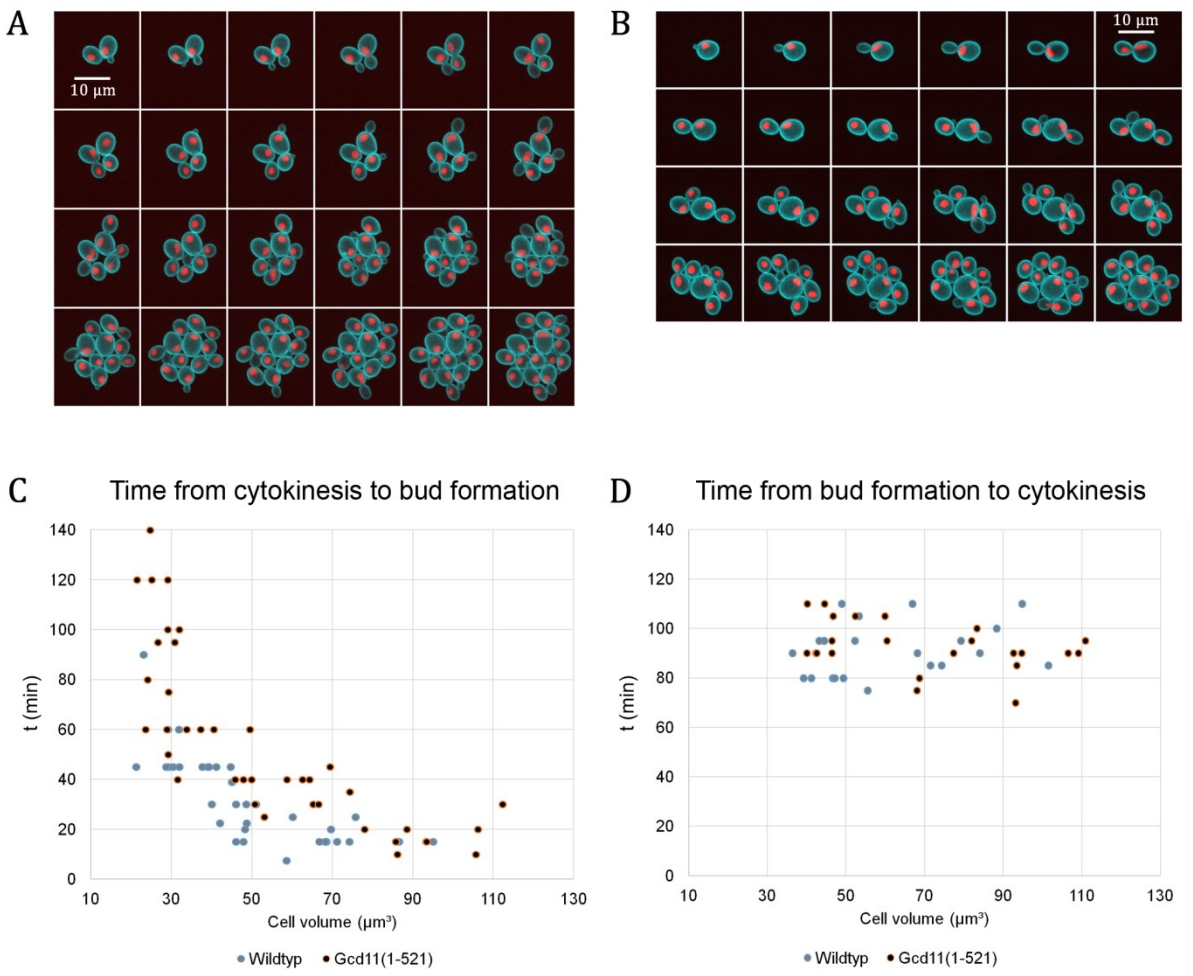

Figure 45: Time lapse of cell divisions in control strain and G521 for visual analysis of cell division. **A:** Time lapse of cell division in wild type strain (W10241) over a time span of 345 min (15 min intervals) **B:** Time lapse of cell division in G521 (W15770) over a time span of 460 min (20 min intervals). **C:** Cell volume at cytokinesis plotted against the time until a bud is be formed after cytokinesis. **D:** Cell volume at the start of bud formation plotted against the time needed from the start of bud formation to cytokinesis.

Yeast cells continue to grow throughout all cell cycle phases and tend to increase in size the more cell cycles they have completed. Newly born cells are generally much smaller than their mothers. While having the same DNA content, their biosynthetic capacity is much lower. It was therefore of interest to examine aged cells and newly born cells separately. Using the same timelapses as before, several differences between wt and G521 were identified and quantified. Cells that had just separated from their mother cell and formed their first bud were of the same average size in both strains (figure 46C), while their birth size was significantly smaller: ~40 μm^3 for wild type cells and only ~30μm^3 for G521 cells (figure 46D). The smaller birth size necessitated a prolonged G1 phase and indeed, the time from budding to formation of the first bud was around 45 min in wt cells but on average 80 min in G521 (figure 46F). In aged cells, the difference between both strains was smaller (figure 46G), indicating that the reduced biosynthetic capacity became less of a limitation as the cells increased their volume from cell cycle to cell cycle. The combined duration of S-, G2- and M-phase, as seen in figure 46H, hardly differed between strains. Growth of the bud takes place during this period, which explains why

G521 with its slower growth gives rise to smaller daughter cells. Average cell size at the start of bud formation was slightly larger in G521 (figure 46A), though the difference was more pronounced in aged cells (figure 46B). Taken together, these data suggest a model where G521 cells sense their lower biosynthetic capacity and compensate for it with increased cell volume. Their increased doubling time is largely caused by the small size of newly born cells, which need more time than wild type cells to reach a size appropriate for cell cycle entry.

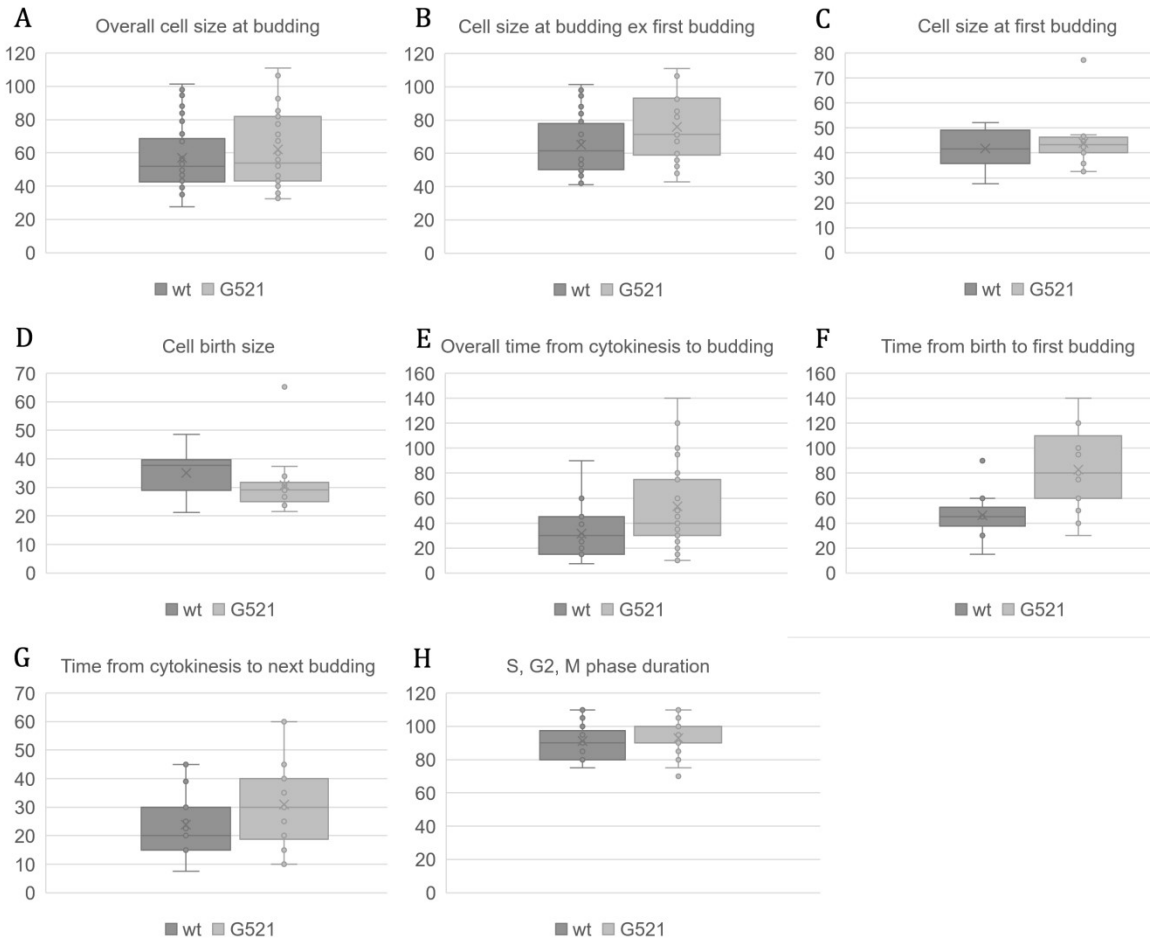

Figure 46: Cell size and cell division in G521 and wild type yeast. Volume is given in μm^3, time in minutes. The number of cells included in each data set is indicated as follows: n(wt); n(G521) **A:** Cell volume at the time point of bud formation, averaged over all cells (n = 37; 39). **B:** Volume of cells at bud formation, first budding excluded (n = 24; 22). **C:** Volume of cells at formation of their first bud after birth (n = 13; 17). **D:** Volume of cells at birth (n = 13; 17). **E:** Time interval from birth/ cytokinesis to bud formation, averaged over all cells (n = 37; 39). **F:** Time interval from cytokinesis to first bud formation after birth (n = 13; 17). **G:** Time interval from cytokinesis to next bud formation, newly born cells excluded (n = 24; 22) . **H:** Time interval from bud formation to completion of cytokinesis (n = 21; 23).

3 Discussion

Translation initiation factor 2, which consists of three protein subunits (α, β, γ) and forms a ternary complex (TC) with GTP and Met-tRNA$_i^{Met}$, is a fundamental component of the translation machinery in archaea and eukaryotes. Its assembly into a trimeric protein complex seems to occur spontaneously in archaea but largely relies on the ATP grasp-related protein Cdc123 in eukaryotes. Originally linked to cell cycle progression (Ohno et al., 1984), it was later found that Cdc123 is involved in the regulation of eIF2 abundance. At first, it was thought that Cdc123 controlls the degradation of eIF2γ (Bieganowski et al., 2004), but later studies demonstrated that it is indeed needed for eIF2 assembly (Perzlmaier et al., 2013; Richter, 2006). While it was known that Cdc123 binds to the C-terminus of eIF2γ and facilitates the binding of eIF2α and –β, the order of the assembly and how Cdc123 affected eIF2γ remained unclear. In this work, a more detailed model for eIF2 assembly and intersubunit interactions of eIF2 was established. Experiments in human cell culture indicate that eIF2 assembly is fundamentally similar in yeast and human cells. Moreover, a potentially important link between Cdc123 function and eIF2γ self-interaction was uncovered. An investigation into the stability of human eIF2γ in yeast cells revealed a stabilizing, transient interaction of heIF2γ with hCdc123, which strongly hints towards a permanent modification of eIF2γ, covalent or allosteric, that is catalyzed by Cdc123. Mutational analyses of eIF2γ domain 1 mutants in yeast demonstrated how eIF2 assembly and potentially TC assembly fail, if the GTP binding properties or structure of domain 1 are compromised. Finally, the effect of deficient eIF2 function on cell cycle progression was assessed in flow cytometry and live cell microscopy. The use of a yeast strain with C-terminally truncated Gcd11 confirmed the difficulties of eIF2 deficient mutants to pass START. Additionally, a link between low biosynthetic capacity, small birth size and prolonged G1 phase, that had been established pharmacologically before (reviewed in Polymenis and Aramayo, 2015), was replicated in a yeast strain under normal growth conditions.

3.1 New model for eIF2 assembly

Many large protein complexes or protein-RNA complexes rely on assembly factors or scaffold proteins to kinetically enable the assembly of in some cases dozens of subunits and cofactors. Since eIF2 consists of only three subunits, the requirement for an assembly factor seems counterintuitive. Given that no such factor was found in archaea, it seems likely that while eIF2 could be able to assemble spontaneously, evolution has favored a mechanism that requires the protein Cdc123, owing to the higher complexity of eukaryotic cellular biochemistry and a greater need for regulation compared to archaea. The data obtained in this work suggest an assembly mechanism in which eIF2 is formed in three steps. First, Cdc123 binds eIF2γ at its C-terminus. This triggers a structural change in the protein. Covalent modification of eIF2γ by Cdc123 is conceivable and would be consistent with its membership in the family of ATP grasp proteins, which catalyze carboxylation or phosphorylation of biomolecules (Fawaz et al., 2011). However, an enzymatic activity of Cdc123 has yet to be found, which makes a mere allosteric effect on eIF2γ the more likely mechanism. In yeast, interaction between domain 1 and domain 2+3 fragments of Gcd11 was shown in Y2H and Co-IP experiments. The binding of the two fragments to each other was stable enough to activate the reporter gene β-Galactosidase in the

Y2H assay and to withstand lysis of the yeast cells and the IP procedure. The interaction was interrupted by overexpression of Cdc123 in the same cells (see section 2.2.3). This intramolecular interaction could thus be a feature of immature eIF2γ. The self-interaction might prevent eIF2α and –β from binding, possibly by hiding important interaction surfaces. The discovery of human eIF2γ versions that bind Cdc123, but do not assemble into eIF2, demonstrates that binding of the two proteins is necessary, but not sufficient to elicit the putative conformational change of eIF2γ. The heIF2γ variant 1-464SQQ*, found in some patients suffering from MEHMO syndrome, seemingly forms an unproductive heIF2γ-hCdc123 complex that has trouble binding heIF2α and –β. It follows that the very C-terminus of human eIF2γ must have a vital role in its conformational maturation, assuming that the model proposed thus far is correct. After the change in conformation, eIF2α and –β bind eIF2γ. Their binding to –γ is not strictly dependent on each other (section 2.1.2) and may thus occur in arbitrary order. Evidence suggests that eIF2α binding quickly triggers the release of Cdc123, as their interaction is direct, but few complexes containing eIF2α and Cdc123 can be found in Co-IP (sections 2.1.3, 2.1.7). The step is also rate-limiting for eIF2 assembly, as demonstrated by the inverse relationship between eIF2α abundance and eIF2γ-β-Cdc123 assembly intermediates (section 2.1.5). Quantification of Cdc123 complexes with eIF2 subunits revealed that eIF2γ-Cdc123 complexes are a lot more abundant than complexes containing eIF2β (~20%) or –α (<5%). These numbers are consistent with the role of eIF2α as a release factor, but compatible with a model in which the order of eIF2α and eIF2β binding to eIF2γ does not necessarily occur in a strict order. eIF2γ is the primary interaction partner of Cdc123, which explains the high abundance of eIF2γ-Cdc123 complexes. eIF2β later binds this dimeric complex but on its own does not trigger the release of Cdc123. Only after the binding of eIF2α, the interaction between eIF2γ and Cdc123 is destabilized and the assembly factor is released. Accordingly, complexes containing Cdc123 and eIF2α are very short-lived and least abundant. However, it is likely that efficient release of Cdc123 by Sui2 can only occur if Sui3 is also bound to eIF2γ, as Gcd11 mutants with a defect in Sui3 binding can be toxic if overexpressed (section 2.2.4). The relative levels of complexes containing Cdc123 and eIF2 subunits are similar in yeast and humans, suggesting a similar assembly mechanism (see section 2.1.7). It was demonstrated before that in yeast, deletion of the essential *CDC123* gene can be rescued by combined overexpression of Gcd11 and Sui2 (Richter, 2006). Since in wild type cells, Sui3 binding does not strictly depend on prior binding of Sui2, but overexpression of Gcd11 and Sui2 rescues assembly in the mutants, the effect might be explained by a stabilization of the assembly competent conformation of Gcd11 by Sui2 binding. Recycled eIF2γ that was used in translation initiation before and a fraction of newly synthesized eIF2γ proteins have GDP in their nucleotide binding pocket. GDP release is catalyzed by eIF2B, GTP can bind and TC formation is completed by the binding of Met-tRNA$_i^{Met}$.

In conclusion, the most important findings about eIF2 assembly are the independence of Sui2 and Sui3 binding, the need for an intact domain 1 for binding of both eIF2α and -β, and the role of Sui2 as the Cdc123 release factor. An extremely interesting aspect that requires further investigation is the potential self-interaction of eIF2γ as a hallmark of an immature protein and the reorganization of eIF2γ structure by Cdc123 that ends the self-interaction and enables eIF2 assembly.

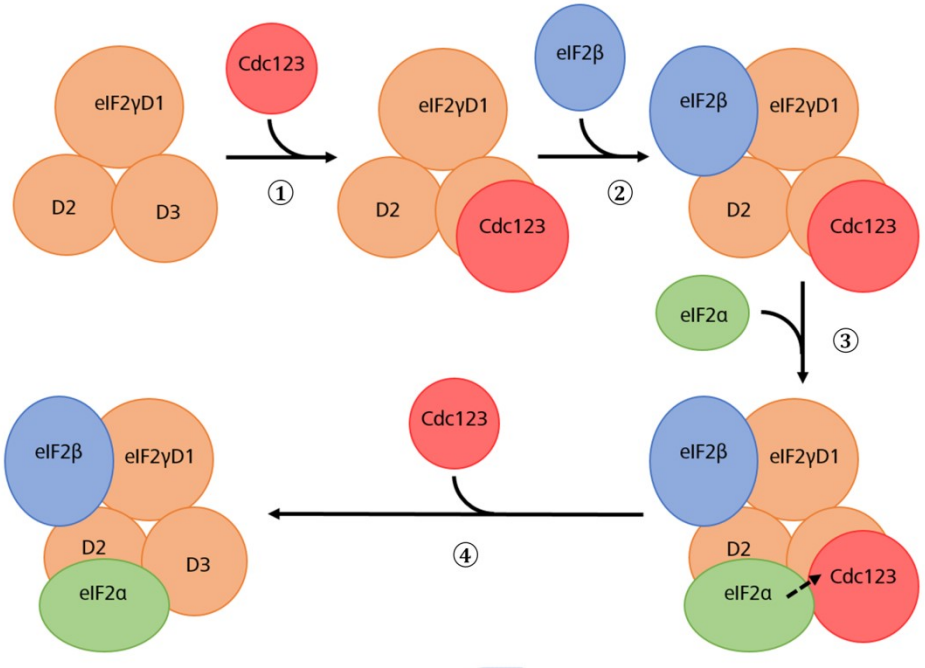

Figure 47: New model for eIF2 assembly. **(1)** Cdc123 binds to the C-terminus of eIF2γ. A conformational change, possibly opening up interaction surfaces for eIF2α and –β, is introduced. **(2)** eIF2β binds to eIF2γ. **(3)** Upon binding of eIF2α, the interaction with Cdc123 with eIF2γ is destabilized. Steps 2 and 3 may occur in a defined order or at the same time, but 3 is rate limiting**. (4)** Cdc123 is released from the trimeric eIF2 complex.

To definitively answer, whether the model proposed here or Young-Baird et al's model is more accurate, the experiment shown in section 2.1.5 would have to be repeated and refined. Reducing the background signal, e.g. by using an αFLAG matrix with lower unspecific binding for the immunoprecipitation, might expose a potential effect of Gcd11 overexpression on the Cdc123-Sui2 interaction.

3.2 Impact of eIF2γ mutations on eIF2 function

In this work, multiple mutants of yeast eIF2γ (Gcd11) were created and analyzed to assess their functionality in eIF2 assembly as well as the consequences of their overexpression on eIF2 assembly and downstream processes. The impact of their overexpression on cell viability depends on the stage of eIF2 assembly that is affected.

Gcd11 variants that show only defects in Cdc123 binding are nonfunctional or hypofunctional proteins. If expressed alongside functional Gcd11, they do not interfere with cellular biochemistry in a negative way, other than using up a small proportion of cellular resources. These variants include C-terminally truncated Gcd11 proteins, e.g. the low functioning 1-519 and nonfunctional 1-514 mutants. However, these proteins cannot functionally replace endogenous Gcd11. Failure to form assembled eIF2 reduces TC availability, leads to decreased protein synthesis and activates the ISR. One example for such an eIF2γ mutation found in humans is the I464SQQ* variant, found in a few families affected by X-linked intellectual deficiency (Moortgat et al., 2016). Hyperactive ISR seems to play a major role in pathogenesis

and its inhibition normalizes growth of iPSCs, derived from patient cells (Young-Baird et al., 2019b).

Gcd11 variants that bind Cdc123 but do not assemble properly do not support cell growth and additionally hinder eIF2 function even when functional Gcd11 is present at physiological levels. Examples for such Gcd11 variants are N-terminal truncation mutants that do not bind Sui2 and Sui3 (e.g. 201-527), the cystein mutants C150A and C174A and subunit specific binding mutants (e.g. D403R and V281R). Mutation of zinc binding amino acids C150 and C174 results in a structural change of a protrusion in domain 1 of Gcd11 and, similar to removal of amino acids from the N-terminus, likely compromises the structure of domain 1. The explanation that is best supported by data is that these variants sequester Cdc123, because efficient release of the assembly factor requires completion of assembly. Since all eIF2 subunits are expressed at up to ten times higher levels than Cdc123, the pool of free Cdc123 quickly drops below the threshold for cell viability if a significant amount of Gcd11 proteins permanently bind the assembly factor. The extent to which these Gcd11 variants are toxic and the maximum expression level of each mutant that is compatible with cell growth can provide additional information about eIF2 assembly. The N-terminal truncation mutants and the double mutant V281R/D403R, all of which cannot bind Sui2 or Sui3 are toxic even at endogenous expression levels. Transformation of yeast cells with variant 91-527, expressed with p*GCD11*, yields a low number of transformants, all of which express the protein at levels that are significantly lower than the endogenous level (see figure S3). The double mutant V281R/D403R and cystein mutants C150A and C174A cannot be expressed under p*GCD11* at all. The Gcd11 variants V281R and D403R, which do not bind Sui3 or Sui2 but bind the respective other subunit, can be expressed at endogenous levels but are toxic at higher expression levels (compare sections 2.1.2 and 2.2.4). This suggests that Cdc123 remains bound to Gcd11 more strongly if neither subunit can bind. While Sui2 is more important in this regard, as shown by the higher toxicity of D403R compared to V281R, Sui3 binding also enhances Cdc123 release, because the double mutant is multiple times as toxic as either single mutant. Since Cdc123 availability becomes a bottleneck for eIF2 assembly when Cdc123 sequestering mutants are expressed at high enough levels, overexpression of the assembly factor resolves the issue and restores cell growth to normal (see sections 2.2.4, 2.2.5). The eIF2γ mutation I222T, identified in some patients with MEHMO syndrome, showed decreased affinity for eIF2β. The carriers of the mutation had similar symptoms as those with the 1-464SQQ* variant, but overall, the syndrome was milder (Borck et al., 2012). Since the mutated copy of EIF2S3 is the only source of eIF2γ protein, sequestration of Cdc123 does not play a role in the molecular etiology of the syndrome. However, it is still conceivable that eIF2 function in these patients could profit from higher Cdc123 levels.

In this study, three Gcd11 variants with point mutations that affect the G-nucleotide related functions of Gcd11 were analyzed. The spectrum of mutants includes the GTP binding motif mutants S114A/T115A (ST/AA) and K250A as well as the ΔSw1 motif deletion mutant. The effects these mutants had on eIF2 function were more complex than those of the aforementioned assembly mutants and required a more sophisticated approach. Combined Gcd11(mut) and Sui2, Sui3, Cdc123 overexpressions in cell growth assays was used to assess the mechanisms underlying their toxicity. The toxicity of all three proteins at least in part stems from sequestration of Cdc123. ΔSw1 is able to assemble into eIF2 (see section 2.2.5.1) and cannot be

rescued by overexpression of Cdc123 or any other combination of Sui2, Sui3 and Cdc123 (table 6). It was concluded that the protein affects downstream processes, e.g. the interaction with eIF2B. Lack of the ΔSw1 motif affects GTP binding and likely also the conformational change Gcd11 undergoes as GTP is hydrolyzed. IP data from Sandra Rast (Rast, 2020) showed that ΔSw1 is uncompromised in its ability to bind Gcd6 and Gcd7, two proteins from the eIF2B complex. It is thus conceivable that a tetrameric complex, containing Gcd11(ΔSw1), Sui2, Sui3 and Cdc123, sequesters eIF2B in a similar fashion as it does Cdc123. This is supported by the fact that like Cdc123, eIF2B is expressed at ~2-10 fold lower levels than eIF2 (Wang et al., 2012). Interference with translation initiation itself remains another possibility. If ΔSw1 is integrated into the 43S PIC, its lack of G-protein functionality would disrupt start codon recognition and transition to the P_{in}/ closed 40S state. In order to examine this possibility, interaction with 43S components, e.g. eIF3, eIF4 and/or ribosomal proteins would have to be tested. Quantification of $tRNA_i$ binding by IP of Gcd11(ΔSw1), followed by qPCR, would provide additional information about its integration into TCs. Gcd11 variant ST/AA was rescued partially by Cdc123 but rescue was reversed if in addition, Sui2 and Sui3 were overexpressed (table 6). The most reasonable explanation for this is that Cdc123 overexpression alleviates the negative impact of Cdc123 sequestration but also enhances integration of the ST/AA variant, whose ability to bind Sui2 and Sui3 is somewhat compromised, into eIF2 complexes. The aberrant eIF2 complex then affects downstream processes, possibly in a similar fashion ΔSw1 might do. Overexpression of Gcd11(K250A) was fully rescued by coexpression with Cdc123, because the protein has a severe Sui3 binding deficiency and does not easily assemble into eIF2 complexes (see figure 2.2.5.2). Additional overexpresseion of Sui3, however, enhances eIF2 assembly and disrupts cell growth again, possibly due to titration of Sui2.

The mutational analyses highlight how both Cdc123 availability and abundance of active eIF2B can become bottlenecks in the eIF2 cycle. While eIF2B inhibition as a consequence of eIF2α phosphorylation has been established as the major target for regulation of translation initiation, no comparable mechanism has been found for Cdc123.

3.3 Interdomain interaction of eIF2γ

The Gcd11 mutant R510D unites many features of eIF2γ mutations but is different in other regards. When looking only at eIF2 assembly, the protein behaves in a very similar fashion as C-terminally truncated Gcd11 variants, with reduced Cdc123 binding and lower integration into eIF2 complexes. As has been established earlier, interaction with eIF2B occurs only via trimeric eIF2. Accordingly, less complexes of Gcd11(R510D) with eIF2B are found compared to the wild type protein. The mutant is insufficient as sole source of Gcd11 in yeast cells (section 2.2.1). When overexpressing the mutant protein and Cdc123 at the same time, the difference to the wild type protein in terms of eIF2 assembly and interaction with eIF2B becomes smaller. However, this does not restore cell viability but instead creates a lethal dominant negative effect. Judging from the experience gained from other dominant negative mutations, a logical assumption would be that eIF2 complexes, containing the mutated Gcd11(R510D) protein affect eIF2B function or translation initiation negatively but it requires high levels of the protein and its assembly factor to reach toxic levels of the aberrant complex. As to why R510D exerts a

dominant negative effect, the available data is not sufficient for a definite conclusion. However, the newly gained information, combined with older data can be used to outline a rough model of the role residue R510 has. As described earlier, its mutation to histidine results in a slow growth phenotype and inaccurate start codon recognition. The slow growth can probably be explained by low TC availability. Start codon recognition, on the other hand, is not dependent on Cdc123 and low availability of TC generally results in a Gcd^-, not a Sui^- phenotype (Harashima and Hinnebusch, 1986). Interestingly, residue R510 is in close proximity to residue E231 in domain 1. The homologous amino acids R406 and E131 contact each other in archaea (figure 48, Kashiwagi et al., 2019; Panvert et al., 2015). The crystal structure of Gcd11, which was taken from an eIF2-eIF2B complex, shows that the amino acids are close to each other but are not in direct contact (figure 48). Possibly, the two residues contact each other directly in the premature, self-interacting state of Gcd11 but are separated by interaction with Cdc123. Archaea do not rely on a factor for eIF2 assembly, which might explain why the positioning of the homologous Asp and Arg residues to each other differs between *S. solfataricus* and *S. cerevisiae*. Since Cdc123 is required to facilitate the interaction with Sui2 and Sui3, and the positioning of both proteins is essential for accurate start-codon selection (Hinnebusch, 2017), the altered structure of Gcd11 in the R510H mutant might also impact the structure of trimeric eIF2 sufficiently to influence fidelity of start codon recognition. Mutation of R510 to Asp rather than His, which constitutes a more drastic alteration, affects the function of eIF2 even stronger and might thereby become toxic if the protein is integrated into eIF2 complexes.

While a possible involvement of R510 in interdomain interaction and the link to Cdc123-mediated eIF2 assembly are exciting thoughts, more data must be generated to validate the hypothesis. One important and potentially insightful experiment is the repetition of the IP and Y2H experiments that were used to test self-interaction (section 2.2.3) with Gcd11 mutant R510D. If R510 is a key residue for interdomain interaction, its mutation should weaken the interaction between the domain 1 and domain 2+3 fragments. Even more informative would be a Cryo-EM structure of Gcd11 variant 1-514 that cannot interact with Cdc123 or, alternatively, wild type Gcd11 from a yeast strain in which the deletion of Cdc123 has been rescued by overexpression of Gcd11 and Sui2. According to the described model, R510 and E231 would be in direct contact in the protein because the lack of interaction with Cdc123 prevents refolding.

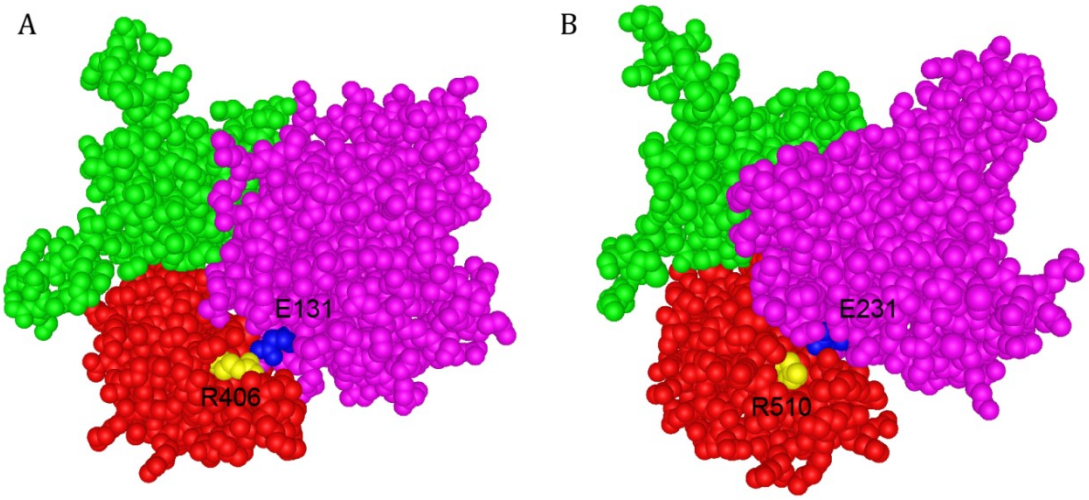

Figure 48: 3D structures of eIF2γ in archaea (A) and yeast (B). The homologous Arg residues (R404/R510) are highlighted in yellow, the homologous Asp residues (E131/E231) are highlighted in blue. Domain 1 is shown in magenta, domain 2 in green, domain 3 in red. aIF2 structure taken from Adomavicius et al. (Adomavicius et al., 2019, MMDB-ID: 6I7T), eIF2 structure taken from Dubiez et al. (Dubiez et al., 2015, MMDB-ID: 4RD6)

3.4 Mass spectrometric analysis of Cdc123 binding partners

Cdc123 is an essential protein in yeast and its deletion or inactivation causes G1 arrest. In yeast, its essentiality can be circumvented by combined overexpression of Gcd11 and Sui2. In this case, the lack of efficiency in eIF2 assembly is compensated by the higher abundance of eIF2 proteins. The essential function of Cdc123 is therefore the facilitation of eIF2 assembly. However, mass spectrometry analysis of Cdc123 binding partners in yeast cells and HEK cells indicated that a large proportion of Cdc123 proteins is in contact with nuclear transport proteins and proteins involved in pre-ribosomal processing. Surprisingly, their scores in the post-MS data analysis, which are calculated based on the number of identified unique peptides, were often on par with those of bona fide interaction partners, such as eIF2γ and –β (both species) or Chf1/2 (yeast). This raises the question whether Cdc123 has a function in the nucleus. Nuclear pore proteins interact with a wide variety of proteins, including many that are located in and fulfil their function in the cytoplasm. For that reason, their identification in mass spectrometry does not support the idea that Cdc123 is a nuclear protein on its own. The identification of nucleolar proteins, particularly such that participate in pre-ribosomal processing, however, justifies a deeper look into a possible function of Cdc123 unrelated to eIF2 regulation. Proteins with a dual function in translation and pre-ribosome processing are not unheard of; human eIF6 is both involved in ribosomal subunit joining and pre-ribosome processing (Sanvito et al., 1999). Interestingly, eIF6 was identified in this study as a binding partner of human Cdc123 (see table 2), which could indicate the participation of both proteins in the same complex, e.g. the pre-60S processing machinery. This could therefore be the startpoint for an investigation into yet unknown functions of Cdc123. To begin, one could use the *CDC123* deletion strain, rescued by Gcd11 and Sui2 overexpression, to look into a potential effect on pre-ribosome processing.

Another finding, raising important questions about eIF2 function in higher eukaryotes, was the identification of eIF2γ-like protein as a very strong interaction partner of hCdc123. Despite the strong interaction with hCdc123, the protein most likely cannot functionally replace the *EIF2S3*

gene product, because mutations in *EIF2S3* have major consequences in higher eukaryotes. According to tissue-specific gene expression data compiled on ensemble.org (Yates et al., 2020), both gene products are expressed in various tissues, including the developing brain. A different publication, which identified EIF2S3B as a retrogene, found significant expression levels only in testes, small intestine and skeletal muscle (Marques et al., 2005). Differential expression of EIF2S3 and EIF2S3B during development could explain why the latter does not functionally replace mutated EIF2S3 in MEHMO. Alternatively, the seven AA exchanges could be sufficient to alter the protein's function. One of the exchanges, T109M, indeed affects a verified phosphorylation site. Hence, it would be worthwhile to look into a potential regulatory function of eIF2γL. To this end, tagged versions of the protein could be expressed in yeast and HEK cells to analyze interaction with human eIF2 subunits and hCdc123. If the protein indeed has a regulatory function, it would be interesting to analyze the effect its overexpression has on translation initiation and ISR activation.

3.5 Role of the eIF2γ - Cdc123 interaction

Experiments by Semmelmann had demonstrated that overexpression of Gcd11 decreases the stability of endogenous Gcd11. It was concluded that the disproportionally high level of Gcd11 compared to Sui2 and Sui3 lead to a large pool of monomeric, unassembled Gcd11, which was more prone to degradation than Gcd11 in complex. A stabilizing effect of Cdc123 on the free pool was also discussed as a secondary mechanism of Gcd11 stabilization (Semmelmann, 2019).

The expression of human eIF2γ in yeast cells in this study revealed the very low stability of the protein in absence of hCdc123 (section 2.2.6). This effect was observed for both wild type heIF2γ and the mutant 1-464SQQ* variant. The stabilizing effect was not further enhanced by heIF2α or –β, which indicates that only hCdc123, but not assembly into trimeric eIF2 is necessary for the effect. However, heIF2γ can interact with yeIF2α, which could potentially enhance stability. Since heIF2γ(1-464SQQ*) assembles inefficiently compared to wt but is stabilized to the same degree, the stabilization could be independent from the mechanism by which Cdc123 facilitates eIF2 assembly. It is also not reliant on permanent association of the two proteins, as substoichiometric amounts of hCdc123 are sufficient to stabilize heIF2γ. These data suggest that Cdc123 introduces a stabilizing change into eIF2γ that occurs in both the human and yeast systems. The decrease of stability observed when Gcd11 was overexpressed likely stems from the disproportionate amount of Gcd11 molecules, for whose stabilization the endogenous expression level of Cdc123 was insufficient.

How exactly Cdc123 prepares eIF2γ for eIF2 assembly remains a complicated topic and is insufficiently explained by the available data. The fact that Cdc123 can stabilize eIF2γ in a transient interaction, even when that interaction does not facilitate eIF2 assembly, as seen for heIF2γ(1-464SQQ*), indicates that the putative structural rearrangement has more than one stage. This assumption is corroborated by the analysis of different hCdc123 mutants and their effect on heIF2γ and assembly of heIF2. The hCdc123 variants 1-314 were able to bind heIF2γ, but were not capable of facilitating heIF2γ's association with heIF2α. Similar to the observation for the interaction between heIF2γ(1-464SQQ*) and its binding partners, binding of heIF2β was less affected. As mentioned before, the mutated variants were also able to stabilize heIF2γ

(Dlugosch, 2019). The differential requirements for the stabilization effect and facilitation of eIF2α and –β binding show that the interaction between Cdc123 and eIF2γ is highly complex and worthy of deeper analysis.

3.6 eIF2 defects and cell cycle

Failure to form trimeric eIF2 and TC results in G1 arrest, as demonstrated by cell lines with temperature sensitive Cdc123 or shutdown of eIF2 subunit expression in yeast cells. The arrest does not occur because eIF2 and Cdc123 have a specific function in cell cycle progression, but because cells without sufficient TC fail to pass the G1-S transition checkpoint (Ohno and Kimura, 1984). As described earlier, nutritional availability, or, more broadly, ability to synthesize biomolecules and grow, is one of the most fundamental requirement for mitosis (Alberghina et al., 1998) and not met if an essential component of the translational machinery is missing (Weinzierl, 2011). In this study, the work on a yeast strain with a C-terminally truncated version of Gcd11, named G521, showed that cells with decreased TC activity have a disproportially prolonged G1 phase and ~40% of cells in a given population are in G1, unlike in wild type cells, where G1 phase is short and most cells have passed START. On the other hand, S-, G2- and M-phase are completed in similar time intervals by the mutant and wild type cell line (section 2.3.4). This indicates that the mutant cells sense their lower biosynthetic capacity and compensate for it in G1, e.g. by increasing the number of ribosomes and auxiliary protein complexes, including TIFs.

A variety of size sensing mechanisms has been uncovered and discussed before. One of those found in yeast is the Cln3-Whi5 sensor. According to Schmoller and others, the antimitotic protein Whi5 is present in yeast cells at almost constant molecule numbers, so that the concentration is highest in small cells and becomes gradually lower as cells grow. The pro-mitotic regulator Cln3 on the other hand is synthesized proportionally to cell size, as most proteins are. At a certain point, Cln3 wins the tug-of-war with Whi5 and the cell cycle block is removed (Schmoller et al., 2015). A few publications contested this view, as they did not find decreasing Whi5 concentrations over the course of G1 (Dorsey et al., 2018). Drastic increases in Cln3 expression due to bursts of glycolytic flux, metabolism and protein synthesis were proposed as the actual mechanism to overcome the Whi5 block (Litsios et al., 2019). Others yet found no correlation between a drop of Whi5 concentration and the spread of cell volumes of individual cells at the time point of entering cell cycle, but acknowledge the effect Whi5 levels have on cell size. According to these data, Whi5 dilution would be one mechanism among others (Barber et al., 2020). Yet another level of Cln3 regulation is the interaction with chaperones, that promote stability and nuclear localization of Cln3 (Moreno et al., 2019). Therefore, the mechanism of cell size control in yeast is unresolved as of 2020 and it is unlikely that one protein or one pathway alone is responsible for it.

How do the results obtained from the work on yeast strain G521 fit to the already published data? Do they favor the Whi5 dilution model or the metabolic burst model over the respective other?

First of all, the experiments show that the metabolic requirements for cell cycle entry are checked in each cell cycle before START, but biosynthetic capacity and related factors play at best a minor role in post-START cell cycle checkpoints. Cell cycle profiling via flow cytometry, Sic1 expression levels and Sic1 nuclear localization all demonstrate that a disproportionate amount of G521 cells are in G1 (section 2.3.4), likely because they need more time to prepare for cell cycle than wild type strains. Cell sizes at cell cycle entry are relatively similar in G521 and wild type control cells, but a tendency towards larger cells, particularly in aged cells, seems to exist in G521. The size difference was seen both in microscopic data (section 2.3.5) and in flow cytometry, where forward scatter (FSC) was significantly higher for G521 cells (section 2.3.4).

Since cell division cycles in wild type cells are ~40% shorter compared to G521, it can be estimated that biosynthetic capacity is lower to a similar degree. Cell volume, however, is not increased proportionally, which would be expected for a Whi5-only model, since Cln3 levels are roughly proportional to its rate of synthesis. Whi5 dilution is therefore unlikely to be the only mechanism of cell size control; this, however, does not constitute a contradiction of the Whi5 dilution model, which could describe one mechanism of cell size control among others.

Other data from this work seems to contradict Litsios et al.'s publication (Litsios et al., 2019), where increases in glycolytic activity were proposed to be at the top of the pathway that leads to Cln3 level increases. Both doubling time and cell cycle phase distribution were more similar between wt and G521 in media with poor carbon sources (glycerol, acetate) that are not metabolized in glycolysis. Poor carbon sources should therefore hamper G521's capability of having metabolic bursts as much as that of the wild type strain, rather than flattening the difference between the two strains.

The general importance of glucose levels and glycolysis as a pro-mitotic signal, however, is well established (Peeters et al., 2017) and compatible with the observations reported here. High translational activity might be a prerequisite for glucose-activated mitosis. In cells with high biosynthetic activity, the poor carbon sources create a bottleneck, but not in G521, where protein biosynthesis is already slow. Yeast cells react to poor media by decreasing the number of ribosomes. This also lowers the translation of the *CLN3* mRNA and delays cell cycle entry (Polymenis and Schmidt, 1997). While the total number of ribosomes might be normal in G521, the number of active 43S- and 48S PICs should already be lower in rich media due to a decreased number of TCs. The decrease of ribosome numbers in poor media therefore does not lower the number of actively translating ribosomes and does not impair cell growth as much as in wild type cells.

The link between protein synthesis activity and cell cycle entry, according to the data presented here and many previous publications, is conserved over most, if not all eukaryotes. From an evolutionary point of view, it seems reasonable that translation initiation, which is the first step of protein synthesis and a known target for cell cycle regulation, would also be sensitive to glucose availability. eIF2 is at the center of the ISR to respond to cell stressors and poor availability of nutrients and it is not unreasonable to think that it could be used as a sensor for the general fitness of cells to enter the cell cycle.

4 Materials

4.1 Chemicals

Table 8: List of chemicals

Chemical	Manufacturer
3xFLAG peptide (5 mg/ ml in TBS pH = 7.4)	Sigma Aldrich, St. Louis, USA
Amino acids, uracil, adenine	Sigma Aldrich, St. Louis, USA
Anti-FLAG Affinity Gel (1E6 antibody)	Bimake, Houston, USA
Anti-FLAG M2-Agarose	Sigma Aldrich, St. Louis, USA
AEBSF	Serva, Heidelberg, Germany
Ampicillin	Sigma Aldrich, St. Louis, USA
Aprotinin	Fluka, Seelze, Germany
Blasticidin	Invivogen, San Diego, USA
β-Mercaptoethanol	Applichem, Darmstadt, Germany
BSA	Sigma Aldrich, St. Louis, USA
Dimethyl formamide (DMFA)	Sigma Aldrich, St. Louis, USA
dNTPs	New England Biolabs, Ipswich, USA
G418	Calbiochem (Merck), Burlington, USA
Guanidinium hydrochloride	Sigma Aldrich, St. Louis, USA
Hygromycin B	Sigma Aldrich, St. Louis, USA
Nourseothricin (NAT)	Clontech (Takara Bio), Kusatsu, Japan
ONPG	Applichem, Darmstadt, Germany
Pepstatin	Sigma Aldrich, St. Louis, USA
Sodium lauryl sulfate (SDS)	Roth, Karlsruhe, Germany
Tetracyclin	Roth, Karlsruhe, Germany
Zeocin	Invivogen, San Diego, USA
X-Gal	Applichem, Darmstadt, Germany

4.1.1 Enzymes

Table 9: List of enzymes

Enzyme	Manufacturer
KOD polymerase	RG Seufert
Novozyme 234	Novozyme, Bagsværd, Denmark
Proteinase K	Roche, Basel, Switzerland
Restriction enzymes	New England Biolabs, Ipswich, USA
Recombinant Shrimp Alkaline Phosphatase	New England Biolabs, Ipswich, USA
RNase A	Applichem, Darmstadt, Germany
T4 ligase	New England Biolabs, Ipswich, USA
Taq polymerase	RG Seufert

4.1.2 Buffers and solutions

Table 10: List of buffers and solutions

Buffer/ solution	Ingredients/ Manufacturer	
5 x Bradford assay solution	Biorad, Hercules, USA	
Buffer 3	NaCl	150 mM
	Tris/HCl pH = 7.5	50 mM
	NaF	50 mM
	EDTA	5 mM
	IGEPAL CA-630	0.1%
Cell lysis buffer	NaCl	150 mM
	Tris-HCl pH = 8.2	50 mM
AEBSF, Aprotinin and Pepstatin are added freshly before use.	Triton X-100	1%
	EDTA	5 mM
	NaF	5 mM
	AEBSF	0.2 mM
	Aprotinin	2 µg/ ml
	Pepstatin	2.5 µg/ ml
Colloidal coomassie staining solution	Coomassie Brilliant Blue G250	0.8%
	Citric acid	10%
	Ammonium sulfate	8%
	Methanol (add before usage)	20%
6 x DNA purple loading dye	New England Biolabs, Ipswich, USA	
EasyPrep buffer	Tris/HCl pH = 8	10 mM
	EDTA	1 mM
	Sucrose	150 mg/ml
	Lysozyme	2 mg/ml
	RNaseA	0.2 mg/ml
	BSA	0.1 mg/ml
10 x KOD buffer	Tris-HCl pH = 8	1,2 M
	KCl	100 mM
	$(NH_4)_2SO_4$	60 mM
	Triton X-100	1%
	BSA	100 µg/ml
10 x Laemmli running buffer (LRB)	Tris-Base	250 mM
	Glycine	9.46 M
	SDS	1 %
4 x Laemmli sample buffer	Tris/HCl pH = 6.8	200 mM
	SDS	8 %
	Glycerol	40%
	β-Mercaptoethanol	20%
	Bromophenol blue	0.05%
PBS for cell culture	NaCl	137 mM
	Phosphate buffer pH = 7.35	10 mM
	KCl	2.7 mM
PEG/LiAc	Tris/HCl pH = 7.5	10 mM
	EDTA	1 mM
	Lithium acetate pH = 7.5	100 mM
	PEG 3350	40%
Ponceau S staining solution	Ponceau S	1g /l
	Glacial acetic acid	5%
	H_2O to 1 l	
Salmon sperm DNA	DNA	10 µg/ µl
	Dissolved in TE pH = 8	

SDS PAGE separating gel (6 ml, 10% acrylamide)	1.5M Tris-HCl pH = 8.8 10 % SDS 30% Acrylamide 37.5:1 APS TEMED H_2O	1.5 ml 60 µl 2 ml 36.5 µl 3,5 µl 2,4 ml
SDS PAGE stacking gel (2.5 ml)	0.5M Tris-HCl pH = 6.8 10 % SDS 30% Acrylamide 37.5:1 APS TEMED	625 µl 25 µl 335 µl 25 µl 2.5 µl
Sodium citrate buffer (0.5M)	Na-Citrate H_2O pH adjusted to 7 with HCl	129 g ad 1 l
T4 ligase buffer	New England Biolabs, Ipswich, USA	
50 x Tris-Acetate-EDTA (TAE)	Tris-Base EDTA Glacial acetic acid to pH = 8	2 M 50 mM
10 x Taq buffer	Tris-HCl KCl $MgCl_2$	125 mM 560 mM 15 mM
10 x Tris buffered saline solution (TBS)	Tris base NaCl pH adjusted to 7.6 with HCl	200 mM 1.37 M
TBS-T	10 x TBS Tween-20 H_2O to 1 l	100 ml 0.1%
10 x Tris-EDTA (TE)	Tris/HCl pH7.5 EDTA	100 mM 10 mM
TE/LiAc	Tris/HCl pH7.5 EDTA Lithium acetate pH = 7.5	10 mM 1 mM 100 mM
Western Blot stripping buffer	Tris-HCl pH = 7 Guanidinium chloride Triton X-100 β-Mercaptoethanol (add before use)	20 mM 6 M 0.2% 100 mM
Western Blot transfer buffer	Tris-Base Glycine SDS Methanol	5.8 g/l 2.9 g/l 370 mg/l 10 %
Z-buffer	Na_2HPO_4 NaH_2PO_4 KCl $MgSO_4$ β-Mercaptoethanol adjust pH to 7	16.1 g/l 5.5 g/l 0.75 g/l 0.246 g/l 2.7 ml/l

4.2 Growth media

4.2.1 *E. coli* growth media

Table 11: List of E. coli growth media

Medium	Ingredients	
LB liquid medium	Yeast extract	5 g/l
	Tryptone	10 g/l
	NaCl	10 g/l
	NaOH	300 µM
SOC medium	Yeast extract	5 g/l
	Tryptone	20 g/l
	NaCl	10 mM
	KCl	2.5 mM
	$MgCl_2$	10 mM
	Glucose	20 mM

4.2.2 Yeast growth media

Carbon sources were added to media after autoclaving to prevent caramelization. If not stated otherwise, final concentration was 2%. For agar plates, 1.5% agar was added.

Table 12: List of yeast growth media

Medium	Ingredients	
Synthetic growth medium (500 ml)	10 x Dropout	50 ml
	10 x Yeast nitrogen base (YNB)	50 ml
	Carbon source	2 %
	steril H_2O to 1 l	
XY medium	Yeast extract	10 g/l
	Tryptone	20 g/l
	KH_2PO_4	50 mM
	Adenine	100 mg/l
	Tryptophane	200 mg/l
Carbon sources	Sodium Acetate pH = 7	20%
	Galactose	20%
Carbon sources were dissolved in water and autoclaved.	Glucose	20%
	Glycerol	20%
	Raffinose	10%
	Sucrose	20%
10 x Dropout ++	Adenine	500 mg/l
	Alanine	500 mg/l
For 10 x Dropout -5, adenine, histidine, leucine, tryptophane and uracil were omitted.	Arginine	500 mg/l
	Asparagine	500 mg/l
	Aspartic acid	1000 mg/l
For 10x Dropout -6, these five ingredients and methionine were omitted.	Cysteine	500 mg/l
	Glutamine	500 mg/l
	Glutaminic acid	1000 mg/l
For selective medium, adenine, histidine, leucine, tryptophane and uracil were added separately if needed.	Glycine	500 mg/l
	Histidine	500 mg/l
	(myo-) Inositol	500 mg/l
	Isoleucine	500 mg/l
	Leucine	1000 mg/l
	Lysine	500 mg/l
	Methionine	500 mg/l
	p-Aminobenzoic acid	50 mg/l

	Phenylalanine	500 mg/l
	Proline	500 mg/l
	Serine	1000 mg/l
	Threonine	1000 mg/l
	Tryptophane	1000 mg/l
	Tyrosine	500 mg/l
	Uracil	500 mg/l
	Valine	1000 mg/l
100 x Adenine (sterile filtered)	Adenine	5 g/l
100 x Histidine (sterile filtered)	Histidine	5 g/l
100 x Leucine (sterile filtered)	Leucine	10 g/l
100 x Methionine (sterile filtered)	Methionine	5 g/l
100 x Tryptophane (sterile filtered)	Tryptophane	10 g/l
50 x Uracil (sterile filtered)	Uracil	2.5 g/l
10 x Yeast Nitrogen Base (5.88 l)	YNB	100 g
	Ammonium sulfate	294 g
Novozyme medium	Sorbitol	1 M
	Tris/HCl pH = 7.5	10 mM
	EDTA	1 mM
	Novozyme 234	2 mg
	Dithiothreitol (add freshly)	50 mM

4.2.3 Mammalian cell media

Table 13: List of mammalian cell media

Medium	**Manufacturer/ recipe**	
Dulbecco's Modified Eagle Medium (DMEM)	Thermo Fisher Scientific, Waltham, USA	
Fetal bovine serum (FBS)	Thermo Fisher Scientific, Waltham, USA	
HEK cell growth medium (500 ml)	DMEM	450 ml
	FBS	50 ml
Freezing medium (10 ml)	DMEM	7 ml
	FBS	2 ml
	DMSO	1 ml

4.3 Biological materials

4.3.1 Primary Antibodies

Rabbit sera were obtained from Davids Biotechnologie in Regensburg. Rabbits were immunized with recombinant proteins produced by the Seufert research group.

Table 14: List of primary antibodies and their usage

Antigen	**Description**	**Dilution**	**Use in figure**
S.c Cdc123	rabbit serum, affinity purified, Davids Biotechnologie, Regensburg, Germany	1:1000	8A, 9, 10A, 11A, 17C, 22B, 24, 25B, 26C, 31A, S1, S2
H. s. Cdc123	rabbit serum, affinity purified, Davids Biotechnologie, Regensburg, Germany	1:500	14D, 15A/D
H. s. EIF2S1	FL-315, rabbit polyclonal, Santa Cruz, Dallas, USA	1:1000	14D, 15D
H. s. EIF2S2	Rabbit polyclonal (90-960), Prosci, Poway, USA	1:200	14D, 15D
H. s. EIF2S3	A31100, rabbit, Bioworld (Genelinx), Dublin, USA	1:200	15D

FLAG	M2, mouse monoclonal, Thermo Scientific, Waltham, USA	1:20000	8A, 9, 10A, 11, 14A/B/D, 15A/B, 17A/B/C, 22B/C, 24, 25, 26C, 31A, 33, 34A, 36A/C, S1, S2, S4
FLAG	F7425, rabbit polyclonal, Thermo Scientific, Waltham, USA	1:3000	8A, 10C, 12A/C, 13, 15D, 16A, 17A/B, 18, 31A, 39A
Gcd11	Rabbit serum, Davids Biotechnologie, Regensburg, Germany	1:2500	10C, 11, 12A/C, 13, 42, S4
HA	12CA5, mouse monoclonal, cell culture supernatant	1:100	9B, 12A, 26C, S2
HA	Y11, rabbit polyclonal, Santa Cruz, Dallas, USA	1:1000	17A/B, 18, 39A
MYC	9E10, mouse monoclonal, cell culture supernatant	1:100	10C, 11A, 13, 25B, 33, 36C, 44A
MYC	A14, rabbit polyclonal, Santa Cruz, Dallas, USA	1:500	11B, 17A/B, 17C, 18, 22C, 39A
Sui2	rabbit serum, Davids Biotechnologie, Regensburg, Germany	1:1000	8A, 9, 11A, 12B, 17C, 22B, 24, 31A, S1, S2
Sui3	rabbit serum, Davids Biotechnologie, Regensburg, Germany	1:1000	8A, 9, 10C, 11B, 12A/C, 22B, 24, 31A, S1, S2

4.3.2 Secondary antibodies

Table 15: List of secondary antibodies and their usage

Name	Manufacturer	Dilution
α-rabbit-IRDye®800CW	Li-COR Biosciences, Lincoln, USA	1:15000
α-rabbit-IRDye®680CW	Li-COR Biosciences, Lincoln, USA	1:15000
α-mouse-IRDye®800CW	Li-COR Biosciences, Lincoln, USA	1:15000
α-mouse-IRDye®680CW	Li-COR Biosciences, Lincoln, USA	1:15000

4.4 Oligonucleotides

Oligonucleotides were obtained from Eurofins Genomics in Ebersber, Germany.

Table 16: List of oligonucleotides used in this study

Name	Sequence	Description
WS84	TTCCCAGTCACGACGTTG	F sequencing primer, binds outside of MCS in pUC18-derived plasmids
WS85	CACACAGGAAACAGCTATG	R sequencing primer, binds outside of MCS in pUC18-derived plasmids
WS883	GGAGGATCCATGAAGAAGGAGCATGTG	F-primer for PCR-amplification of hCDC123, contains BamHI site
WS979	CCAGAAGTGTCAGTTTCCCTTCCTCCTAGCCCGTTTCTTATCTTCGAATTCGAGCTCGTTTAAAC	F-Primer for genomic integration of *GCD11(1-519)* with pFA6A-GFP(S65T)-KanMX6 (Longtine-System)
WS884	GGACTCGAGTCAGTCGTCCTCCTGCTG	R-primer for PCR-amplification of hCDC123, contains XhoI site
WS1140	CGTAGTCGACTTAAGCGATGGGTTCCAATGTAGTAC	R-Primer for PCR-amplification of *GCD11*, contains stop and SalI site
WS2369	TCTCTTTCTAATATATAAATTC	F sequencing primer, binds in pTEF2

WS2493	ATTGAATTCGGTCTCGGATCCATG GCGGGCGGAGAAGCTG	F-Primer for PCR-amplification of human eIF2γ, contains EcoRI and BsaI (->BamHI) sites
WS2494	AATGTCGACGGTCTCAAGCTTCTA GTCATCATCTACTGTTGGCTTG	R-Primer for PCR-amplification of human eIF2γ, contains SalI and BsaI (->HindIII) sites
WS3004	ACTGAATTCGGATCCATGAGTACT ATGTTATCAGGTGCT	F-Primer for PCR-amplification of *GCD11 (AA201-)*
WS3015	ATATGAATTCGGATCCGAAGAAGA AAAAAGGAAAAGGG	F-Primer for PCR-amplification of *GCD11 (AA61-)*
WS3016	ATATGAATTCGGATCCTTAGGTTA CGCTAATGCTAAAATTT	F-Primer for PCR-amplification of *GCD11 (AA140-)*
WS3021	CATTGCTGACGGTGCTCCTATTAG ACCAATATCCGCTCAGTTGAAG	F-Primer for mutagenesis of *GCD11 (V281R)*, (GTA->AGA)
WS3022	CTTCAACTGAGCGGATATTGGTCT AATAGGAGCACCGTCAGCAATG	R-Primer for mutagenesis of *GCD11 (V281R)*, (GTA->AGA)
WS3054	ACTGAATTCGGATCCATGGGTGGT GGTTTGCCCGAAC	F-Primer for PCR-amplification of *GCD11 (AA72-)*
WS3055	ACTGAATTCGGATCCATGAACCCT GATTTTTCAAAATTAAACCCACTA TCC	F-Primer for PCR-amplification of *GCD11 (AA81-)*
WS3091	ATATGTCGACCTAACCCCAACCAA TTAAACGCC	R-Primer for PCR-amplification of EIF2S3 (AA-457), contains stop and Sal site
WS3092	ATATGTCGACCTATGTCACTCCTCT TCTTATCTGAC	R-Primer for PCR-amplification of EIF2S3 (AA-464), contains stop and Sal site
WS3093	ATATGTCGACTCATCTACTGTTGG CTTGTCACTCCTCTTCTTATCTGAC	R-Primer for PCR-amplification of EIF2S3 (AA-I465SQQ*), contains stop and Sal site
WS3157	ATATGTCGACCTACTGTTGGCTTG TAGTACCCTTTTTAATGGTTG	R-Primer for PCR-amplification of *GCD11 (AA-L523SQQ*)*, contains stop and SalI site
WS3163	GACTGTCGACTTATGTAGTACCCT TTTTAATGGTTGC	R-Primer for PCR-amplification of *GCD11 (AA-522)*, contains stop and SalI site
WS3170	AAAGCATTGGCGTTTGATTGGTTG GGCAACCATTAAAAAGTAATGAGG CGCGCCACTTCTAAA	F-Primer for genomic integration of *GCD11(1-519)* with pFA6A-GFP(S65T)-KanMX6 (Longtine-System), R-Primer = WS979
WS3174	AACAAGAAGTTGGCCTACCTGCTG CAGAGTTATTATCTAGATTTTTC	F-Primer for mutagenesis of *SUI3 (Y131A/S132A)*, creates ApeKI-site
WS3175	GAAAAATCTAGATAATAACTCTGC AGCAGGTAGGCCAACTTCTTGTT	R-Primer for mutagenesis of *SUI3* (Y131A/S132A), creates ApeKI-site
WS3176	TTGGCCTACCTTATTCAGAGAGAA GATCTAGATTTTTCAATATTCTAA G	F-Primer for mutagenesis of *SUI3* (L134A/L135A)
WS3177	CTTAGAATATTGAAAAATCTAGAT CTTCTCTCTGAATAAGGTAGGCCA A	R-Primer for mutagenesis of *SUI3* (L134A/L135A)
WS3186	GTCACTCGAGTCAAGAGAGGTCTA CAAAGTCCTTGG	R-Primer for PCR-amplification of hCDC123 (AA-314), contains stop and XhoI site
WS3187	GTCACTCGAGTCAACTGTTTGTGC AACGGAAAGC	R-Primer for PCR-amplification of hCDC123 (AA-292), contains stop and XhoI site
WS3188	GCCCAGCCCCTATTTGAGTGGCCGG CTACCCAAGGACTTTG	F-Primer for mutagenesis of hCDC123 (Y304G), creates NaeI site
WS3189	CAAAGTCCTTGGGTAGCCGGCCAC TCAAATAGGGGCTGGGC	R-Primer for mutagenesis of hCDC123 (Y304G), creates NaeI site
WS3196	CCGAAAATCATGTTCCACAGCGAC TAGTAGAAGCTAGTTTAAATCC	F-Primer for mutagenesis of *CDC123 (D323R)*, creates SpeI site

WS3197	GGATTTAAACTAGCTTCTACTAGT CGCTGTGGAACATGATTTTCGG	R-Primer for mutagenesis of *CDC123 (D323R)*, creates SpeI site
WS3200	GACGTATCGAAAAGCATTGGGACC TGATTGGTTGGGCAACCATTAAAA AG	F-Primer for mutagenesis of *GCD11 (R510D)*, creates AvaII site
WS3201	CTTTTTAATGGTTGCCCAACCAAT CAGGTCCCAATGCTTTTCGATACG TC	R-Primer for mutagenesis of *GCD11 (R510D)*, creates AvaII site
WS3203	GCGTTTGATTGGTTGGGCAACCAT TAAAAAGGGTACTACATAATGAGG CGCGCCACTTCTAAA	F-Primer for genomic integration of *GCD11(1-522)* with pFA6A-GFP(S65T)-KanMX6 (Longtine-System), R-Primer = WS979
WS3208	GGTGTTGGTACTAAAGTTAGGCCT ACCTTGTGTAGAGCTG	F-Primer for mutagenesis of *GCD11 (D403R)*, creates StuI site
WS3209	CAGCTCTACACAAGGTAGGCCTAA CTTTAGTACCAACACC	R-Primer for mutagenesis of *GCD11 (D403R)*, creates StuI site
WS3210	GCATTGGCGTTTGATTGGTTGGGC AACCATTAAAAAGGGTTAATGAGG CGCGCCACTTCTAAA	F-Primer for genomic integration of *GCD11(1-520*) with pFA6A-GFP(S65T)-KanMX6 (Longtine-System), R-Primer = WS979
WS3211	TTGGCGTTTGATTGGTTGGGCAAC CATTAAAAAGGGTACTTAATGAGG CGCGCCACTTCTAAA	F-Primer for genomic integration of *GCD11*(1-521) with pFA6A-GFP(S65T)-KanMX6 (Longtine-System), R-Primer = WS979
WS3246	GTATCGATGCCATTAAAGACGCAG AAAAATCAGCTGAAGACATGTC	F-Primer for mutagenesis of *SUI2 (L205E)*
WS3247	GACATGTCTTCAGCTGATTTTTCT GCGTCTTTAATGGCATCGATAC	R-Primer for mutagenesis of *SUI2 (L205E)*
WS3248	CAGAACAAATGCAAGTTAAAGAAA AATTAGTCGCCGCCCCATTATATG	F-Primer for mutagenesis of *SUI2 (V220E)*
WS3249	CATATAATGGGGCGGCGACTAATT TTTCTTTAACTTGCATTTGTTCTG	R-Primer for mutagenesis of *SUI2 (V220E)*
WS3456	AGTCGTCGACCTAGTCATCATCTA CTGTTGGCTTG	R-Primer for PCR-Amplifikation of EIF2S3, contains stop and SalI site
WS3461	AGTCGAATTCGGTCTCAAGCTTAT GTCTGACTACAAAGACCATGACG	F-Primer for PCR-Amplifikation of FLAG peptide sequence, contains EcoRI and BsaI (->HindIII) sites
WS3551	GTAAAATTGTTTTGACCAATAGCG TCTGCACAGAGGTAGGAGAAAAAA TTG	F-Primer for mutagenesis of EIF2S3 (P432S), erzeugt eine BsgI-Schnittstelle, Sven V. 27.03.2019
WS3552	CAATTTTTTCTCCTACCTCTGTGCA GACGCTATTGGTCAAAACAATTTT AC	R-Primer for mutagenesis ofEIF2S3 (P432S), erzeugt eine BsgI-Schnittstelle, Sven V. 27.03.2019
WS3721	GTCATGTCGCCCACGGTAAAGCTG CAGTAGTTAGGGCTATTTCAG	F-Primer for mutagenesis of *GCD11 (S114A, T115A)*, creates PstI site
WS3722	CTGAAATAGCCCTAACTACTGCAG CTTTACCGTGGGCGACATGAC	R-Primer for mutagenesis of *GCD11 (S114A, T115A*), creates PstI site
WS3723	CACGTCATCATCTTACAGAATGCG GTCGATTTAATGCGTGAAGAAAGT GC	F-Primer for mutagenesis of *GCD11 (K250A)*
WS3724	GCACTTTCTTCACGCATTAAATCG ACCGCATTCTGTAAGATGATGACG TG	R-Primer for mutagenesis of *GCD11 (K250A)*

4.5 Plasmids

Table 17: All plasmids used in this work, sorted alphabetically

Name	Construkt	Vector	Source
pcDNA5-FRT/TO			Thermo Fisher Waltham, USA
pFA6a-13MYC-HIS3MX6			Longtine et al.
pFA6a-3HA-kanMX6			Longtine et al.
pFA6a-GFP(S65T)-kanMX6			Longtine et al.
pFA6a-NatNT2			Longtine et al.
pRS303			Sikorski RS, Hieter P.
pRS304			
pRS305			
pRS306			
pWS3395	GCN4(5'-UTR)-lacZ	pRS314	RG Seufert
pWS3912	pTEF2-FLAG3-hD123-tCYC1-LEU2	pRS305	RG Seufert
pWS4018	pADH-LexA-heIF2alpha	pEG202	RG Seufert
pWS4023	pGAL1-AD-heIF2gamma	pJG4-5	RG Seufert
pWS4488	pTEF2-CDC123-3xFLAG-tCYC1-URA3	pRS306	RG Seufert
pWS4731	pGAL1-HA4-SUI2-tCYC1-LEU2	pRS305	RG Seufert
pWS5041	pGAL1-FLAG3-GCD11(1-527)-tCYC1-LEU2	pRS305	This study
pWS5042	pGAL1-FLAG3-GCD11(310-527)-tCyc-LEU2	pRS305	This study
pWS5043	pGAL1-FLAG3-GCD11(410-527)-tCyc-LEU2	pRS305	This study
pWS5073	pGAL1-FLAG3-GCD11(201-527)-tCyc-LEU2	pRS305	This study
pWS5095	pGAL1-FLAG3-GCD11(61-527)-tCYC1-LEU2	pRS305	This study
pWS5096	pGAL1-FLAG3-GCD11(140-527)-tCyc-LEU2	pRS305	This study
pWS5097	pGAL1-FLAG3-GCD11(91-527)-tCyc-LEU2	pRS305	This study
pWS5114	pGCD11-FLAG3-GCD11(V281R)-tCYC1-HIS3	pRS303	This study
pWS5123	pGAL1-FLAG3-GCD11(72-527)-tCYC1-LEU2	pRS305	This study
pWS5124	pGAL1-FLAG3-GCD11(81-527)-tCYC1-LEU2	pRS305	This study
pWS5143	pTEF2-MYC3-hD123-tCYC1-LEU2	pRS305	RG Seufert
pWS5154	pMET25-ha3-heIF2beta-tCYC-TRP1	pRS304	This study
pWS5158	pGAL1-AD-heIF2gamma(1-457)-tADH	pJG4-5	This study
pWS5159	pGAL1-AD-heIF2gamma(1-464)-tADH	pJG4-5	This study
pWS5160	pGAL1-AD-heIF2gamma(1-464fs4*)-tADH	pJG4-5	This study
pWS5173	pGCD11-FLAG3-heIF2gamma(1-457)-tCYC-HIS3	pRS303	This study
pWS5174	pGCD11-FLAG3-heIF2gamma(1-464)-tCYC-HIS3	pRS303	This study
pWS5175	pGCD11-FLAG3-heIF2gamma(1-464fs4*)-tCYC-HIS3	pRS303	This study
pWS5185	pGCD11-FLAG3-heIF2gamma-tCYC1-HIS3	pRS303	This study
pWS5218	pGAL1-pGAL1-3xFLAG-SUI3-tCYC1-URA3	pRS306	RG Seufert
pWS5271	pGCD11-FLAG3-GCD11(L523SQQ)-tCYC1-HIS3	pRS303	This study
pWS5274	pGCD11-FLAG3-GCD11(1-522)-tCYC1-HIS3	pRS303	This study
pWS5311	pGAL1-FLAG3-SUI3(YS/AA)-tCYC1-URA3	pRS306	This study
pWS5312	pGAL1-FLAG3-SUI3(LL/RR)-tCYC1-URA3	pRS306	This study

pWS5324	pTEF2-MYC3-hD123(1-314)-tCYC1-LEU2	pRS305	RG Seufert
pWS5325	pTEF2-FLAG3-hD123(1-314)-tCYC1-LEU2	pRS305	RG Seufert
pWS5326	pTEF2-MYC3-hD123(1-292)-tCYC1-LEU2	pRS305	RG Seufert
pWS5327	pTEF2-FLAG3-hD123(1-292)-tCYC1-LEU2	pRS305	RG Seufert
pWS5328	pTEF2-MYC3-hD123(Y304G)-tCYC1-LEU2	pRS305	RG Seufert
pWS5329	pTEF2-FLAG3-hD123(1-Y304G)-tCYC1-LEU2	pRS305	RG Seufert
pWS5334	pTEF2-MYC3-CDC123(D323R)-tCYC1-URA3	pRS306	This study
pWS5342	pTEF2-MYC3-CDC123-tCYC1-URA3	pRS306	This study
pWS5353	pGCD11-FLAG3-GCD11(D403R)-tCYC1-HIS3	pRS303	This study
pWS5356	pTEF2-FLAG3-SUI2-tCYC1-TRP1	pRS304	RG Seufert
pWS5358	pGALL-FLAG3-GCD11(R510D)-tCYC1-HIS3	pRS303	This study
pWS5361	pGALL-FLAG3-GCD11-tCYC1-HIS3	pRS303	This study
pWS5365	pTEF2-FLAG3-SUI2(C192E)-tCYC1-TRP1	pRS304	RG Seufert
pWS5367	pTEF2-FLAG3-SUI2(V220E)-tCYC1-TRP1	pRS304	RG Seufert
pWS5376	pGCD11-FLAG3-GCD11(R510D)-tCYC1-HIS3	pRS303	This study
pWS5383	pGAL1-HA4-SUI2(C193E)-tCYC1-LEU2	pRS305	This study
pWS5384	pGAL1-HA4-SUI2(V220E)-tCYC1-LEU2	pRS305	This study
pWS5452	pGAL1-FLAG3-GCD11(201-514)-tCYC1-LEU2	pRS305	This study
pWS5495	pCMV-FLAG3-EIF2S3-tbGH	pcDNA5-FRT-TO	This study
pWS5501	pGALL-FLAG3-GCD11(V281R)-tCYC1-HIS3	pRS303	RG Seufert
pWS5502	pGALL-FLAG3-GCD11(D403R)-tCYC1-HIS3	pRS303	RG Seufert
pWS5503	pGALL-FLAG3-GCD11(V281R, D403R)-tCYC1-HIS3	pRS303	RG Seufert
pWS5603	pMET3-3HA-GCD11-tCYC1-URA3	pRS306	This study
pWS5632	pGAL1-AD-heIF2gamma(1-252)	pJG4-5	This study
pWS5633	pGAL1-AD-heIF2gamma(1-373)	pJG4-5	This study
pWS5634	pADH-LexA-heIF2gamma(251-472)	pEG202	This study
pWS5635	pADH-LexA-heIF2gamma(251-464 fs*4)	pEG202	This study
pWS5636	pADH-LexA-heIF2gamma(351-472)	pEG202	This study
pWS5637	pADH-LexA-heIF2gamma(351-464 fs*4)	pEG202	This study
pWS5639	pGCD11-FLAG3-heIF2gamma(P432S)-tCYC1 HIS3	pRS303	This study
pWS5644	pCMV-FLAG3-hD123-tbGH	pcDNA5-FRT-TO	This study
pWS5657	pCDC123-FLAG3-D123-tCYC1-LEU2	pRS305	RG Seufert
pWS5658	pGCD11-FLAG3-D123-tCYC1-LEU2	pRS305	RG Seufert
pWS5695	pGALL-FLAG3-heIF2gamma-tCYC1-HIS3	pRS303	This study
pWS5750	pMET3-FLAG3-GCD11(91-527)-tCYC1-LEU2	pRS305	This study
pWS5751	pMET3-FLAG3-GCD11(C150A)-tCYC1-LEU2	pRS305	This study
pWS5752	pMET3-FLAG3-GCD11(C174A)-tCYC1-LEU2	pRS305	This study
pWS5753	pMET3-FLAG3-GCD11(K250A)-tCYC1-LEU2	pRS305	This study
pWS5754	pMET3-FLAG3-GCD11(S114A/T115A)-tCYC1-LEU2	pRS305	This study
pWS5755	pMET3-FLAG3-GCD11(ΔSw1)-tCYC1-LEU2	pRS305	This study
pWS5789	pMET3-3HA-GCD11(C150A)-tCYC1 URA3	pRS306	This study
pWS5790	pMET3-3HA-GCD11(C174A)-tCYC1 URA3	pRS306	This study

pWS5791	pMET3-3HA-GCD11(K250A)-tCYC1 URA3	pRS306	This study
pWS5792	pMET3-3HA-GCD11(S114A/T115A)-tCYC1 URA3	pRS306	This study
pWS5793	pMET3-3HA-GCD11(deltaSw1)-tCYC1 URA3	pRS306	This study
pWS5825	pMET3-HA3-GCD11(D2,3)-tCYC1 URA3	pRS306	This study
pWS5826	pGCD11-FLAG3-GCD11(D1)-tCYC1 HIS3	pRS303	This study

4.6 Yeast strains

Table 18: Yeast strains used in this work, sorted by experiment

Experiment	Name	MAT	Genotype	Source
2.1.1 (Figure 8A)	K700	α		RG Seufert
	W15011	α	leu2::pGAL1-FLAG3-GCD11(1-527)-tCYC1-LEU2	This study
	W14924	α	leu2::pGAL1-FLAG3-GCD11(AA61-527)-tCYC1-LEU2	This study
	W15009	α	leu2::pGAL1-FLAG3-GCD11(72-527)-tCYC1-LEU2	This study
	W15010	α	leu2::pGAL1-FLAG3-GCD11(81-527)-tCYC1-LEU2	This study
	W14925	α	leu2::pGAL1-FLAG3-GCD11(AA91-527)-tCYC1-LEU2	This study
	W14926	α	leu2::pGAL1-FLAG3-GCD11(AA140-527)-tCYC1-LEU2	This study
	W14927	α	leu2::pGAL1-FLAG3-GCD11(AA201-527)-tCYC1-LEU2	This study
	W14928	α	leu2::pGAL1-FLAG3-GCD11(AA310-527)-tCYC1-LEU2	This study
	W14929	α	leu2::pGAL1-FLAG3-GCD11(AA410-527)-tCYC1-LEU2	This study
2.1.2 (Figure 9A)	W12626	a/α	GCD11/gcd11-delta::kanMX6	RG Seufert
	W12783	a/α	GCD11/gcd11-delta::kanMX6 his3/his3::pGCD11-FLAG3-GCD11-tCYC1-HIS3	RG Seufert
	W15419	a/α	GCD11/gcd11-delta::kanMX6 his3/his3::pGCD11-FLAG3-GCD11(1-514)-tCYC1-HIS3	This study
	W15558	a/α	GCD11/gcd11-delta::kanMX6 his3/his3::pGCD11-FLAG3-GCD11(D403R)-tCYC1-HIS3	This study
	W15416	a/α	GCD11/gcd11-delta::kanMX6 his3/his3::pGCD11-FLAG3-GCD11(V281R)-tCYC1-HIS3	This study
2.1.2 (Figure 9B)	W15500	a/α	his3/his3::HIS3 GCD6/GCD6-HA3-KanMX6	This study
	W15512	a/α	his3/his3::pGCD11-FLAG3-GCD11-tCYC1-HIS3 GCD6/GCD6-HA3-KanMX6	This study
	W15506	a/α	his3/his3::pGCD11-FLAG3-GCD11(1-514)-tCYC1-HIS3 GCD6/GCD6-HA3-KanMX6	This study
	W15771	a/α	his3/his3::pGCD11-FLAG3-GCD11(D403R)-tCYC1-HIS3 GCD6/GCD6-HA3-KanMX6	This study
	W15503	a/α	his3/his3::pGCD11-FLAG3-GCD11(V281R)-tCYC1-HIS3 GCD6/GCD6-HA3-KanMX6	This study
	W15501	a/α	his3/his3::HIS3 GCD7/GCD7-HA3-KanMX6	This study
	W15513	a/α	his3/his3::pGCD11-FLAG3-GCD11-tCYC1-HIS3	This study

			GCD7/GCD7-HA3-KanMX6	
	W15507	a/α	his3/his3::pGCD11-FLAG3-GCD11(1-514)-tCYC1-HIS3 GCD7/GCD7-HA3-KanMX6	This study
	W15772	a/α	his3/his3::pGCD11-FLAG3-GCD11(D403R)-tCYC1-HIS3 GCD7/GCD7-HA3-KanMX6	This study
	W15504	a/α	his3/his3::pGCD11-FLAG3-GCD11(V281R)-tCYC1-HIS3 GCD7/GCD7-HA3-KanMX6	This study
2.1.3 (Figure 10A)	W10953	a	TIF5-HA3-HIS3MX6	RG Seufert
	W15228	a	kanMX4-pSUI2-FLAG3-SUI2 TIF5-HA3-HIS3MX6	RG Seufert
	W15230	a	kanMX4-pSUI3-FLAG3-SUI3 TIF5-HA3-HIS3MX6	RG Seufert
	W15232	a	kanMX4-pGCD11-FLAG3-GCD11 TIF5-HA3-HIS3MX6	RG Seufert
2.1.3 (Figure 10C)	W9878	α	SUI2-myc13-HIS3MX6	RG Seufert
	W14424	α	ura3::pTEF2-CDC123-FLAG3-tCYC1-URA3 SUI2-MYC13-HIS3MX6	RG Seufert
2.1.4 (Figure 11A top)	K700	α		RG Seufert
	W15193	α	ura3::pGAL1-3xFLAG-SUI3-tCYC1-URA3	RG Seufert
	W15428	α	ura3::pGAL1-FLAG3-SUI3(YS/AA)-tCYC1-URA3	This study
	W15429	α	ura3::pGAL1-FLAG3-SUI3(LL/RR)-tCYC1-URA3	This study
2.1.4 (Figure 11A bottom)	W15773	a/α	ura3/ura3::URA3 TIF5/TIF5-myc13-HIS3MX6	This study
	W15441	a/α	ura3/ura3::pGAL1-3xFLAG-SUI3-tCYC1-URA3 TIF5/TIF5-myc13-HIS3MX6	This study
	W15444	a/α	ura3/ura3::pGAL1-FLAG3-SUI3(YS/AA)-tCYC1-URA3 TIF5/TIF5-myc13-HIS3MX6	This study
	W15447	a/α	ura3/ura3::pGAL1-FLAG3-SUI3(LL/RR)-tCYC1-URA3 TIF5/TIF5-myc13-HIS3MX6	This study
2.1.4 (Figure 11B)	W5077	a	CDC123-MYC13-HIS3MX6	RG Seufert
	W15714	a	trp1::pTEF2-FLAG3-SUI2-tCYC1-TRP1 CDC123::CDC123-MYC13-HIS3MX6	This study
	W15720	a	trp1::pTEF2-FLAG3-SUI2(L205E)-tCYC1-TRP1 CDC123::CDC123-MYC13-HIS3MX6	This study
	W15723	a	trp1::pTEF2-FLAG3-SUI2(V220E)-tCYC1-TRP1 CDC123::CDC123-MYC13-HIS3MX6	This study
2.1.5 (Figure 12A)	K699	a		RG Seufert
	W14058	a	ura3::pTEF2-CDC123-3xFLAG-tCYC1-URA3	RG Seufert
	W15914	a	ura3::pTEF2-CDC123-FLAG3-tCYC1-URA3 leu2::pGAL1-HA4-SUI2-tCYC1-LEU2	This study
	W15915	a	ura3::pTEF2-CDC123-FLAG3-tCYC1-URA3 leu2::pGAL1-HA4-SUI2(L205E)-tCYC1-LEU2	This study
	W15916	a	ura3::pTEF2-CDC123-FLAG3-tCYC1-URA3 leu2::pGAL1-HA4-SUI2(V220E)-tCYC1-LEU2	This study
2.1.5 (Figure 12C)	W15910	a/α	ura3/ura3::pTEF2-CDC123-3xFLAG-tCYC1-URA3	This study
	W15911	a/α	SUI2/sui2delta::natNT2 ura3/ura3::pTEF2-CDC123-3xFLAG-tCYC1-URA3	This study
2.1.5 (Figure 13)	W17923	a	SUI2-myc13-HIS3MX6	This study
	W17924	a	SUI2-myc13-HIS3MX6 CDC123-FLAG12-HIS3MX6	This study
	W17925	a	SUI2-myc13-HIS3MX6	This study

			trp1::pTEF2-GCD11-tCYC1-TRP1	
	W17926	a	SUI2-myc13-HIS3MX6 CDC123-FLAG12-HIS3MX6 trp1::pTEF2-GCD11-tCYC1-TRP1	This study
2.1.8 (Figure 16)	W276	α	his3, trp1, ura3-52::URA3-lexA-op-lacZ, leu2::pLEU2-lexA-op	RG Seufert
	W15023	α	his3, trp1, ura3-52::URA3-lexA-op-lacZ, leu2::pTEF2-FLAG3-hD123-tCYC1-LEU2	This study
2.1.8 (Figure 17A)	W14736	a/α	ura3/ura3::pTEF2-MYC3-heIF2alpha-tCYC1-URA3	This study
	W15260	a/α	ura3/ura3::pTEF2-MYC3-heIF2α-tCYC1-URA3 leu2/leu2::pTEF2-MYC3-hD123-tCYC1-LEU2 his3/his3::pGCD11-FLAG3-heIF2gamma-tCYC1-HIS3	This study
	W15261	a/α	ura3/ura3::pTEF2-MYC3-heIF2α-tCYC1-URA3 leu2/leu2::pTEF2-MYC3-hD123-tCYC1-LEU2 his3/his3::pGCD11-FLAG3-heIF2gamma(1-457)-tCYC1-HIS3	This study
	W15262	a/α	ura3/ura3::pTEF2-MYC3-heIF2α-tCYC1-URA3 leu2/leu2::pTEF2-MYC3-hD123-tCYC1-LEU2 his3/his3::pGCD11-FLAG3-heIF2gamma(1-464)-tCYC1-HIS3	This study
	W15263	a/α	ura3/ura3::pTEF2-MYC3-heIF2α-tCYC1-URA3 leu2/leu2::pTEF2-MYC3-hD123-tCYC1-LEU2 his3/his3::pGCD11-FLAG3-heIF2gamma(1-464fs*4)-tCYC1-HIS3	This study
	W15026	a	ura3::pTEF2-MYC3-heIF2beta-tCYC1-URA3	This study
	W15125	a	ura3::pTEF2-MYC3-heIF2beta-tCYC1-URA3 his3::pGCD11-FLAG3-heIF2gamma-tCYC1-HIS3	This study
	W15126	a	ura3::pTEF2-MYC3-heIF2beta-tCYC1-URA3 his3::pGCD11-FLAG3-heIF2gamma (1-457)-tCYC1-HIS3	This study
	W15127	a	ura3::pTEF2-MYC3-heIF2beta-tCYC1-URA3 his3::pGCD11-FLAG3-heIF2gamma (1-464)-tCYC1-HIS3	This study
	W15128	a	ura3::pTEF2-MYC3-heIF2beta-tCYC1-URA3 his3::pGCD11-FLAG3-heIF2gamma (1-464fs4*)-tCYC1-HIS3	This study
	W15034	a	leu2::pTEF2-MYC3-hD123-tCYC1-LEU2	This study
	W15129	a	leu2::pTEF2-MYC3-hD123-tCYC1-LEU2 his3::pGCD11-FLAG3-heIF2gamma-tCYC1-HIS3	This study
	W15130	a	leu2::pTEF2-MYC3-hD123-tCYC1-LEU2 his3::pGCD11-FLAG3-heIF2gamma (1-457)-tCYC1-HIS3	This study
	W15131	a	leu2::pTEF2-MYC3-hD123-tCYC1-LEU2 his3::pGCD11-FLAG3-heIF2gamma (1-464)-tCYC1-HIS3	This study
	W15132	a	leu2::pTEF2-MYC3-hD123-tCYC1-LEU2 his3::pGCD11-FLAG3-heIF2gamma (1-464fs4*)-tCYC1-HIS3	This study
2.1.8 (Figure 17B)	W18017		ura3/ura3::pTEF2-MYC3-heIF2alpha-tCYC1-URA3 leu2/leu2::pTEF2-MYC3-hD123-tCYC1-	This study

			LEU2 trp1/trp1::pMET25-HA3-heIF2beta-tCYC1-TRP1	
	W15350		ura3/ura3::pTEF2-MYC3-heIF2α-tCYC1-URA3 leu2/leu2::pTEF2-MYC3-hD123-tCYC1-LEU2 his3/his3::pGCD11-FLAG3-heIF2gamma-tCYC1-HIS3 trp1/trp1::pMET25-HA3-heIF2beta-tCYC1-TRP1	This study
	W16360		ura3/ura3::pTEF2-MYC3-heIF2α-tCYC1-URA3 leu2/leu2::pTEF2-MYC3-hD123-tCYC1-LEU2 his3/his3::pGCD11-FLAG3-heIF2gamma(1-457)-tCYC1-HIS3 trp1/trp1::pMET25-HA3-heIF2beta-tCYC1-TRP1	This study
	W16361		ura3/ura3::pTEF2-MYC3-heIF2α-tCYC1-URA3 leu2/leu2::pTEF2-MYC3-hD123-tCYC1-LEU2 his3/his3::pGCD11-FLAG3-heIF2gamma(1-464)-tCYC1-HIS3 trp1/trp1::pMET25-HA3-heIF2beta-tCYC1-TRP1	This study
	W16362		ura3/ura3::pTEF2-MYC3-heIF2α-tCYC1-URA3 leu2/leu2::pTEF2-MYC3-hD123-tCYC1-LEU2 his3/his3::pGCD11-FLAG3-heIF2gamma(1-464 fs*4)-tCYC1-HIS3 trp1/trp1::pMET25-HA3-heIF2beta-tCYC1-TRP1	This study
2.1.8 (Figure 17C)	W12626	a/α	GCD11/gcd11-delta::kanMX6	RG Seufert
	W12790	a/α	GCD11/gcd11-delta::kanMX6 his3/his3::pGCD11-FLAG3-GCD11(1-514)-tCYC1-HIS3	RG Seufert
	W12788	a/α	GCD11/gcd11-delta::kanMX6 his3/his3::pGCD11-FLAG3-GCD11(1-519)-tCYC1-HIS3	RG Seufert
	W16160	a/α	GCD11/gcd11-delta::kanMX6 his3/his3::pGCD11-FLAG3-GCD11(1-522)-tCYC-HIS3	This study
	W12786	a/α	GCD11/gcd11-delta::kanMX6 his3/his3::pGCD11-FLAG3-GCD11(1-523)-tCYC1-HIS3	RG Seufert
	W16199	a/α	GCD11/gcd11-delta::kanMX6 his3/his3::pGCD11-FLAG3-GCD11(L523S QQ)-tCYC-HIS3	This study
	W12784	a/α	GCD11/gcd11-delta::kanMX6 his3/his3::pGCD11-FLAG3-GCD11-tCYC1-HIS3	RG Seufert
2.1.9 (Figure 18)	W18017		ura3/ura3::pTEF2-MYC3-heIF2alpha-tCYC1-URA3 leu2/leu2::pTEF2-MYC3-hD123-tCYC1-LEU2 trp1/trp1::pMET25-HA3-heIF2beta-tCYC1-TRP1	This study
	W15350		ura3/ura3::pTEF2-MYC3-heIF2α-tCYC1-URA3 leu2/leu2::pTEF2-MYC3-hD123-tCYC1-LEU2 his3/his3::pGCD11-FLAG3-heIF2gamma-tCYC1-HIS3 trp1/trp1::pMET25-HA3-heIF2beta-tCYC1-TRP1	This study
	W16360		ura3/ura3::pTEF2-MYC3-heIF2α-tCYC1-URA3 leu2/leu2::pTEF2-MYC3-hD123-tCYC1-LEU2 his3/his3::pGCD11-FLAG3-heIF2gamma(1-457)-tCYC1-HIS3 trp1/trp1::pMET25-HA3-heIF2beta-tCYC1-TRP1	This study

Yeast strains

	W16362		ura3/ura3::pTEF2-MYC3-heIF2α-tCYC1-URA3 leu2/leu2::pTEF2-MYC3-hD123-tCYC1-LEU2 his3/his3::pGCD11-FLAG3-heIF2gamma(1-464 fs*4)-tCYC1-HIS3 trp1/trp1::pMET25-HA3-heIF2beta-tCYC1-TRP1	This study
	W18018		ura3/ura3::pTEF2-MYC3-heIF2alpha-tCYC1-URA3 leu2/leu2::pTEF2-MYC3-hD123-tCYC1-LEU2 his3/his3::pGCD11-FLAG3-heIF2gamma(P432S)-tCYC1-HIS3 trp1/trp1::pMET25-HA3-heIF2beta-tCYC1-TRP1	This study
2.1.10	K699	a		RG Seufert
	W14058	a	ura3::pTEF2-CDC123-3xFLAG-tCYC1-URA3	RG Seufert
2.2.1 (Figure 22A/B)	W12626	a/α	GCD11/gcd11-delta::kanMX6	RG Seufert
	W12783	a/α	GCD11/gcd11-delta::kanMX6 his3/his3::pGCD11-FLAG3-GCD11-tCYC1-HIS3	RG Seufert
	W15907	a/α	GCD11/gcd11-delta::kanMX6 HIS3/his3::pGCD11-FLAG3-GCD11(R510D)-tCYC1-HIS3	This study
2.2.1 (Figure 22C); 2.2.2 (Figure 23)	W15678	a/α	his3/his3::pGALL-FLAG3-GCD11-tCYC1-HIS3 ura3/ura3::pTEF2-MYC3-CDC123-tCYC1-URA3	This study
	W15679	a/α	his3/his3::pGALL-FLAG3-GCD11-tCYC1-HIS3 ura3/ura3::pTEF2-MYC3-CDC123(D323R)-tCYC1-URA3	This study
	W15680	a/α	his3/his3::pGALL-FLAG3-GCD11(R510D)-tCYC1-HIS3 ura3/ura3::pTEF2-MYC3-CDC123-tCYC1-URA3	This study
	W15681	a/α	his3/his3::pGALL-FLAG3-GCD11(R510D)-tCYC1-HIS3 ura3/ura3::pTEF2-MYC3-CDC123(D323R)-tCYC1-URA3	This study
2.2.2 (Figure 25A)	W17931	a/α	his3::HIS3 TIF5-MYC13-natMX6	This study
	W15469	a/α	his/his3::pGCD11-FLAG3-GCD11-tCYC1-HIS3 TIF5/TIF5-myc13-natMX6	This study
	W17934	a/α	his3::pGCD11-FLAG3-GCD11(R510D)-tCYC1-HIS3 TIF5-MYC13-natMX6	This study
	W17932	a/α	his3::HIS3 GCD6-MYC13-natMX6	This study
	W15470	a/α	his/his3::pGCD11-FLAG3-GCD11-tCYC1-HIS3 GCD6/GCD6-MYC13-natMX6	This study
	W17935	a/α	his3::pGCD11-FLAG3-GCD11(R510D)-tCYC1-HIS3 GCD6-MYC13-natMX6	This study
	W17933	a/α	his3::HIS3 GCD7-MYC13-natMX6	This study
	W15471	a/α	his/his3::pGCD11-FLAG3-GCD11-tCYC1-HIS3 GCD7/GCD7-MYC13-natMX6	This study
	W17936	a/α	his3::pGCD11-FLAG3-GCD11(R510D)-tCYC1-HIS3 GCD7-MYC13-natMX6	This study
	W16286	a/α	his3::HIS3 RPS2-MYC13-natMX6	This study
	W16287	a/α	his3/his3::pGCD11-FLAG3-GCD11-tCYC1-HIS3 RPS2/RPS2-MYC13-NatMX6	This study
	W17937	a/α	his3::pGCD11-FLAG3-GCD11(R510D)-tCYC1-HIS3 RPS2-MYC13-natMX6	This study
2.2.2 (Figure 25B)	W16030	a/α	trp1/trp1::pGAL1-CDC123-tCYC1-TRP1 TIF5/TIF5-MYC13-NatMX6	This study
	W16018	a/α	his3/his3::pGALL-FLAG3-GCD11-tCYC1-HIS3 trp1/trp1::pGAL1-CDC123-tCYC1-TRP1	This study

			TIF5/TIF5-MYC13-natMX6	
	W16022	a/α	his3/his3::pGALL-FLAG3-GCD11(R510D)-tCYC1-HIS3 trp1/trp1::pGAL1-CDC123-tCYC1-TRP1 TIF5/TIF5-MYC13-natMX6	This study
	W16031	a/α	trp1/trp1::pGAL1-CDC123-tCYC1-TRP1 GCD6/GCD6-MYC13-NatMX6	This study
	W16019	a/α	his3/his3::pGALL-FLAG3-GCD11-tCYC1-HIS3 trp1/trp1::pGAL1-CDC123-tCYC1-TRP1 GCD6/GCD6-MYC13-natMX6	This study
	W16023	a/α	his3/his3::pGALL-FLAG3-GCD11(R510D)-tCYC1-HIS3 trp1/trp1::pGAL1-CDC123-tCYC1-TRP1 GCD6/GCD6-MYC13-natMX6	This study
	W16032	a/α	trp1/trp1::pGAL1-CDC123-tCYC1-TRP1 GCD7/GCD7-MYC13-NatMX6	This study
	W16020	a/α	his3/his3::pGALL-FLAG3-GCD11-tCYC1-HIS3 trp1/trp1::pGAL1-CDC123-tCYC1-TRP1 GCD7/GCD7-MYC13-natMX6	This study
	W16024	a/α	his3/his3::pGALL-FLAG3-GCD11(R510D)-tCYC1-HIS3 trp1/trp1::pGAL1-CDC123-tCYC1-TRP1 GCD7/GCD7-MYC13-natMX6	This study
	W16033	a/α	trp1/trp1::pGAL1-CDC123-tCYC1-TRP1 RPS2/RPS2-MYC13-NatMX6	This study
	W16021	a/α	his3/his3::pGALL-FLAG3-GCD11-tCYC1-HIS3 trp1/trp1::pGAL1-CDC123-tCYC1-TRP1 RPS2/RPS2-MYC13-NatMX6	This study
	W16025	a/α	his3/his3::pGALL-FLAG3-GCD11(R510D)-tCYC1-HIS3 trp1/trp1::pGAL1-CDC123-tCYC1-TRP1 RPS2/RPS2-MYC13-NatMX6	This study
2.2.3 (Figure 26A/B)	W276	α	his3, trp1, ura3-52::URA3-lexA-op-lacZ, leu2::pLEU2-lexA-op	RG Seufert
	W16901	α	his3, trp1, ura3-52::URA3-lexA-op-lacZ, leu2::pTEF2-CDC123-tCYC1	This study
2.2.3 (Figure 26C)	W17918	a/α	ura3/ura3::pMET3-HA3-GCD11(D2,3)-tCYC1 URA3 his3::HIS3	This study
	W17919	a/α	ura3/ura3::pMET3-HA3-GCD11(D2,3)-tCYC1 URA3 his3/his3::pGCD11-FLAG3-GCD11(D1)-tCYC1 HIS3	This study
	W17920	a/α	ura3/ura3::pMET3-HA3-GCD11(D2,3)-tCYC1 URA3 leu2/leu2::pTEF2-CDC123-tCYC1-LEU2 his3::HIS3	This study
	W17921	a/α	ura3/ura3::pMET3-HA3-GCD11(D2,3)-tCYC1 URA3 leu2/leu2::pTEF2-CDC123-tCYC1-LEU2 his3/his3::pGCD11-FLAG3-GCD11(D1)-tCYC1 HIS3	This study
2.2.4 (Figure 28)	W11164	α	leu2::LEU2	This study
	W15011	α	leu2::LEU2 leu2::pGAL1-FLAG3-GCD11-tCYC1-LEU2	This study
	W16200	α	leu2::pGAL1-FLAG3-GCD11(1-514)-tCYC1-LEU2	This study
	W16201	α	leu2::pGAL1-FLAG3-GCD11(201-527)-tCYC1-LEU2	This study
	W16202	α	leu2::pGAL1-FLAG3-GCD11(201-514)-tCYC1-LEU2	This study
2.2.4 (Figure	W18061	a/α	his3/his3::pTEF2-CDC123-tCYC1-HIS3	This study

28)			leu2/leu2::LEU2	
	W18062	a/α	his3/his3::pTEF2-CDC123-tCYC1-HIS3 leu2/leu2::pGAL1-FLAG3-GCD11-tCYC-LEU2	This study
	W18063	a/α	his3/his3::pTEF2-CDC123-tCYC1-HIS3 leu2/leu2::pGAL1-FLAG3-GCD11(1-514)-tCYC-LEU2	This study
	W18064	a/α	his3/his3::pTEF2-CDC123-tCYC1-HIS3 leu2/leu2::pGAL1-FLAG3-GCD11(201-527)-tCYC-LEU2	This study
	W18065	a/α	his3/his3::pTEF2-CDC123-tCYC1-HIS3 leu2/leu2::pGAL1-FLAG3-GCD11(201-514)-tCYC-LEU2	This study
2.2.4 (Figure 29)	K700	α		This study
	W15672	α	his3::pGALL-FLAG3-GCD11-tCYC1-HIS3	This study
	W16441	α	his3::pGALL-FLAG3-GCD11(D403R)-tCYC1-HIS3	This study
	W16442	α	his3::pGALL-FLAG3-GCD11(V281R, D403R)-tCYC1-HIS3	This study
	W16443	α	his3::pGALL-FLAG3-GCD11(1-521)-tCYC1-HIS3	This study
2.2.4 (Figure 29)	W17745	a/α	leu2::leu2::pTEF2-CDC123-tCYC1-LEU2 his3::HIS3	This study
	W17746	a/α	leu2::leu2::pTEF2-CDC123-tCYC1-LEU2 his3::his3::pGALL-FLAG3-GCD11-tCYC1-HIS3	This study
	W17747	a/α	leu2::leu2::pTEF2-CDC123-tCYC1-LEU2 his3::his3::pGALL-FLAG3-GCD11(V281R)-tCYC1-HIS3	This study
	W17748	a/α	leu2::leu2::pTEF2-CDC123-tCYC1-LEU2 his3::his3::pGALL-FLAG3-GCD11(D403R)-tCYC1-HIS3	This study
	W17749	a/α	leu2::leu2::pTEF2-CDC123-tCYC1-LEU2 his3::his3::pGALL-FLAG3-GCD11(V281R, D403R)-tCYC1-HIS3	This study
2.2.5.1 (Figure 31)	K700	α		This study
	W12629	α	leu2::pMET3-FLAG3-GCD11-tCYC1-LEU2	
	W17422	α	leu2::pMET3-FLAG3-GCD11(91-527)-tCYC1 LEU2	This study
	W17423	α	leu2::pMET3-FLAG3-GCD11(C150A)-tCYC1 LEU2	This study
	W17424	α	leu2::pMET3-FLAG3-GCD11(C174A)-tCYC1 LEU2	This study
	W17425	α	leu2::pMET3-FLAG3-GCD11(K250A)-tCYC1 LEU2	This study
	W17426	α	leu2::pMET3-FLAG3-GCD11(S114A/T115A)-tCYC1 LEU2	This study
	W17427	α	leu2::pMET3-FLAG3-GCD11(deltaSw1)-tCYC1 LEU2	This study
2.2.5.2 (Figure 32)	W16899	a	kanMX4-pGCD11-FLAG3-GCD11 ura3::pMET3-3HA-GCD11-tCYC1-URA3	This study
	W16903	a	GCD11/kanMX4-pGCD11-FLAG3-GCD11 ura3::pMET3-HA3-Gcd11(C150A)-tCYC1 URA3	This study
	W16904	a	GCD11/kanMX4-pGCD11-FLAG3-GCD11 ura3::pMET3-HA3-Gcd11(C174A)-tCYC1 URA3	This study

	W16905	a	GCD11/kanMX4-pGCD11-FLAG3-GCD11 ura3::pMET3-HA3-Gcd11(K250A)-tCYC1 URA3	This study
	W16906	a	GCD11/kanMX4-pGCD11-FLAG3-GCD11 ura3::pMET3-HA3-Gcd11(S114A/T115A)-tCYC1 URA3	This study
	W16907	a	GCD11/kanMX4-pGCD11-FLAG3-GCD11 ura3::pMET3-HA3-Gcd11(deltaSw1)-tCYC1 URA3	This study
2.2.5.3 (Table 6, figure S3)	W17699	α	leu2::pMET3-FLAG3-GCD11-tCYC1 LEU2 ade2::ADE2	RG Seufert
	W17700	α	leu2::pMET3-FLAG3-GCD11(91-527)-tCYC1 LEU2 ade2::ADE2	RG Seufert
	W17701	α	leu2::pMET3-FLAG3-GCD11(C150A)-tCYC1 LEU2 ade2::ADE2	RG Seufert
	W17702	α	leu2::pMET3-FLAG3-GCD11(C174A)-tCYC1 LEU2 ade2::ADE2	RG Seufert
	W17703	α	leu2::pMET3-FLAG3-GCD11(K250A)-tCYC1 LEU2 ade2::ADE2	RG Seufert
	W17704	α	leu2::pMET3-FLAG3-GCD11(S114A/T115A)-tCYC1 LEU2 ade2::ADE2	RG Seufert
	W17705	α	leu2::pMET3-FLAG3-GCD11(deltaSw1)-tCYC1 LEU2 ade2::ADE2	RG Seufert
	W15495	a	his3::HIS3	RG Seufert
	W5542	a	ura3::pTEF2-SUI2-tCYC1-URA3	RG Seufert
	W5546	a	trp1::pTEF2-SUI3-tCYC1-TRP1	RG Seufert
	W17707	a	leu2::pTEF2-CDC123-tCYC1-LEU2 his3::HIS3	RG Seufert
	W17439	a	ura3::pTEF2-SUI2-tCYC1-URA3 trp1::pTEF2-SUI3-tCYC1-TRP1	This study
	W17709	a	ura3::pTEF2-SUI2-tCYC1-URA3 leu2::pTEF2-CDC123-tCYC1-LEU2	RG Seufert
	W17710	a	trp1::pTEF2-SUI3-tCYC1-TRP1 leu2::pTEF2-CDC123-tCYC1-LEU2	RG Seufert
	W17711	a	ura3::pTEF2-SUI2-tCYC1-URA3 trp1::pTEF2-SUI3-tCYC1-TRP1 leu2::pTEF2-CDC123-tCYC1-LEU2	RG Seufert
2.2.6.1 (Figure 33)	W15350	a/α	ura3/ura3::pTEF2-MYC3-heIF2α-tCYC1-URA3 leu2/leu2::pTEF2-MYC3-hD123-tCYC1-LEU2 his3/his3::pGCD11-FLAG3-heIF2gamma-tCYC1-HIS3 trp1/trp1::pMET25-HA3-heIF2beta-tCYC1-TRP1	RG Seufert
	W16360	a/α	ura3/ura3::pTEF2-MYC3-heIF2α-tCYC1-URA3 leu2/leu2::pTEF2-MYC3-hD123-tCYC1-LEU2 his3/his3::pGCD11-FLAG3-heIF2gamma(1-457)-tCYC1-HIS3 trp1/trp1::pMET25-HA3-heIF2beta-tCYC1-TRP1	RG Seufert
	W16362	a/α	ura3/ura3::pTEF2-MYC3-heIF2α-tCYC1-URA3 leu2/leu2::pTEF2-MYC3-hD123-tCYC1-LEU2 his3/his3::pGCD11-FLAG3-heIF2gamma(1-464 fs*4)-tCYC1-HIS3 trp1/trp1::pMET25-HA3-heIF2beta-tCYC1-TRP1	RG Seufert
2.2.6.2 (Figure 34)	W16353	a	his3::pGCD11-FLAG3-heIF2gamma -tCYC1-HIS3	RG Seufert
2.2.6.3 (Figure 36A/B)	W17743	α	his3::pGALL-FLAG3-heIF2gamma-tCYC1-HIS3	This study
	W17744	α	leu2::pTEF2-MYC3-hD123-tCYC1-LEU2	This study

			his3::pGALL-FLAG3-heIF2gamma-tCYC1-HIS3	
2.2.6.3 (Figure 36C/D)	W16916	α	ura3::pMET3-MYC3-D123-tCYC1-URA3 leu2::pMET-FLAG3-heIF2gamma-tCYC-LEU2	RG Seufert
	W16919	α	ura3::pTEF2-MYC3-D123-tCYC1-URA3 leu2::pMET-FLAG3-heIF2gamma-tCYC-LEU2	RG Seufert
2.2.7.1 (Figure 38)	W15568	a/α	CDC123/cdc123-delta::kanMX4 leu2/leu2::pTEF2-MYC3-hD123-tCYC1-LEU2	This study
	W15573	a/α	CDC123/cdc123-delta::kanMX4 leu2/leu2::pTEF2-MYC3-hD123(1-314)-tCYC1-LEU2	This study
	W15578	a/α	CDC123/cdc123-delta::kanMX4 leu2/leu2::pTEF2-MYC3-hD123(1-292)-tCYC1-LEU2	This study
	W15581	a/α	CDC123/cdc123-delta::kanMX4 leu2/leu2::pTEF2-MYC3-hD123(Y304G)-tCYC1-LEU2	This study
2.2.7.2 (Figure 39A)	W15164	α	trp1::pMET25-HA3-heIF2beta-tCYC1-TRP1 ura3::pTEF2-MYC3-heIF2gamma-tCYC1-URA3	This study
	W15165	α	leu2::pTEF2-FLAG3-hD123-tCYC1-LEU2 trp1::pMET25-HA3-heIF2beta-tCYC1-TRP1 ura3::pTEF2-MYC3-heIF2gamma-tCYC1-URA3	This study
	W17059	α	trp1::pMET25-HA3-heIF2beta-tCYC1-TRP1 ura3::pTEF2-MYC3-heIF2gamma-tCYC1-URA3 leu2::pTEF2-FLAG3-D123(1-314)-tCYC1-LEU2	This study
	W17060	α	trp1::pMET25-HA3-heIF2beta-tCYC1-TRP1 ura3::pTEF2-MYC3-heIF2gamma-tCYC1-URA3 leu2::pTEF2-FLAG3-D123(1-292)-tCYC1-LEU2	This study
	W17061	α	trp1::pMET25-HA3-heIF2beta-tCYC1-TRP1 ura3::pTEF2-MYC3-heIF2gamma-tCYC1-URA3 leu2::pTEF2-FLAG3-D123(Y304G)-tCYC1-LEU2	This study
2.2.7.2 (Figure 39B)	W276	α	his3, trp1, ura3-52::URA3-lexA-op-lacZ, leu2::pLEU2-lexA-op	RG Seufert
	W15023	α	his3, trp1, ura3-52::URA3-lexA-op-lacZ, leu2::pTEF2-FLAG3-hD123-tCYC1-LEU2	This study
	W15592	α	his3, trp1, ura3-52::URA3-lexA-op-lacZ, leu2::pTEF2-FLAG3-D123(1-314)-tCYC1-LEU2	This study
	W15593	α	his3, trp1, ura3-52::URA3-lexA-op-lacZ, leu2::pTEF2-FLAG3-D123(1-292)-tCYC1-LEU2	This study
	W15594	α	his3, trp1, ura3-52::URA3-lexA-op-lacZ, leu2::pTEF2-FLAG3-hD123(Y304G)-tCYC1-LEU2	This study
2.3.1 (Figure 40)	K842	a/α		RG Seufert
	W12626	a/α	GCD11/gcd11-delta::kanMX6	RG Seufert
	W8907	a/α	SUI2/sui2delta::HIS3MX6	RG Seufert
	W9883	a/α	SUI3/sui3-delta::kanMX6	RG Seufert
	W4443	a/α	CDC123/cdc123-delta::kanMX4	RG Seufert
2.3.2 (Figure 41)	W15565	a/α	GCD11/GCD11(1-521)-KanMX6	This study
	W15566	a	GCD11(1-521)-KanMX6	This study
	W15567	α	GCD11(1-521)-KanMX6	This study
2.3.4 (Figure 43C)	K699	a		RG Seufert
	W15566	a	GCD11(1-521)-KanMX6	This study
	W14785	a	gcn4-delta::natNT2	RG Seufert

	W15747	a	GCD11(1-521)-KanMX6 gcn4-delta::natNT2	RG Seufert
2.3.4 (Figure 44A)	W4331	α	SIC1-MYC13-His3MX6	RG Seufert
	W4332	a	SIC1-MYC13-His3MX6	RG Seufert
	W16293	a	GCD11(1-521)-KanMX6 SIC1-MYC13-His3MX6	This study
	W16294	α	GCD11(1-521)-KanMX6 SIC1-MYC13-His3MX6	This study
2.3.4 (Figure 44B/C/D)	W13701	α	SIC1-GFP-SpHIS5 trp1::pTEF2-mCherry-SWI5-S/A-tCYC1-TRP1	RG Seufert
	W15753	α	GCD11::GCD11(1-521)-KanMX6 leu2::pSIC1-SIC1-GFP-tCYC1-LEU2 trp1::pTEF2-mCherry-SWI5-S/A-tCYC1-TRP1	RG Seufert
2.3.5 (Figure 45)	W10241	α	pTEF2-GFP-SSO1-tCYC1-URA3 pTEF2-mCherry-SWI5-S/A-tCYC1-TRP1	RG Seufert
	W15770	α	GCD11::GCD11(1-521)-KanMX6 ura::pTEF2-GFP-SSO1-tCYC1-URA3 trp1::pTEF2-mCherry-SWI5-S/A-tCYC1-TRP1	RG Seufert

4.7 Other materials

4.7.1 Kits

Table 19 : List of kits used

Name	Use	Manufacturer
NucleoSpin® Plasmid Mini Kit	Small scale plasmid purification	Macherey-Nagel, Düren, Germany
GenElute™ HP Plasmid Midiprep Kit	Medium scale plasmid purification	Sigma Aldrich, St. Louis, USA
QIAquick PCR Purification Kit	PCR purification	Qiagen, Venlo, Netherlands
QIAquick Gel Extraction Kit	Plasmid clean-up after gel preparation	

4.7.2 Machines

Table 20 : List of machines used

Name	Use	Manufacturer
Axio Observer.Z1	Inverse microscope	Carl Zeiss, Oberkochen, Germany
Axiocam MRm	Microscope camera	
Blue/Green LED Transilluminator XL	Agarose gel documentation	Nippon genetics Europe, Düren, Germany
CSU-XI	Spinning disk module	Yokogawa, Musashino, Japan
Cyflow Space	Flow cytometry	Sysmex-Partec, Görlitz, Germany
DS-11 FX+ photometer	Microspectrometer	DeNOVIX, Wilmington, USA
Electroporator 2510	Electroporation	Eppendorf, Hamburg, Germany
Imager M1	Fluorescence microscope	Carl Zeiss, Oberkochen, Germany
Mixer mill MN200	Cell homogenization	Retsch, Haan, Germany
Mixer mill MN2000	Cell homogenization	
LICOR Odyssey	WB infrared scanner	Li-COR, Lincoln, USA
UVP GelStudio PLUS	Agarose gel documentation	Analytik Jena, Jena, Germany
RotorGenQ	qPCR	Qiagen, Venlo, Netherlands
Singer MSM	Tetrad dissection	Singer Instruments, Watchet, UK
SONOPULS HD 2070	Cell decollating, cell lysis	Bandelin, Berlin, Germany

4.7.3 Softwares and webtools

Table 21 : List of softwares used

Software	Use	Manufacturer
Clone Manager 6	Sequence editing	Sci Ed Software, Westminster, USA
Clustal ω	Multiple sequence alignment	EBI, Hinxton, UK
Corel Draw graphics suite	Image editing	Corel Corporation, Ottawa, Canada
EMBOSS water	Pairwise sequence alignment	EBI, Hinxton, UK
ExPASy Translate	In silico translation	Bioinformatics Recource Portal
FCS Express 4	Flow cytometry analysis	Denovo Software, Glendale, USA
ImageJ	Image editing, data analysis	Open project
Image Studio 5.2	Control software for LiCOR Odyssey, WB data analysis	LICOR, Lincoln, USA
Jalview	Sequence alignment	Open project
Microsoft Access 2013	Data base management	Microsoft, Redmond, USA
Microsoft Excel	Data management and visualization	Microsoft, Redmond, USA
Microsoft Powerpoint	Data management, visualization and presentation	Microsoft, Redmond, USA
Microsoft Word	Writing	Microsoft, Redmond, USA
Odyssey v3.0	WB data analysis	LICOR, Lincoln, USA
Oligo Calculator	Oligonucleotide analysis	Northwestern University, USA
re site finder	Cryptic restriction site finder	University of Chicago, USA
SnapGene viewer 5.1	Plasmid map editing	GSL Biotech, Vadodara, India
WebGestalt	Overrepresentation analysis	http://www.webgestalt.org
WinMDI2.8	Flow cytometry analysis	Joe Trotter
ZEN 2.3	Control software for Zeiss microscopes	Carl Zeiss, Oberkochen, Germany

5 Methods

5.1 Molecular cloning and genetics

All plasmids constructed in this study are based on previously cloned genes *from Saccharomyces cerevisiae* (*S. c.*) or *Homo sapiens* (*H. s.*). The backbone of cloning plasmids is pBluescript II SK+, a cloning vector derived from pUC19. Plasmids for expression of proteins in yeast are based on the pRS series of shuttle vectors, which were constructed from pBluescript, too, but contain yeast specific elements for selection and propagation (Sikorski and Hieter, 1989). Plasmids for stable transfection of mammalian cells were constructed by inserting the genes of interest into pcDNA5-FRT/TO. For modification of endogenous yeast genes, the pFA6a series of plasmids was used. Primer design, PCR and subsequent steps were carried out as described in the original publication (Longtine et al., 1998).

5.1.1 Polymerase chain reaction (PCR)

PCR is a method for in-vitro DNA amplification first published in 1986 (Mullis et al., 1986). First, double stranded DNA is melted at 94 °C. After lowering the temperature, single stranded DNA oligos, complementary to the end sequences of the DNA fragment to be amplified, bind to the single stranded template DNA. In a third step, a DNA polymerase synthesizes the new DNA strands, starting from the primer oligonucleotide. These steps are repeated in a cyclical manner until a sufficient amount of DNA has been synthesized. Important breakthroughs for the method of PCR have been the use of thermostable polymerases to avoid degradation of the enzyme after each cycle (Saiki et al., 1988) and the discovery of thermostable polymerases with proofreading activity (Lundberg et al., 1991).

For applications that do not require accurate amplification of DNA, the highly active and fast *Taq* polymerase from hyperthermophilic archaeon *Thermus aquaticus* was used. Whenever the amplified DNA fragments were used in subsequent steps, such as molecular cloning or yeast transformation, DNA was amplified with the more accurate *KOD* polymerase, which possesses a 3'-5' proofreading activity.

5.1.1.1 Amplification of DNA sequences for molecular cloning

For molecular cloning, DNA fragments were amplified with KOD polymerase. The primers contained a sequence complementary to the end sequences of the template (around 20 bp), restriction enzyme recognition sites and a spacer sequence at the 5'-end to help the restriction enzymes attach to the fragment. The melting temperature was calculated based on the sequences complementary to the template with the online tool Oligo Calculator. For annealing, a temperature (T_A) slightly below the melting temperature was chosen. The conditions and time profile of a typical PCR for gene amplification are shown in the table below.

Table 22: Program for standard gene amplification PCR

PCR reaction		**Time profile**			
10 x KOD buffer	5 µl	Denaturation	94 °C	5 min	
$MgSO_4$ (25 mM)	3 µl				
dNTPs (2 mM)	5 µl	Denaturation	94 °C	1 min	
f-Primer (10 µM)	3 µl	Annealing	T_A -1	1 min	x 25
r-Primer (10 µM)	3 µl	Elongation	72 °C	1 min/ kb	
Template	1-100 ng				
KOD polymerase	1 µl	Terminal	72 °C	5 min	
H_2O	ad 50 µl	Elongation			

5.1.1.2 Site-directed mutagenesis

Point mutations can be introduced into plasmid DNA in-vitro using the QuikChange protocol (by Agilent). Two reverse complementary primers are designed that contain a point mutation or a few mutations in close proximity and ~20 nucleotides upstream and downstream of the mutation that are complementary to the template. After denaturation of the template, the primers bind to each of the two template strands and the entire plasmid is replicated. According to the original protocol, the amplification reaction is linear rather than a true PCR, as the newly synthesized mutated DNA products are not suitable as templates. The PCR products are circular plasmids that can be readily taken up and used by *E. coli* cells. A newer study disputes this and claims an exponential amplification is possible and the products are linear double stranded DNA molecules with homologous ends that are recombined into circular plasmids in *E. coli* (Xia et al., 2015). However, before transforming *E. coli* with the DNA, the PCR product is first treated with *Dpn*I, a restriction enzyme that recognizes methylated DNA (which the PCR product is not), to degrade the unmutated template. If possible, the mutagenesis should create or eliminate a restriction site in the plasmid to simplify the screening of mutants. Table 23 shows composition and time profile of a site-directed mutagenesis reaction.

Table 23: Program for site-directed mutagenesis

PCR reaction		**Time profile**			
10 x KOD buffer	5 µl	Denaturation	94 °C	5 min	
$MgSO_4$ (25 mM)	3 µl				
dNTPs (2 mM)	5 µl	Denaturation	94 °C	1 min	
fwd-Primer (10 µM)	3 µl	Annealing	50 °C	1 min	x 20
rev-Primer (10 µM)	3 µl	Elongation	72 °C	1 min/ kb +	
Template	1-50 ng			1 min	
KOD polymerase	1 µl				
H_2O	ad 50 µl	Terminal Elongation	72 °C	5 min	

5.1.1.3 PCR for genomic modifications in yeast

The modification of endogenous genes in yeast is, compared to multicellular organisms, simple and efficient, as yeast cells can be easily transformed with circular and linear DNA. Yeasts integrate linear DNA into their genome by homologous recombination. The pFA6a series of plasmids offers a variety of modules that, if amplified with primers containing 5'-tails homologous to their target site in the genome, allow deletion and truncation of genes, exchange of promotors as well as C-terminal tagging (Longtine et al., 1998). For gene deletion, a plasmid

such as pFA6a-HISMX6 can be used. Oligonucleotides are designed that prime the template DNA outside of the HISMX6 cassette. They must also contain 5'-tails, around 45 bp in length, that are homologous to the sequences upstream of the start codon and downstream of the stop codon of the target gene. HISMX6 contains a *HIS3* gene from *Saccharomyces kluyveri,* flanked by a *TEF2* promotor and a *TEF2* terminator. The cassette is amplified with flanking homologous tails, used in a yeast transformation, and integrated into the genome to replace the gene of interest. *HIS3* from *S. kluyveri* can complement the defective *HIS3* genes in *S. cerevisiae* laboratory strains and serve as a selection marker. Composition and time profile of the PCR are similar to a regular gene amplification with KOD polymerase.

5.1.1.4 Colony PCR

Colony PCR is a simple and quick method for identifying presence or absence of genes, mutations and modifications in genomic DNA without the need for clean genomic DNA preparation. A small amount of yeast cells is resuspended in 5 µl of water in a PCR Tube. The PCR master mix, containing primers specific for the genomic constellation to be analyzed, is prepared separately on ice and mixed with the yeast cells by pipetting up and down shortly before starting the PCR. During the first denaturation step, a sufficient amount of genomic DNA is released from the cells to enable the amplification reaction. The program for colony PCR is similar to a regular gene amplification, though Taq polymerase is used preferably and a small volume (15-25 µl) is sufficient.

Mating type PCR

An essential part of yeast genetics is identification of the mating type of haploid spores after tetrad dissection. The mating type of a yeast cells is determined by whether a MATa or MATα allele is present in the MAT locus on chromosome 3. Unlike natural yeast strains, laboratory strains are unable to undergo mating type switch. Before invention of the MAT-PCR technique, mating types were determined by crossbreeding of the strain in question against other haploid strains of known mating type; only yeast cells of opposite mating type can mate. MAT-PCR involves the use of three primers (WS826, WS827, WS828, see table 16), one of which binds outside of the MAT locus independently of the mating type. The other two are specific for either of the two MAT alleles. In MATa cells, the two primers WS826 and WS828 bind and yield a product of 544 bp, whereas in MATα cells, WS827 instead of WS828 binds and a product of 404 bp is synthesized. Diploid cells usually contain both MATa and MATα alleles, thus yielding both fragments. The PCR product is analyzed on a 1.5% agarose gel. Table 24 shows the composition and time profile of a MAT-PCR.

Table 24: Program for mating type (MAT-) PCR

PCR reaction		**Time profile**			
10 x Taq buffer	1.5 µl	Denaturation	94 °C	5 min	
dNTPs (2 mM)	1.5 µl				
Primer mix	1 µl	Denaturation	94 °C	40 s	
(WS826/7/8), 10 µM each		Annealing	55 °C	40 s	x 35
Taq polymerase	1-100 ng	Elongation	72 °C	40 s	
Template: Yeast in H_2O	5 µl				
H_2O	ad 15 µl	Terminal Elongation	72 °C	5 min	

5.1.2 Plasmid construction

5.1.2.1 Restriction digestion

The amounts of DNA and restriction enzymes and the reaction volume were chosen according to the required amount of digested DNA. In order to insert a DNA fragment into a vector, they must be cut with compatible restriction enzymes. Usually, two different restriction enzymes which create overhangs (sticky ends) and are active in the same reaction buffer and at the same temperature were used. Restriction digestion was also used to verify the identity of plasmids by making use of their individual restriction site profile. Typical reaction conditions for three applications are listed in the table below.

Table 25: Composition of different restriction digest reactions

Analytical digestion		**Preperative digestion/ plasmid linearization**	
DNA	100-300 ng	DNA	2-3 µg
Enzyme	2 U	Enzyme	10 U
10 x buffer	1 µl	10 x buffer	2 µl
H_2O	ad 10 µl	H_2O	ad 20 µl

5.1.2.2 Gel preparation

After restriction digestion, the desired vector and insert fragments were purified via gel electrophoresis. The reaction products were mixed with 6x purple loading dye and loaded onto a 1% agarose gel. After the gel run, the bands were identified on an illumination table (Blue/Green LED Transilluminator XL) and cut out with a scalpel. The DNA was extracted from the gel pieces using the QIAquick Gel Extraction Kit.

5.1.2.3 Ligation of DNA fragments

Vector and insert were combined in a stoichiometric ratio of 1:5, together with 1 U of T4 ligase and 2 µl 10x ligase buffer in a volume of 20 µl. The relative DNA concentrations were assessed by visual judgement on an agarose gel. Typically, 1 µl of vector and an appropriate volume of insert were used. The reaction mix was incubated at room temperature (RT) for at least 1 h. Before electroporation (see section 5.3.2), the product was desalted by dialysis against demineralized water for 20 min.

5.1.2.4 Screening of *E. coli* transformants

Some of the grown single colonies were picked with 200 µl pipette tips and cultivated overnight in 2 ml LB_{Amp}. Next day, plasmid DNA was prepared from these cultures by EasyPrep method. Depending on the amount of probes, the DNA samples were run on 1% agarose gels undigested, with an empty vector as negative control, or digested with appropriate restriction enzymes first to identify the correct plasmid. In the former case, some of the positive samples were chosen for restriction digestion in a second round of analysis. Typically, the restriction analysis was carried out using the same enzymes that were used to generate the vector- and insert fragments. One positive clone per generated plasmid was picked for a clean DNA preparation (see section 5.3.3.2). If the insert had been amplified via PCR, the new plasmid had to be sequenced to avoid unwanted mutations. Here, the sequencing services of Seqlab/ Microsynth and GATC/ Eurofins were used. For most plasmids, the primers WS84/ WS85 were used, as they bind upstream and downstream of the LacZ fragment in all pUC19 based plasmids, which includes pBluescript and pRS vectors.

5.2 Working with yeast

All yeast strains in this work are derived from lab strain W303, which in turn was created by cross-breeding different yeast strains into S288c, the most commonly used laboratory yeast strain (Ralser et al., 2012). W303 can be efficiently transformed and sporulated, making it a go-to strain for studies that involve extensive yeast transformation, cross-breeding and tetrad dissection (Matheson et al., 2017). However, W303-derived yeasts require media enriched in adenine and tryptophane for optimal growth.

5.2.1 Yeast cultivation

Yeast cells were cultivated in XY(-D) medium for growth. It is similar to YEPD but contains additional adenine, tryptophane and buffering KH_2PO_4. In XY-D medium, W303 cells have a generation time of 1.75 h at 25 °C and 1.35 h at 30 °C. Alternative carbon sources were used to change expression conditions and synthetic medium was used for selection after yeast transformation and cross breeding.

5.2.1.1 Agar plate culture

XY medium was autoclaved with agar and without sugar in glass bottles. After autoclaving, sugar was added and the medium were poured into petri dishes directly, or the bottles were left to cool down. In the latter case, the medium was heated in a water bath to melt the agar, sugar was added and the plate was cast. The plates were left to dry for three days and stored at 4 °C.

Yeast cells were streaked out to obtain single colonies by using toothpicks or inoculation loops. Typically, yeast cells were incubated at 30 °C for two days or at 25 °C for three days and then stored at 4 °C for weeks to months.

5.2.1.2 Liquid culture

Yeast cells were taken from a single colony (if available) on an agar plate, using a 200 µl pipette, and resuspended in the appropriate liquid medium. For a dense overnight culture, a small amount of cells was resuspended in medium and incubated at 30 °C until the next morning. If exponentially growing cells were needed, a preculture was inoculated during the day. In the evening, a defined amount of cells was transferred to new culture medium. The amount was dependent on the density of the preculture, the doubling time and cultivation time, as well as the desired volume and cell density of the main culture.

5.2.1.3 Freezing and thawing of cells

To preserve newly created yeast strains, a 5 ml XY-D culture of each strain was incubated overnight at 30 °C in test tubes to obtain dense, stationary cultures. The next day, the test tubes were centrifuged at 800 x g for 2 minutes and the supernatant was removed. The pellet was resuspended in 15% sterile-filtered glycerol and transferred into steril 2 ml screw cap tubes. The cells were then frozen at -80 °C. For thawing, a small amount of cells was taken from the tube with an inoculation loop and streaked out on an XY-D plate. The plate was then incubated as described above.

5.2.2 Cell cycle profiling with Flow cytometry

The DNA content of cells varies during the cell cycle. In G1 phase, DNA content is n = 1. In S-phase, the genome is replicated and DNA content is between n = 1 and n = 2, depending on the progression status of genome replication. In G2 and M phase, when DNA replication is completed, DNA content is n = 2. During cytokinesis, mother and daughter cell are separated into two distinct particles and DNA content is again n = 1. In diploid yeasts, DNA content per particle is twice the amount of that in haploid yeast cells. If a yeast culture contains cells of only one ploidy, the DNA content of a cell is an excellent surrogate marker for its cell cycle stage.

With flow cytometry, fluorescently labelled DNA can be measured in single particles. An equivalent of 1 ml of yeast cells at an OD_{600} of 0.25 was harvested by centrifugation and resuspended in 150 µl of water. To fixate the cells, 350 µl of pure ethanol were added dropwise while the cells were carefully mixed on a vortexer. The fixed cells were centrifuged and washed in 50 mM NaCitrate buffer (pH = 7) and resuspended in 250 µl of the same buffer. During the fixation process, the cells agglomerate. To separate them, the cells were treated with six ultrasound pulses at 40% intensity. At this point, the cells still contained protein and RNA, which had to be removed. First, 100 µg of RNAse A were added and the cells were shaken at 50 °C for 1 h. Then, proteinase K was added and the cells were shaken at 50 °C for one more hour. Thereafter, cells were washed with NaCitrate buffer and resuspended in NaCitrate buffer with 1 µM of the nucleic acid stain Sytox green. The cells were repeatedly inverted at 4 °C overnight to stain the DNA. Before the flow cytometric analysis, they were again treated with ultrasound to resolve clumps. Flow cytometry was then performed with the cytometer Cyflow space. Cell cycle profiles were analyzed with WinMDI2.8 and FCS Express 4.

5.2.3 Yeast genetics

The exceptional usefulness of *S. cerevisiae* in genetics and molecular biology in part stems from the ease with which yeast genomes can be altered by transformation, cross-breeding and meiotic recombination during sporulation. While the development of methods to introduce DNA into yeast cells that are both effective and easy took many decades, the cells readily integrate DNA into their genomes if it contains ends that are homologous to genomic sequences. Circular plasmids can be propagated in yeast cells if they contain an origin of replication. Unlike *E. coli*, yeasts can occur as haploid or diploid organisms. Haploid cells of different mating types quickly mate to form diploid cells with combined genomes. Diploid cells in turn can undergo sporulation under certain conditions, during which two meiotic cell divisions occur. As in higher eukaryotes, homologous chromatids align in the first meiotic division and genetic material is exchanged during crossover events. Four spores, coated with an ascus, are formed in which the genetic material of the mother cell is distributed according to the laws of inheritance. This can be used to recombine genetic traits and generate new yeast strains.

5.2.3.1 Yeast transformation

DNA constructs were introduced into yeast cells by using a variant of the lithium acetate - PEG method. The method was first described in 1983 (Ito et al., 1983) and further improved by additionally using an excess of single stranded DNA, usually from salmon or herring sperm (Gietz and Woods, 2002).

One day before the transformation, a small overnight yeast culture is prepared. In the morning, the culture is diluted in fresh liquid medium. The DNA is prepared for transformation. PCR products can be readily used, whereas plasmid DNA must be linearized first to create homologous ends. Usually, the plasmid is cut at its selection marker, e.g. HIS3, to later allow the yeast cell to integrate the expression construct into its HIS3 locus. At the time of transformation, 2 ml of a culture at a cell density of ~OD = 1.0 are harvested by centrifugation. The cells are first washed in sterile water and then in TE-LiAc buffer. For quick transformations with a high expected efficiency, e.g. transformation with a plasmid, the reaction mix, consisting of 2 µg DNA, 240 µl PEG 3350, 36 µl 10 x TE 36 µl 1M LiAc and 50 µg ssDNA, was given onto the cells and thoroughly mixed. For transformations with a low expected yield of transformants, such as with pFA6a PCR products, the cells were incubated in TE-LiAc for several minutes and LiAc was not added to the reaction mix until the cells were already well resuspended. For either variant, the cells were shaken or inverted for 20 min at RT and then incubated at 42 °C for 15-45 min without shaking. Then, the cells were centrifuged, resuspended in water and streaked out on a selection plate or, if transformants were selected with an antibiotic, given time to recover for 2 h in XY-D at 30 °C before being plated onto selection medium agar. The plates were incubated at 30 °C for 2-3 days until large colonies of transformed yeast cells had grown. A few transformants were selected and streaked out on new selection plates to avoid carry-over of untransformed yeast cells into non-selective cultures. Once established, the new yeast strains were cultivated in XY-D. However, transient transformation with plasmids required permanent cultivation under selective conditions.

5.2.3.2 Crossbreeding, sporulation and tetrad dissection

Yeast cells express mating type specific pheromones, the a- and α-factor, as well as a- and α-factor specific receptors to recognize yeast cells of the opposite mating type. When MATa- and MATα cells are in close proximity, they form a projection towards each other and the two cells, including their genomes, combine. The combined cell divides, giving rise to a new diploid yeast cell lineage. Breeding of yeast cells can be induced by simply combining two strains of opposite mating types in the same medium; in this work, yeasts were resuspended in a small amount of water and spotted together on an XY-D plate. If the two yeast strains contain different marker genes, diploid yeasts can be selected for by streaking out cells from the spot on double selection plates. If this is not the case, cells from the spot are streaked out on another XY-D plate and single colonies are analyzed for diploidy by MAT PCR.

In nature, sporulation of yeast cells usually occurs under conditions of nutritional scarcity. The recombination of genetic traits enables the emergence of new yeast lineages that are more resistant to changing conditions; additionally, spores are more durable towards harsh conditions than vegetative cells. Spores quickly germinate if sufficient nutrients are available. Under laboratory conditions, sporulation can be induced by growing cells under nutrient-poor conditions. Diploid yeast cells are resuspended in 2 ml of presporulation medium with 10 % glucose and an excess of nutrients. The cells are incubated at 30 °C until they have reached late log phase. Alternatively, they can be incubated overnight. Then, the cells are washed with water to remove presporulation medium. Sporulation is induced by adding the nutrient-poor sporulation medium with little glucose or amino acids and acetate as the main carbon source. After three days of incubation at 25 °C, >50% of cells should have formed four spores, the so-

called tetrad. To separate the spores, the ascus must be removed from the tetrad, first. To this end, an enzymatic solution, containing 2 mg of novozyme 234 in 1 ml novozyme medium is prepared and mixed 1:1 with 50 µl of sporulated yeast cells. Novozyme 234 is an enzyme preparation from the slime of *Helix pomatia*, which digests the ascus wall. After 20 minutes at RT, a small amount of cells is pipetted onto the edge of a clear XY-D plate, letting the liquid run down the side of the plate. As soon as the liquid is absorbed into the plate, the tetrads can be separated in a micromanipulator. The spores of each tetrad are aligned in rows to be able to observe the growth of each spore of a tetrad. Genetic traits that are coupled to an antibiotic resistance or prototrophy can be identified in haploid colonies by spotting them on selection plates.

5.2.3.3 Yeast promoters used in this work

In this work, a variety of promoters were used to express proteins in different amounts and under different conditions. In the table below, all used promoters are listed. For each one, its estimated relative strength and conditions for its activity are noted. Note that expression varies from protein to protein and depends on the number of genomic integrations of a given expression construct during yeast transformation.

Table 26: Promoters used in this work

Name	Strength	Induction/ repression
p*CDC123*	0.1	constitutively active
p*GCD11*	1	constitutively active
p*TEF2*	10	constitutively active
p*MET25*	untested	moderate repression in methionine-rich medium
p*MET3*	4	strong repression in methionine-rich medium
p*GALL*	10	repression in glucose medium, induction in galactose medium
p*GAL1*	20	

5.2.4 Spot dilution growth test

A simple way to test the toxicity of a protein is the yeast spot test. Yeast strains, expressing the protein of interest conditionally are grown under repressive conditions in liquid culture. They are transferred to a 96-well plate and diluted serially in water (figure), starting at an OD_{600} of 1. Then, they are spotted on agar plates, one of which represses expression of the protein, whereas the other induces its expression. On the same plate, a strain lacking the coding gene is spotted. If the protein of interest is a mutant, a third strain, expressing the wild type protein is included, too. Growth is then monitored over several days and compared between tested strain and controls. The same test can be applied to testing temperature sensitivity of a yeast strain or tolerance to substances in the medium. Toxicity of the protein is evaluated by cell density in the highly concentrated spots and size of individual colonies in the diluted spots.

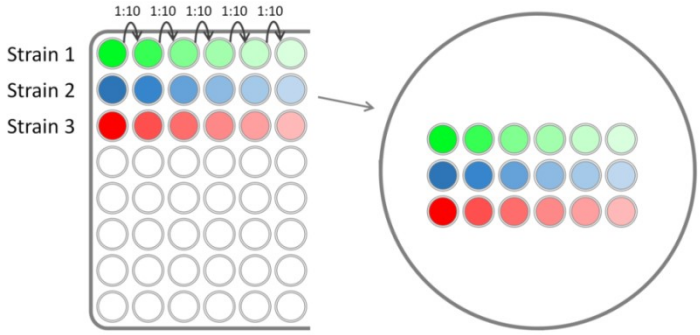

Figure 49: Schematic representation of the dilution spot test.

5.2.5 Live cell microscopy

Yeast cells were transferred to a small volume of growth medium in the morning. When the cells had reached exponential growth phase, a defined amount was used to inoculate an overnight culture. In the morning, OD_{600} of the culture was measured. A part of the culture was concentrated to OD_{600} = 4/ ml by centrifugation and resuspension. For single images, 4 µl of the cell suspension were pipetted onto a large cover slip and covered with a piece of SD++ agar 1 cm^2 in size. For time lapses, cells were kept in the HT200 chamber by ibidi, which can be placed on the microscope table, covered by a piece of SD++ agar inside the chamber. The chamber can keep the cells at a defined temperature to standardize growth conditions. All images and time lapses were taken at 630x magnification. Zeiss microscope Axio Observer.Z1, together with the spinning disk module CSU-XI and AxioCam MRm were used. GFP-tagged proteins were excited at 488 nm and mCherry-tagged proteins at 561 nm. Excitation time and laser intensity depended on the fluorescent strength of the tag protein and the expression level of each fusion protein. In the table below, excitation times and laser intensities are listed. Microscopic images and time lapses were analyzed with ImageJ.

Table 27: Laser intensities and excitation times for fluorescent proteins in this work.

Protein	Laser intensity	Excitation time
mCherry-NLS	8%	200 ms
$Sic1^{GFP}$	10%	200 ms
$Sso1^{GFP}$	2.5%	100 ms

5.2.6 Morphological analysis of yeast cells

Cell size, budding, cytokinesis and the temporal relationship between these were analyzed by observation of yeast cells in live cell microscopy. GFP-tagging of Sso1 was used as a tool to increase the visibility of cell borders. Sso1 is a t-SNARE protein located in the cytoplasmic membrane. The Sso1-GFP fusion protein allows visualization of cellular borders at a higher resolution than phase contrast

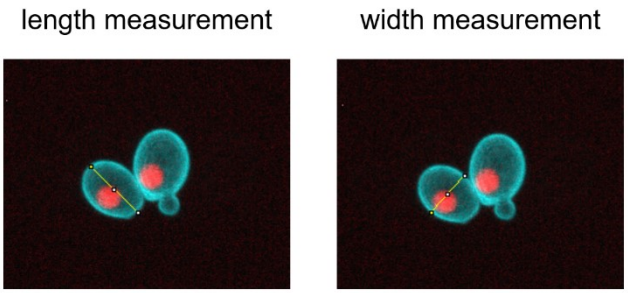

Figure 50: Volume measurement in yeast cells. Width (right) and length (left) of yeast cells were measured in ImageJ.

microscopy. Using ImageJ, length and width of dividing cells were measured. Cell shape was assumed to be an ellipsoid with a circular cross-section and a long side. Volume was calculated accordingly via the following formula (a = short side, b = long side):

$$V = \frac{\pi}{6} * a^2 * b$$

Time lapses of dividing cells were used to estimate time intervals from cytokinesis to budding, from budding to completion of cell division etc.

5.2.7 *LacZ* reporter assay

The translation of an mRNA is dependent on properties of its untranslated regions. Depending on the conditions in a cell, certain properties, such as highly structured 5'-leaders, uORFs or miRNA binding sites can influence the rate of translation initiation at the main ORF. Here, expression of *GCN4*, the main activator of the ISR in yeast, was tested with a reporter plasmid, in which the *GCN4* 5'-leader was fused to the *LacZ* gene, which encodes β-galactosidase. In the assay, ONPG, an artificial galactopyranoside, is cleaved by β-galactosidase and releases yellow o-nitrophenol. Yeast strains of interest were transformed with the reporter plasmid. A few colonies were picked and grown in selective medium overnight. The cells were harvested and resuspended in Z-buffer. An amount of OD_{600} = 0.5 was taken and suspended in 1 ml of Z-buffer. SDS was added to a final concentration of 0.0025% and 50 µl of chloroform were added. Cells were shaken at 37 °C for 15 min. Then, 200 µl of an aqueous 0.4% ONPG solution were added and incubated with the cells for an appropriate amount of time. Thereafter, 500 µl of 1M Na_2CO_3 were added to stop the reaction and increase color intensity. OD_{420} was measured for all probes. The blank value was generated with a sample in which a yeast strain without the reporter plasmid was used. From the OD_{420} value, miller units (Miller, 1972) were calculated (see formula below), which indicate lacZ activity and thus translation intitiation of the *GCN4* ORF.

$$U = 1000\, x \frac{OD420}{t * V * OD600}$$

U = Miller units t = reaction time (min) V = reaction volume

OD_{600}: indicates the amount of cells used in the assay

5.3 Working with *E. coli*

5.3.1 *E. coli* cultivation

In this work, the *E. coli* strain DH5α (genotype: *F- φ80dlacZΔM15 Δ(lacZYA-argF)-U169 deoR endA1 gyrA96 hsdR17(rk-, mk+) phoA recA1 relA1 supE44 thi-1 λ-)* was used for amplification of plasmid DNA. The cells were cultivated in LB medium or on LB agar plates, respectively. For selective media, the antibiotic Ampicillin was added at a concentration of 100 µg/ ml after autoclaving. Liquid LB_{Amp} was stored at 4 °C, LB_{Amp} agar plates were prepared by adding the antibiotic freshly before pouring the medium into petri dishes. *E. coli* cells were grown in liquid culture or on agar plates overnight at 37 °C.

5.3.2 *E. coli* transformation

DH5α cells were transformed with plasmid DNA by electroporation. Competent cells, stored at -80 °C in 10% glycerol stocks of 100 µl, were slowly thawed on ice. Electroporation cuvettes were placed on ice as well to cool them down. After the cells had thawed, 50 µl were used for one transformation and mixed with an equal amount of sterile water, containing the plasmid DNA. The mixture was transferred to the cuvette and electroporated (electric field: 12.5 kV/cm, resistance: 200 Ω, capacitance: 25 µF, voltage: 2.5 kV). The cells were quickly given into prewarmed SOC medium and given 30-60 min to recover at 37 °C. After recovery, 100 µl of the cell suspension were plated on 1/2 of an LB_{Amp} agar plate and some material was streaked onto the rest of the plate to obtain single colonies. The plate was incubated at 37 °C overnight, 30 °C for two days or 25 °C for three days.

5.3.3 Plasmid preparation

For quick screenings after transformation of *E. coli* with ligated plasmids, the fast "EasyPrep" boiling method was used. For larger scale, clean preparations, *E. coli* cells were subjected to alkaline lysis and plasmid DNA was purified with commercially available mini- or midiprep kits (see table 19).

5.3.3.1 EasyPrep boiling lysis

For quick screenings, 2 ml overnight *E. coli* cultures were centrifuged in 1.5 ml microtubes. The supernatant was removed completely and cells were resuspended in 50 µl EasyPrep buffer. In EasyPrep boiling lysis, the cells are lysed by a combination of lysozyme, an enzyme that digests the bacterial cell wall, and heat. The heat also denaturates all proteins and double stranded DNA, whereas RNase A degrades most of the RNA. The tubes were placed on a heating block at 95 °C and lysed for one minute. Thereafter, the lysate was quickly cooled down on ice to allow the plasmid DNA, but not the genomic DNA, to renaturate. The lysate was centrifuged for 10 minutes at max. rpm to pellet insoluble cell components and most of the genomic DNA. The supernatant now contained a crude plasmid DNA preparation that could be used for analytical restriction digestion and sequencing.

5.3.3.2 Column preparation

Plasmid-DNA stocks for molecular cloning, yeast transformation and other applications were prepared by alkaline lysis and subsequent column preparation. For minipreparations, 5-20 ml of *E. coli* culture in LB_{Amp} were grown overnight. For midipreparations, 50-100 ml were used, depending on the expected yield. Low-copy plasmids were prepared by lysing a large amount (200 ml) of transformed *E. coli* cells with the alkaline method. The DNA in the lysate was precipitated with isopropanol and cleaned up through a miniprep column. Alkaline lysis and column preparation were performed according to protocols provided by the kit manufacturers.

5.3.3.3 DNA precipitation

Crude DNA preparations and DNA with low concentrations can be precipitated to remove contaminants like proteins and RNA or increase concentration. The basic principle behind DNA precipitation is the lowering of its solubility by adding organic solvents, such as ethanol or isopropanol. Only DNA salt, not free DNA acid can be precipitated. Therefore, ions must be added

to the solution if its ionic strength is very low. Here, sodium acetate (pH = 5.3) was added in a final concentration of 100 mM. Lysates from alkaline lysis contain sufficient amounts of ions. Then, three volumes of ethanol or one volume of isopropanol were added. The mixture was placed in a freezer at -20 °C for one hour to speed up DNA precipitation. Then, the solution was centrifuged, e.g. at 4000 x g for 20 min or 20000 x g for 5 minutes. The pellet was washed twice, first with 70% ethanol to remove sodium acetate and then with 100% ethanol to remove water. The pellet was dried and dissolved in buffer solution.

5.4 Working with mammalian cells

Interactions between components of human eIF2 were analyzed in yeast cells, but also in the human cell line Flp-In™ T-REx™-293. This cell line serves as a host cell line for the expression plasmid pcDNA5-FRT/TO. It is commercially available from Thermo Scientific or can be created by transfection of HEK-293 with plasmids pFRT/lacZeo and pcDNA™6/TR. The first plasmid introduces a Flippase recognition target (FRT) into the genome of the cell. Transfectants are selected for by the Zeocin resistance they receive from the plasmid. Cells are tested for a single integration. FRT sites are recognized by the Flippase recombinase and serve as a target for a directed insertion of plasmid DNA that contains an FRT sites itself. The second plasmid, pcDNA™6/TR, introduces a TET-On operator that is used to regulate expression of the inserted gene at the FRT site, and a resistance towards blasticidin. Here, the Flp-In™ T-REx™-293 cell line was obtained from a collaborating research group.

5.4.1 Cell cultivation

Cells were grown in DMEM + 10% Fetal Bovine Serum (FBS) at 37 °C and a CO_2 concentration of 5%. If not stated otherwise, DMEM refers to DMEM + 10% FBS. Depending on the required amount of cells, they were cultivated in 6-well, 12-well and 24-well plates or 25 cm^2 and 75 cm^2 culture flasks. Flp-In™ T-REx™-293 host cells are resistant towards zeocin and blasticidin. It is recommended to cultivate cells under selective conditions at all times, so zeocin was added at a concentration of 100 µg/ ml and blasticidin at 10 µg/ ml. In Flp-In™ T-REx™-293 expression cell lines, the zeocin resistance is swapped for hygromycin B resistance (see section 5.4.2). The required hygromycin B concentration was assessed empirically and 100 µg/ ml was used for established cell lines. No additional antibiotics (e.g. Penicillin-Streptomycin) were used. Cells were passaged with trypsin. Before trypsination, medium was removed and cells were washed with PBS. Since HEK cells do not strongly attach to the culture flask, trypsin was diluted to 0.3x of the recommended concentration. Detached cells were centrifuged to remove trypsin and transferred to a new flask or well plate. Cells were split at ratios of 1:4 to 1:15.

5.4.2 Cell transfection

Stable expression cell lines were created via lipofection, using lipofectamine 3000. Flp-In™ T-REx™-293 cells, as mentioned, contain one FRT site and a Tet-On element. The expression plasmid pcDNA5-FRT/TO is a vector into which genes of interest can be inserted. The genes are expressed under control of a hybrid CMV-TetO promotor, which is as strong as a regular CMV promotor but controlled by the TetO element in the host cell's genome. The vector also contains

a hygromycin B resistance gene without a proprietary start codon. The gene is placed next to the FRT site and, upon recombination with the FRT site in the host cell's genome, receives a start codon from the zeocin resistance gene, which in turn loses its start codon. This way, zeocin resistance is swapped for hygromycin B resistance; randomly integrated and episomal plasmids do not mediate hygromycin B resistance. Recombination of the plasmid with the host FRT site is catalyzed by Flippase recombinase. Cells must therefore be cotransfected with pcDNA5-FRT/TO and pOG44, from which the recombinase is transiently expressed, to achieve stable transfection.

The transfection was performed according to recommendations from the Lipofectamine 3000 and pcDNA5-FRT/TO protocols (Thermo Fisher). One day before transfection, healthy Flp-In™ T-REx™-293 cells were passaged into 6-wells without any antibiotics to reach a density of around 80% the next day. In the morning, medium was removed and replaced with 1 ml of fresh DMEM without antibiotics per well. Transfection was carried out according to protocol with two different concentrations of lipofectamine. Two negative controls were performed: One without any DNA and one with 0.5 µg of the expression plasmid but without pOG44 (flippase recombinase). The third reaction included 0.5 µg of the expression plasmid and 4.5 µg of pOG44, as recommended in the manual. After 4-6 h, the medium was removed and exchanged for 3 ml of fresh DMEM without antibiotics. Then, cells were grown for 2 days and passaged into 75 cm^2 flasks with 20 ml DMEM + 50 µg/ ml Hygromycin B. Hygromycin B kills sensitive cells after 4-7 days, but quickly impairs their metabolism so that many of the untransfected cells do not attach to the flask surface quickly. This was taken advantage of by carefully exchanging medium after one day. The cells were now left in the incubator until clonal foci of transfected cells appeared, which can take up to 3 weeks. Ideally, no foci should emerge in the negative control flasks. Some of the foci were selected and passaged into 24-well plates with 1 ml DMEM + 100 µg Hygromycin B. After one week, the cells were passaged to larger flasks to perform test expressions of the clonal lineages and obtain sufficient material for cryoconservation and experiments.

5.4.3 Protein expression in HEK cells

Each cell lineage to be tested was passaged into two wells of a multi well plate. When a confluency of 80% was reached, cells in one of the wells were induced with 2 µg/ ml tetracyclin (from a 20 mg/ ml stock, dissolved in 70% ethanol), whereas vehicle control (70% ethanol) was added to the other. After one day, the cells were harvested and lyzed as described in section 5.5.2 and analyzed via Western Blot. Test expression was used first to identify positive lineages that expressed the protein of interest and then to optimize expression conditions. For the expression of larger amounts of proteins, cells in multiple 75 cm^2 flasks were induced and harvested.

5.4.4 Cryoconservation

Healthy, growing cells in a 75 cm^2 flask at a confluency of 100% were washed with PBS, trypsinated and transferred to a 15 ml tube. Cells were pelleted at 200 x g for 3 minutes. The supernatant was removed and cells were resuspended in 6 ml of freezing medium. They were aliquoted in cryotubes at 1 ml each and put into a thin styrofoam box. The box was placed in a -

80 °C freezer for at least a few hours. In order to test cell viability in the cryoculture, one cryotube was thawed in a water bath at 37 °C and the cells were transferred to a 25 cm^2 flask with 5 ml DMEM and incubated. Viable cells should not take longer than 2 days to attach. If successful, the remaining tubes were stored in a liquid nitrogen tank.

5.5 Protein analytics

5.5.1 Yeast lysates for Western Blot

For small-scale analyses, such as test expression of transformed yeast strains, 6 ml of exponentially growing yeast cultures at an OD_{600} of 1 are harvested by centrifugation, washed with water and transferred to screw cap microtubes with 100 µl of glass beads. From now on, the probes must be handled at 4 °C or on ice. The cells are pelleted by centrifugation and 100 µl of buffer 3 + 60 mM β-glycerophosphate (buffer 3+) are added. They are mechanically lysed in a mixer mill (MN200, MN2000) and centrifuged for 4 minutes at 20,000 x g in a cooled centrifuge. Protein concentration in the lysates is measured by combining 0.25 µl of lysate in 500 µl of water with an equal amount of Bradford assay solution in 1 ml cuvettes (for details, see section 5.5.4). During the incubation time of 5-10 minutes, 75 µl of lysate are heated in a block with 25 µl 4x LSB for 5-10 min. Then, OD_{595} of the Bradford samples is measured. In most cases, relative rather than absolute protein concentrations were calculated; the amount of lysate in LSB used for the SDS gel was determined by calculating 1 µl/ OD_{595}. Depending on how much of the protein of interest (POI) was expected to be in the probes, a smaller or larger numerator was used.

5.5.2 Mammalian cell lysates for Western Blotting

In this work, stably transfected T-REx-293 cells were used for protein expression. The cells were grown to a confluency of around 80% and induced with 2 µg/ ml tetracyclin for two days. Before the harvest, the medium was removed and the cells were washed with PBS once. As HEK cells are only loosely attached to their flask, they were detached by repeatedly pipetting PBS onto the cell layer. The detached cells were centrifuged at 200 x g for 3 minutes in 15 ml tubes and frozen or lysed directly. Protease inhibitors were added freshly to the lysing buffer, which was added to the cells. After resuspension, the cells were transferred to a 2 ml microtube, inverted for 20 min at 4 °C and centrifuged in a cooled centrifuge for 10-30 min, depending on the amount of cells. Protein concentration in the lysate was measured in a Bradford assay, the rest was mixed with 4 x LSB and heated for 5-10 minutes.

5.5.3 Immunoprecipitation with αFLAG agarose beads

Immunoprecipitation was used to identify and quantify interaction partners of a POI. This protein was tagged with a FLAG tag at its endogenous locus or expressed from an exogenous construct. Ideally, the FLAG-tagged protein should behave similarly to the untagged protein in terms of its function and interaction with binding partners. The cells expressing the POI are lysed and the lysate is incubated with agarose beads, coupled with αFLAG IgG. The FLAG-tagged

protein (bait) is pulled from the lysate, still in complex with some of its binding partners (prey). Bait and prey proteins are then eluted and analyzed. The method is used to quantify the amount of coprecipitated binding partners under different conditions and to identify new interaction partners.

Preparation of protein lysates was carried out in a similar fashion as described above (section 5.5.1), albeit on a larger scale. 50 ml of yeast culture were pelleted, washed with water and transferred to two screw-cap tubes with 200 µl of glass beads in each tube. The cells were lysed, centrifuged for 10 min, lysates from the same probe were combined and centrifuged again for 15 min. 25 µl of the lysate were cooked with 25 µl 2x LSB for 5-10 min to WCEs. If not stated otherwise, 100 µl/ OD_{595} of protein lysates were used for the IP. The IgG agarose beads were washed with lysis buffer three times, transferred to 1.5 ml screw-cap tubes and the lysate was pipetted onto the washed beads. In order to achieve similar reaction conditions for all samples, all IPs of one experiment were performed in the same volume. Differences in volume were adjusted by adding lysis buffer. The reaction tubes were inverted at 4 °C for 2 h. Then, they were washed with lysis buffer three times and all of the supernatant was removed with a syringe. In this work, two different types of αFLAG agarose bead were used. Beads with M2 antibody are suited for competitive elution with 3xFLAG peptide. Therefy, denaturation of the antibody is avoided, which results in a cleaner eluate. The FLAG affinity gel by Bimake was used for most IPs because of its higher capacity. Elution with 3xFLAG peptide is ineffective with these beads, so the samples were heated in 1x LSB (50 µl, if not stated otherwise) for 10 min. During the elution, the tubes were carefully agitated a few times to distribute the eluted proteins equally in the solution. For the elution with 3xFLAG peptide, one bead volume of a 1:20 dilution of 3xFLAG peptide in lysis buffer was incubated with the beads for 30 minutes with shaking. The beads were centrifuged, the supernatant was collected and the elution step was repeated two times. The combined supernatants of each probe were mixed with 4x LSB and heated. Finally, the IP probes, together with the WCE probes, were subjected to Western Blot analysis.

For quantification of cellular protein complexes, IPs were performed in triplicates. To this end, yeast cells of a given strain were cultivated, lyzed and analyzed by WB independently.

5.5.4 Bradford protein assay

Protein concentrations in cell lysates were determined via Bradford assay. Typically, a small amount of lysate, e.g. 5 µl, was diluted 1:20 in distilled water and thoroughly mixed. From the diluted sample, 5 µl were taken again and transferred to a cuvette with 495 µl of water in it. Use of 4x LSB rather than 2x LSB yields a 50% greater protein concentration in the final sample, which was accounted for by using 7.5 µl instead of 5 µl to the cuvette. Then, 500 µl of Bradford staining solution, that had already been diluted 1:5, was added to the cuvette, achieving a dilution factor of 1:2000 for the protein lysates. The probes were incubated for 5-10 minutes until protein-dye complexes had formed. Absorption at 595nm was measured and Bradford staining solution, mixed with 500 µl of water without any added protein lysate, was used as a blank. OD_{595} values were noted. For most purposes, absolute protein concentrations were not determined, but the probe volume to be used for SDS-PAGE was determined by dividing a variable factor (x) by the OD_{595} value. A small factor (e.g. 0.5, 0.25) was chosen when the signal

was expected to be strong, e.g. for overexpressed, FLAG-tagged proteins. For the detection of proteins that were expected to yield a weak signal, a larger factor was chosen (e.g. 1 or 2).

$$V\ (sample) = \frac{x}{OD595}$$

The amount of protein contained in 5 µl of a protein sample in 1x LSB is around 20 µg, if the OD595 value is at 0.2, as determined by Bradford standard curve. For reasons of simplicity, this amount of protein is referred to as 1 OD_{595} (5 µl * 0.2). As the absorption properties of the assay solution may vary from batch to batch and depending on the age of the solution, the relationship between OD_{595} and protein concentration can vary.

5.5.5 SDS-Polyacrylamide gel electrophoresis (SDS-PAGE)

SDS-PAGE is a method for the separation of proteins according to their molecular weight, developed in the late 1960s by Ullrich Laemmli (Laemmli, 1970). It has since become one of the widest-used methods in biology. The gel contains acrylamide and bisacrylamide in buffered solution and SDS. Addition of APS, a radical starter, and TEMED, a catalyst, starts a polymerization reaction. Acrylamide polymerizes to form linear chains that are linked by bisacrylamide. This 3D network allows small molecules to pass through more quickly than large molecules. As proteins are charged, they migrate through the gel once an electrical field is applied. Proteins are denaturated by heating and addition of reducing agents to prevent differences between their tertiary and quaternary structure to influence their migration through the gel. SDS serves a dual function: As a denaturing agent, it prevents proteins from renaturating and, being negatively charged, it masks the proteins' individual charge to make molecular weight the only major influencing factor to their migration speed. Acrylamide gels consist of an alkaline separating gel with varying acrylamide concentration, depending on the size of the analyzed proteins, and a neutral stacking gel on top of the separating gel. A comb is inserted into the stacking gel to create wells for the samples. The gel is placed in a running buffer which contains Glycine and SDS and an electric field is applied, with the negative cathode being at the top of the gel and the anode at the bottom. The stacking effect relies on the zwitterionic property of glycine, which is part of the running buffer. In the stacking gel, glycine is weakly charged and runs behind the proteins. As it approaches the basic separating gel, its charge becomes more negative and it overtakes the proteins. In the process of overtaking them, it compresses all proteins into a thin band, which drastically improves the resolution. In the separating gel, larger proteins migrate slower than small proteins; the size of proteins in the probes can be estimated in comparison to a ladder of prestained proteins of known sizes. Here, the separating gels were 9 cm wide, 6 cm high and 1 mm thick. SDS-PAGE was run at 150 V for 1.5 h ± 10 minutes until the Bromophenol blue from the sample buffer had reached the bottom of the gel. The proteins in the gel can be visualized in two ways: Unspecific staining of all proteins directly in the gel, or transfer of proteins to a membrane and subsequent detection of specific proteins with antibodies.

5.5.6 Coomassie staining

Proteins can be visualized in SDS gels directly with chemical dyes that bind to proteins. Such staining methods are unspecific and do not differenciate between proteins. Traditionally, coomassie staining with Brilliant Blue G250 was used as a quick, cost-efficient, but not very sensitive staining method (>100 ng per band) and silver staining was the preferred method for visualizing smaller amounts of protein (5 ng per band). Newer, colloidal formulations of Coomassie Brilliant Blue (see table 10) are similarly sensitive as the silver staining method. Coomassie Brilliant blue G250 binds amino acids of the proteins unspecifically. Whereas the dye is quickly washed out of the gel after staining, the proteins bound dye molecules remain.

In this work, the colloidal Coomassie staining method was used. After the gel run, the stacking gel was discarded and the separating gel was washed with water for a few minutes to remove most of the SDS. The staining solution, made from 20 ml of Colloidal Coomassie stock solution and 5 ml of methanol, was prepared and the gel was stained for a few hours or overnight. Then, the dye was discarded and the gel was washed several times with water for 30 min until the proteins bands became visible. The gels were scanned at 700 nm in the Infraredscanner LICOR Odyssey; band signals were quantified with LICOR softwares Odyssey v3.0 and the newer Image Studio v5.2.

Coomassie staining can also be used for the quantification of purified proteins. The color intensity of a protein band can be correlated with a set of samples containing a purified protein in known concentrations. In this work, BSA was used to generate a standard curve. The relationship between protein amount and color intensity was linear over a range from 10 ng to 1 µg.

5.5.7 Western Blot

While Coomassie staining is useful to visualize all proteins in a sample or purified and abundant proteins, the detection of single proteins in WCEs requires higher specificity and sensitivity. The method of transferring proteins to a membrane and detecting it with antibodies was described in three different publications in 1979 and 1981 (Burnette, 1981; Renart et al., 1979; Towbin et al., 1979). The electroblot method was first published by Towbin. Burnette coined the term “Western Blot”. In this work, the semidry electroblotting method was used. The proteins are transferred from the seperating gel to a nitrocellulose membrane in an electric field. From bottom to top, a “blotting sandwich” is made, consisting of filter paper – membrane – gel – filter paper. All components are washed in or soaked with transfer buffer and placed between the anode (bottom) and cathode (top). A current of 40 mA per gel was applied for 90 min. The sandwich was disassembled and the membrane was stained with Ponceau S for a few minutes to visualize the protein bands. Thereby, the amount of total protein in each probe and the evenness of protein bands could be checked. The stained membrane was scanned and then blocked with TBS-T + 5% milk powder for at least 30 min.

Now, the primary antibody, specific for the POI or its tag, was diluted in TBS-T + milk powder and incubated with the membrane for 2 h at RT or overnight at 4 °C. Then, the membrane was washed with TBS-T 3x for 5 min and the secondary antibody, targeted against the species

specific F_C part of the primary antibody, was added. Since secondary antibodies with specificity for mouse or rabbit primary antibodies were available with coupled fluorophores at two wavelengths, 680 nm and 800 nm, two proteins could be detected on the same membrane at the same time. The membrane was washed again 3 times with TBS-T for 5 minutes and scanned in the LICOR Odyssey scanner. The scans were analyzed with Odyssey v3.0 or Image Studio v5.2.

If more proteins had to be detected on the same membrane, the antibodies were stripped from the membrane with a stripping buffer (see table 10). This solution contained Guanidinium hydrochloride and β-mercaptoethanol, which denature the antibodies and remove them from the membrane. The solution was incubated with the membrane for 10 min at RT and then washed off. Before adding new primary antibodies, the membrane was blocked again with 5% milk powder in TBS-T for 30 min. The stripping process removes not only the antibodies, but also up to 30% of the proteins bound to the membrane. Therefore, membranes were reused only once.

5.5.8 Yeast two hybrid (Y2H) protein interaction assay

The Yeast-two-hybrid screen is a method to study interaction of two proteins inside yeast cells. Unlike *in-vitro* assays, Y2H provides an environment that resembles that of intracellular proteins more than buffer solutions. Natural glycosylation and interaction with chaperones is more likely to occur in the eukaryote *S. cerevisiae* than it is in *E. coli*, commonly used for heterologous gene expression. Protein expression and test of interaction take place in the same working step, which enables the test of many protein interactions. The method was originally published in 1989 (Fields and Song, 1989).

The basic principle of Y2H is the coexpression of two proteins, fused to two parts of a transcriptional activator, in a reporter yeast strain. Interaction of the two proteins inside the nucleus reconstitutes the transcription factor and activates expression of a reporter gene (figure 51A). Here, a yeast strain with two reporter genes was used. The first reporter gene is β-galactosidase that can cleave X-gal, releasing an indole that quickly dimerizes to form a blue pigment. The second reporter gene is the endogenous *LEU2* gene of *S. cerevisiae.* In the reporter strain, both genes are controlled by the bacterial *lexA* operator. The proteins whose interaction is to be tested are cloned into two reporter plasmids, pJG4-5 and pEG202. Both are 2µ plasmids that are replicated in high numbers in yeast. pJG4-5 encodes the lexA DNA binding domain that is upstream of the multiple cloning site where the gene, encoding the first protein, is inserted (figure 51B). Expression of the fusion gene is dependent on the strong, inducible *GAL1* promoter. pEG202 adds the B42 activator domain to the N-terminus of the second protein (see figure 51C). Its expression is controlled by the constitutively active *ADH1* promoter. The reporter strain is cotransformed with both plasmids. Since pJG4-5 and pEG202 contain *TRP1* and *HIS3* genes as selection markers, transformed yeast cells are streaked out on SD-HT plates. Several transformants are picked, spotted and grown for 2-3 days at 25 °C on SG-HT or SRG-HT for the β-galactosidase assay and SG-HTL or SRH-HTL to test expression of the LEU2 reporter. To test β-galactosidase expression, a reaction mix, containing X-gal, is prepared, mixed with agarose (see table 28) and poured onto the yeast cells. The plates are incubated at 37 °C and monitored for formation of the blue pigment. Cell growth on SG/SRG-HTL plates indicates *LEU2* expression in a

very sensitive way, as even a fraction of the highest expression level allows visible, albeit slow growth of colonies.

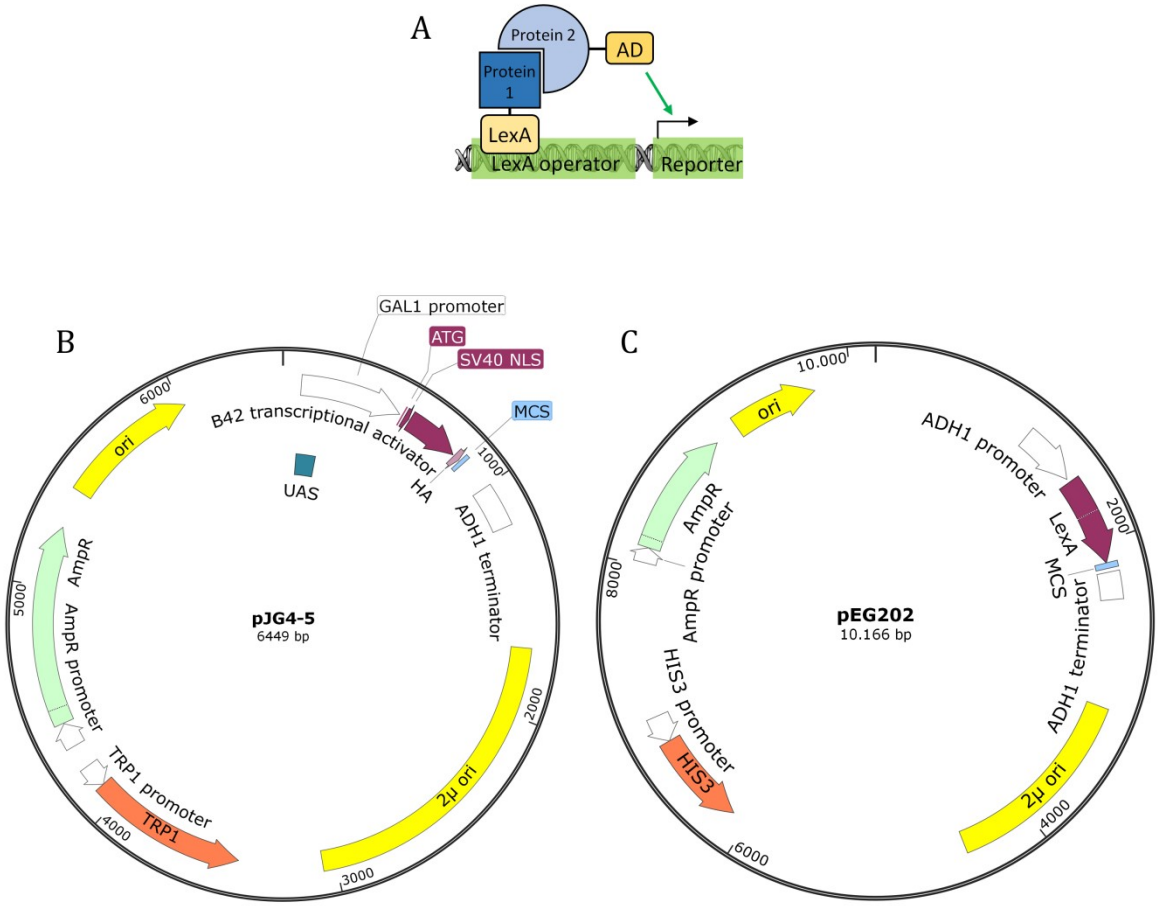

Figure 51: Principle of the Y2H assay. **A:** Activation of a LexA operator dependent reporter gene by a reconstituted transcriptional activator, consisting of the LexA DBD and B42 transcriptional activator. **B:** Map of pJG4-5 vector. **C:** Map of pEG202 vector.

Table 28: Composition of Y2H reaction mix

Chemical	concentration	volume
Na-Phosphate buffer pH = 7	1 M	5 ml
SDS	10%	0.1 ml
X-Gal	20 mg/ ml	0.1 ml
DMFA	100%	600 µl
Agarose	1%	5 ml

5.5.9 Affinity purification of antibodies from sera

Crude sera from immunized rabbits contain many antibodies besides the desired ones and often show crossreactivity towards a variety of other antigens. The recombinant protein with which the rabbit was immunized can also be used to pull antibodies with an affinity for the protein from the serum.

A large amount of the recombinant protein is loaded onto a whole acrylamide gel and transferred to a nitrocellulose membrane via Western Blot. The protein band is visualized with Ponceau S and cut out. The membrane piece is blocked with TBS-T + 5% milk powder and incubated with the serum (~10 ml) overnight at 4 °C. The membrane is washed 3x with TBS-T. Then it is cut into smaller pieces and put into a 2 ml plastic tube. The bound antibody is eluted by incubation with 0.5 ml acidic glycine solution (0.2M glycine, pH = 2.2). The elution is repeated three times in total and all three elutions are pooled. Finally, the eluate must be dialyzed to remove glycine and neutralize pH. Here, the eluate was dialyzed against a buffer containing 20 mM Tris-HCl pH = 7.5 and 50% glycerol. Success of the purification is verified by Western Blot.

5.5.10 Mass spectrometry

Mass spectrometry is used to find interaction partners of a POI. For this purpose, a large amount of cells expressing FLAG-tagged protein and an equal amount of non-transfected cells (~100 million each) are harvested and lyzed. The lysates are used for immunoprecipitation with αFLAG agarose beads (Sigma) and the bait protein is eluted by competition with 3xFLAG peptide. A small amount of eluate from both samples is run on an SDS gel together with a BSA standard to visually assess the amount of purified Cdc123 and its binding partners. The rest of the probes is run on a gradient SDS-gel (4-12%). The proteins in the gel are prepared for mass spectrometry according to an established protocol described in the following passage.

First, appropriate amounts of the protein samples, dissolved in 1x LSB, are loaded onto a 4-12% gradient gel. After the gel run, the gel is stained with Coomassie staining solution. Following destaining of the background, the sample and control lanes are cut into 5-10 pieces. Each piece is transferred to a 2 ml microtube and washed first in 50 mM NH_4HCO_3, then a 3:1 ammonium carbonate + acetonitrile mix, followed by a 1:1 mix and lastly 200 µl of pure acetonitrile to destain the gel pieces and remove water. Remaining liquid is removed by lyophilization. Now, cysteine residues are reduced by addition of 200 µl of 1mg/ mL DTT in 50 mM NH_4HCO_3 and incubation of the samples at 56 °C for 35 min. Disulphide bonds are a hinderance for the tryptic digestion of the proteins and must be broken up. To avoid reformation of disulfide bonds, cysteines are then carbamidomethylated with a freshly prepared 5 mg/ ml iodoacetamide solution in 50 mM NH_4HCO_3 at room temperature for 30 min. Following this reaction, the gel pieces are again washed and dried as described above. Finally, the proteins in the gel pieces are trypsinated with 20 µl 0.04 µg/ ml Trypsin in 50 mM NH_4HCO_3. The digestion is carried out at 37 °C overnight. The peptides are then eluted from the gel pieces by addition of a small amount of 50 mM NH_4HCO_3, incubation at 37 °C for one hour and collection of the supernatant. This step is repeated once with 50 mM NH_4HCO_3 and again with a 1:1 acetonitrile mixture. The eluate is then carefully dried by lyophilization, making sure not to spill any of the samples. The dried samples are then ready for mass spectrometry.

Table 29: Buffers and solutions used in the preparation of protein samples for mass spectrometry

Solution	**Recipe**	
Ammonium carbonate buffer	50 mM NH_4HCO_3 in water, prepared from 100 mM NH_4HCO_3 stock	
3:1 mixture	3 parts 50 mM NH_4HCO_3 + 1 part acetonitrile	
1:1 mixture	1 parts 50 mM NH_4HCO_3 + 1 part acetonitrile	
DTT solution	50 mM NH_4HCO_3 25 mg/ ml DTT	950 µl 50 µl
Iodoacetamide solution (5 mg/ ml)	50 mM NH_4HCO_3 Iodoacetamide	1 ml 5 mg
Trypsin solution (0.04 µg/ µl)	50 mM NH_4HCO_3 4 µg trypsin in 1 mM HCl	70 µl 30 µl

Literature

Acker, M.G., Shin, B.-S., Dever, T.E., Lorsch, J.R., 2006. *Interaction between eukaryotic initiation factors 1A and 5B is required for efficient ribosomal subunit joining.* J. Biol. Chem. 281, 8469–75.

Adomavicius, T., Guaita, M., Zhou, Y., Jennings, M.D., Latif, Z., Roseman, A.M., Pavitt, G.D., 2019. *The structural basis of translational control by eIF2 phosphorylation.* Nat. Commun. 10, 2136.

Aitken, C.E., Lorsch, J.R., 2012. *A mechanistic overview of translation initiation in eukaryotes*. Nat. Struct. Mol. Biol. 19, 568–576.

Alberghina, L., Smeraldi, C., Ranzi, B.M., Porro, D., 1998. *Control by nutrients of growth and cell cycle progression in budding yeast, analyzed by double-tag flow cytometry.* J. Bacteriol. 180, 3864–72.

Alberts, bruce; Johnson, Alexander; Lewis, Julian; Raff, Martin; Roberts, Keith; Walter, P., 2004. Molekularbiologie der Zelle.

Algire, M.A., Maag, D., Lorsch, J.R., 2005. *P_i release from eIF2, not GTP hydrolysis, is the step controlled by start-site selection during eukaryotic translation initiation*. Mol. Cell 20, 251–262.

Anand, A.A., Kenner, L.R., Nguyen, H.C., Myasnikov, A.G., Klose, C.J., McGeever, L.A., Tsai, J.C., Miller-Vedam, L.E., Walter, P., Frost, A., 2018. *Structural basis of eIF2B-catalyzed GDP exchange and phosphoregulation by the integrated stress response*. bioRxiv 495, 504654.

Anderson, J., Phan, L., Cuesta, R., Carlson, B.A., Pak, M., Asano, K., Björk, G.R., Tamame, M., Hinnebusch, A.G., 1998. *The essential Gcd10p-Gcd14p nuclear complex 15 required for 1-methyladenosine modification and maturation of initiator methionyl-tRNA*. Genes Dev. 12, 3650–3662.

Andreou, A.Z., Klostermeier, D., 2014. *eIF4B and eIF4G jointly stimulate eIF4A ATPase and unwinding activities by modulation of the eIF4A conformational cycle.* J. Mol. Biol. 426, 51–61.

Asano, K., Shalev, A., Phan, L., Nielsen, K., Clayton, J., Valásek, L., Donahue, T.F., Hinnebusch, A.G., 2001. *Multiple roles for the C-terminal domain of eIF5 in translation initiation complex assembly and GTPase activation.* EMBO J. 20, 2326–37.

Barber, F., Amir, A., Murray, A.W., Murray, A.W., 2020. *Cell-size regulation in budding yeast does not depend on linear accumulation of Whi5*. Proc. Natl. Acad. Sci. U. S. A. 117, 14243–14250.

Ben-Shem, A., Jenner, L., Yusupova, G., Yusupov, M., 2010. *Crystal structure of the eukaryotic ribosome.* Science 330, 1203–9.

Bieganowski, P., Shilinski, K., Tsichlis, P.N., Brenner, C., 2004. *Cdc123 and checkpoint forkhead associated with RING proteins control the cell cycle by controlling eIF2γ abundance*. J. Biol. Chem. 279, 44656–44666.

Bogorad, A.M., Lin, K.Y., Marintchev, A., 2018. *EIF2B Mechanisms of Action and Regulation: A Thermodynamic View*. Biochemistry 57, 1426–1435.

Borck, G., Shin, B.S., Stiller, B., Mimouni-Bloch, A., Thiele, H., Kim, J.R., Thakur, M., Skinner, C., Aschenbach, L., Smirin-Yosef, P., Har-Zahav, A., Nürnberg, G., Altmüller, J., Frommolt, P., Hofmann, K., Konen, O., Nürnberg, P., Munnich, A., Schwartz, C.E., Gothelf, D., Colleaux, L., Dever, T.E., Kubisch, C., Basel-Vanagaite, L., 2012. *EIF2γ Mutation that Disrupts eIF2 Complex Integrity Links Intellectual Disability to Impaired Translation Initiation*. Mol. Cell 48, 641–646.

Breker, M., Gymrek, M., Schuldiner, M., 2013. *A novel single-cell screening platform reveals proteome plasticity during yeast stress responses.* J. Cell Biol. 200, 839–50.

Burnette, W.N., 1981. *"Western Blotting": Electrophoretic transfer of proteins from sodium dodecyl sulfate-polyacrylamide gels to unmodified nitrocellulose and radiographic detection with antibody and radioiodinated protein A*. Anal. Biochem.

Burroughs, A.M., Zhang, D., Aravind, L., 2015. *The eukaryotic translation initiation regulator CDC123 defines a divergent clade of ATP-grasp enzymes with a predicted role in novel protein modifications.* Biol. Direct 10, 21.

Campbell, S.G., Hoyle, N.P., Ashe, M.P., 2005. *Dynamic cycling of eIF2 through a large eIF2B-containing cytoplasmic body: implications for translation control.* J. Cell Biol. 170, 925–34.

Cardozo, T., Pagano, M., 2004. *The SCF ubiquitin ligase: insights into a molecular machine.* Nat. Rev. Mol. Cell Biol. 5, 739–51.

Chang, K.-J., Wang, C.-C., 2004. *Translation initiation from a naturally occurring non-AUG codon in Saccharomyces cerevisiae.* J. Biol. Chem. 279, 13778–85.

Chong, Y.T., Koh, J.L.Y., Friesen, H., Duffy, S.K., Duffy, K., Cox, M.J., Moses, A., Moffat, J., Boone, C., Andrews, B.J., 2015. *Yeast Proteome Dynamics from Single Cell Imaging and Automated Analysis.* Cell 161, 1413–24.

Cigan, A.M., Feng, L., Donahue, T.F., 1988a. *tRNAi(met) functions in directing the scanning ribosome to the start site of translation.* Science 242, 93–7.

Cigan, A.M., Pabich, E.K., Donahue, T.F., 1988b. *Mutational analysis of the HIS4 translational initiator region in Saccharomyces cerevisiae.* Mol. Cell. Biol. 8, 2964–75.

Dever, T.E., Kinzy, T.G., Pavitt, G.D., 2016. *Mechanism and Regulation of Protein Synthesis Initiation in Eukaryotes*. Genetics 203, 1–83.

Diffley, J.F.X., 2004. *Regulation of early events in chromosome replication.* Curr. Biol. 14, R778-86.

Dlugosch, A., 2019. Analyse der Interaktion des humanen Assemblierungsfaktors D123 mit seinem Zielprotein heIF2γ.

Dorris, D.R., Erickson, F.L., Hannig, E.M., 1995. *Mutations in GCD11, the structural gene for eIF-2 gamma in yeast, alter translational regulation of GCN4 and the selection of the start site for protein synthesis.* EMBO J. 14, 2239–2249.

Dorsey, S., Tollis, S., Cheng, J., Black, L., Notley, S., Tyers, M., Royer, C.A., 2018. *G1/S Transcription Factor Copy Number Is a Growth-Dependent Determinant of Cell Cycle Commitment in Yeast*. Cell Syst. 6, 539-554.e11.

Dubiez, E., Aleksandrov, A., Lazennec-Schurdevin, C., Mechulam, Y., Schmitt, E., 2015. *Identification of a second GTP-bound magnesium ion in archaeal initiation factor 2.* Nucleic Acids Res. 43, 2946–57.

Enserink, J.M., Kolodner, R.D., 2010. *An overview of Cdk1-controlled targets and processes*. Cell Div. 5, 1–41.

Evans, T., Rosenthal, E.T., Youngblom, J., Distel, D., Hunt, T., 1983. *Cyclin: a protein specified by maternal mRNA in sea urchin eggs that is destroyed at each cleavage division.* Cell 33, 389–96.

Fawaz, M. V, Topper, M.E., Firestine, S.M., 2011. *The ATP-grasp enzymes.* Bioorg. Chem. 39, 185–91.

Fekete, C.A., Mitchell, S.F., Cherkasova, V.A., Applefield, D., Algire, M.A., Maag, D., Saini, A.K., Lorsch, J.R., Hinnebusch, A.G., 2007. *N- and C-terminal residues of eIF1A have opposing effects on the fidelity of start codon selection.* EMBO J. 26, 1602–14.

Fields, S., Song, O., 1989. *A novel genetic system to detect protein-protein interactions.* Nature 340, 245–6.

Gietz, R.D., Woods, R.A., 2002. *Transformation of yeast by lithium acetate/single-stranded carrier DNA/polyethylene glycol method*. Methods Enzymol.

Gordiyenko, Y., Llácer, J.L., Ramakrishnan, V., 2019. *Structural basis for the inhibition of translation through eIF2α phosphorylation*. Nat. Commun. 10, 1–11.

Gregory, L.C., Ferreira, C.B., Young-Baird, S.K., Williams, H.J., Harakalova, M., van Haaften, G., Rahman, S.A., Gaston-Massuet, C., Kelberman, D., GOSgene, Qasim, W., Camper, S.A., Dever, T.E., Shah, P., Robinson, I.C.A.F., Dattani, M.T., 2019. *Impaired EIF2S3 function associated with a novel phenotype of X-linked hypopituitarism with glucose dysregulation*. EBioMedicine 42, 470–480.

Gupta, N., Lorsch, J.R., Hinnebusch, A.G., 2018. *Yeast Ded1 promotes 48S translation pre-initiation complex assembly in an mRNA-specific and eIF4F-dependent manner.* Elife 7.

Haase, S.B., Wittenberg, C., 2014. *Topology and control of the cell-cycle-regulated transcriptional circuitry*. Genetics 196, 65–90.

Harashima, S., Hinnebusch, A.G., 1986. *Multiple GCD genes required for repression of GCN4, a transcriptional activator of amino acid biosynthetic genes in Saccharomyces cerevisiae.* Mol. Cell. Biol. 6, 3990–8.

Hartwell, L.H., Culotti, J., Pringle, J.R., Reid, B.J., 1974. *Genetic Control of the Cell Division Cycle in Yeast*. Science (80-.). 183, 46 LP – 51.

Hinnebusch, A.G., 2017. *Structural Insights into the Mechanism of Scanning and Start Codon Recognition in Eukaryotic Translation Initiation*. Trends Biochem. Sci. 42, 589–611.

Hinnebusch, A.G., 2014. *The Scanning Mechanism of Eukaryotic Translation Initiation*. Annu. Rev. Biochem. 83, 779–812.

Hinnebusch, A.G., 2011. *Molecular Mechanism of Scanning and Start Codon Selection in Eukaryotes*. Microbiol. Mol. Biol. Rev. 75, 434–467.

Hinnebusch, A.G., 2005. *Translational Regulation of GCN4 and the General Amino Acid Control of Yeast*. Annu. Rev. Microbiol. 59, 407–450.

Hinnebusch, A.G., 1985. *A hierarchy of trans-acting factors modulates translation of an activator of amino acid biosynthetic genes in Saccharomyces cerevisiae.* Mol. Cell. Biol. 5, 2349–60.

Holcik, M., Sonenberg, N., 2005. *Translational control in stress and apoptosis*. Nat. Rev. Mol. Cell Biol. 6, 318–327.

Howell, A.S., Lew, D.J., 2012. *Morphogenesis and the cell cycle*. Genetics 190, 51–77.

Huang, H.K., Yoon, H., Hannig, E.M., Donahue, T.F., 1997. *GTP hydrolysis controls stringent selection of the AUG start codon during translation initiation in Saccharomyces cerevisiae.* Genes Dev. 11, 2396–413.

Humphrey, T., Pearce, A., 2005. *Cell cycle molecules and mechanisms of the budding and fission yeasts.* Methods Mol. Biol. 296, 3–29.

Ito, H., Fukuda, Y., Murata, K., Kimura, A., 1983. *Transformation of intact yeast cells treated with alkali cations*. J. Bacteriol.

Jackson, R.J., Hellen, C.U.T., Pestova, T. V, 2010. *The mechanism of eukaryotic translation initiation and principles of its regulation.* Nat. Rev. Mol. Cell Biol. 11, 113–127.

Jan, E., Mohr, I., Walsh, D., 2016. *A Cap-to-Tail Guide to mRNA Translation Strategies in Virus-Infected Cells*. Annu. Rev. Virol. 3, 283–307.

Jennings, M.D., Pavitt, G.D., 2014. *A new function and complexity for protein translation initiation factor eIF2B*. Cell Cycle 13, 2660–2665.

Jennings, M.D., Pavitt, G.D., 2010. *eIF5 has GDI activity necessary for translational control by eIF2 phosphorylation.* Nature 465, 378–81.

Jennings, M.D., Zhou, Y., Mohammad-Qureshi, S.S., Bennett, D., Pavitt, G.D., 2013. *eIF2B promotes eIF5 dissociation from eIF2*GDP to facilitate guanine nucleotide exchange for translation initiation.* Genes Dev. 27, 2696–707.

Kachroo, A.H., Laurent, J.M., Yellman, C.M., Meyer, A.G., Wilke, C.O., Marcotte, E.M., 2015. *Evolution. Systematic humanization of yeast genes reveals conserved functions and genetic modularity.* Science 348, 921–5.

Kashiwagi, K., Yokoyama, T., Nishimoto, M., Takahashi, M., Sakamoto, A., Yonemochi, M., Shirouzu, M., Ito, T., 2019. *Structural basis for eIF2B inhibition in integrated stress response*. Science 364, 495–499.

Kertesz, M., Wan, Y., Mazor, E., Rinn, J.L., Nutter, R.C., Chang, H.Y., Segal, E., 2010. *Genome-wide measurement of RNA secondary structure in yeast.* Nature 467, 103–7.

Kochetov, A. V., 2008. *Alternative translation start sites and hidden coding potential of eukaryotic mRNAs*. BioEssays 30, 683–691.

Kozak, M., 1987. *An analysis of 5'-noncoding sequences from 699 vertebrate messenger RNAs.* Nucleic Acids Res. 15, 8125–48.

Kwan, T., Thompson, S.R., 2019. *Noncanonical Translation Initiation in Eukaryotes.* Cold Spring Harb. Perspect. Biol. 11.

Laemmli, U.K., 1970. *Cleavage of structural proteins during the assembly of the head of bacteriophage T4.* Nature 227, 680–5.

Lee, J.H., Pestova, T. V, Shin, B.-S., Cao, C., Choi, S.K., Dever, T.E., 2002. *Initiation factor eIF5B catalyzes second GTP-dependent step in eukaryotic translation initiation.* Proc. Natl. Acad. Sci. U. S. A. 99, 16689–94.

Lee, M., Nurse, P., 1988. *Cell cycle control genes in fission yeast and mammalian cells.* Trends Genet. 4, 287–90.

Litsios, A., Huberts, D.H.E.W., Terpstra, H.M., Guerra, P., Schmidt, A., Buczak, K., Papagiannakis, A.,

Rovetta, M., Hekelaar, J., Hubmann, G., Exterkate, M., Milias-Argeitis, A., Heinemann, M., 2019. *Differential scaling between G1 protein production and cell size dynamics promotes commitment to the cell division cycle in budding yeast*. Nat. Cell Biol. 21, 1382–1392.

Llácer, J.L., Hussain, T., Marler, L., Aitken, C.E., Thakur, A., Lorsch, J.R., Hinnebusch, A.G., Ramakrishnan, V., 2015. *Conformational Differences between Open and Closed States of the Eukaryotic Translation Initiation Complex*. Mol. Cell 59, 399–412.

Longhese, M.P., Foiani, M., Muzi-Falconi, M., Lucchini, G., Plevani, P., 1998. *DNA damage checkpoint in budding yeast*. EMBO J. 17, 5525–5528.

Longtine, M.S., McKenzie, A., Demarini, D.J., Shah, N.G., Wach, A., Brachat, A., Philippsen, P., Pringle, J.R., 1998. *Additional modules for versatile and economical PCR-based gene deletion and modification in Saccharomyces cerevisiae*. Yeast 14, 953–961.

Lundberg, K.S., Shoemaker, D.D., Adams, M.W.W., Short, J.M., Sorge, J.A., Mathur, E.J., 1991. *High-fidelity amplification using a thermostable DNA polymerase isolated from Pyrococcus furiosus*. Gene.

Maag, D., Fekete, C.A., Gryczynski, Z., Lorsch, J.R., 2005. *A conformational change in the eukaryotic translation preinitiation complex and release of eIF1 signal recognition of the start codon.* Mol. Cell 17, 265–75.

Marques, A.C., Dupanloup, I., Vinckenbosch, N., Reymond, A., Kaessmann, H., 2005. *Emergence of young human genes after a burst of retroposition in primates*. PLoS Biol. 3, 1970–1979.

Marston, A.L., 2014. *Chromosome segregation in budding yeast: sister chromatid cohesion and related mechanisms.* Genetics 196, 31–63.

Martin-Marcos, P., Cheung, Y.-N., Hinnebusch, A.G., 2011. *Functional Elements in Initiation Factors 1, 1A, and 2 Discriminate against Poor AUG Context and Non-AUG Start Codons*. Mol. Cell. Biol. 31, 4814–4831.

Matheson, K., Parsons, L., Gammie, A., 2017. *Whole-genome sequence and variant analysis of W303, a widely-used strain of Saccharomyces cerevisiae*. G3 Genes, Genomes, Genet.

Mayr, C., 2019. *What are 3′ utrs doing?* Cold Spring Harb. Perspect. Biol. 11.

Miller, J.H., 1972. Experiments in molecular genetics.

Moortgat S, Desir J, Benoit V, Boulanger S, Pendeville H, Nassogne M-C, Lederer D, M.I., 2016. *Two novel EIF2S3 mutations associated with syndromic intellectual disability with severe microcephaly, growth retardation, and epilepsy.* Am. J. Med. Genet. A 170, 2927–2933.

Moreno, D.F., Parisi, E., Yahya, G., Vaggi, F., Csikász-Nagy, A., Aldea, M., 2019. *Competition in the chaperone-client network subordinates cell-cycle entry to growth and stress*. Life Sci. Alliance 2, 1–16.

Mullis, K., Faloona, F., Scharf, S., Saiki, R., Horn, G., Erlich, H., 1986. *Specific enzymatic amplification of DNA in vitro: The polymerase chain reaction*. Cold Spring Harb. Symp. Quant. Biol.

Nanda, J.S., Cheung, Y.-N., Takacs, J.E., Martin-Marcos, P., Saini, A.K., Hinnebusch, A.G., Lorsch, J.R., 2009. *eIF1 controls multiple steps in start codon recognition during eukaryotic translation initiation.* J. Mol. Biol. 394, 268–85.

Naveau, M., Lazennec-Schurdevin, C., Panvert, M., Dubiez, E., Mechulam, Y., Schmitt, E., 2013. *Roles of yeast eIF2α and eIF2β subunits in the binding of the initiator methionyl-tRNA*. Nucleic Acids Res. 41, 1047–1057.

Naveau, M., Lazennec-Schurdevin, C., Panvert, M., Mechulam, Y., Schmitt, E., 2010a. *TRNA binding properties of eukaryotic translation initiation factor 2 from encephalitozoon cuniculi*. Biochemistry 49, 8680–8688.

Naveau, M., Lazennec-Schurdevin, C., Panvert, M., Mechulam, Y., Schmitt, E., 2010b. *TRNA binding properties of eukaryotic translation initiation factor 2 from encephalitozoon cuniculi*. Biochemistry 49, 8680–8688.

Newcomb, L.L., Diderich, J.A., Slattery, M.G., Heideman, W., 2003. *Glucose regulation of Saccharomyces cerevisiae cell cycle genes*. Eukaryot. Cell 2, 143–149.

Ohno, K., Kimura, G., 1984. *Genetic analysis of control of proliferation in fibroblastic cells in culture. II. Alteration in proliferative and survival phenotypes in a set of temperature-sensitive mutants of rat 3Y1 cells after infection or transformation with simian virus 40.* Somat. Cell Mol. Genet. 10, 29–36.

Ohno, K., Okuda, A., Ohtsu, M., Kimura, G., 1984. *Genetic analysis of control of proliferation in fibroblastic cells in culture. I. Isolation and characterization of mutants temperature-sensitive for proliferation or survival of untransformed diploid rat cell line 3Y1.* Somat. Cell Mol. Genet. 10, 17–28.

Okuda, A., Kimura, G., 1996. *An amino acid change in novel protein D123 is responsible for temperature-sensitive G1-phase arrest in a mutant of rat fibroblast line 3Y1*. Exp. Cell Res. 223, 242–249.

Okuda, A., Ohtsu, M., Kimura, G., 2001. *Reversion of temperature-sensitive mutation by inhibition of proteasome-mediated degradation of mutated D123 protein.* Cell Struct. Funct. 26, 205–14.

Okuda, A., Ohtsu, M., Kimura, G., 1999. *Extensive degradation of mutant-type D123 protein is responsible for temperature-sensitive proliferation inhibition in 3Y1tsD123 cells.* Cell Struct. Funct. 24, 443–9.

Onisto, M., Zeilante, P., Scannapieco, P., Pellati, D., Pozza, M., Caenazzo, C., Negro, A., Garbisa, S., 1998. *Expression study on D123 gene product: Evidence for high positivity in testis*. Exp. Cell Res. 242, 451–459.

Pakos-Zebrucka, K., Koryga, I., Mnich, K., Ljujic, M., Samali, A., Gorman, A.M., 2016. *The integrated stress response*. EMBO Rep. 17, 1374–1395.

Panvert, M., Dubiez, E., Arnold, L., Perez, J., Mechulam, Y., Seufert, W., Schmitt, E., 2015. *Cdc123, a Cell Cycle Regulator Needed for eIF2 Assembly, Is an ATP-Grasp Protein with Unique Features*. Structure 23, 1596–1608.

Passmore, L.A., Schmeing, T.M., Maag, D., Applefield, D.J., Acker, M.G., Algire, M.A., Lorsch, J.R., Ramakrishnan, V., 2007. *The eukaryotic translation initiation factors eIF1 and eIF1A induce an open conformation of the 40S ribosome.* Mol. Cell 26, 41–50.

Peeters, K., Van Leemputte, F., Fischer, B., Bonini, B.M., Quezada, H., Tsytlonok, M., Haesen, D., Vanthienen, W., Bernardes, N., Gonzalez-Blas, C.B., Janssens, V., Tompa, P., Versées, W., Thevelein, J.M., 2017. *Fructose-1,6-bisphosphate couples glycolytic flux to activation of Ras.* Nat. Commun. 8, 922.

Peguero-Sanchez, E., Pardo-Lopez, L., Merino, E., 2015. *IRES-dependent translated genes in fungi: computational prediction, phylogenetic conservation and functional association.* BMC Genomics 16, 1059.

Perzlmaier, A.F., 2012. Die Rolle des Zellproliferationsproteins Cdc123 bei der Initiation der Translation.

Perzlmaier, A.F., Richter, F., Seufert, W., 2013. *Translation initiation requires cell division cycle 123 (Cdc123) to facilitate biogenesis of the eukaryotic initiation factor 2 (eIF2)*. J. Biol. Chem. 288, 21537–21546.

Polymenis, M., Aramayo, R., 2015. *Translate to divide: control of the cell cycle by protein synthesis*. Microb. Cell 2, 94–104.

Polymenis, M., Schmidt, E. V, 1997. *Coupling of cell division to cell growth by translational control of the G1 cyclin CLN3 in yeast.* Genes Dev. 11, 2522–31.

Ralser, Markus, Kuhl, H., Ralser, Meryem, Werber, M., Lehrach, H., Breitenbach, M., Timmermann, B., 2012. *The Saccharomyces cerevisiae W303-K6001 cross-platform genome sequence: Insights into ancestry and physiology of a laboratory mutt*. Open Biol.

Rast, S., 2020. Testing of different eIF2γ variants regarding complementation, eIF2 assembly and interaction with its guanosine exchange factor. Regensburg.

Renart, J., Reiser, J., Stark, G.R., 1979. *Transfer of proteins from gels to diazobenzyloxymethyl-paper and detection with antisera: A method for studying antibody specificity and antigen structure*. Proc. Natl. Acad. Sci. U. S. A.

Reynolds, P.R., 2002. *In sickness and in health: The importance of translational regulation*. Arch. Dis. Child. 86, 322–324.

Richter, F., 2006. Das konservierte Zellproliferationsgen CDC123 kodiert für einen Initiationsfaktor der Translation: 2gamma-AP.

Roll-Mecak, A., Alone, P., Cao, C., Dever, T.E., Burley, S.K., 2004. *X-ray Structure of Translation Initiation Factor eIF2γ: Implications for tRNA and eIF2α binding*. J. Biol. Chem. 279, 10634–10642.

Saiki, R.K., Gelfand, D.H., Stoffel, S., Scharf, S.J., Higuchi, R., Horn, G.T., Mullis, K.B., Erlich, H.A., 1988. *Primer-directed enzymatic amplification of DNA with a thermostable DNA polymerase*. Science (80-.).

Sanvito, F., Piatti, S., Villa, A., Bossi, M., Lucchini, G., Marchisio, P.C., Biffo, S., 1999. *The beta4 integrin interactor p27(BBP/eIF6) is an essential nuclear matrix protein involved in 60S ribosomal subunit assembly.* J. Cell Biol. 144, 823–37.

Schmitt, E., Naveau, M., Mechulam, Y., 2010. *Eukaryotic and archaeal translation initiation factor 2: A heterotrimeric tRNA carrier*. FEBS Lett. 584, 405–412.

Schmitt, E., Panvert, M., Lazennec-Schurdevin, C., Coureux, P.D., Perez, J., Thompson, A., Mechulam, Y., 2012. *Structure of the ternary initiation complex aIF2-GDPNP-methionylated initiator tRNA*. Nat. Struct. Mol. Biol. 19, 450–454.

Schmoller, K.M., Turner, J.J., Kõivomägi, M., Skotheim, J.M., 2015. *Dilution of the cell cycle inhibitor Whi5 controls budding-yeast cell size*. Nature 526, 268–272.

Schwob, E., Nasmyth, K., 1993. *CLB5 and CLB6, a new pair of B cyclins involved in DNA replication in Saccharomyces cerevisiae.* Genes Dev. 7, 1160–75.

Semmelmann, A., 2019. Studien zur Cdc123- vermittelten Assemblierung des Translationsfaktors eIF2.

Sen, N.D., Zhou, F., Ingolia, N.T., Hinnebusch, A.G., 2015. *Genome-wide analysis of translational efficiency reveals distinct but overlapping functions of yeast DEAD-box RNA helicases Ded1 and eIF4A.* Genome Res. 25, 1196–205.

Shiber, A., Döring, K., Friedrich, U., Klann, K., Merker, D., Zedan, M., Tippmann, F., Kramer, G., Bukau, B., 2018. *Cotranslational assembly of protein complexes in eukaryotes revealed by ribosome profiling*. Nature 561, 268–272.

Shin, B.-S., Maag, D., Roll-Mecak, A., Arefin, M.S., Burley, S.K., Lorsch, J.R., Dever, T.E., 2002. *Uncoupling of initiation factor eIF5B/IF2 GTPase and translational activities by mutations that lower ribosome affinity.* Cell 111, 1015–25.

Shin, B.S., Kim, J.R., Walker, S.E., Dong, J., Lorsch, J.R., Dever, T.E., 2011. *Initiation factor eIF2γ promotes eIF2-GTP-Met-tRNA iMet ternary complex binding to the 40S ribosome*. Nat. Struct. Mol. Biol. 18, 1227–1234.

Sikorski, R.S., Hieter, P., 1989. *A system of shuttle vectors and yeast host strains designed for efficient manipulation of DNA in Saccharomyces cerevisiae.* Genetics.

Singh, C.R., Lee, B., Udagawa, T., Mohammad-Qureshi, S.S., Yamamoto, Y., Pavitt, G.D., Asano, K., 2006. *An eIF5/eIF2 complex antagonizes guanine nucleotide exchange by eIF2B during translation initiation.* EMBO J. 25, 4537–46.

Sokabe, M., Fraser, C.S., Hershey, J.W.B., 2012. *The human translation initiation multi-factor complex promotes methionyl-tRNAi binding to the 40S ribosomal subunit.* Nucleic Acids Res. 40, 905–13.

Sokabe, Masaaki, Yao, M., Sakai, N., Toya, S., Tanaka, I., 2006. *Structure of archaeal translational initiation factor 2 betagamma-GDP reveals significant conformational change of the beta-subunit and switch 1 region.* Proc. Natl. Acad. Sci. U. S. A. 103, 13016–21.

Sokabe, M., Yao, M., Sakai, N., Toya, S., Tanaka, I., 2006. *Structure of archaeal translational initiation factor 2 beta -GDP reveals significant conformational change of the beta-subunit and switch 1 region*. Proc. Natl. Acad. Sci. 103, 13016–13021.

Spriggs, K.A., Bushell, M., Mitchell, S.A., Willis, A.E., 2005. *Internal ribosome entry segment-mediated translation during apoptosis: the role of IRES-trans-acting factors.* Cell Death Differ. 12, 585–91.

Stanik, J., Skopkova, M., Stanikova, D., Brennerova, K., Barak, L., Ticha, L., Hornova, J., Klimes, I., Gasperikova, D., 2018. *Neonatal hypoglycemia, early-onset diabetes and hypopituitarism due to the mutation in EIF2S3 gene causing MEHMO syndrome*. Physiol. Res. 67, 331–337.

Starck, S.R., Tsai, J.C., Chen, K., Shodiya, M., Wang, L., Yahiro, K., Martins-Green, M., Shastri, N., Walter, P., 2016. *Translation from the 5' untranslated region shapes the integrated stress response*. Science (80-.). 351.

Szamecz, B., Rutkai, E., Cuchalová, L., Munzarová, V., Herrmannová, A., Nielsen, K.H., Burela, L., Hinnebusch, A.G., Valásek, L., 2008. *eIF3a cooperates with sequences 5' of uORF1 to promote resumption of scanning by post-termination ribosomes for reinitiation on GCN4 mRNA.* Genes

Dev. 22, 2414–25.
Towbin, H., Staehelin, T., Gordon, J., 1979. *Electrophoretic transfer of proteins from polyacrylamide gels to nitrocellulose sheets: Procedure and some applications*. Proc. Natl. Acad. Sci. U. S. A. 76, 4350–4.
Tyers, M., Tokiwa, G., Nash, R., Futcher, B., 1992. *The Cln3-Cdc28 kinase complex of S. cerevisiae is regulated by proteolysis and phosphorylation.* EMBO J. 11, 1773–84.
Valásek, L., Mathew, A.A., Shin, B.-S., Nielsen, K.H., Szamecz, B., Hinnebusch, A.G., 2003. *The yeast eIF3 subunits TIF32/a, NIP1/c, and eIF5 make critical connections with the 40S ribosome in vivo.* Genes Dev. 17, 786–99.
Veitia, R.A., 2007. *Exploring the molecular etiology of dominant-negative mutations.* Plant Cell 19, 3843–51.
Wang, M., Weiss, M., Simonovic, M., Haertinger, G., Schrimpf, S.P., Hengartner, M.O., von Mering, C., 2012. *PaxDb, a database of protein abundance averages across all three domains of life.* Mol. Cell. Proteomics 11, 492–500.
Weinzierl, S., 2011. Genetische Studien zur Kopplung von Proteinsynthese und Zellteilung in Saccharomyces cerevisiae.
Xia, Y., Chu, W., Qi, Q., Xun, L., 2015. *New insights into the QuikChangeTM process guide the use of Phusion DNA polymerase for site-directed mutagenesis*. Nucleic Acids Res. 43, e12.
Yamamoto, Y., Singh, C.R., Marintchev, A., Hall, N.S., Hannig, E.M., Wagner, G., Asano, K., 2005. *The eukaryotic initiation factor (eIF) 5 HEAT domain mediates multifactor assembly and scanning with distinct interfaces to eIF1, eIF2, eIF3, and eIF4G.* Proc. Natl. Acad. Sci. U. S. A. 102, 16164–9.
Yamano, H., 2019. *APC/C: current understanding and future perspectives.* F1000Research 8.
Yates, A.D., Achuthan, P., Akanni, W., Allen, James, Allen, Jamie, Alvarez-Jarreta, J., Amode, M.R., Armean, I.M., Azov, A.G., Bennett, R., Bhai, J., Billis, K., Boddu, S., Marugán, J.C., Cummins, C., Davidson, C., Dodiya, K., Fatima, R., Gall, A., Giron, C.G., Gil, L., Grego, T., Haggerty, L., Haskell, E., Hourlier, T., Izuogu, O.G., Janacek, S.H., Juettemann, T., Kay, M., Lavidas, I., Le, T., Lemos, D., Martinez, J.G., Maurel, T., McDowall, M., McMahon, A., Mohanan, S., Moore, B., Nuhn, M., Oheh, D.N., Parker, A., Parton, A., Patricio, M., Sakthivel, M.P., Abdul Salam, A.I., Schmitt, B.M., Schuilenburg, H., Sheppard, D., Sycheva, M., Szuba, M., Taylor, K., Thormann, A., Threadgold, G., Vullo, A., Walts, B., Winterbottom, A., Zadissa, A., Chakiachvili, M., Flint, B., Frankish, A., Hunt, S.E., IIsley, G., Kostadima, M., Langridge, N., Loveland, J.E., Martin, F.J., Morales, J., Mudge, J.M., Muffato, M., Perry, E., Ruffier, M., Trevanion, S.J., Cunningham, F., Howe, K.L., Zerbino, D.R., Flicek, P., 2020. *Ensembl 2020.* Nucleic Acids Res. 48, D682–D688.
Yatime, L., Mechulam, Y., Blanquet, S., Schmitt, E., 2006. *Structural switch of the γ subunit in an archaeal aIF2αγ heterodimer*. Structure 14, 119–128.
Yatime, L., Schmitt, E., Blanquet, S., Mechulam, Y., 2005. *Structure - Function relationships of the intact aIF2α subunit from the archaeon Pyrococcus abyssi*. Biochemistry 44, 8749–8756.
Young-Baird, S.K., Lourenço, M.B., Elder, M.K., Klann, E., Liebau, S., Dever, T.E., 2019a. *Suppression of MEHMO Syndrome Mutation in eIF2 by Small Molecule ISRIB*. Mol. Cell 1–12.
Young-Baird, S.K., Lourenço, M.B., Elder, M.K., Klann, E., Liebau, S., Dever, T.E., 2019b. *Suppression of MEHMO Syndrome Mutation in eIF2 by Small Molecule ISRIB*. Mol. Cell 77.
Young-Baird, S.K., Shin, B.S., Dever, T.E., 2019c. *MEHMO syndrome mutation EIF2S3-I259M impairs initiator Met-tRNAiMet binding to eukaryotic translation initiation factor eIF2*. Nucleic Acids Res. 47, 855–867.
Zhou, F., Walker, S.E., Mitchell, S.F., Lorsch, J.R., Hinnebusch, A.G., 2014. *Identification and characterization of functionally critical, conserved motifs in the internal repeats and N-terminal domain of yeast translation initiation factor 4B (yeIF4B).* J. Biol. Chem. 289, 1704–22.

Supplementary data

Table S1: Quantification of Cdc123 precipitation by ^{FLAG}Gcd11 variants D403R and V281R. *For each sample, the Cdc123 was quantified relative to the FLAG signal in the same probe (Cdc123/FLAG). The ratio of the wt sample in each experiment was set to 1. Then, the average value (Avg) and Mean Square Error (MSE) for each Gcd11 variant was calculated.*

Gcd11 variant	experiment No.	FLAG signal	Cdc123 signal	Cdc123/ FLAG	relative to wt	Avg	MSE
wt	1	61.66	8.32	0.13	1.00	1.00	0
	2	41.17	4.98	0.12	1.00		
	3	28	1.1	0.04	1.00		
D403R	1	66.87	35.8	0.54	3.97	5.42	1.19
	2	35.42	23.22	0.66	5.42		
	3	20	5.4	0.27	6.87		
V281R	1	70.49	29.88	0.42	3.14	3.14	0.02
	2	47.38	18.17	0.38	3.17		
	3	18	2.2	0.12	3.11		

Table S2: Quantification of coprecipitation of Cdc123 with ^{FLAG}eIF2 subunits. *Cdc123 signals were quantified relative to the FLAG signal in each sample (Cdc123/FLAG). The ratio of the Gcd11 sample in each experiment was set to 1. Then, the average value (Avg) and Mean Square Error (MSE) for each eIF2 subunit was calculated.*

bait	experiment No.	Cdc123	FLAG	Cdc123/ FLAG	relative to wt	Avg	MSE
Sui2	1	0.02	9.67	0.0021	0.017	0.033	0.019
	2	0.01	7.47	0.0027	0.021		
	3	0.07	7.15	0.0098	0.059		
Sui3	1	0.91	33.13	0.0275	0.225	0.227	0.013
	2	0.85	27.82	0.0309	0.245		
	3	0.89	25.13	0.0354	0.213		
Gcd11	1	4.9	40.02	0.1224	1	1	0.000
	2	4.21	33.42	0.1263	1		
	3	5.46	32.88	0.1661	1		

Table S3: Quantification of coprecipitation of eIF2 subunits with Cdc123^{FLAG}. *The enrichment of each eIF2 subunit in the IP eluate, compared to each respective WCE was calculated for each sample (IP/ WCE). The ratio of the Gcd11 sample in each experiment was set to 1. Then, the average value (Avg) and Mean Square Error (MSE) for each eIF2 subunit was calculated.*

prey	experiment No.	WCE signal	IP signal	IP/ WCE	relative to Gcd11	Avg	MSE
Sui2	1	62.88	11.02	0.18	0.02	0.04	0.022
	2	16.47	4.89	0.30	0.02		
	3	70.55	26.63	0.38	0.07		
Sui3	1	11	36.17	3.29	0.34	0.41	0.050
	2	2.28	13.88	6.09	0.46		
	3	23.37	55.79	2.39	0.43		
Gcd11	1	6.77	65.37	9.66	1	1.00	0
	2	2.68	35.54	13.26	1		
	3	9.89	55.05	5.57	1		

***Table S4: Complete list of proteins associated with ^{FLAG}hCdc123 in Flp-In™ T-REx™-293**, identified by mass spectrometry. Proteins with a score < 100 were excluded. A represents the positive sample, B the negative control without ^{FLAG}hCdc123. Proteins with a score less than 3 times higher in the positive sample, compared to that in the negative sample (column A/B), were excluded. "Peptides" indicates the number of identified unique tryptic peptides from each protein.*

		Scores			Peptides	
Accession No.	**Name**	**A**	**B**	**A/B**	**A**	**B**
sp|P20042|IF2B_H.s.	Eukaryotic translation initiation factor 2 subunit 2	4655	202	23.0	55	4
sp|P41091|IF2G_H.s.	Eukaryotic translation initiation factor 2 subunit 3	4067	184	22.1	52	5
sp|Q2VIR3|IF2GL_H.s.	Eukaryotic translation initiation factor 2 subunit 3B	3124			41	
sp|O75794|CD123_H.s.	Cell division cycle protein 123 homolog	2892	126	23.0	37	4
sp|Q8IUD2|RB6I2_H.s.	ELKS/Rab6-interacting/CAST family member 1	1408			27	
sp|P55010|IF5_H.s.	Eukaryotic translation initiation factor 5	1384	64	21.8	23	2
sp|P34931|HS71L_H.s.	Heat shock 70 kDa protein 1-like	1286			18	
sp|P30153|2AAA_H.s.	Serine/threonine-protein phosphatase 2A	1033	288	3.6	18	6
sp|Q13428|TCOF_H.s.	Treacle protein	717	71	10.1	16	2
sp|Q96KR1|ZFR_H.s.	Zinc finger RNA-binding protein	679	197	3.4	13	5
sp|P22087|FBRL_H.s.	rRNA 2'-O-methyltransferase fibrillarin	636	194	3.3	11	6
sp|O75821|EIF3G_H.s.	Eukaryotic translation initiation factor 3 subunit G	553	168	3.3	11	4
sp|P61254|RL26_H.s.	60S ribosomal protein L26	548			12	
sp|Q04695|K1C17_H.s.	Keratin, type I cytoskeletal 17	533			10	
sp|Q14978|NOLC1_H.s.	Nucleolar and coiled-body phosphoprotein 1	480			10	
sp|P46778|RL21_H.s.	60S ribosomal protein L21	470	138	3.4	9	3
sp|Q9Y2X3|NOP58_H.s.	Nucleolar protein 58	468	59	8.0	7	2
sp|O75534|CSDE1_H.s.	Cold shock domain-containing protein E1	466	121	3.9	10	4
sp|P05141|ADT2_H.s.	ADP/ATP translocase 2	462	144	3.2	11	4
sp|P12814|ACTN1_H.s.	Alpha-actinin-1	450			9	
sp|Q562R1|ACTBL_H.s.	Beta-actin-like protein 2	447			7	
sp|P05023|AT1A1_H.s.	Sodium/potassium-transporting ATPase subunit alpha-1	444	96	4.6	9	3
sp|P09543|CN37_H.s.	2',3'-cyclic-nucleotide 3'-phosphodiesterase	378			10	
sp|O00203|AP3B1_H.s.	AP-3 complex subunit beta-1	376	112	3.4	10	4
sp|Q7Z794|K2C1B_H.s.	Keratin, type II cytoskeletal 1b	368			6	
sp|Q71UM5|RS27L_H.s.	40S ribosomal protein S27-like	367			6	
sp|O95071|UBR5_H.s.	E3 ubiquitin-protein ligase UBR5	367	98	3.7	8	3
sp|Q13547|HDAC1_H.s.	Histone deacetylase 1	352			9	
sp|O43660|PLRG1_H.s.	Pleiotropic regulator 1	351	68	5.2	10	2
sp|P00558|PGK1_H.s.	Phosphoglycerate kinase 1	339	109	3.1	7	3
sp|Q9BTD8|RBM42_H.s.	RNA-binding protein 42	323	94	3.4	6	3

sp|Q00325|MPCP_H.s.	Phosphate carrier protein, mitochondrial	320	67	4.8	8	2
sp|P18206|VINC_H.s.	Vinculin	317	73	4.3	7	2
sp|P12236|ADT3_H.s.	ADP/ATP translocase 3	314			8	
sp|O60282|KIF5C_H.s.	Kinesin heavy chain isoform 5C	310			8	
sp|O43684|BUB3_H.s.	Mitotic checkpoint protein BUB3	310	76	4.1	7	1
sp|P20020|AT2B1_H.s.	Plasma membrane calcium-transporting ATPase 1	306			6	
sp|P61964|WDR5_H.s.	WD repeat-containing protein 5	302	60	5.0	6	2
sp|P47755|CAZA2_H.s.	F-actin-capping protein subunit alpha-2	284			6	
sp|Q96F07|CYFP2_H.s.	Cytoplasmic FMR1-interacting protein 2	269			6	
sp|Q16659|MK06_H.s.	Mitogen-activated protein kinase 6	265	54	4.9	5	1
sp|P28066|PSA5_H.s.	Proteasome subunit alpha type-5	263	34	7.7	6	1
sp|Q96A65|EXOC4_H.s.	Exocyst complex component 4	261	60	4.4	7	2
sp|P05198|IF2A_H.s.	Eukaryotic translation initiation factor 2 subunit 1	260	75	3.4	5	2
sp|P63173|RL38_H.s.	60S ribosomal protein L38	260	45	5.8	5	1
sp|Q9UJZ1|STML2_H.s.	Stomatin-like protein 2, mitochondrial	259	72	3.6	6	2
sp|Q8ND56|LS14A_H.s.	Protein LSM14 homolog A	258	42	6.2	6	1
sp|O75153|CLU_H.s.	Clustered mitochondria protein homolog	256	66	3.9	7	2
sp|P56537|IF6_H.s.	Eukaryotic translation initiation factor 6	256			6	
sp|Q5VTR2|BRE1A_H.s.	E3 ubiquitin-protein ligase BRE1A	256			4	
sp|P49721|PSB2_H.s.	Proteasome subunit beta type-2	249	55	4.5	8	2
sp|Q9UKV8|AGO2_H.s.	Protein argonaute-2	249	71	3.5	6	2
sp|Q9NSB2|KRT84_H.s.	Keratin, type II cuticular Hb4	244			5	
sp|Q32MZ4|LRRF1_H.s.	Leucine-rich repeat flightless-interacting protein 1	237	72	3.3	4	2
sp|Q9BSD7|NTPCR_H.s.	Cancer-related nucleoside-triphosphatase	237			4	
sp|P62140|PP1B_H.s.	Serine/threonine-protein phosphatase PP1-beta catalytic subunit	235			5	
sp|Q9P258|RCC2_H.s.	Protein RCC2	234	64	3.7	7	2
sp|Q99497|PARK7_H.s.	Protein/nucleic acid deglycase DJ-1	234	76	3.1	7	2
sp|P25787|PSA2_H.s.	Proteasome subunit alpha type-2	233	73	3.2	6	2
sp|O14818|PSA7_H.s.	Proteasome subunit alpha type-7	232	48	4.9	4	1
sp|Q9UL25|RAB21_H.s.	Ras-related protein Rab-21	232			6	
sp|Q99714|HCD2_H.s.	3-hydroxyacyl-CoA dehydrogenase type-2	230	33	7.0	6	1
sp|Q9Y2L1|RRP44_H.s.	Exosome complex exonuclease RRP44	224			6	
sp|Q9Y3B7|RM11_H.s.	39S ribosomal protein L11, mitochondrial	222			5	
sp|Q15370|ELOB_H.s.	Elongin-B	221			5	
sp|P42695|CNDD3_H.s.	Condensin-2 complex subunit D3	218	60	3.6	5	1
sp|P78344|IF4G2_H.s.	Eukaryotic translation initiation factor 4 gamma 2	212			5	
sp|P18669|PGAM1_H.s.	Phosphoglycerate mutase 1	210			4	

sp|P51570|GALK1_H.s.	Galactokinase	210			6	
sp|Q9UI10|EI2BD_H.s.	Translation initiation factor eIF-2B subunit delta	207	51	4.0	5	1
sp|P78362|SRPK2_H.s.	SRSF protein kinase 2	205	36	5.6	5	1
sp|P04844|RPN2_H.s.	Dolichyl-diphosphooligosaccharide protein glycosyltransferase subunit 2	204	48	4.2	4	1
sp|O95816|BAG2_H.s.	BAG family molecular chaperone regulator 2	204	63	3.2	4	2
sp|P63167|DYL1_H.s.	Dynein light chain 1, cytoplasmic	203			4	
sp|P61962|DCAF7_H.s.	DDB1- and CUL4-associated factor 7	201	41	4.9	4	1
sp|P19784|CSK22_H.s.	Casein kinase II subunit alpha	200	31	6.4	5	1
sp|Q9Y2R9|RT07_H.s.	28S ribosomal protein S7, mitochondrial	200	57	3.5	5	2
sp|P51149|RAB7A_H.s.	Ras-related protein Rab-7a	196			5	
sp|P37802|TAGL2_H.s.	Transgelin-2	195			6	
sp|Q7Z7L1|SLN11_H.s.	Schlafen family member 11	194			4	
sp|Q8N684|CPSF7_H.s.	Cleavage and polyadenylation specificity factor subunit 7	193			4	
sp|Q9UDY2|ZO2_H.s.	Tight junction protein ZO-2	193	35	5.5	5	1
sp|O60684|IMA7_H.s.	Importin subunit alpha-7	192			4	
sp|Q8WW12|PCNP_H.s.	PEST proteolytic signal-containing nuclear protein	190			5	
sp|P07237|PDIA1_H.s.	Protein disulfide-isomerase	190	56	3.4	4	1
sp|Q9BT78|CSN4_H.s.	COP9 signalosome complex subunit 4	189	44	4.3	5	1
sp|P27797|CALR_H.s.	Calreticulin	188			5	
sp|Q9NVI7|ATD3A_H.s.	ATPase family AAA domain-containing protein 3A	188			5	
sp|O60841|IF2P_H.s.	Eukaryotic translation initiation factor 5B	188	56	3.4	4	2
sp|Q8NFC6|BD1L1_H.s.	Biorientation of chromosomes in cell division protein 1-like 1	186	47	4.0	4	1
sp|Q29RF7|PDS5A_H.s.	Sister chromatid cohesion protein PDS5 homolog A	186	31	6.0	5	1
sp|O00487|PSDE_H.s.	26S proteasome non-ATPase regulatory subunit 14	185	45	4.1	4	1
sp|Q9Y5M8|SRPRB_H.s.	Signal recognition particle receptor subunit beta	185			4	
sp|P30101|PDIA3_H.s.	Protein disulfide-isomerase A3	180	36	4.9	5	1
sp|Q9NWU2|GID8_H.s.	Glucose-induced degradation protein 8 homolog	177			4	
sp|Q9Y312|AAR2_H.s.	Protein AAR2 homolog	175	32	5.4	5	1
sp|P78347|GTF2I_H.s.	General transcription factor II-I	173			5	
sp|P37268|FDFT_H.s.	Squalene synthase	171			4	
sp|P62304|RUXE_H.s.	Small nuclear ribonucleoprotein E	171	44	3.9	3	1
sp|Q9Y3B2|EXOS1_H.s.	Exosome complex component CSL4	171			3	
sp|P35080|PROF2_H.s.	Profilin-2	170	32	5.4	3	1
sp|Q14157|UBP2L_H.s.	Ubiquitin-associated protein 2-like	169			5	
sp|Q9NQ55|SSF1_H.s.	Suppressor of SWI4 1 homolog	169			4	
sp|P31751|AKT2_H.s.	RAC-beta serine/threonine-protein kinase	168	45	3.8	4	1

sp|P83881|RL36A_H.s.	60S ribosomal protein L36a	167	54	3.1	4	1
sp|Q9GZT3|SLIRP_H.s.	SRA stem-loop-interacting RNA-binding protein, mitochondrial	163	39	4.2	3	1
sp|Q9Y2S7|PDIP2_H.s.	Polymerase delta-interacting protein 2	162			4	
sp|Q9NR28|DBLOH_H.s.	Diablo homolog, mitochondrial	162	46	3.5	4	1
sp|P25788|PSA3_H.s.	Proteasome subunit alpha type-3	161	31	5.3	3	1
sp|Q9ULK4|MED23_H.s.	Mediator of RNA polymerase II transcription subunit 23	161			5	
sp|O75832|PSD10_H.s.	26S proteasome non-ATPase regulatory subunit 10	161	31	5.3	2	1
sp|P49720|PSB3_H.s.	Proteasome subunit beta type-3	160			4	
sp|Q7L1Q6|BZW1_H.s.	Basic leucine zipper and W2 domain-containing protein 1	159			4	
sp|P81605|DCD_H.s.	Dermcidin	158	46	3.4	4	1
sp|P09936|UCHL1_H.s.	Ubiquitin carboxyl-terminal hydrolase isozyme L1	157			4	
sp|O75616|ERAL1_H.s.	GTPase Era, mitochondrial	156	40	3.9	3	1
sp|Q8NF37|PCAT1_H.s.	Lysophosphatidylcholine acyltransferase 1	156			3	
sp|Q13043|STK4_H.s.	Serine/threonine-protein kinase 4	148	32	4.6	4	1
sp|P42025|ACTY_H.s.	Beta-centractin	146			4	
sp|Q99733|NP1L4_H.s.	Nucleosome assembly protein 1-like 4	146			4	
sp|Q8WTT2|NOC3L_H.s.	Nucleolar complex protein 3 homolog	146			4	
sp|Q8NB90|AFG2H_H.s.	ATPase family protein 2 homolog	142			3	
sp|Q13257|MD2L1_H.s.	Mitotic spindle assembly checkpoint protein MAD2A	142	34	4.2	3	1
sp|Q92665|RT31_H.s.	28S ribosomal protein S31, mitochondrial	140			3	
sp|P62306|RUXF_H.s.	Small nuclear ribonucleoprotein F	140	40	3.5	2	1
sp|Q9NZN8|CNOT2_H.s.	CCR4-NOT transcription complex subunit 2	140			3	
sp|P49643|PRI2_H.s.	DNA primase large subunit	139	32	4.3	4	1
sp|Q7L5Y9|MAEA_H.s.	E3 ubiquitin-protein transferase MAEA	139	43	3.3	3	1
sp|O60832|DKC1_H.s.	H/ACA ribonucleoprotein complex subunit DKC1	139			4	
sp|P67870|CSK2B_H.s.	Casein kinase II subunit beta	137			3	
sp|Q8IY17|PLPL6_H.s.	Neuropathy target esterase	136			3	
sp|Q9P035|HACD3_H.s.	Very-long-chain (3R)-3-hydroxyacyl-CoA dehydratase 3	135			2	
sp|Q8N3U4|STAG2_H.s.	Cohesin subunit SA-2	135			3	
sp|Q9NQT4|EXOS5_H.s.	Exosome complex component RRP46	132			3	
sp|P19367|HXK1_H.s.	Hexokinase-1	132	32	4.1	4	1
sp|Q8WY22|BRI3B_H.s.	BRI3-binding protein	131	36	3.6	2	1
sp|Q8NFH3|NUP43_H.s.	Nucleoporin Nup4	130			3	
sp|Q99653|CHP1_H.s.	Calcineurin B homologous protein 1	129			3	
sp|P12532|KCRU_H.s.	Creatine kinase U-type, mitochondrial	129			3	
sp|P30086|PEBP1_H.s.	Phosphatidylethanolamine-binding protein 1	129			3	
sp|Q06609|RAD51_H.s.	DNA repair protein RAD51 homolog 1	128			2	

sp|Q9NPD3|EXOS4_H.s.	Exosome complex component RRP41	127	38	3.3	3	1
sp|P35241|RADI_H.s.	Radixin	125			3	
sp|Q9Y3C1|NOP16_H.s.	Nucleolar protein 16	124			3	
sp|Q9Y388|RBMX2_H.s.	RNA-binding motif protein, X-linked 2	124			2	
sp|O15047|SET1A_H.s.	Histone-lysine N-methyltransferase SETD1A	122	40	3.1	3	1
sp|P50454|SERPH_H.s.	Serpin H1	122			2	
sp|Q8N4Q1|MIA40_H.s.	Mitochondrial intermembrane space import and assembly protein 40	120			2	
sp|P06454|PTMA_H.s.	Prothymosin alpha	120			2	
sp|Q9UJA5|TRM6_H.s.	tRNA (adenine(58)-N(1))-methyltransferase non-catalytic subunit TRM6	119			3	
sp|O75822|EIF3J_H.s.	Eukaryotic translation initiation factor 3 subunit J	119			3	
sp|Q00403|TF2B_H.s.	Transcription initiation factor IIB	119			3	
sp|Q9UNL2|SSRG_H.s.	Translocon-associated protein subunit gamma	118	39	3.1	1	1
sp|Q13185|CBX3_H.s.	Chromobox protein homolog 3	118			4	
sp|P51572|BAP31_H.s.	B-cell receptor-associated protein 31	118			3	
sp|Q9NPH2|INO1_H.s.	Inositol-3-phosphate synthase 1	117			2	
sp|Q9NP72|RAB18_H.s.	Ras-related protein Rab-18	114			3	
sp|O75190|DNJB6_H.s.	DnaJ homolog subfamily B member 6	114			3	
sp|Q96DH6|MSI2H_H.s.	RNA-binding protein Musashi homolog 2	113	33	3.4	2	1
sp|Q96HR3|MED30_H.s.	Mediator of RNA polymerase II transcription subunit 30	112			3	
sp|P49006|MRP_H.s.	MARCKS-related protein	111			3	
sp|Q8IX01|SUGP2_H.s.	SURP and G-patch domain-containing protein 2	111			3	
sp|Q9UKN7|MYO15_H.s.	Unconventional myosin-XV	110			2	
sp|P84243|H33_H.s.	Histone H3.3	109			3	
sp|P04279|SEMG1_H.s.	Semenogelin-1	108			2	
sp|Q9NQG5|RPR1B_H.s.	Regulation of nuclear pre-mRNA domain-containing protein 1B	108			2	
sp|Q9UL18|AGO1_H.s.	Protein argonaute-1	107			3	
sp|Q9NP97|DLRB1_H.s.	Dynein light chain roadblock-type 1	106			2	
sp|P43490|NAMPT_H.s.	Nicotinamide phosphoribosyltransferase	106			2	
sp|P61803|DAD1_H.s.	Dolichyl-diphosphooligosaccharide protein glycosyltransferase subunit DAD1	105			2	
sp|P41219|PERI_H.s.	Peripherin	105			2	
sp|Q5C9Z4|NOM1_H.s.	Nucleolar MIF4G domain-containing protein 1	104			2	
sp|Q9Y5S9|RBM8A_H.s.	RNA-binding protein 8A OS=Homo sapiens	102			3	
sp|O00264|PGRC1_H.s.	Membrane-associated progesterone receptor component 1	102			2	
sp|P52294|IMA5_H.s.	Importin subunit alpha-5	102			3	
sp|P63092|GNAS2_H.s.	Guanine nucleotide-binding protein	101			2	

	G(s) subunit alpha isoforms short					
sp|O60231|DHX16_H.s.	Pre-mRNA-splicing factor ATP-dependent RNA helicase DHX16	101			2	
sp|Q9NUP9|LIN7C_H.s.	Protein lin-7 homolog C	101			3	
sp|O60343|TBCD4_H.s.	TBC1 domain family member 4	101			3	
sp|Q9H3K6|BOLA2_H.s.	BolA-like protein 2	101			3	
sp|Q9BYD2|RM09_H.s.	39S ribosomal protein L9, mitochondrial	101			3	
sp|O95819|M4K4_H.s.	Mitogen-activated protein kinase kinase kinase kinase 4	101			2	
sp|P50570|DYN2_H.s.	Dynamin-2	100			3	
sp|Q9Y6A4|CFA20_H.s.	Cilia- and flagella-associated protein 20	100			2	
sp|P10155|RO60_H.s.	60 kDa SS-A/Ro ribonucleoprotein	100			2	

Table S5: Complete list of proteins associated with ^{FLAG}yCdc123 in vivo*, identified by mass spectrometry. Proteins with a score < 100 were excluded. A represents the positive sample, B the negative control without ^{FLAG}hCdc123. Proteins with a score less than 3 times higher in the positive sample, compared to that in the negative sample (column A/B), were excluded. "Peptides" indicates the number of identified unique tryptic peptides from each protein.*

Accession No.	**Name**	**A**	**B**	**A/B**	**A**	**B**
sp|Q05791|CD123_S.c.	Cell division cycle protein 123	4908	66	74.4	56	2
sp|P32481|IF2G_S.c.	Eukaryotic translation initiation factor 2 subunit gamma	3344	832	4.0	43	16
sp|Q12019|MDN1_S.c.	Midasin	3122	986	3.2	65	24
sp|Q08972|NEW1_S.c.	[NU+] prion formation protein 1	2045	672	3.0	38	16
sp|P40069|IMB4_S.c.	Importin subunit beta-4	1912	640	3.0	32	13
sp|P53924|DMA2_S.c.	E3 ubiquitin-protein ligase DMA2	1445			21	
sp|P0C2I9|YP12B_S.c.	Transposon Ty1-PR1 Gag-Pol polyprotein	1387			30	
sp|P47100|YJ12B_S.c.	Transposon Ty1-JR2 Gag-Pol polyprotein	1386			31	
sp|P07244|PUR2_S.c.	Bifunctional purine biosynthetic protein ADE5,7	1186	174	6.8	18	4
sp|P09064|IF2B_S.c.	Eukaryotic translation initiation factor 2 subunit beta	1159	205	5.7	15	4
sp|P25655|NOT1_S.c.	General negative regulator of transcription subunit 1	1150	305	3.8	25	8
sp|P41810|COPB_S.c.	Coatomer subunit beta	1071	333	3.2	21	9
sp|P38708|YHI0_S.c.	Putative proline--tRNA ligase YHR020W	1023	295	3.5	19	6
sp|P30822|XPO1_S.c.	Exportin-1	1013	169	6.0	23	4
sp|P47912|LCF4_S.c.	Long-chain-fatty-acid--CoA ligase 4	902	210	4.3	16	6
sp|P14742|GFA1_S.c.	Glutamine--fructose-6-phosphate aminotransferase	870	257	3.4	18	7
sp|Q07878|VPS13_S.c.	Vacuolar protein sorting-associated protein 13	829	234	3.5	21	7
sp|P05453|ERF3_S.c.	Eukaryotic peptide chain release factor GTP-binding subunit	821	254	3.2	16	6
sp|P38823|DMA1_S.c.	E3 ubiquitin-protein ligase DMA1	788			10	
sp|P47047|MTR4_S.c.	ATP-dependent RNA helicase DOB1	780	186	4.2	16	4

sp|P30665|MCM4_S.c.	DNA replication licensing factor MCM4	767	36	21.3	17	1
sp|P15303|SEC23_S.c.	Protein transport protein SEC23	758	130	5.8	15	4
sp|P00330|ADH1_S.c.	Alcohol dehydrogenase 1	741			14	
sp|P28274|URA7_S.c.	CTP synthase 1 OS=Saccharomyces cerevisiae	739	108	6.8	15	3
sp|Q03640|TCB3_S.c.	Tricalbin-3	737	131	5.6	15	4
sp|P20449|DBP5_S.c.	ATP-dependent RNA helicase DBP5	734	167	4.4	16	5
sp|P42842|EMW1_S.c.	Essential for maintenance of the cell wall protein 1	711	30	23.7	14	1
sp|P25293|NAP1_S.c.	Nucleosome assembly protein	710	211	3.4	13	4
sp|Q12754|RRP12_S.c.	Ribosomal RNA-processing protein 12	700	160	4.4	15	5
sp|Q06685|VIP1_S.c.	Phosphatase VIP1	688			15	
sp|P38737|ECM29_S.c.	Proteasome component ECM29	674	71	9.5	16	2
sp|P47054|NU192_S.c.	Nucleoporin NUP192	622	33	18.8	15	1
sp|Q12213|RL7B_S.c.	60S ribosomal protein L7-B	610			10	
sp|Q07844|RIX7_S.c.	Ribosome biogenesis ATPase RIX7	551			12	
sp|P53091|MCM6_S.c.	DNA replication licensing factor MCM6	533	44	12.1	11	1
sp|P0CX63|YF21B_S.c.	Transposon Ty2-F Gag-Pol polyprotein	532			13	
sp|P0CX41|RL23A_S.c.	60S ribosomal protein L23-A	529	184	2.9	9	4
sp|P39993|GEA2_S.c.	ARF guanine-nucleotide exchange factor 2	528	139	3.8	13	4
sp|Q04175|SXM1_S.c.	Importin beta SMX1	525	129	4.1	11	3
sp|P30624|LCF1_S.c.	Long-chain-fatty-acid-CoA ligase 1	523	123	4.3	11	3
sp|P52918|MSN5_S.c.	Protein MSN5	522	67	7.8	12	2
sp|P53261|PESC_S.c.	Pescadillo homolog	507	80	6.3	9	3
sp|P39986|ATC6_S.c.	Manganese-transporting ATPase 1	484			12	
sp|P40469|MET18_S.c.	DNA repair/transcription protein MET18/MMS19	478	124	3.9	10	4
sp|P29469|MCM2_S.c.	DNA replication licensing factor MCM2	475			10	
sp|P40850|MKT1_S.c.	Protein MKT1	473	38	12.4	9	1
sp|P32590|HSP79_S.c.	Heat shock protein homolog SSE2	446			7	
sp|P12688|YPK1_S.c.	Serine/threonine-protein kinase YPK1	442			10	
sp|P32337|IMB3_S.c.	Importin subunit beta-3	432	69	6.3	10	2
sp|P40212|RL13B_S.c.	60S ribosomal protein L13-B	422			8	
sp|P18759|SEC18_S.c.	Vesicular-fusion protein SEC18	418			10	
sp|P24279|MCM3_S.c.	DNA replication licensing factor MCM3	414			10	
sp|P32501|EI2BE_S.c.	Translation initiation factor eIF-2B subunit epsilon	410	117	3.5	9	3
sp|P22276|RPC2_S.c.	DNA-directed RNA polymerase III subunit RPC2	405	115	3.5	9	2
sp|P38144|ISW1_S.c.	ISWI chromatin-remodeling complex ATPase ISW1	393	79	5.0	8	2
sp|Q08217|PSK2_S.c.	Serine/threonine-protein kinase PSK2	370			9	

sp|P40482|SEC24_S.c.	Protein transport protein SEC2	368	100	3.7	7	2
sp|P38112|MAK5_S.c.	ATP-dependent RNA helicase MAK5	365	57	6.4	8	1
sp|P53172|SDS23_S.c.	Protein SDS23	357	39	9.2	7	1
sp|P53303|ZPR1_S.c.	Zinc finger protein ZPR1	340			6	
sp|P29496|MCM5_S.c.	Minichromosome maintenance protein 5	325			9	
sp|P21147|ACO1_S.c.	Acyl-CoA desaturase 1	323			6	
sp|Q12114|CHS5_S.c.	Chitin biosynthesis protein CHS5	322	39	8.3	6	1
sp|P38811|TRA1_S.c.	Transcription-associated protein 1	310			8	
sp|P53313|SDA1_S.c.	Protein SDA1	307	94	3.3	6	2
sp|P38314|SDS24_S.c.	Protein SDS24	305			6	
sp|P31380|FUN30_S.c.	ATP-dependent helicase FUN30	290			8	
sp|P47037|SMC3_S.c.	Structural maintenance of chromosomes protein 3	284			7	
sp|P09734|TBA3_S.c.	Tubulin alpha-3 chain	281			7	
sp|P33418|XPOT_S.c.	Exportin-T	276			7	
sp|Q06706|ELP1_S.c.	Elongator complex protein 1	275	61	4.5	8	2
sp|P11076|ARF1_S.c.	ADP-ribosylation factor 1	272	32	8.5	6	1
sp|P54861|DNM1_S.c.	Dynamin-related protein DNM1	264			7	
sp|P43621|COPD_S.c.	Coatomer subunit delta OS=Saccharomyces cerevisiae	257	71	3.6	6	2
sp|P39743|RV167_S.c.	Reduced viability upon starvation protein 167	249			5	
sp|P08678|CYAA_S.c.	Adenylate cyclase	244			6	
sp|P19812|UBR1_S.c.	E3 ubiquitin-protein ligase UBR1	243	37	6.6	6	1
sp|Q12451|OSH2_S.c.	Oxysterol-binding protein homolog 2	242			6	
sp|P46970|NMD5_S.c.	Nonsense-mediated mRNA decay protein 5	242	59	4.1	4	2
sp|O14455|RL36B_S.c.	60S ribosomal protein L36-B	240			5	
sp|Q12466|TCB1_S.c.	Tricalbin-1	239	32	7.5	6	1
sp|Q05029|BCH1_S.c.	Protein BCH1	238			6	
sp|P35729|NU120_S.c.	Nucleoporin NUP120	237	31	7.6	6	1
sp|P31384|CCR4_S.c.	Glucose-repressible alcohol dehydrogenase transcriptional effector	235			5	
sp|Q12122|HOSM_S.c.	Homocitrate synthase, mitochondrial	234			5	
sp|P09032|EI2BG_S.c.	Translation initiation factor eIF-2B subunit gamma	228	32	7.1	5	1
sp|P30771|NAM7_S.c.	ATP-dependent helicase NAM7	228			5	
sp|P12754|EI2BD_S.c.	Translation initiation factor eIF-2B subunit delta	227	56	4.1	5	1
sp|P33338|SLA2_S.c.	Protein SLA2	214			6	
sp|P32836|GSP2_S.c.	GTP-binding nuclear protein GSP2/CNR2	213			5	
sp|P32767|KA122_S.c.	Importin beta-like protein KAP122	211			4	
sp|Q12028|AP1G1_S.c.	AP-1 complex subunit gamma-1	200			5	
sp|P33202|UFD4_S.c.	Ubiquitin fusion degradation protein 4	197			5	
sp|P18961|YPK2_S.c.	Serine/threonine-protein kinase YPK2/YKR2	195			5	

sp|P38989|SMC2_S.c.	Structural maintenance of chromosomes protein 2	194			5	
sp|P38712|RRP3_S.c.	ATP-dependent rRNA helicase RRP3	192	33	5.8	5	1
sp|P49687|NU145_S.c.	Nucleoporin NUP145	191	32	6.0	4	1
sp|Q02206|RSC4_S.c.	Chromatin structure-remodeling complex subunit RSC4	187			4	
sp|P47108|URB2_S.c.	Nucleolar pre-ribosomal-associated protein 2	186			5	
sp|P53140|RMD9_S.c.	Protein RMD9, mitochondrial	184			3	
sp|P46673|NUP85_S.c.	Nucleoporin NUP85	176			3	
sp|P32333|MOT1_S.c.	TATA-binding protein-associated factor MOT1	174			4	
sp|P36048|SN114_S.c.	Pre-mRNA-splicing factor SNU114	174			4	
sp|P20485|KICH_S.c.	Choline kinase	173			4	
sp|P38850|RT107_S.c.	Regulator of Ty1 transposition protein 107	172			4	
sp|P32349|RPC3_S.c.	DNA-directed RNA polymerase III subunit RPC3	171			3	
sp|P38426|TPS3_S.c.	Trehalose synthase complex regulatory subunit TPS3	171			4	
sp|P23255|TAF2_S.c.	Transcription initiation factor TFIID subunit 2	169			5	
sp|P36015|YKT6_S.c.	Synaptobrevin homolog YKT6	168			3	
sp|P40856|SA185_S.c.	SIT4-associating protein SAP185	163			5	
sp|P33307|CSE1_S.c.	Importin alpha re-exporter	163			5	
sp|P16603|NCPR_S.c.	NADPH-cytochrome P450 reductase	162			4	
sp|P31374|PSK1_S.c.	Serine/threonine-protein kinase PSK1	160			4	
sp|P25298|RNA14_S.c.	mRNA 3'-end-processing protein RNA14	159			4	
sp|P25847|MSH2_S.c.	DNA mismatch repair protein MSH2	159			4	
sp|P53067|IMB5_S.c.	Importin subunit beta-5	158			5	
sp|P36009|DHR2_S.c.	Probable ATP-dependent RNA helicase DHR2	158			4	
sp|P38630|RFC1_S.c.	Replication factor C subunit 1	157			4	
sp|P17442|PHO81_S.c.	Phosphate system positive regulatory protein PHO81	155			5	
sp|Q99257|MEX67_S.c.	mRNA export factor MEX67	154			3	
sp|P53734|DBP6_S.c.	ATP-dependent RNA helicase DBP6	151			4	
sp|Q12018|CDC53_S.c.	Cell division control protein 53	150			4	
sp|P48562|CLA4_S.c.	Serine/threonine-protein kinase CLA4	150			4	
sp|Q08773|ISW2_S.c.	ISWI chromatin-remodeling complex ATPase ISW2	147			4	
sp|P47169|MET5_S.c.	Sulfite reductase [NADPH] subunit beta	147			3	
sp|P54860|UFD2_S.c.	E4 ubiquitin-protein ligase UFD2	145			4	
sp|P22213|SLY1_S.c.	Protein SLY1	145			3	
sp|Q03653|EFR3_S.c.	Protein EFR3	143			4	
sp|Q02555|RNT1_S.c.	Ribonuclease 3	142			4	
sp|P38129|TAF5_S.c.	Transcription initiation factor TFIID	140			4	

	subunit 5					
sp|P50101|UBP15_S.c.	Ubiquitin carboxyl-terminal hydrolase 15	139			3	
sp|Q12453|CEX1_S.c.	Cytoplasmic export protein	138			4	
sp|P32608|RTG2_S.c.	Retrograde regulation protein 2	134			4	
sp|Q03195|RLI1_S.c.	Translation initiation factor RLI1	134			2	
sp|Q92331|VPS5_S.c.	Vacuolar protein sorting-associated protein 5	132			2	
sp|P40164|PP4R3_S.c.	Serine/threonine-protein phosphatase 4 regulatory subunit 3	130			3	
sp|P25644|PAT1_S.c.	DNA topoisomerase 2-associated protein PAT1	130			4	
sp|P32492|MYO4_S.c.	Myosin-4	129			3	
sp|P38181|NU170_S.c.	Nucleoporin NUP170	128			4	
sp|Q08971|YP225_S.c.	Protein PBDC1 homolog	128			4	
sp|P48563|MON2_S.c.	Protein MON2	128			4	
sp|P53327|SLH1_S.c.	Antiviral helicase SLH1	127			3	
sp|Q06488|RSC2_S.c.	Chromatin structure-remodeling complex subunit RSC2	127			2	
sp|P12753|RAD50_S.c.	DNA repair protein RAD50	126	37	3.4	3	1
sp|P39526|LAA1_S.c.	AP-1 accessory protein LAA1	124			4	
sp|P47031|IML2_S.c.	Inclusion body clearance protein IML2	124			4	
sp|P52593|NU188_S.c.	Nucleoporin NUP188	124			3	
sp|Q00578|RAD25_S.c.	General transcription and DNA repair factor IIH helicase subunit XPB	119			3	
sp|Q08924|WDR6_S.c.	Regulator of Ty1 transposition protein 10	117			4	
sp|P25623|SYP1_S.c.	Suppressor of yeast profilin deletion	116			4	
sp|Q02932|KA120_S.c.	Importin beta-like protein KAP120	115			3	
sp|P17883|SKI3_S.c.	Superkiller protein 3	115			3	
sp|P38217|IMB2_S.c.	Importin subunit beta-2	113			3	
sp|P25303|SCJ1_S.c.	DnaJ-related protein SCJ1	112			2	
sp|P38993|FET3_S.c.	Iron transport multicopper oxidase FET3	112			3	
sp|P39960|BEM2_S.c.	GTPase-activating protein BEM2/IPL2	109			3	
sp|P25632|RSC6_S.c.	Chromatin structure-remodeling complex protein RSC6	109			4	
sp|P34221|PP2C3_S.c.	Protein phosphatase 2C homolog 3	106			3	
sp|P15731|UBC4_S.c.	Ubiquitin-conjugating enzyme E2 4	105			2	
sp|P34110|VPS35_S.c.	Vacuolar protein sorting-associated protein 35	104			3	
sp|P53893|RIA1_S.c.	Ribosome assembly protein 1	102			2	
sp|P22204|DBF2_S.c.	Cell cycle protein kinase DBF2	101			3	
sp|P52891|NUP84_S.c.	Nucleoporin NUP84	100	33	3.0	2	1
sp|P14747|PP2B2_S.c.	Serine/threonine-protein phosphatase 2B catalytic subunit A2	100			2	

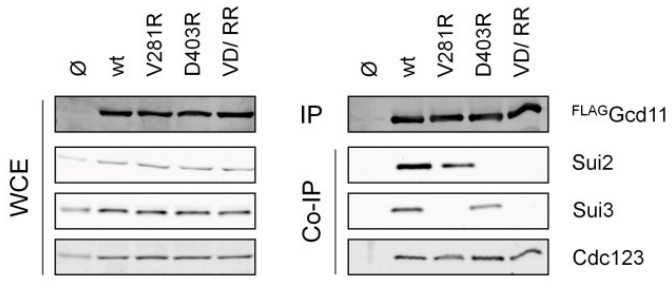

Figure S1: Immunoprecipitation of ^{FLAG}Gcd11 mutants and detection of coprecipitated Sui2, Sui3 and Cdc123. Gcd11 variants were expressed under control of p*GALL*, expression was induced two hours before harvest. The respective Gcd11 variant in each sample is indicated on top of the figure. VD/ RR = V281R, D403R double mutant.

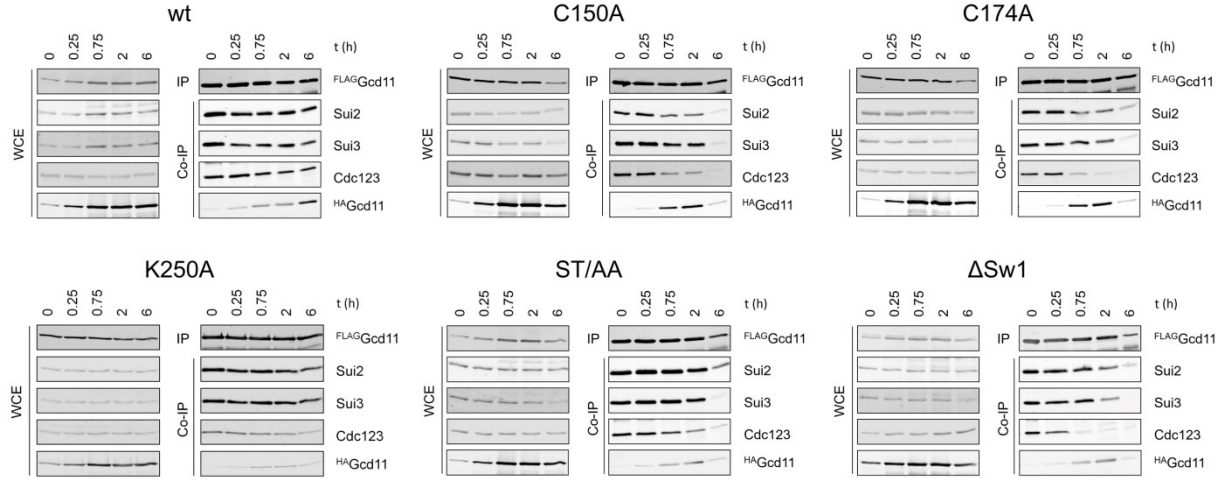

Figure S2: Monitoring of endogenous eIF2 assembly in yeast strains during overexpression of mutated Gcd11 variants. The respective mutated Gcd11 variant is indicated on top of each Western Blot. Below, the time after induction is denoted.

Table S6: Raw data from two independent IPs of Gcd11 D1 mutants*. Coprecipitation of Sui2, Sui3 and Cdc123 was quantified and normalized to the FLAGGcd11 signal in each probe.*

	IP FLAG	**Co-IP Sui2**	**Co-IP Sui3**	**Co-IP Cdc123**	**Sui2/ FLAG**	**Sui3/ FLAG**	**Cdc123/ FLAG**	**Sui2 %**	**Sui3 %**	**Cdc123 %**
wt	53.52	15.41	11.89	12.15	0.288	0.222	0.227	1.00	1.00	1.00
91-527	27.19	0.25	0.51	7.88	0.009	0.019	0.290	0.03	0.08	1.28
C150A	38.5	0.14	0.06	6.68	0.004	0.002	0.174	0.01	0.01	0.76
C174A	36.36	0.2	0.04	7.15	0.006	0.001	0.197	0.02	0.00	0.87
K250A	33.37	7.01	0.42	7.05	0.210	0.013	0.211	0.73	0.06	0.93
ST/AA	36.68	4.85	1.15	6.01	0.132	0.031	0.164	0.46	0.14	0.72
ΔSw1	42.1	10.42	6.52	22.17	0.248	0.155	0.527	0.86	0.70	2.32
	IP FLAG	**Co-IP Sui2**	**Co-IP Sui3**	**Co-IP Cdc123**	**Sui2/ FLAG**	**Sui3/ FLAG**	**Cdc123/ FLAG**	**Sui2 %**	**Sui3 %**	**Cdc123 %**
wt	49.02	8.47	8.39	5.5	0.173	0.171	0.112	1.00	1.00	1.00
91-527	42.27	0.15	0.5	3.46	0.004	0.012	0.082	0.02	0.07	0.73
C150A	36.84	0.18	0.07	2.56	0.005	0.002	0.069	0.03	0.01	0.62
C174A	48.68	0.19	0.16	4.18	0.004	0.003	0.086	0.02	0.02	0.77
K250A	55.39	3.53	0.63	3.75	0.064	0.011	0.068	0.37	0.07	0.60
ST/AA	44.05	2.82	2.21	3.3	0.064	0.050	0.075	0.37	0.29	0.67
ΔSw1	56.42	6.45	6.85	9.96	0.114	0.121	0.177	0.66	0.71	1.57

Table S7: Averages and MSEs for raw data shown in table S6

	Averages			MSE		
	Sui2	**Sui3**	**Cdc123**	**Sui2 %**	**Sui3 %**	**Cdc123 %**
wt	1.00	1.00	1.00	0.00	0.00	0.00
91-527	0.03	0.08	1.00	0.01	0.01	0.27
C150A	0.02	0.01	0.69	0.01	0.00	0.07
C174A	0.02	0.01	0.82	0.00	0.01	0.05
K250A	0.55	0.06	0.77	0.18	0.00	0.16
ST/AA	0.41	0.22	0.69	0.04	0.08	0.03
ΔSw1	0.76	0.70	1.95	0.10	0.01	0.37

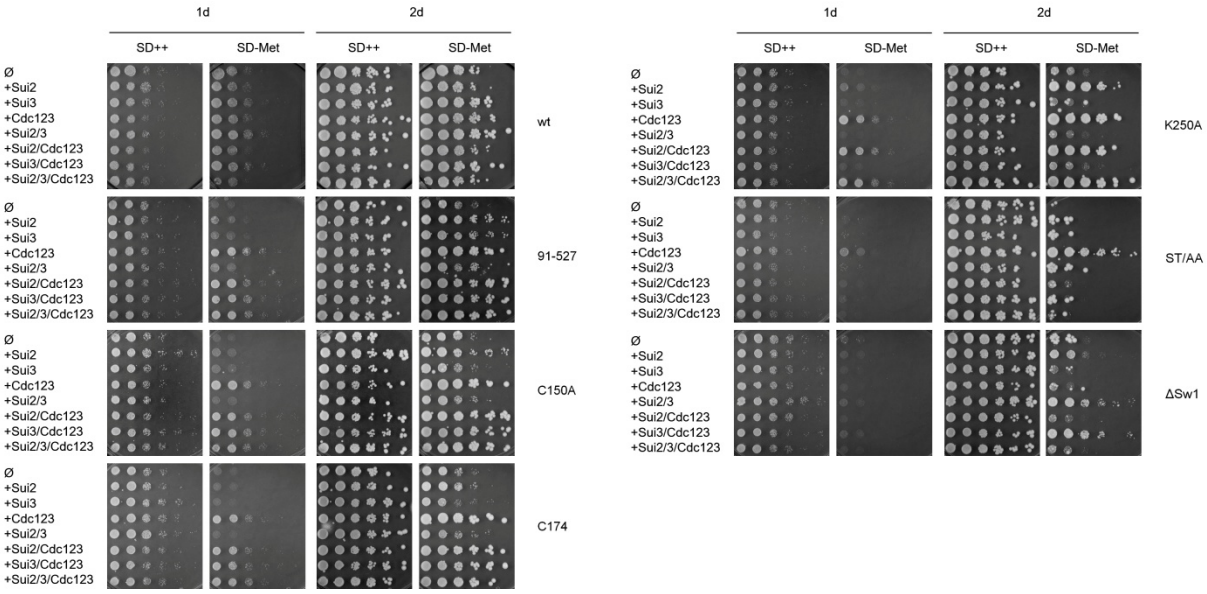

Figure S3: Spot growth test of yeast strains, expressing Gcd11 variants conditionally (p*MET3*) and overexpressing eIF2 subunits, Cdc123 and combinations thereof. For each strain, growth on SD++ and SD-Met was documented after 1 and 2 days (top of figure). Proteins that were overexpressed are indicated on the left, Gcd11 variants are indicated on the right.

Table S8: Quantification of ^{FLAG}heIF2γ signals over time *in one yeast strain with (*hCdc123 (+)*) and one without (*hCdc123(-)*) hCdc123. Columns hCdc123(+) and hCdc123(-) show absolute strengths of heIF2γ signals, t/t=0 (hCdc123(+)) and t/t=0 (heIF2γ(-)) show signal strengths relative to the values at t = 0.*

time (h)	hCdc123 (+)	hCdc123 (-)	t/ t(0) (hCdc123 (+))	t/ t(0) (hCdc123 (-))
0	96054	30121	1.000	1.000
0.25	102729	27068	1.069	0.899
0.75	87443	11748	0.910	0.390
1.5	70666	3004	0.736	0.100
2.5	53788	941	0.560	0.031
4	34957	421	0.364	0.014
6	13637	137	0.142	0.005
9	3204	39	0.033	0.001

Table S9: Quantification of ^{MYC}hCdc123 and ^{FLAG}heIF2γ signals over time. Both proteins were expressed dependent on pGALL. Columns hCdc123 and heIF2γ show absolute signal strengths, t/t=0 (hCdc123) and t/t=0 (heIF2γ) show signal strengths relative to the values at t = 0.

time (h)	hCdc123	heIF2γ	t/t=0 (hCdc123)	t/t=0 (heIF2γ)
0	97600	568000	1.00	1.00
0.25	72700	479000	0.74	0.84
0.75	53200	379000	0.55	0.67
1.5	42100	341000	0.43	0.60
2.5	15900	222000	0.16	0.39
4	7120	166000	0.07	0.29
6	1880	96500	0.02	0.17
9	782	41700	0.01	0.07

Table S10: Quantification of ^{MYC}hCdc123 and ^{FLAG}heIF2γ signals over time*. hCdc123 was expressed constitutively with pTEF2, heIF2γ was expressed dependent on pGALL. Columns hCdc123 and heIF2γ show absolute signal strengths, t/t=0 (hCdc123) and t/t=0 (heIF2γ) show signal strengths relative tot he values at t = 0.*

time (h)	hCdc123	heIF2γ	t/t=0 (hCdc123)	t/t=0 (heIF2γ)
0	112000	709000	1	1
0.25	106000	597000	0.95	0.84
0.75	122000	523000	1.09	0.74
1.5	125000	468000	1.12	0.66
2.5	99600	274000	0.89	0.39
4	110000	199000	0.98	0.28
6	101000	101000	0.9	0.14
9	94400	43600	0.84	0.06

Table S11: Average doubling times of diploid, heterozygous yeasts in liquid XY-D medium at 25 °C in overnight cultures*. wt = unaltered, diploid laboratory strain K842. - /SUI2, etc: strains with heterozygous deletion of the respective gene, based on K842.*

	Repl. No	OD600 (t = 0)	Cultivation time (x)	OD600 (t = x)	Genera-tions	Doubling Time (h)	Average (h)	MSE (h)
wt	1	0.002	14.75	0.78	8.61	1.71	1.73	0.02
	2	0.002	14.75	0.652	8.35	1.77		
	3	0.002	14.75	0.76	8.57	1.72		
	4	.000 86	17	0.8	9.86	1.72		
- /*SUI2*	1	0.002	14.75	0.148	6.21	2.38	2.38	0.04
	2	0.002	14.75	0.132	6.04	2.44		
	3	0.002	14.75	0.16	6.32	2.33		
	4	.000 86	17	0.128	7.22	2.36		
- /*SUI3*	1	0.002	14.75	0.192	6.58	2.24	2.17	0.04
	2	0.002	14.75	0.236	6.88	2.14		
	3	0.002	14.75	0.244	6.93	2.13		
	4	.000 86	17	0.192	7.80	2.18		
- /*GCD11*	1	0.002	14.75	0.48	7.91	1.87	1.92	0.04
	2	0.002	14.75	0.416	7.70	1.92		
	3	0.002	14.75	0.4	7.64	1.93		
	4	.000 86	17	0.344	8.64	1.97		
- /*CDC123*	1	0.002	14.75	0.724	8.50	1.74	1.74	0.00
	2	0.002	14.75	0.7	8.45	1.75		
	3	0.002	14.75	0.716	8.48	1.74		
	4	.000 86	17	0.732	9.73	1.75		

Table S12: Raw data for calculation of β-galactosidase activity in Miller units for K699 and G521 with ΔGCN4

	Repl. No.	OD_{420nm}	t (min)	V_{sample} (ml)	OD_{600}	Miller-Units	Avg.	MSE
K699	1	0.071	10	1.75	0.5	8.1	6.2	1.7
	2	0.062	10	1.75	0.5	7.1		
	3	0.031	10	1.75	0.5	3.5		
	4	0.053	10	1.75	0.5	6.1		
G521	1	0.302	10	1.75	0.5	34.5	31.8	4.9
	2	0.28	10	1.75	0.5	32.0		
	3	0.322	10	1.75	0.5	36.8		
	4	0.208	10	1.75	0.5	23.8		

Table S13: Quantification of cell cycle phases in wild type strain and G521*, grown in XY-D, XY-Gly and XY-A*

Strain	Carbon source	%G1 phase	%S phase	%G2/M phase
wt	glucose	11.09	30.19	58.72
G521	glucose	33.09	24.29	42.62
wt	glycerol	56	14.35	29.65
G521	glycerol	56.12	17	26.88
wt	acetate	73.74	10.39	15.87
G521	acetate	70.25	13.28	16.48

Table S14: Quantification of nuclear Sic1 accumulation in detail

Gcd11(wt) in glucose

Image	Total nuclei	Sic1 in nucleus	% Sic1 in Nucleus
1	76	19	25.0
2	104	16	15.4
3	119	15	12.6
4	89	11	12.4
5	105	19	18.1
6	99	19	19.2
7	91	25	27.5
8	122	18	14.8
9	107	18	16.8
10	101	19	18.8
Total	1013	179	**18.0**
MSE			**4.7**

Gcd11(1-521) in glucose

Image	Total nuclei	Sic1 in nucleus	% Sic1 in Nucleus
1	42	17	40.5
2	46	15	32.6
3	39	14	35.9
4	53	16	30.2
5	41	15	36.6
6	50	16	32.0
7	45	12	26.7
8	43	19	44.2
9	65	25	38.5
10	32	15	46.9
11	47	18	38.3
12	43	16	37.2
Total	546	198	**36.6**
MSE			**5.5**

Table S15: Quantification of nuclear Sic1 accumulation in glycerol

Gcd11(wt) in glycerol				*Gcd11(1-521) in glycerol*			
Image	**Total nuclei**	**Sic1 in nucleus**	**% Sic1 in Nucleus**	**Image**	**Total nuclei**	**Sic1 in nucleus**	**% Sic1 in Nucleus**
1	39	17	43.6	1	30	15	50.0
2	43	15	34.9	2	102	49	48.0
3	48	26	54.2	3	87	33	37.9
4	50	19	38.0	4	98	33	33.7
5	25	11	44.0	5	85	29	34.1
Total	205	88	**42.9**	**Total**	402	159	**39.6**
MSE			**6.6**	**MSE**			**6.9**

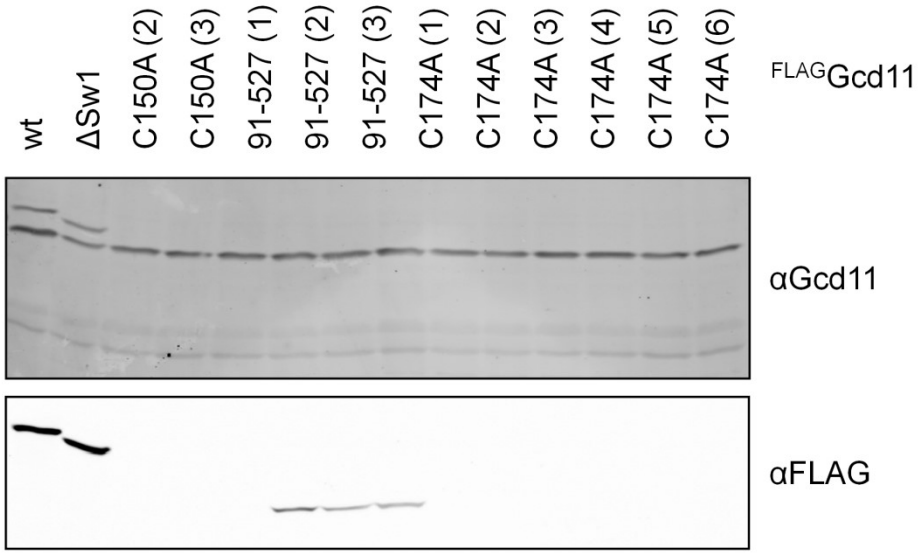

Figure S4: Test expression of different variants of Gcd11 under control of pGCD11 in addition to endogenous Gcd11. The upper panel shows detection of all Gcd11 proteins by αGcd11 antiserum, the lower panel shows bands from monoclonal αFLAG antibody. Note that variant 91-527 is not detectable with αGcd11 serum.

Abbreviations

Table 30: Abbreviations in alphabetical order

Abbreviation	Meaning
AA	Amino acid
APC/C	Anaphase promoting complex/ cyclosome
APS	Ammonium persulfate
ARS-CEN	Autonomously replicating sequence - Centromere region
A-site	Aminoacyl site
bp	Base pair
Buffer 3+	Buffer 3 + 60 mM phosphoglycerophosphate
BSA	Bovine serum albumine
CAK	Cdk activating kinase
CDK	Cyclin dependent kinase
CKI	Cdk inhibitor
CTD	Carboxy-terminal domain
CTT	Carboxy-terminal tail
DBD	DNA binding domain
DMEM	Dulbecco's modified Eagle Medium
DMFA	Dimethyl formamide
DMSO	Dimethyl sulphoxide
dNTP	Desoxynucleoside triphosphate
DTT	Dithiothreitol
EBI	European Bioinformatics Institute
E. coli	*Escherichia coli*
EDTA	Ethylenediaminetetraacetic acid
E-site	Exit site
FBS	Fetal Bovine Serum
FRT/TO	Flippase recognition target/ Tet-On
GAP	GTPase activating protein
Gcd^-	General control derepressed
GDF	GDI dissociation factor
GDI	Guanosine dissociation inhibitor
GEF	Guanosine exchange factor
HA (tag)	Hemagglutinine epitope (tag)
H. sapiens/ H. s.	Homo sapiens
HEK (cells)	Human embryonic kidney (cells)
heIF2x	human eIF2 subunit x (x = α, β, γ)
hCdc123	human Cdc123
(Co-)IP	(Co-)Immunoprecipitation
IRES	Internal Ribosome Entry Structure
Kb(p)	Kilobase (pair)
K_D	Dissociation constant
KOD (polymerase)	*Pyrococcus* sp. strain from Kodakara island (polymerase)
LB_{Amp}	LB medium with ampicillin
LiAc	Lithium acetate
LRB	Laemmli running buffer
LSB	Laemmli sample buffer
LSU	Large subunit (referring to the 60S ribosomal subunit)
MAT	Mating type
MS	Mass spectrometry
MSE	Mean square error

MYC (tag)	c-MYC epitope (tag)
NLS	Nuclear localization signal (peptide)
NTD	Amino-terminal domain
NTT	Amino-terminal tail
OD	Optical density
(u)ORF	(upstream) Open reading frame
PAGE	Polyacrylamide gel electrophoresis
PBS	Phosphate buffered saline
PCR	Polymerase chain reaction
p(*GENE* name)	Gene specific promoter (e.g. p*GAL1* = *GAL1* promoter)
PEG	Polyethylene glycol
P_i	Anorganic phosphate (Nucleotriphosphate hydrolysis product)
PIC	Preinitiation complex
POI	Protein of interest
P-site	Peptidyl site
RG	Research group
(t)RNA	(transcription) ribonucleic acid
rpm	Rounds per minute
RT	Room temperature
SCF	Skp1 cullin f-box protein complex
S. cerevisiae/ *S. c.*	Saccharomyces cerevisiae
SDS	Dodium dodecyl sulfate
SDS-PAGE	Polyacrylamide electrophoresis (SDS-PAGE)
SV40	Simian Virus 40
ssDNA	Single stranded DNA
SSU	Small subunit (referring to the 40S ribosomal subunit)
ssu$^-$	Suppressor of sui$^-$ (phenotype)
sui$^-$	Suppressor of initiation codon (phenotype)
T_A	Annealing temperature
TAE	Tris-Acetate-EDTA
TBS(-T)	Tris buffered saline (with tween 20)
TC	Ternary complex
TE	Tris-EDTA
Tet	Tetracyclin
TEMED	Tetramethylethylenediamine
$tRNA_e$	Elongator tRNA
$tRNA_i$	Met-$tRNA_i^{MET}$
UTR	Untranslated region
WCE	Whole cell extract
XLID	X-linked intellectual deficiency
Y2H	Yeast-two-hybrid assay
y/heIF2x	Yeast/ human eIF2 subunit x (x = α, β, γ)
y/hCdc123	Yeast/ human Cdc123

Figures

Tables

Acknowledgements

This thesis wouldn't have been possible without the help and previous work from numerous other people.

I want to thank my supervisor, Prof. Dr. Wolfgang Seufert for his supervision, constant preparedness for discussion, and helping me finalizing my thesis.

Furthermore, I want to thank my mentors, Prof. Dr. Gunter Meister of the University of Regensburg and Dr. Emmanuelle Schmitt of the École Polytechnique in Paris. Thanks also to Prof. Dr. Seufert, Prof. Dr. Tschochner and Dr. Medenbach for assessing and examining my thesis.

My thanks also go to my predecessors and colleagues Dr. Lea Neumann-Arnold, Dr. Angelika Perzlmaier and Dr. Frank Richter whose work enabled me to do my research in the first place.

Special thanks also goes to Dr. Jan Medenbach, Stefan Reich and Dr. Astrid Bruckmann for being extremely helpful. Without them my cell culture work and mass spectrometry wouldn't have been possible.